Janus fluorocyclohexanes as facially polarised motifs for organized supramolecular materials

Thomas J. Poskin

A thesis submitted for the degree of PhD
at the
University of St Andrews

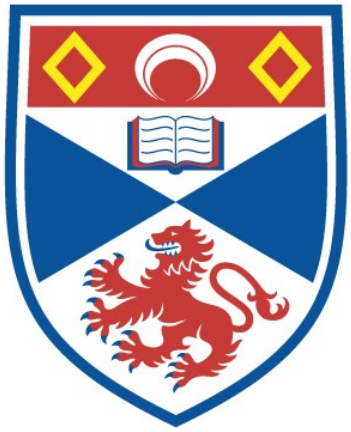

2025

Full metadata for this thesis is available in
St Andrews Research Repository
at:
https://research-repository.st-andrews.ac.uk/

Identifier to use to cite or link to this thesis:
DOI: https://doi.org/10.17630/sta/1204

This item is protected by original copyright

This item is licensed under a
Creative Commons Licence

https://creativecommons.org/licenses/by-nc/4.0/

Candidate's declaration

Candidate's declaration

I, Thomas Joseph Poskin, do hereby certify that this thesis, submitted for the degree of PhD, which is approximately 56,000 words in length, has been written by me, and that it is the record of work carried out by me, or principally by myself in collaboration with others as acknowledged, and that it has not been submitted in any previous application for any degree. I confirm that any appendices included in my thesis contain only material permitted by the 'Assessment of Postgraduate Research Students' policy.

I was admitted as a research student at the University of St Andrews in September 2020.

I received funding from an organisation or institution and have acknowledged the funder(s) in the full text of my thesis.

Date 09/09/2024 Signature of candidate

Supervisor's declaration

I hereby certify that the candidate has fulfilled the conditions of the Resolution and Regulations appropriate for the degree of PhD in the University of St Andrews and that the candidate is qualified to submit this thesis in application for that degree. I confirm that any appendices included in the thesis contain only material permitted by the 'Assessment of Postgraduate Research Students' policy.

Date 09/09/2024 Signature of supervisor

Permission for publication

In submitting this thesis to the University of St Andrews we understand that we are giving permission for it to be made available for use in accordance with the regulations of the University Library for the time being in force, subject to any copyright vested in the work not being affected thereby. We also understand, unless exempt by an award of an embargo as requested below, that the title and the abstract will be published, and that a copy of the work may be made and supplied to any bona fide library or research worker, that this thesis will be electronically accessible for personal or research use and that the library has the right to migrate this thesis into new electronic forms as required to ensure continued access to the thesis.

Candidate's declaration

I, Thomas Joseph Poskin, confirm that my thesis does not contain any third-party material that requires copyright clearance.

The following is an agreed request by candidate and supervisor regarding the publication of this thesis:

Printed copy
No embargo on print copy.

Electronic copy

No embargo on electronic copy.

Date 09/09/2024 Signature of candidate

Date 09/09/2024 Signature of supervisor

Candidate's declaration

Underpinning Research Data or Digital Outputs

Candidate's declaration

I, Thomas Joseph Poskin, understand that by declaring that I have original research data or digital outputs, I should make every effort in meeting the University's and research funders' requirements on the deposit and sharing of research data or research digital outputs.

Date 09/09/2024 Signature of candidate

Permission for publication of underpinning research data or digital outputs
We understand that for any original research data or digital outputs which are deposited, we are giving permission for them to be made available for use in accordance with the requirements of the University and research funders, for the time being in force.

We also understand that the title and the description will be published, and that the underpinning research data or digital outputs will be electronically accessible for use in accordance with the license specified at the point of deposit, unless exempt by award of an embargo as requested below.

The following is an agreed request by candidate and supervisor regarding the publication of underpinning research data or digital outputs:

No embargo on underpinning research data or digital outputs.

Date 09/09/2024 Signature of candidate

Date 09/09/2024 Signature of supervisor

Research data underpinning this thesis are available at

https://doi.org/10.17630/676501a7-cb0d-4e9f-85a7-f393178f5de8

Abstract

A Janus-face cyclohexane has a single fluorine on each carbon and with all *syn* configuration, creating a face of fluorines on one side of the ring and hydrogens on the other. This thesis prepares and explores the properties of derivatives of this class of molecule. **Chapter 1** introduces organofluorine chemistry, its applications, and an overview of the evolution of Janus fluorocyclohexanes, detailing their initial synthesis and highlighting their unique polar properties. **Chapter 2** describes the synthesis of mono-, di-, and tri-alkylated Janus fluorocyclohexane derivatives. In particular the influence of peripheral substituents on supramolecular packing was explored. The tri-alkylated systems adopted columnar discotic stacking. This research suggests that the 2,4,6 tri-alkylated ring systems have potential as a motif for ordered supramolecular assemblies and as they exhibit multiple polymorphs, they offer potential as liquid crystalline materials. **Chapter 3** focuses on the synthesis of two novel Janus Organic Framework (JOF) struts, featuring carboxylic acid linkers with either tri- or penta-fluorinated Janus rings. Single crystal X-ray analysis confirmed their structure, and preliminary findings demonstrated increased porosity in first-generation JOF-MOFs compared to isolated JOF struts. Second-generation JOF-MOFs were developed through exchange synthesis with MOF-808, confirming this new class of framework, with initial results showing potential for further porosity enhancements and applications in supramolecular porous materials. **Chapter 4** discusses the development of Janus cyclohexanes with a 3,6-dialkyl ether linkage, investigated for their dielectric anisotropic properties and potential use in memory storage devices. These compounds, which possess a long-chain phosphonic acid group for self-assembly on a TiN substrate were designed as potential memory storage molecules. **Chapter 5** explores nucleophilic aromatic substitution reactions of pentafluoro aryl ethers, focusing on the *para* selectivity of these reactions and leading to the generation of Janus 3,6-di alkyl ethers, compounds which displayed significant polymorphism, suggesting potential for liquid crystal applications. In overview this body of work demonstrates new approaches to the synthesis of Janus fluorocyclohexanes and highlights possibilities for their potential applications in supramolecular assembly, liquid crystals, and organic materials science more generally.

General Acknowledgement

First and foremost, I would like to thank my supervisor, Professor David O'Hagan for his continuous support throughout the years. David's love for organofluorine chemistry has inspired me throughout not only my PhD but my undergraduate degree as well.

I would like to thank all the members of the DOH group both past and present for all of their support and help throughout my PhD. Specifically, I would like to thank Dr. Phill Lowe, Dr. Rifahath Mon Neyya Ppadath, Dr. Qingzhi Zhang, Dr. Marta Wojnowska, Dr. Joshua Clark, Dr. Cihang Yu, Dr. Yohann Renault, Dr. Yawen Chen, Dr. Luca Dobson, Dr. Dom Spurling, Dr. Mengfan He, Josephine Stewart, George Kingsley-Moore, Oluwayinka Oke, and Nachiket Deepak More. In particular I want to thank Mengfan, Luca, and George for their constant chat and support being in the same fume hood bay once we moved into the BMS building in the second year of my PhD. I want to thank the project students I supervised throughout my PhD allowing my love for chemistry to be passed on to eager minds. I want to thank our collaborators on the projects within this thesis: Bruno Piscelli and Dr. Rodrigo Cormanich at the State University of Campinas in Brazil for their computational studies used in chapters 2 and 5; Keigo Yoshida and Dr. Shigeyuki Yamada at Kyoto Institute of Technology for their DSC analysis in chapters 2 and 5; Dr. David Cordes and Dr. Alexandra Slawin for solving my X-ray structures; Romy Ettlinger, Russell Main, and Prof. Russell Morris for their help in synthesizing the JOF-MOFs of chapter 3; Dr. Peer Kirsch for his attempts at developing the SAM memory storage device of chapter 4; Dr. Taiju Takahashi for his investigation into the properties of targets synthesized in chapter 5; Dr. Siobhan Smith, Prof. Thomas Lebl, and Dr. Maria Papa for their help with NMR; Alan Taylor and the Edinburgh mass spectrometry centre for running my mass spectrometry samples.

I want to thank the Ultimate frisbee club of St Andrews and all its members over these last nine years. Finding this sport back in 2015 has been one of the best decisions of my life. To find a sport and team I have enjoyed so much as a relief from the lab has been vital to my success over the years. The people of the club have become some of my closest and dearest friends.

General Acknowledgment

None of this would have been possible without the continued love and support of my fiancée Dr. Lucy Dale, you are my rock. All that I am and all that I will do is yours. I am my beloved, and my beloved is mine.

I would like to thank the EPSRC and EaSi-CAT for funding my PhD.

Funding

This work was supported by The University of St Andrews under the EaSi-CAT program.

Abbreviations

Å	Angstrom
Ac	Acetyl
AGSS	Anaesthetic gas scavenging system
Ar	Aryl
aq	Aqueous
Ax	Axial
BARF	Tetrakis[3,5-bis(trifluoromethyl)phenyl]borate
BET	Brunauer-Emmett-Teller
Bn	Benzyl
Boc	*tert*-butyloxycarbonyl
br	Broad
Bz	Benzoyl
c	Concentration
°C	Celsius
CAAC	Cyclic(alkyl)(amino)carbene
Cat	catalyst
COD	1,5-Cyclooctadiene
COF	Covalent organic framework
COSY	Correlation spectroscopy
2D	Two-dimensional
d	Doublet
D	Debye
DAST	Diethylaminosulfur trifluoride
1,2-DCE	1,2-Dichloroethane Diethylaminosulfur trifluoride
DFT	Density-functional theory
DIBALH	Diisobutylaluminium hydride
DMAP	4-Dimethylaminopyridine
DMF	*N*,*N*-Dimethylformamide
DMSO	Dimethylsulfoxide
E1cB	Elimination unimolecular conjugate base

Abbreviations

E2	Bimolecular elimination
EC_{50}	Half maximal effective concentration
ED_{50}	Median effective dose
EDG	Electron Donating Group
Ee	Enantiomeric excess
EI	Electron impact
Eq	Equatorial
ESI	Electrospray
Et	Ethyl
ε_r	High dielectric constant
equiv	Equivalent(s)
eV	Electronvolt
EWG	Electron Withdrawing Group
FTJ	Ferroelectric tunnel junction
GHG	Greenhouse gases
GWP	Global warming potential
h	Hour(s)
HMBC	Heteronuclear multiple bond correlation spectroscopy
HPLC	High performance liquid chromatography
HSQC	Heteronuclear single-quantum correlation spectroscopy
HOF	Hydrogen-bonded organic framework
HOMO	Highest occupied molecular orbital
HRMS	High-resolution mass spectrometry
Hz	Hertz
^{i}Bu	Isobutyl
IPA	Propan-2-ol / isopropanol / 2-propanol / isopropyl alcohol
^{i}Pr	Isopropyl
IPS	In Plane Switching
IR	Infrared
J	Spin-spin coupling constant
JOF	Janus organic framework

Abbreviations

JOF-MOF	Janus organic framework – metal organic framework
k	capacity factor
K_a	Association constant
K_i	inhibitor constant
LDA	Lithium diisopropylamide
Log D	Distribution coefficient
Log P	Partition coefficient
LSP	Living supramolecular polymerization
LUMO	Lowest unoccupied molecular orbital
M	Molar
m	Multiplet
mCPBA	*meta*-Chloroperbenzoic acid
Me	Methyl
min	Minute(s)
mmol	Millimole(s)
MOF	Metal Organic Framework
mol	Mole(s)
mp	Melting point
MS	Molecular sieves
MW	Microwave
m/z	Mass:charge ratio
N	normal
Na BARF	Sodium tetrakis[3,5-bis(trifluoromethyl)phenyl]borate
NAS	Nucleophilic Aromatic Substitution
^{n}Bu	Butyl
NHC	*N*-Heterocyclic Carbene
NHS	National Health Service
NLO	Non-linear optical
NMR	Nuclear magnetic resonance
NOESY	Nuclear Overhauser effect spectroscopy
NP	Nanoparticle

Abbreviations

OLC	Organic Liquid Crystal
pH	Potential of hydrogen
Ph	Phenyl (C_6H_6)
pK_a	Negative log of K_a
P_s	Spontaneous polarisation
P_{sat}	High saturation polarisation
POM	Polarised Optical Microscopy
PTFE	Poly(tetrafluoroethylene)
q	Quartet
quant.	Quantitative yield
r	Radius
RAM	Random access memory
Ref	Reference
Rf	Retention factor
r.t.	Room temperature
s	Singlet
SAM	Self assembled monolayer
S_NAr	Nucleophilic aromatic substitution
SPS	Solvent purification system
$t_{1/2}$	Half life
t	Triplet
T	Temperature
TBAF	Tetra-n-butylammonium fluoride
TBDMS	*tert*-Butyldimethylsilyl
^{t}Bu	*tert*-Butyl
T_c	Curie temperature
tert	Tertiary
TFA	Trifluoroacetic acid
TFTB	Tri-fluoro *tert*-butyl
THF	Tetrahydrofuran
TLC	Thin-layer chromatography

Abbreviations

TMS	Tetramethylsilane
TMSCl	Trimethylsilyl chloride
TN	Twisted Nematic
Ts	Tosyl
TTMSS	*Tris*(trimethylsilyl)silane
UV	Ultraviolet
VA	Vertical Alignment
VdW	Van der Waals
XPS	X-ray Photoelectron Spectroscopy
δ	Chemical shift

Table of Contents

Contents

Abstract ..... *iv*

General Acknowledgement ..... *v*

Abbreviations ..... *vii*

Contents ..... *xii*

1: Introduction *1*

1.1 Fluorine generation **1**

1.2 First fluorine containing compounds **3**

1.3 Organofluorines **3**

1.31 Stereoelectronic and conformational effects of the C-F bond 5

1.32 Organofluorines in pharmaceuticals 7

1.33 Organofluorines in anaesthetics 9

1.34 Organofluorines in liquid crystals 10

1.4 The history of Janus compounds **16**

1.41 The Zeng cyclic (amino)(alkyl)carbene rhodium catalyst 18

1.42 Novel Janus-faced compounds 22

1.43 The supramolecular Janus motif 23

1.5 Aim **29**

2: Janus cyclohexanes for organic liquid crystals *30*

2.1 Liquid Crystal Displays **30**

2.2 Introduction **32**

2.21 Computational analysis of Janus ring assemblies 33

2.3 Sonogashira cross-coupling reactions **35**

2.4 Hydrogenation of the aryl acetylenes **40**

2.5 Aryl hydrogenations **41**

2.6 POM and DSC analysis **51**

2.7 Conclusions **55**

3: JOF-MOFs *56*

3.1 Introduction **56**

3.2 Organic frameworks **58**

3.21 First generation JOFs 62

3.3 Synthesis of penta- and tri-fluoro JOF-MOF struts **65**

3.31 Initial investigations 65

3.32 Synthesis of JOF struts 70

3.4 JOF-MOF synthesis and analysis **76**

3.41 Preliminary JOF-MOF synthesis 76

3.42 New strategy: Strut replacement from MOF-808 79

3.5 Conclusions **83**

Table of Contents

4: Janus cyclohexanes, a candidate motif for memory storage *85*

4.1 Introduction **85**

4.2 Types of memory storage **90**

4.3 Aim: Organic SAM memory storage project **91**

4.4 Synthesis of Janus containing long chain phosphonic acid **93**

4.41 Initial approaches 93

4.42 Synthesis of Janus SAM precursors 99

4.5 SAM fabrication **102**

4.6 Summary **105**

5: Preparation of the Janus cyclohexane 3,6-diether motif *106*

5.1 Introduction **106**

5.2 Experimental S_NAr study **111**

5.21 Nucleophile scope 116

5.3 Computational study (Dr. Rodrigo Cormanich, University of Campinas) **118**

5.31 Kinetic considerations 118

5.32 Thermodynamic considerations 121

5.4 Synthesis of all-*cis* 3,6-Janus cyclohexanes **122**

5.41 'Equivalent' 3,6-Janus molecules 123

5.42 'Non-equivalent' Janus 3,6-diethers 125

5.5 Conformational equilibrium between *ax/eq* and *eq/ax* Janus 3,6-diethers **133**

5.6 Pentafluoro alkyl ether Janus compound **135**

5.7 Dielectric anisotropy Investigation **138**

5.8 Conclusions **140**

6: Conclusions *142*

7: Experimental *144*

7.1 Analytical Instrumentation supporting synthesis **144**

7.2 Synthetic procedure and characterisation of molecules **145**

7.21 Experimental for Chapter 2 147

7.22 Experimental for Chapter 3 177

7.23 Experimental for Chapter 4 189

7.24 Experimental for Chapter 5 202

8: References *237*

9: Appendix *245*

1: Introduction

1.1 Fluorine generation

Fluorine is an essential element in modern society. The developed world is reliant on pharmaceuticals, agrochemicals, polymers, air conditioning materials, anaesthetic gases, and visual displays, all derived from organic molecules which owe their defining properties to the presence of fluorine.[1] Fluorine is the 13th most abundant element within the Earth's crust and is present in many ores and minerals, however it is only economically accessible via extraction from three mineral classes: cryolite, fluorapatite, and fluorspar.[2] Of these three historical sources, cryolite (AlF_3 or NaF) has been exhausted and is no longer a viable source of fluorine. Fluorapatite ($Ca_5(PO_4)_3F$) a constituent of phosphate rock, is abundant in the United States, however, it is currently not used as a fluorine source even with an estimated 300 billion tones in global reserves.[1] Thus, despite these three mineral classes, all of the fluorine used in chemical industry comes from fluorspar. Fluorspar is commonly mined in Mexico and China and half of the mineral is used as a flux to reduce the melting temperatures of metals in iron and steel production. The remainder is used to manufacture anhydrous hydrogen fluoride (aHF), which is the base chemical for all of the fluorine found in organic products.[1] The most common sources of fluorine in the context of organic chemistry are summarized below in Figure 1.1.

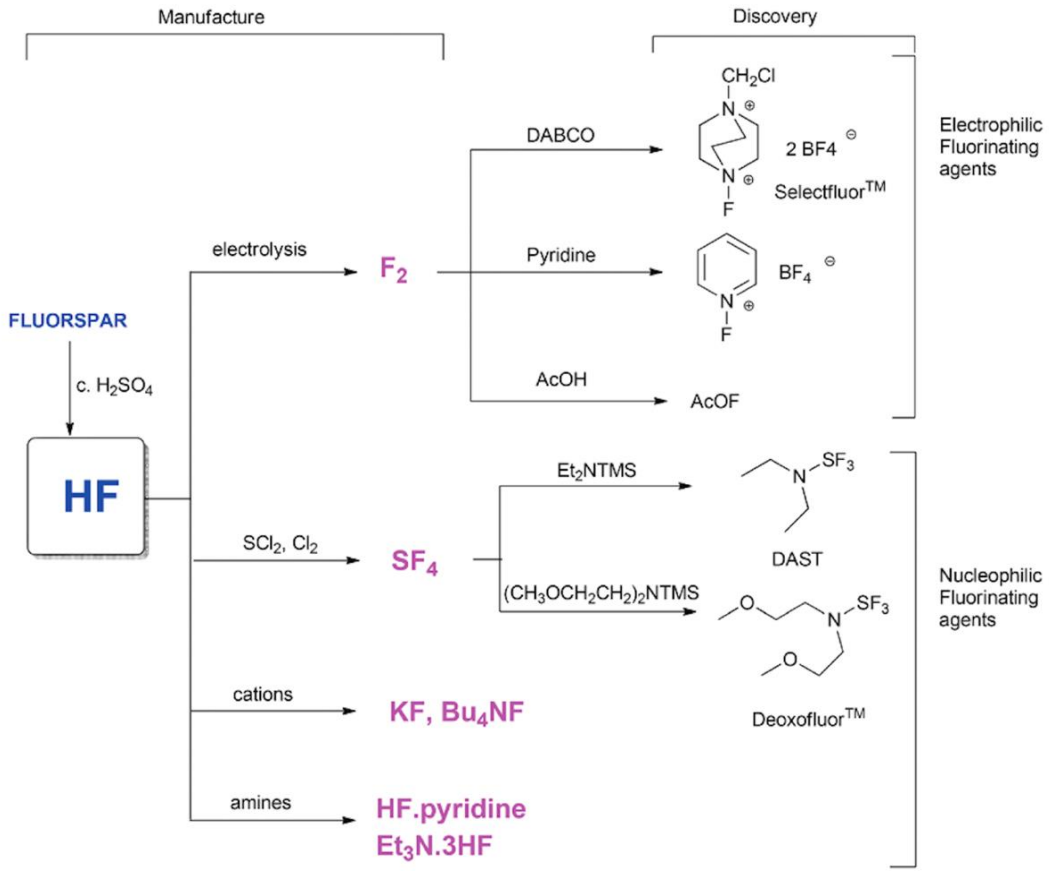

Figure 1.1: Schematic of the specific uses for fluorspar.[1]

Fluorspar is converted into anhydrous hydrogen fluoride by treatment with H_2SO_4. From there, aHF can be processed in several ways, for example, by electrolysis to produce elemental fluorine (F_2) or using SCl_2 and chlorine gas to generate SF_4. These can then be further converted into either electrophilic or nucleophilic fluorinating agents. For example, fluoropyridiniums are generated by reacting F_2 with pyridines, and the common nucleophilic fluorinating agent, Diethylaminosulfur trifluoride (DAST), is generated by reacting sulphur tetrafluoride with diethylamino trimethylsilane. DAST was introduced in the 1970's to replace SF_4 as the main nucleophilic fluorinating agent for the conversion of e.g. carboxylic acids to $-CF_3$, or alcohols to fluorides.[3] Sulphur tetrafluoride is a toxic gas and difficult to handle whereas DAST is a liquid and is a more amenable laboratory chemical.

1.2 First fluorine containing compounds

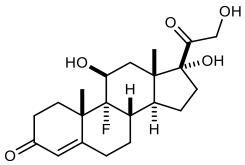

Fludrocrtisone
brand name Florinef acetate

Figure 1.2: First fluorinated drug licenced in 1954.

The first organofluorine compound was made by Alexander Borodin in 1862.[4,5] Later in the late 19th century Swarts developed the first aromatic compounds with fluorinated side chains.[5,6] The first fluorinated drug, the steroidal anti-inflammatory florinef acetate (Figure 1.2), was developed in 1954.[7] By 2012 there were over 140 fluorinated drugs, and by 2019 there were at least 340 licenced for use on the market.[8] This trend is not only obvious in pharmaceuticals, but in agrochemicals too. The importance of food security and safety is particularly challenging as the world population continues to increase and this is tackled by developing improved agrochemical products. According to the 18th edition of the *Pesticide Manual,* roughly 16% of pesticides contain fluorine.[8] This number has increased steadily since the first development of organofluorines. Fluorine has also played a key role in materials perhaps typified by one of the most important fluoropolymers, poly(tetrafluoro)ethylene (PTFE) developed by the Dupont company in the 1930s.[9] PTFE was a revolutionary material as it has enhanced chemical and thermal stability and can survive extreme conditions. The commercial products developed with PTFE are numerous. For example, Teflon (commonly used in coated cookware) or Goretex (used in rainproofing clothing) are used as resistant materials, and the polymer can be fabricated to make components in a range of technologies. Fluoropolymers have been developed for uses ranging from medical implants to aerospace. In 2021 fluoropolymers had an estimated market value at around $7.23 billion per annum and this is expected to grow to $10.31 billion by 2028.[10]

1.3 Organofluorines

Organofluorines are defined by containing at least one C-F bond. Hydrogen and fluorine are of similar size; with atomic radii of 53 pm and 42 pm respectively. As such, they can

be interchangeable in molecules, particularly in pharmaceuticals, as the two atoms have similar steric demands.[11] As hydrogen is partially electropositive in C-H bonds and fluorine is the most electronegative element, the replacement of a hydrogen for a fluorine changes the electronic properties and chemistry of a given molecule after replacement and this has been used widely to tune properties. Fluorine attracts electron density from carbon, polarising the C-F bond.[12] This bond has a significant electrostatic character between $F^{\delta-}$ and the $C^{\delta+}$, more so than a typical covalent bond.[13] Accordingly fluorine forms the shortest and strongest bonds to carbon, apart from the C-H bond, making it one of the strongest bonds in organic chemistry (dissociation energy, 105.4 kcal mol^{-1}) as illustrated in Table 1.1. For comparison the common covalent bond dissociation energies are shown in Table 1.2. This offers advantages when introducing fluorine into drug molecules and materials to improve metabolic, thermal, and chemical stabilities.[14]

Table 1.1: Van der Waals radii and average C-X bond lengths of common elements.[15,16]

van der Waals Radii/Å	H (1.2)	C (1.70)	N (1.55)	O (1.52)	**F (1.47)**
	Si (2.1)	P (1.8)	S (1.8)	Cl (1.74)	
Bond length/Å	C-H (1.09)	C-C 1.54)	C-N (1.47)	C-O (1.43)	**C-F (1.35)**
	C-Si (1.85)	C-P (1.84)	C-S (1.82)	C-Cl (1.77)	

Table 1.2: Bond dissociation energy of common covalent bonds.[15]

Bond	**Bond dissociation energy / kcal mol^{-1}**
C-F	105.4
C-H	98.8
C-O	84.0
C-C	83.1
C-Cl	78.5
C-N	69.7

1.31 Stereoelectronic and conformational effects of the C-F bond

There is a significant polarization of the C-F bond that leads to geometric changes in hydrocarbons,[17] for example, in methane Figure 1.3 indicates that the H-C-H angle widens (113.8°) when two of the hydrogens are replaced with fluorine, and the F-C-F angle narrows (108.4°) relative to the Td angle (109.5°). This is because the fluorine is pulling p-orbital electron density from the sp^3 carbon to the fluorine, making the carbon more sp^2 in character, widening the H-C-H angle and narrowing the F-C-F angle.[17] Bent's rule states "*atomic s character concentrates in orbitals directed toward electropositive substituents*."[18] Thus, more p character in carbon is directed towards electronegative groups such as fluorine.

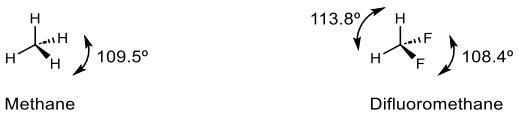

Figure 1.3: Bond angles of methane and fluoromethane derivative.[17]

Introduction of the C-F bond into a molecule can influence conformation as a consequence of stereoelectronic effects. These effects are often discussed in the context of the 'anomeric effect' and the '*gauche* effect' as well as dipole-dipole interactions, and charge-dipole interactions.

1.31.1 The anomeric effect and gauche effect

The anomeric effect is a stereoelectronic effect, most closely associated with carbohydrates, which describes an axial preference for heteroatoms positioned alpha to the oxygen in a pyran ring. An equatorial orientation might be expected based on steric arguments (Figure 1.4).[19]

Hyperconjugation occurs from the non-bonding oxygen lone pair to the LUMO C-O (σ^*) of the C-O bond, but only in the axial (α-) conformer of **1.1** (**1.1a**). This hyperconjugation is not possible in the equatorial (β-) (**1.1b**) conformation due to the poor overlap of orbitals. The anomeric effect is even stronger e.g. if F replaces O in 2-

fluorotetrahydropyran **1.2**, with theory studies estimating ΔE increasing by 2.11 kcal mol^{-1} from **1.1** to **1.2**.[20]

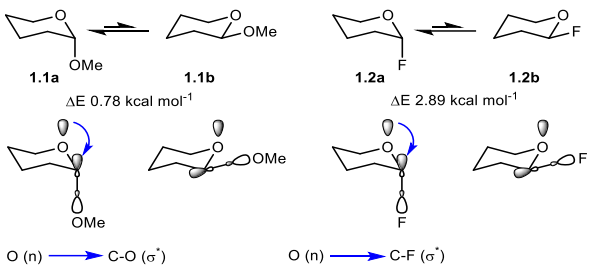

Figure 1.4: The anomeric effect; hyperconjugation interactions supporting a preference for the α-conformer in 2-methoxytetrahydropyran **1.1** and 2-flurorotetrahydropyran **1.2**.[20]

The *gauche* effect recognises that the *gauche* conformation of 1,2-difluoroethane is more stable than the *anti* conformation[21] whereas 1,2-dichloro-, 1,2-dibromo, and 1,2-diiodo-ethanes (**1.3**) all have lower energy *anti*-conformations, consistent with steric arguments (Figure 1.5).[22] For 1,2-difluoroethane the repulsions of the two C-F dipoles is over-ridden by stabilising $\sigma_{C\text{-}H}\ldots\sigma^*_{C\text{-}F}$ hyperconjugative interactions.[22,23]

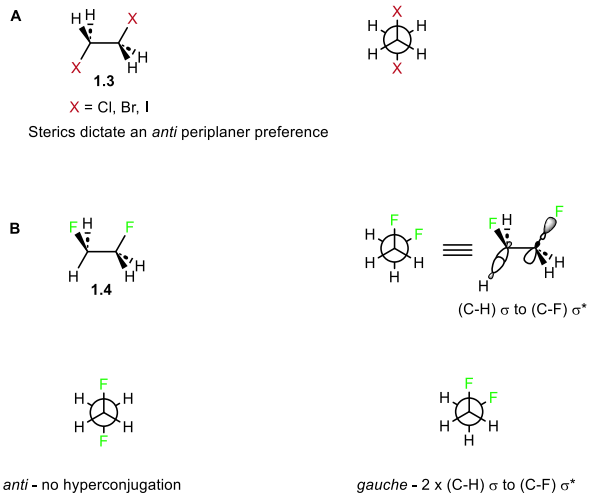

Figure 1.5: A the anti-conformer preference for 1,2-dichalogen-ethane (excluding fluorine) (**1.3**). **B** the gauche-conformer preference for 1,2-difluoroethane (**1.4**) due to hyperconjugation.

1.31.2 Dipole-dipole interactions

The strong dipole associated with the C-F bond influences the conformational behaviour of organofluorine compounds such as α-fluoroacetone (Figure 1.6), [24,25] where the carbonyl and the C-F bond dipoles oppose each other.[22] This phenomenon

extends to esters, ketones, amides, and aldehydes. Additionally polar solvents screen the electrostatics and reduce the energy difference of the isomers; hence the energy difference is larger in the gas phase when compared to DMSO.

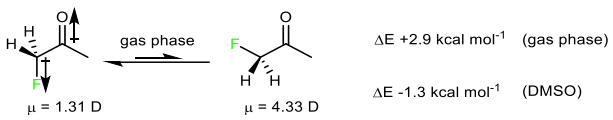

Figure 1.6: Dipolar repulsion favouring the anti-conformation in α-fluoroacetone.

1.31.3 Charge-dipole interactions

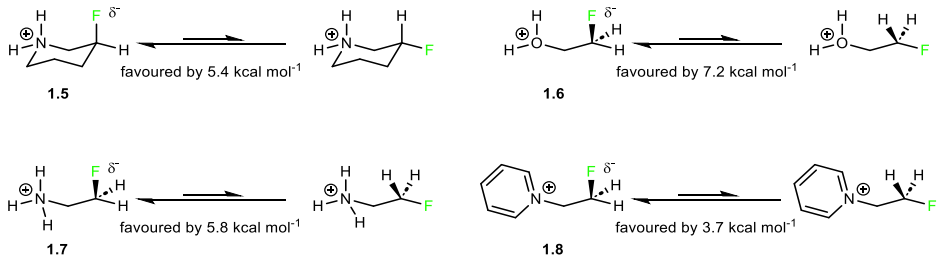

Figure 1.7: Examples of charge-dipole interactions with X^+-H and C-F bonds.[22]

Charge dipole interactions can be relatively strong when the C-F bond dipole interacts with a formal (positive) charge.[22] The result is an enhanced expression of the *gauche* effect. For example in the case of piperidiniums **1.5**-**1.8**, the C-F dipole lies *anti* parallel to the N^+-H dipole or to the O^+-H in the case of **1.6** (Figure 1.7) in the respective axial or *gauche* conformations only and there are electrostatic attractions between the co-aligned and polarised X^+-H and C-F bonds.

1.32 Organofluorines in pharmaceuticals

Lipophilicity is a key factor in drug design and particularly for the uptake and distribution of oral drugs. Lipinski's analysis states that this value should be less than Log P = 5, and for most drugs on the market it is about Log P = 3.[26,27] If the Log P is too low (e.g., 1), the drug may be excreted too quickly due to high hydrophilicity. Conversely, if too high (e.g., Log P > 5), the drug in highly lipophilic and will bind albumin or membranes, hindering its distribution and efficacy. C-F bonds tend to be metabolically inert[26,27] and

the introduction of fluorine can influence Log P, therefore it is increasingly used in tuning pharmaceutical products.

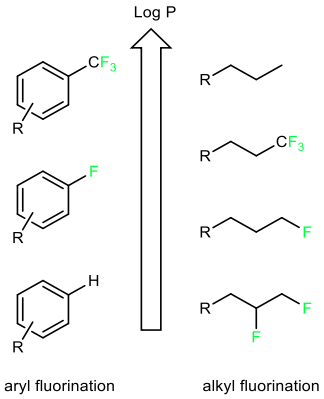

Figure 1.8: Opposite polarity trends of aryl and alkyl fluorination. More fluorines on aromatics increases lipophilicity. More fluorines on alkyl chains decreases lipophilicity.[28]

Aryl-F and aryl-CF_3 tend to increase lipophilicity[29] relative to aryl-H, however alkyl fluorination (e.g. -CH_3 to CH_2F) will decrease lipophilicity (increase in hydrophilicity). This effect is illustrated in Figure 1.8.[28] Thus, selective fluorination of prospective drug molecules has proven useful in controlling lipophilicity, either up or down, whilst preserving target-binding properties.

While fluorine is often introduced to control lipophilicity, its role in drug design can extend beyond this. Aromatic methyl groups, for instance, are rarely seen in pharmaceuticals due to their susceptibility to oxidation by metabolic enzymes such as cytochrome P450s. Replacing these methyl groups with a trifluoromethyl (CF_3) group blocks this metabolism, as fluorine's similar size to hydrogen ensures minimal steric disruption while its metabolic inertness prevents oxidation. Thus, fluorination is frequently employed not only to fine-tune lipophilicity but also to enhance metabolic stability, a critical factor in medicinal chemistry.

1.33 Organofluorines in anaesthetics

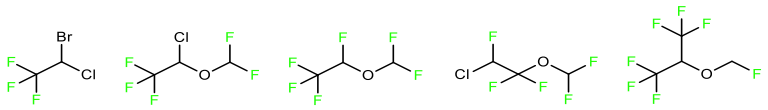

Figure 1.9: Most common inhalation anaesthetics used regularly in surgeries.[30]

Small molecule organofluorine molecules dominate the field of anaesthesiology. These inhalation gases are used regularly, often in conjunction with intravenous anaesthetics in preparation for surgery.[30] In the United States alone, there are over 20 million surgical operations using these forms of anaesthetics.[30] The inhalation anaesthetics illustrated in Figure 1.9 have three to seven C-F bonds, and some are chlorofluorocarbons, which remain in use despite the Montreal Protocol. Unfortunately, all of the current general anaesthetic agents have toxic side effects with no particular agent being most effective, however, these organofluorine inhalation anaesthetics are vastly superior to first-generation anaesthetics which were highly flammable or had a high toxicity profile. For example, diethyl ether, chloroethane, cyclopropane, and chloroform were used for over 100 years until halothane was developed as the first safe and effective inhalation anaesthetic in 1955.[30]

Halogenated gases, particularly chlorofluorocarbons, are however harmful to the ozone layer. The Montreal protocol of 1987 tried to address this issue by banning chlorofluorocarbons. Later, the 2016 Kigali amendment was put in place to phase out hydrofluorocarbons as well, as these had high global warming potential (GWP).[31] However, even though inhaled anaesthetics are hydrofluorocarbons and chlorofluorocarbons, their necessity in surgery exempts them from these protocols. Thus, these agents currently contribute to GWP three orders of magnitude greater than CO_2.[32] In fact one perfluorinated molecule, SF_6 used as a dielectric medium in the electoral industry as well as ultrasound imaging in the medical industry has a GWP 24,300 times that of CO_2.[33] In operating theatres, the use of anaesthetic gas scavenging systems (AGSS) are used to sequester halothanes from patients exhaled airflow, limiting the exposure of these anaesthetics to medical staff. These gases are then passed

through a scrubber, often charcoal or another absorbent, and are then released into the atmosphere from the hospital roof. It is estimated that over 2% of the carbon footprint of the National Health Service (NHS) results from the release of anaesthetic gases alone.[32]

Currently, microporous adsorption-based technologies are being explored for securing anaesthetic gases from AGSS systems thus preventing and limiting their exposure into the environment. The goal of this would be to separate halothanes in the exhaled air for recycling. Metal organic frameworks (MOFs) have been explored in this context, showing some promise.[34] On the basis that 'like attracts like' this thesis introduces JOF-MOFs as offering a possible role in this regard.

1.34 Organofluorines in liquid crystals

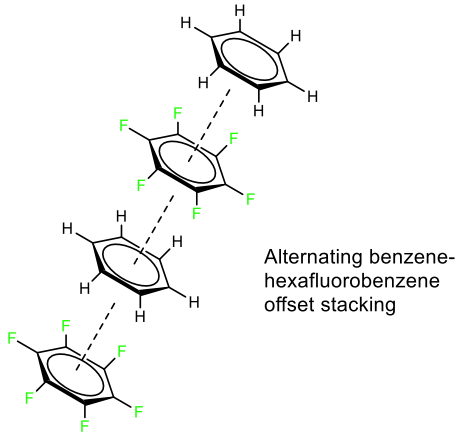

Figure 1.10: Stacking of hexafluorobenzene and benzene adapted from Clark et. al.[35]

In supramolecular chemistry, organofluorines can play a variety of roles. For example, in the early 1960's Patrick and Prosser reported the mixing of benzene and hexafluorobenzene, which are both liquids, to generate a solid with a melting point of 24 °C.[36] At the molecular level this solid was found to arise from the stacking of alternating aryl- and hexafluoro aryl-rings. This alternate stacking arose from complementary electrostatic profiles of the two ring systems.[35] Benzene has an electronegative core and surrounding hydrogens are electropositive, whereas

hexafluorobenzene has an electropositive core with surrounding electronegative fluorine atoms, as illustrated in Figure 1.10.

Fluorine can play multiple roles in noncovalent interactions for supramolecular assembly. The modern IUPAC definition of the hydrogen bond states: "*The hydrogen bond is an attractive interaction between a hydrogen atom from a molecule or a molecular fragment H-X in which X is more electronegative than H and an atom or group of atoms in the same or a different molecule, in which there is evidence of bond formation.*"[37,38] This definition is far more inclusive than the original definitions of hydrogen bonds, such as those from Pauling. This modern definition incorporates the C-H···F-C noncovalent interaction as a weak hydrogen bond. The existence of noncovalent interactions involving fluorine has been widely discussed[37] however such interactions do appear to play a role particularly only when there are no competing hydrogen bonding options.[37,39] The C-H···F-C hydrogen bond interaction has a length range from ~2.2 Å to ~2.7 Å.[37,40] and can be compared with that of more classical hydrogen bonds to N or O, which fall into the range of 1.5 to 2.5 Å.[41]

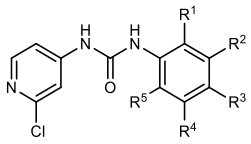

1:R^{1-5}= H
2:R^1= F; R^{2-5}= H
3:R^1= H; R^2= F; R^{3-5}= H
4:R^{1-2}= F; R^{3-5}= H
5:R^{1-4}= F; R^5= H
6:R^1=R^2=R^3=R^5= H; R^4= F
7:R^1=R^2=R^5= H; R^{3-4}= F
8:R^1=R^5= F; R^{2-4}= H

Figure 1.11: Fluoroaryl-phenylureas with differing fluorination patterns, adapted from Abad *et al*.[42]

A case study looked at a series of fluoroaryl-phenylureas as illustrated in Figure 1.11. The study highlighted that crystal packing resulted from short and highly directional C-H···F-C hydrogen bond interactions in the solid state.[37,42] The influence of the fluorine substitution on the crystal packing was attributed to C-F polarity as well as an increase in C-H acidity due to neighbouring fluorine atoms.[37]

A particular branch of supramolecular chemistry of contemporary interest is the generation and development of organic liquid crystals (OLCs). These are utilized in active-matrix display devices.[43] Organofluorines are essential to the development of

commercially successful liquid crystal displays due to the capacity of fluorine substitutions to generate liquid crystals with significantly modified melting points, mesophase morphologies, transition temperatures and optical, dielectric, and viscoelastic properties.[39] Organic liquid crystals order in the fluid phase.[44] They are anisotropic fluids, with a unique combination of flow and molecular ordering, that confers optical, dielectric, and viscoelastic properties. Whilst some of these properties are easily understood, such as melting point, others are more complex. For example, a mesophase is simply a chemical compound that is not a liquid or a solid. The compounds in a mesophase have mechanical properties and symmetry properties that are intermediate between those of a liquid and a single crystal.

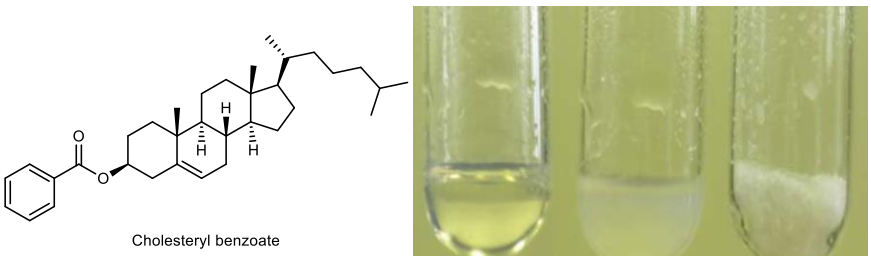

Figure 1.12: Left: first observed liquid crystal, cholesteryl benzoate. Right: image of the liquid, liquid crystal, and crystalline phase of cholesteryl benzoate.[45]

The first liquid crystal was observed in 1888, by the Austrian chemist Friedrich Reinitze[46] who recognised that cholesteryl benzoate (Figure 1.12) had two melting points. At 146 °C the solid melted into a cloudy liquid and at 179 °C it melted again. The liquid became transparent, and purification did not change the observed behaviour.[46] Unable to explain this phenomenon of double melting, Reinitze acquired the help of German physicist Otto Lehmann, an expert in crystal optics. Lehmann deduced that the intermediate cloudy fluid had a unique kind of order, whilst the transparent liquid had the disordered state of all common liquids. This ordered liquid phase was termed a "liquid crystal", as it shared important properties of both states.[47] There are two general types of liquid crystals: lyotropic and thermotropic. If a substance dissolves in water or another solvent and forms the liquid-crystal phase it is a lyotropic liquid crystal.[48] These molecules are usually amphiphilic. A good example is a fatty acid salt such as sodium heptadecanoate shown below (Figure 1.13).[48]

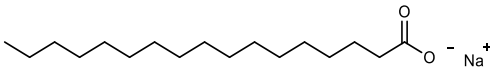

Figure 1.13: Sodium heptadecanoate

Thermotropic liquid crystals possess transition phases determined by temperature. The three general phase transitions are solid or crystalline, liquid crystal, and isotropic liquid.[48] The solid-liquid transition temperature is the melting temperature (T_m) and the liquid crystal-isotropic liquid transition is the elucidation temperature (T_e). Based on the molecular arrangement, liquid crystals are classified into three main types: smectic, nematic and cholesteric.[48] Each type exhibits unique organizational structures and properties.

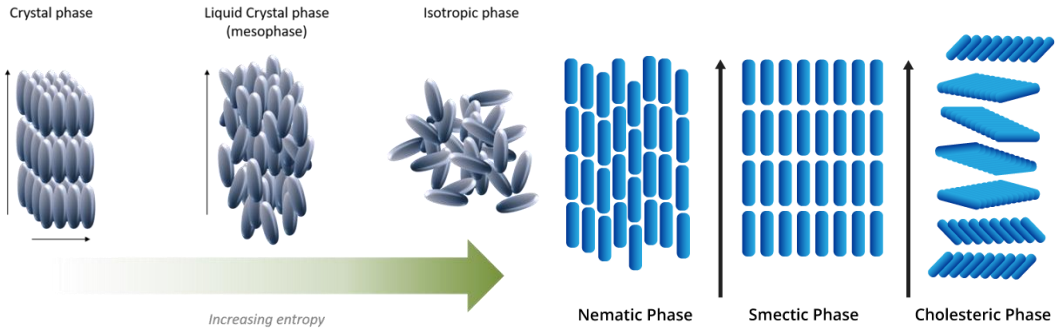

Figure 1.14: Left: Specific liquid crystal phases. Right: Simplified phases of liquid crystals based on increasing entropy.[49]

The smectic phase has the highest level of order, as the molecules possess orientational order and partial positional order (Figure 1.14). There are multiple smectic phases all characterized by different types and degrees of positional and orientational order. One of these is a discotic columnar phase, in which completely isolated systems will stack one on top of another in perfect columns. The nematic phase is the least ordered and possesses no positional order but has orientational order, hence it is the most fluid and least viscous phase.[48] The nematic phase is found in the vast majority of liquid crystal display formats and technologies. Cholesteric liquid crystals are formed from chiral molecules extending from the original cholesterol benzoate observation back in 1888.[46,47] These types of liquid crystals are rarer, and molecules are ordered into layers

and within each layer they are ordered in the same direction. Molecules in each layer are rotated by a defined angle relative to the adjacent layers resulting in a helical assembly.

Liquid-crystalline phases are generally identified using polarising optical microscopy (POM) in conjugation with differential scanning calorimetry (DSC). The most common type of thermotropic liquid crystals are calamitic LCs.[50] These LCs possess long rod-like structure with a high length to breath ratio, the presence of rings provides the backbone of the LC and also affects its properties. Often two rings, ether aromatic or aliphatic, are needed to generate the liquid crystal phase. A generalization of this type of LC is shown below (Figure 1.15).

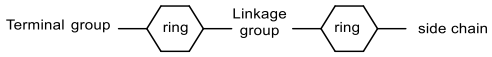

Figure 1.15: The template for calamitic liquid crystals.

Typical ring structures are 1,4-disubstituted aryl rings, *trans* 1,4-disubstituted cyclohexanes, 2,6-disubstituted naphthalenes and so on. The central linkage controls the chemical stability of the liquid crystal, i.e. their resistance to moisture or ultraviolet radiation. The side chain is usually a linearised aliphatic chain since it can strongly influence the viscosity and transition temperate of the LC phases. A very common length is the propyl chain. The terminal group is mostly used to determine the dielectric constant and its anisotropy.

Liquid crystals display birefringence, meaning they possess two distinct principal refractive indices, referred to as n_e and n_o. This property causes them to refract light in two different directions, leading to unique optical effects. The ordinary refractive index (n_o) is for light that is polarized perpendicular to the optical axis of the crystal. The extraordinary refractive index (n_e) is for light that is polarized parallel to the optical axis of the crystal. Unlike the ordinary refractive index (n_o), the extraordinary refractive index varies depending on the angle between the light propagation direction and the optical axis. This variation leads to the phenomenon known as birefringence, where a

crystal exhibits two distinct refractive indices as stated previously. The birefringence is given by the equation:

$$\Delta n = n_e - n_o$$

If $n_e > n_o$, the liquid is said to have a positive birefringence, if $n_e < n_o$, then it is negative. Most liquid crystals possess a positive birefringence ranging from 0.05-0.45.[50] Aryl rings have greater polarizability, therefore materials containing them have higher Δn values than materials containing saturated alicyclic rings.

Typical liquid crystals are uniaxial; therefore, they will have different dielectric constants when an external electric field is applied. The dielectric anisotropy is defined by the equation:

$$\Delta\varepsilon = \varepsilon_{//} - \varepsilon_{\perp}$$

The dielectric constant is termed $\varepsilon_{//}$ when the external electric field is applied parallel to the long axis of the liquid crystal. The dielectric constant is termed $\varepsilon_{\perp}$ when the external electric field is applied perpendicular to the long axis of the liquid crystal. Thus, liquid crystals can be divided into two types: positive and negative dielectric anisotropy liquid crystals.[51] Classic examples of these two types of LCs are illustrated below (Figure 1.16).

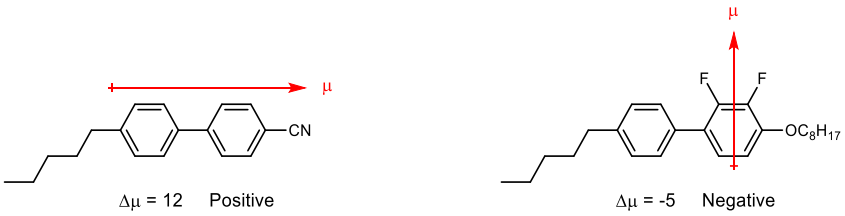

Figure 1.16: Positive and negative dielectric anisotropy liquid crystals.

Due to the development of vertical alignment (VA) liquid crystal display (LCD) technology as well as twisted nematic (TN) display technology that utilize molecules with a dipole perpendicular to the main axis of the molecule, negative dielectric anisotropic LCs have become attractive for use in these visual displays.[51–53] These displays are common in car instrument dashboards, car control indicators, healthcare devices and or elevator displays as they give access to touch-sensitive LCDs.[53]

1.4 The history of Janus compounds

The conformation of alkyl chains possessing multiple vicinal fluorine substituents is dominated by the repulsion between 1,3 fluorine atoms.[54] In this case *gauche* effects play a lesser role over electrostatic repulsions. The influence of 1,3-diploar repulsion was illustrated in the solution (NMR) and solid state (X-ray) conformations of the two stereoisomers of the hexafluoro-vicinally substituted alkanes **1.10** and **1.11** prepared in St Andrews (Figure 1.17).[55,56] The all *syn*-isomer **1.10** adopts a helix conformation which avoids parallel alignment of 1,3-C-F bonds, however isomer **1.11** with the two central fluorines 'back' adopts a linear *anti*-zig-zag conformation as there are no 1,3-dipolar repulsions in that case.[55,56]

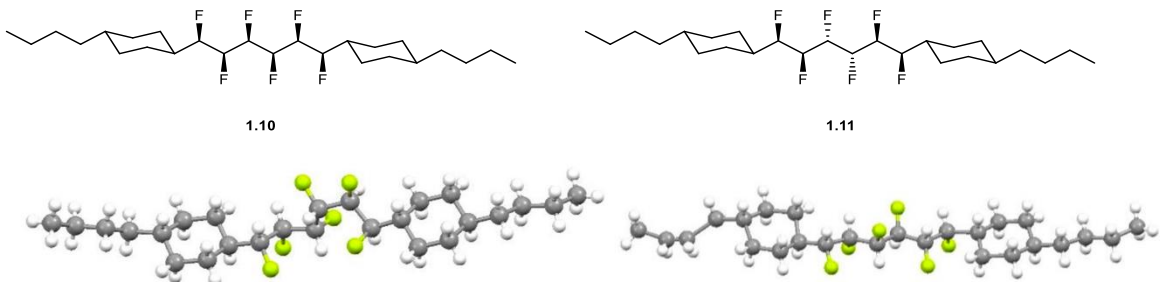

Figure 1.17: Two stereoisomers of all-*cis* **1.10** and anti **1.67** hexafluoroalkane and their crystal structures taken from Clark.[54–56]

Such acyclic multi-vicinal fluorinated alkyl chains can easily rotate and adopt conformations which minimize their net molecular dipole. However, cyclic systems have limited conformational flexibility and the appropriate stereoselective syntheses will access much more stable conformations displaying large dipole moments, particularly if C-F bonds can be made to align.[54] 1,2,3,4-All-*cis*-tetrafluorocyclohexane (**1.12**) was the first fluorinated cyclohexane synthesised in St Andrews (Scheme 1.1) that possessed a large molecular dipole. This compound has two iso-energetic conformers where both have two 1,3-diaxial C-F bonds and this gives the molecule a large molecular dipole moment (μ = 4.91 D).[54,57,58] This facial polarization was later coined a 'Janus' ring, after the two-faced ancient Roman deity.[58]

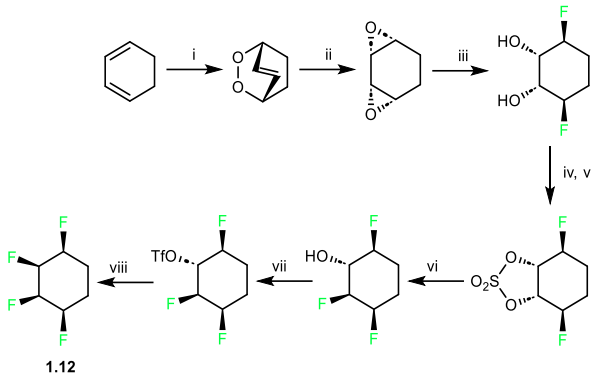

Scheme 1.1: Synthesis of all-*cis*-1,2,3,4-tetrafluorocyclohexane **1.12**; i: $(PhO)_3P$, O_3, CH_2Cl_2, cyclohexa-1,4-diene, -78 °C to -25 °C; ii: $Ru(PPh_3)_3Cl_2$, CH_2Cl_2, 0 °C to r.t., 46% over two steps; iii: $Et_3N.3HF$, 90 °C; iv: thionyl chloride, pyridine, CH_2Cl_2, 0 °C; v: $NaIO_4$, $RuCl_3.xH_2O$, MeCN, H_2O, 35% over three steps; vi: $Et_3N.3HF$, 120 °C, 70%; vii: Tf_2O, pyridine, r.t.; viii: $Et_3N.3HF$, 120 °C, 35% over two steps.[54,57]

An even greater dipole (μ = 5.25 D) was calculated for all-*cis*-1,2,4,5-tetrafluorocyclohexane **1.13**.[59] This cyclohexane was prepared by a shorter route which could be accomplished in only two-steps (Scheme 1.2).

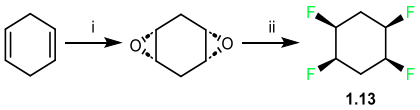

Scheme 1.2: Synthesis of all-*cis*-1,2,4,5-tetrafluorocyclohexane **1.13**; i: mCPBA, CH_2Cl_2, -15 °C to -10 °C, 52%; ii: DAST, 70 °C, 24%. Overall yield of 12%.[59]

Cyclohexane **1.13**, with six all-*cis* fluorine atoms on one face and correspondingly six all-*cis* hydrogen atoms on the other, is shown Scheme 1.3. This became a focus for synthesis as it should have a maximum polarity for a fluorinated 'Janus' ring.

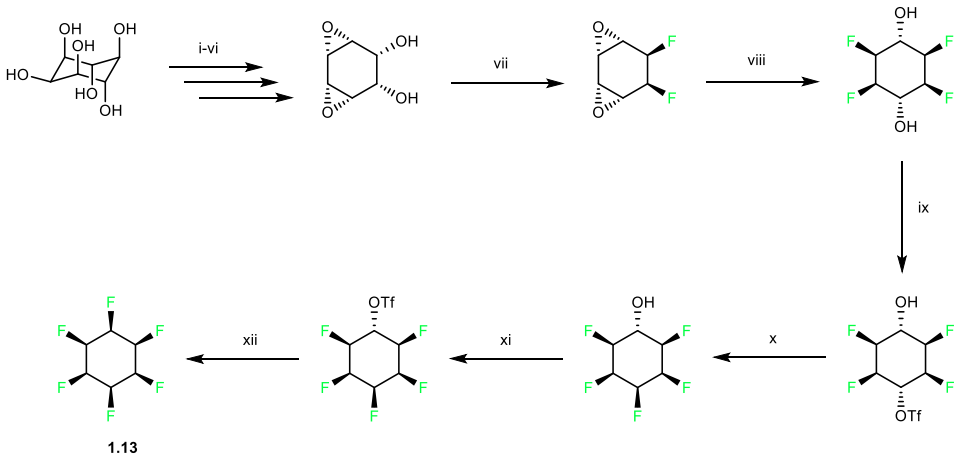

Scheme 1.3: Initial synthesis of all-*cis*-hexafluorocyclohexane **1.13**. i: $HC(OEt)_3$, pTSA, DMF, 5 days, 100 °C, 69%; ii: NaH, BzCl, DMF, 30 min, 55%; iii: TsCl, pyridine, 18 h, 97%; iv: $^{i}BuNH_2$, MeOH, reflux, 4 h, 84%; v: HCl, MeOH, reflux, 4h, 89%; vi: NaOMe, MeOH, $CHCl_3$, 18 h, 85%; vii: Deoxofluor, THF, 60-100 °C, 15 min, MW, 94%; viii: $Et_3N.3HF$, 180 °C, 120 min, MW, 71%; ix:Tf_2O, pyridine, CH_2Cl_2, 88%; x: $Et_3N.3HF$, 120 °C, 2h, MW, 40%; xi: Tf_2O, pyridine, CH_2Cl_2, 71%; xii: $Et_3N.3HF$, 180 °C, 2h, MW, ~10%.[60]

Cyclohexane **1.13** was first synthesised in St Andrews by Dr. Neil Keddie in 2015.[60] This ring system differs from aryl rings which possess negatively charged faces with positively charged rims. As stated, in linear alkanes possessing vicinal fluorines, the C-F bonds tend to orientate away from each other, minimizing the overall molecular dipole. However, in **1.13** the 1,3-alignments of three C-F bonds result in a highly polar cyclohexane. Once the synthesis was accomplished, properties were explored. Cyclohexane **1.13** has a decomposition rather than melting point of 208 °C which is extraordinarily high for a low molecular weight aliphatic compound. This compound is considered to be the most polar aliphatic compound known, with a dipole moment of 6.2D.[60]

1.41 The Zeng cyclic (amino)(alkyl)carbene rhodium catalyst

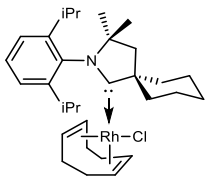

Zeng Catalyst **1.14**

Figure 1.18: Catalyst **1.14**, Zeng catalyst for the stereoselective hydrogenation of fluorobenzene derivatives into Janus-faced fluorocyclohexanes.[61,62]

The original synthesis of **1.13** proved challenging, taking 12 steps, and allowing only a few milligrams of material to be prepared. A Rh CAAC catalyst (Figure 1.18) had been developed by the Zeng group in 2015 for aryl hydrogenations,[61] and this was successfully applied to hexafluorobenzene by Glorius in 2017.[62] With this development, a variety of Janus-faced cyclohexanes became more readily accessible. The Zeng catalyst (**1.14**) was originally developed for the selective hydrogenation of functionalised aromatic ketones and phenols. Cyclic (amino) (alkyl)carbenes (CAACs) have an enhanced nucleophilicity compared to sigma-donating N-heterocyclic carbenes (NHCs). The cyclic (amino) (alkyl)carbene (CAAC) ligand is electron rich and has a strong sigma-donation to the metal centre which enhances the interaction of the metal through aryl back-donation of electron density.[61] The Glorius group used their experience with stereoselective(hetero)arene hydrogenation using Ru-N-heterocyclic carbene (NHC) complexes to develop a pathway to these Janus-faced compounds. They envisioned a catalytic hydrogenation of inexpensive and widely available fluoroarenes since their previous hydrogenations of arenes were highly *cis*-selective.[62] However, when attempting reactions with their NHC catalysts, the results were impeded by competing hydro-defluorination. This competing hydro-defluorination (HDF) reaction takes place via oxidative addition or through nucleophilic aromatic substitution (S_NAr) at the halide. A summary of these undesirable reactions is illustrated in Scheme 1.4.[62]

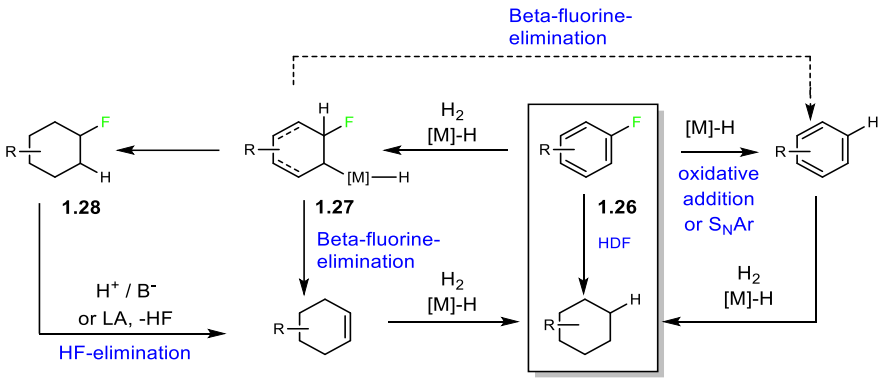

Scheme 1.4: Pathways for competing hydrodefluorination side reactions.

To mitigate the undesirable hydro-defluorination pathway, it was found that performing the reaction in nonpolar solvents greatly reduced this side reaction,[63] as the

defluorination mechanism proceeds via polar intermediates. Additionally, as the solubility of hydrogen gas is higher in nonpolar solvents, the rate of the hydrogenation could be increased.[63] Nonpolar solvents such as *n*-hexane are optimal, and for all total hydrogenations performed in this thesis dry *n*-hexane was used as the solvent.

The Glorius group then decided to use **1.14** resulting in a substantial decrease in the hydro-defluorination pathway and the resulting Janus-faced cyclohexane **1.13** in very good yield (88%). This 2017 paper considerably opened up access to new Janus cyclohexane variants.

The mechanism of the all *cis*-selective hydrogenation was initially thought to be homogeneous. However, a recent paper by Bullock *et al.,* indicates that the process is heterogeneous.[64,65] Bullock identified rhodium nanoparticles (NP) as the active catalyst.[66] The silver salt $AgBF_4$, was used to activate the pre-catalyst in solution (homogeneous) via a cationic pathway rather than supporting the catalyst on molecular sieves or silica gel (heterogeneous).[66] The silver salt did not support aryl hydrogenation of hexafluorobenzene.[66] The need to stabilize the catalyst with either molecular sieves or silica gel, alongside the formation of a dark precipitate after the reaction and the observed induction period all pointed to a heterogenous reaction. Sub-stoichiometric poisoning with tetrahydrothiophene showed loss of catalytic activity, indicative of a heterogeneous process as the reactive sites are buried inside nano particles, requiring less than one equivalent for complete poisoning of reactivity.[66] They also tested the catalyst through filtration, recycling, kinetics as well as spectroscopy and microscopy.[66] These approaches all pointed towards a heterogenous process.

The necessity of silica gel and/or molecular sieves is consistent with the formation of nanoparticles. This, coupled with the observation that increased loadings of silica gel resulted in decreased defluorination and in better yields of the Janus-faced cyclohexanes. The most reactive catalytic species, the smaller nanoparticles, were more abundant after 3 h than after 24 h reaction time.[66] This indicates fresh preparation of small reactive particles, which in turn, explains the high reproducibility of the catalytic

system compared with some commercial heterogenous catalysts possessing varying particle size distribution.[66] This is likely due to commercial heterogenous catalysts possessing varying particle size distributions. The high chemo-selectivity of the catalyst is attributed to the CAAC ligand. X-ray photoelectron spectroscopy (XPS) of the active catalyst had two nitrogen signals in a 1:1 ratio.[66] These signals, along with that obtained from the rhodium itself, were of low intensity due to the sparce dispersion within the silica. However, the two nitrogen signals implied that the CAAC ligand must undergo some type of transformation during reaction. After further study of these complexes though ^{13}C NMR, as well as solid state NMR spectroscopy, the signals were determined to be the CAAC-derived pyrrolidinium and pyrrolidine and they were found to act as key modifiers for controlling the chemo-selectivity of the hydrogenation of these fluorinated aromatics resulting in the all-*cis* products.[66] The preparation and image of the active NP catalyst is illustrated in Scheme 1.5.

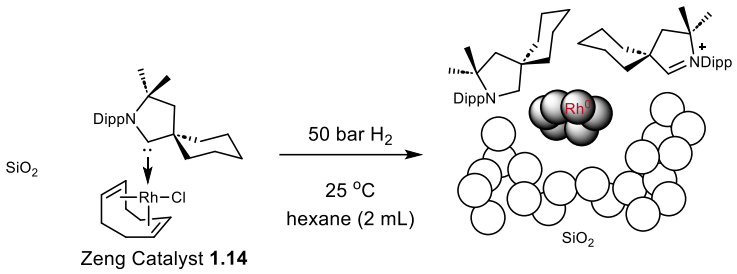

Scheme 1.5: Preparation of silica-supported NPs including different loadings of catalyst and silica gel.[60,62]

1.42 Novel Janus-faced compounds

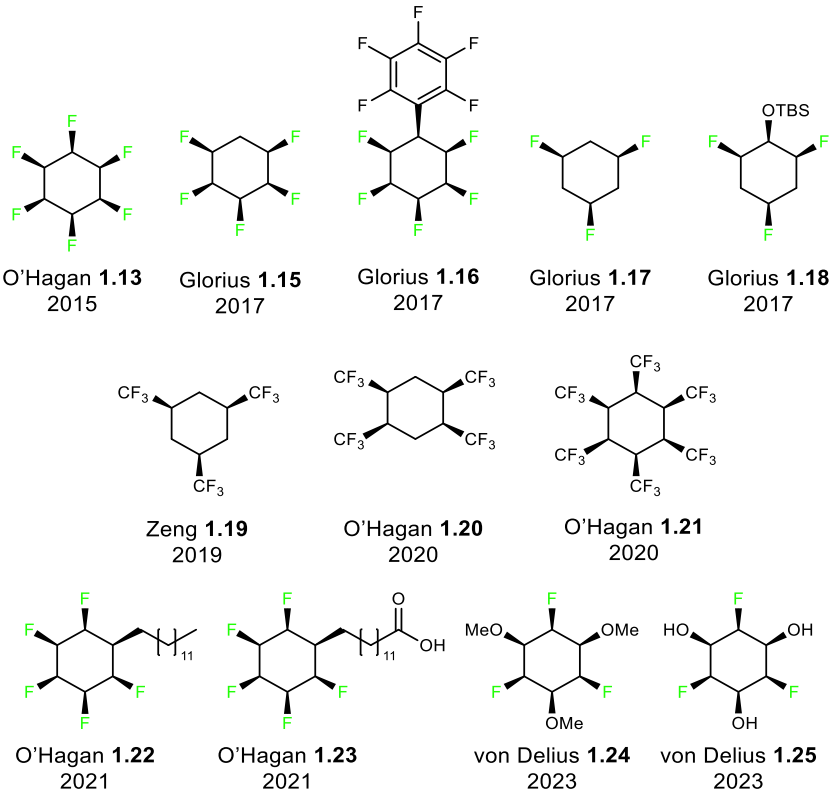

Figure 1.19: List of some relevant Janus compounds.[35,40,62,67,68]

There are recent examples of the synthesis of Janus fluorocyclohexanes from a variety of groups and with a variety of purposes as shown in Figure 1.19. These Janus cyclohexanes have been synthesized with different applications in mind. For instance, compound **1.22** was used to show the supramolecular interactions of the Janus rings with a long chain alkyl group spacer. This improved the supramolecular array in terms of order, but it did not isolate the Janus rings themselves.

Due to the polarity between the faces of the Janus rings, these systems should stack in supramolecular assemblies. Theory studies predict the large and cooperative enhancement of the dipole moment during aggregation in one-dimensional stacks through F···H electrostatic attraction.[69,70] If the crystal structures of these Janus compounds have H and F interaction lengths between 2.2 Å to 2.5 Å, then the interaction is clear. It has been found that the packing of the system increases as more Janus rings are present. Thus, trimers should have an increased interaction energy

compared to dimer or monomers - and this trend can be applied to much larger systems,[71] suggesting a significant force for supramolecular assembly.

1.43 The supramolecular Janus motif

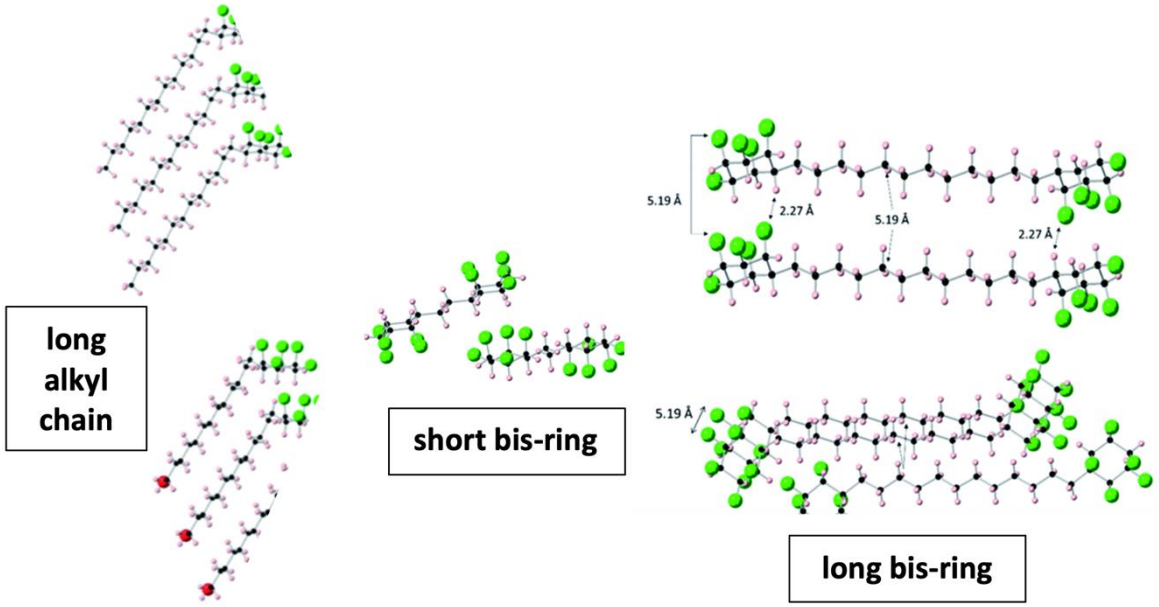

Figure 1.20: Supramolecular packing of alkyl substituted Janus cyclohexanes from crystal structures.[35]

The electropositive and electronegative faces of the cyclohexanes have a strong tendency to associate with one another through intermolecular interactions. Computational calculations suggests the interaction energy between two isolated rings for **1.13** is ~-8.2 kcal mol^{-1} (4.1 kcal mol^{-1} per ring) which is stronger than a good hydrogen bond.[70] The association energy between Janus rings is also larger than that for hexafluorobenzene and benzene (-5.38 kcal mol^{-1}).[72,73] There is an energy gain of ~20 kcal mol^{-1} for stacking trimers of **1.13** (-6.3 kcal mol^{-1} per ring), and this is even increased to ~30 kcal mol^{-1} for a tetramer (-7.7 kcal mol^{-1}).[74] These trends suggest that the binding energy of self-association of the Janus rings will accommodate aggregation and polymerisation to promote supramolecular assembly. This was a key inspiration when developing this thesis. There is an increasing trend to the overall polarity observed. From monomer to aggregated polymers, the polarity of all-*cis*-hexafluorocyclohexane (**1.13**) increased from 6.2 D (monomer) to 9.4 D (crystal asymmetric unit).[70,75] The 'asymmetric unit' is the smallest portion of a crystal structure

to which a symmetry operation can be applied to generate the complete unit cell.[70,75] The overall polarizability of a 1 D crystal of **1.13** resulted in a large macroscopic polarization, which Datta suggests could be designed for the use of novel nonlinear optical materials.[70,75]

The crystal structure of a number of long and short alkyl chain substituted Janus cyclohexanes, as well as some *bis*-ring systems have been solved by Clarke *et al.*[35] structures of which are shown above in Figure 1.20. The substituted alkyl chains were always found to lie equatorial to the cyclohexane ring whilst the three C-F bonds always sit axial. This conformation maintains the high net dipole moment, and the polar arrangement is supported by the strong intermolecular associations between the Janus rings as well as minimising steric repulsions by forcing the alkyl groups equatorial.

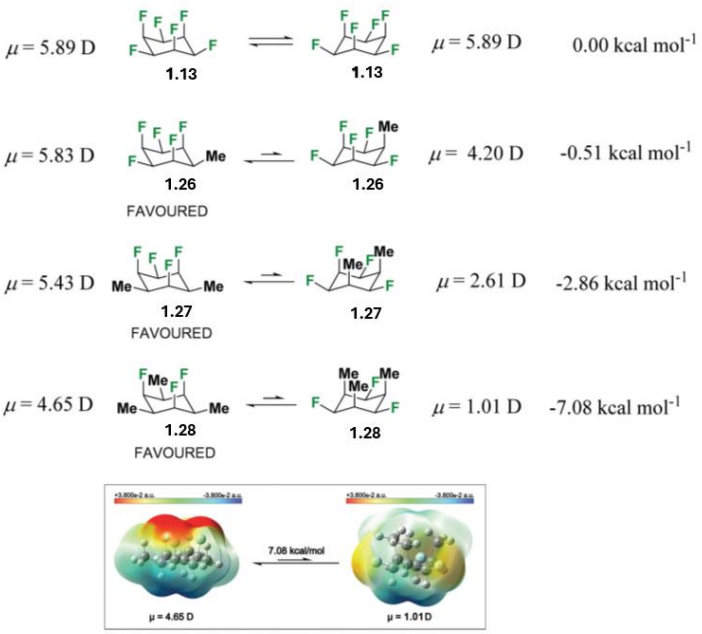

Figure 1.21: Structures optimized at the B3LYPD3/def2-TZVP theory level, with calculated free energy differences and dipole moments between the chair conformations of increasingly alkylated rings. Bottom image indicates a surface electrostatic potential map for the conformers of the all-*cis* 1,3,5-trialkyl2,4,6-trifluorocyclohexane.[76]

Figure 1.21 shows how adding alkyl groups to the 1, 3 and 5 positions of the cyclohexane increasingly favours conformations where the C-F bonds go axial. This is reasonably due to the steric influence of the alky groups relative to fluorine which favours an equatorial orientation.

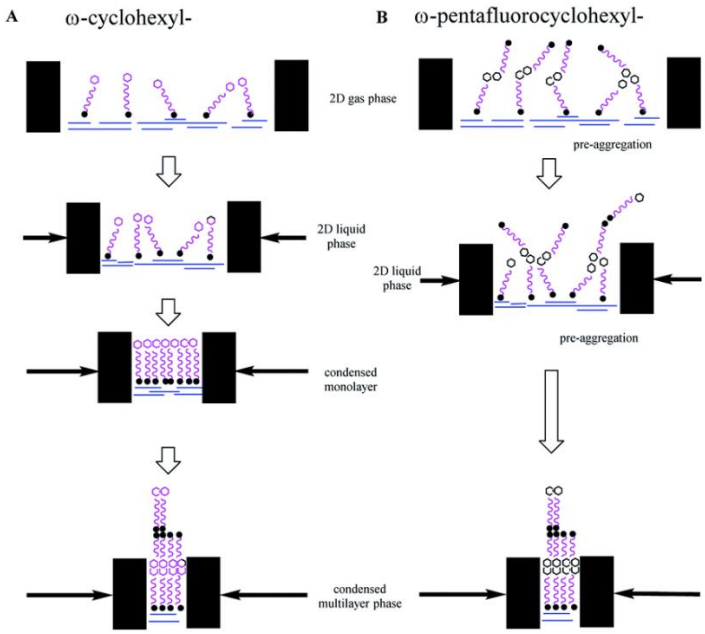

Figure 1.22: Langmuir isotherm behaviour of the ω-cyclohexyl and ω-pentafluorocyclohexyl fatty acids on a water subphase. Image taken from O'Hagan.[35]

The behaviours of Janus cyclohexane terminated fatty acids on a water subphase have been explored by the Guldin and O'Hagan labs in 2021 via Langmuir trough experiments. Langmuir pressure-area isotherm analysis (Figure 1.22) of deposited fatty acids suggested that the Janus cyclohexane motif results in a pre-aggregation and generated bilayers prior to barrier compression.[35,74] This behaviour is not found in a cyclohexyl fatty acid control which forms very coherent monolayers, just like stearic acid, when compressed on a water subphase.[35]

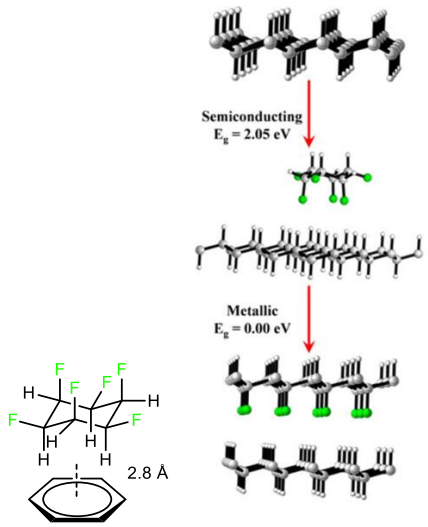

Figure 1.23: All-*cis*-hexafluorocyclohexane (**1.13**) – π interactions with benzene (left) and graphane (right).[75]

The hydrogen face of Janus cyclohexane **1.13** displays a moderate interaction with aromatic rings (Figure 1.23). The interaction energy of one molecule (**1.13**) with benzene was calculated at between -7.9 kcal mol^{-1} and -6.4 kcal mol^{-1} depending on the level of theory used, and with a calculated C-H···π distance of 2.8 Å.[77] **1.13** can pack between graphene and graphane sheets in a sandwich structure at the supramolecular level. **1.13** does this through noncovalent interactions, caused by the enhanced polarity of the axial C-H and C-F bonds, resulting in the formation of a 'triple decker' structure.[77] The interaction with hydro-fluorinated graphene is predicted to present semi-conductivity with a band gap of ~3.0 eV, with associations through a strong C-H···F-C interlayer with graphene to form a stable metallic bilayer.[75]

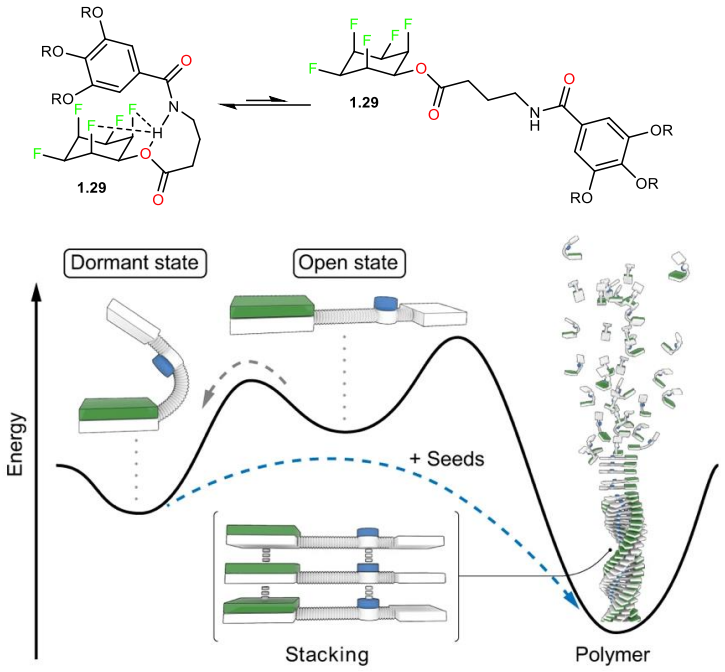

Figure 1.24: Living covalent polymerisation (LPS): Structures and illustration of the partial energy profile with a Janus monomer. Figure was taken and adapted from Shyshov, Haridas, Pesce et al al.[78]

Organic materials science has placed a keen focus on the development of powerful methods for living covalent polymerisation.[78] A supramolecular block co-polymer was prepared by linking the pentafluoro Janus motif to gallic acid to generate monomer **1.29**.[78] The monomer in its dormant state forms intramolecular hydrogen bonding, dipole-dipole, and C-H···π interactions. Living supramolecular polymerisation (LSP) is enabled by intermolecular interaction, interactions which are under kinetic control, for the self-assembly of nanofibers.[78] This illustration in Figure 1.24 shows the folding of a monomer into a dormant state, which inhibits spontaneous aggregation. Seeds can initiate LSP. Depending on the position of the equilibrium, the fibres adjust in length and morphology. This is one of the first examples of supramolecular block copolymers synthesized from kinetically trapped monomers rather than off-pathway aggregation.[74] Monomer **1.29** offers a simple and novel facially polarized building block as an alternative to extended π systems or crosslinks through metal centres.[74,78]

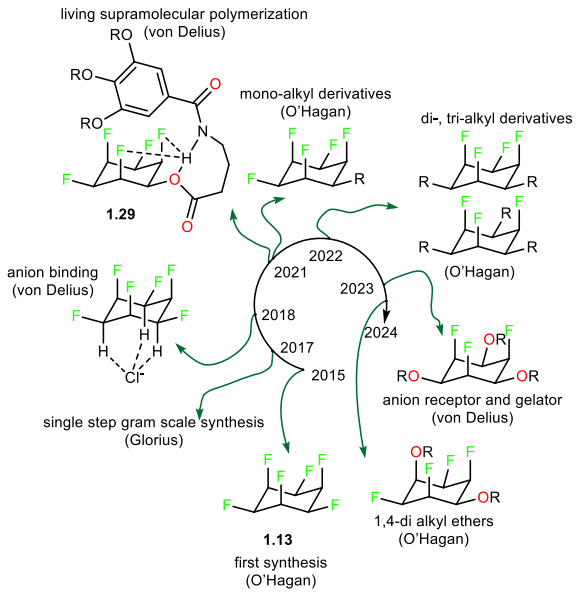

Figure 1.25: Timeline indicating the development of Janus cyclohexanes.[60,62,68,69,76,78]

A recent paper by von Delius demonstrated another Janus cyclohexane for supramolecular assembly (Figure 1.25). Alternating fluorine and 1,3,5-tri-ether systems **1.30** and **1.31** were utilized in a proof-of-principle study as simple gelators, and as tripodal receptors for chloride ion.[68] The binding affinity was also enhanced by hydrogen / halogen bonding with triazole / iodotriazole side arms in **1.31** (Figure 1.26).[68]

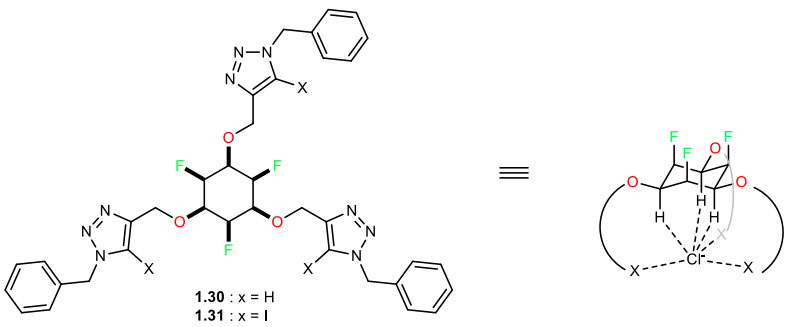

	K_a (M^{-1})	Solvent
1.30	~29	CH_2Cl_2
1.31	~140	CH_2Cl_2

Figure 1.26: Visual representation of **1.30** and **1.31** coordination with chloride ions with association energies.[68]

1.5 Aim

This thesis embarked on a journey to deepen our knowledge of organo-fluorine compounds through the lens of the Janus cyclohexane motif. The primary aim of the work focussed on developing novel Janus molecules tailored for supramolecular assembly. The work explores four aspects, the findings of which are detailed in Chapters 2 - 5. Chapter 2 focuses on developing all-*cis* 1,3,5-trialkylated tri-fluorinated Janus cyclohexanes as discotic columnar materials. Chapter 3 describes research into building blocks as potential struts for JOF-MOFs. Chapter 4 explores the synthesis and properties of Janus cyclohexanes but assembled as 3,6-dialkyl ethers. Finally, Chapter 5 investigates nucleophilic aromatic substitution on pentafluoroaryl ethers and as a methodology for the synthesis of the 3,6-dialkyl ether Janus cyclohexanes discussed in Chapter 4.

2: Janus cyclohexanes for organic liquid crystals

2.1 Liquid Crystal Displays

The development of vertical alignment (VA) and twisted nematic (TN) liquid crystal display (LCD) technologies has stimulated the use of negative dielectric anisotropic LCs in visual displays.[51–53] Such displays are typically found in car dashboards,[79] healthcare devices,[80] and elevators,[81] as they give access to touch-sensitive LCDs.[53]

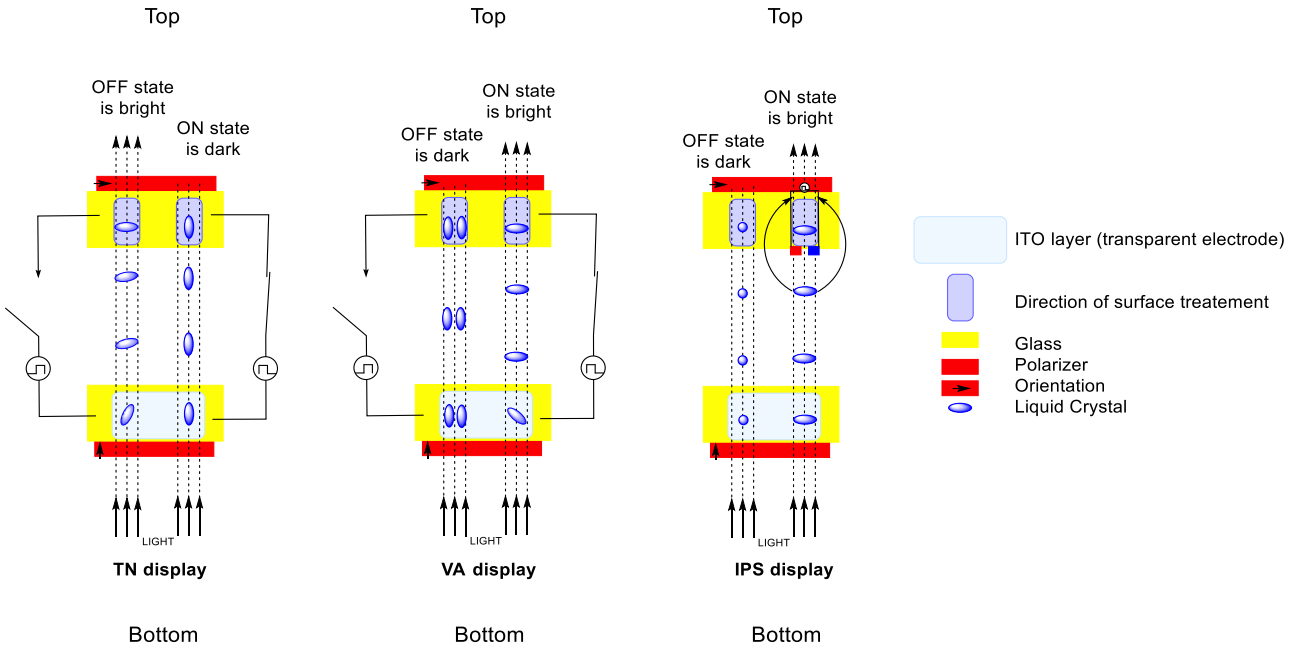

Figure 2.1: Liquid crystal display diagram. Left: Twisted Nematic (TN) display technology. Centre: Vertical Alignment (VA) display technology. Right: In Plane Switching (IPS) display.

TN, VA, and in-plane switching (IPS) display technologies, represented above in Figure 2.1, each have the direction of the surface treatment at the top and bottom of the device oriented at 90° to each other. This means that the two surfaces are oriented in a cross- or T-shape, preventing light passing through. In Twisted Nematic (TN) displays, liquid crystal molecules “twist” 90° between two glass layers. Without an applied voltage, polarized light traverses these twisted crystals, which align with the top polarizer to produce a bright display, known as the 'normal white mode’. Applying a voltage across the display causes the crystals to align parallel to the electric field, blocking the light at the top polarizer, and resulting in a dark or 'black mode' display (Figure 2.1 – left).

In Vertical Alignment (VA) displays, liquid crystal molecules start fully aligned with the bottom polarizer, allowing light to pass initially without any change in polarization but it is eventually blocked by the top polarizer, resulting in a 'black mode' with no applied voltage. Upon applying a voltage the LC molecules re-orient perpendicular to the electric field, due to their negative dielectric anisotropy, thus orientating with the top polarizer and permitting light to pass through, resulting in the 'normal white mode' (Figure 2.1 – centre).

Vertical Alignment displays offer several benefits when compared to traditional TN displays.[82] VA displays achieve nearly complete light blockage, with only 1% leakage compared to 5%, with TN's, enabling higher contrast ratios. Furthermore, VA panels can have faster response times as the liquid crystal (LC) molecules switch directly between vertical and horizontal alignments. In VA displays, LC molecules align either vertically or horizontally, enhancing the viewing angle beyond that which TN displays offer (where the LC molecules are not perfectly perpendicular). These advantages have made VA display technology a popular choice for PC monitors,[83] laptops, TV screens,[84] and projectors,[85] driving demand for liquid crystals with negative dielectric anisotropy.[82]

A third type of LCD, known as in-plane switching (IPS) visual displays, are significantly brighter and have more colour accuracy and coverage.[86] However IPS systems cannot compete with VA displays as VA displays have less backlight bleeding with wider viewing angels. IPS displays work in a similar manner to VA displays; however, they align their liquid crystals horizontally between the two glass surfaces (possessing positive dielectric anisotropy), shown in Figure 2.1 - right. They run perpendicular to the glass surface rather than parallel to it, and when a voltage is applied, the crystals tilt letting light through and producing colour (Figure 2.1). IPS and VA displays are currently the most popular used in LCD technology, with both having distinct advantages depending on their application.[87,88] For instance for larger brighter displays, such as those in airport departure boards, an IPS display performs better. But for a laptop screen trying to produce the best contrast in colours and displaying a range of images, VA displays often prove superior. The critical component in these diverse visual displays are the liquid

crystals that comprise them. These molecules exhibit negative dielectric anisotropy, whereby the dipole of the molecule aligns perpendicular to its long molecular axis. It was in this context that the project focused on the synthesis of *tris*-alkylated Janus molecules, to assess if they displayed LC polymorphism and if they had the potential to act as a new class of negative dielectric anisotropic LC materials (Figure 2.2).

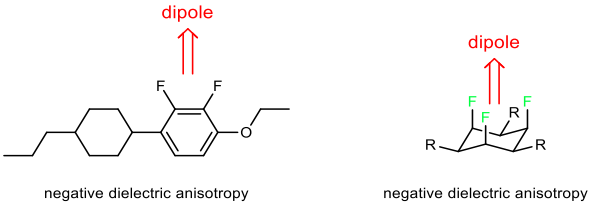

Figure 2.2: Left: known negative dielectric LC.[89] Right: proposed new 3D negative dielectric LC.

2.2 Introduction

The aim of this project was to develop novel Janus fluorocyclohexane derivatives that may display organic liquid crystal (OLC) properties. The compounds were designed with only three fluorines and with long alkyl chains attached at the 2, 4 and 6 positions of the cyclohexane, alternating with fluorines at the 1, 3 and 5 positions, where stereochemistry is retained, all substituents are on the same face of the cyclohexane ring (all-*cis*). A concise and general synthesis protocol was developed to generate all-*cis* mono-, di-, and tri-alkylated fluorocyclohexanes. In each case, and particularly for the trialkylated series, it is predicted that the alkyl groups will adopt equatorial orientations forcing the three C-F bonds axial. This arrangement retains a molecular dipole and polarity perpendicular to the ring system.[76,90–92] Intermolecular electrostatic interactions in the solid-state structures of these compounds result in supramolecular ordering of the cyclohexanes and open up prospects for the design of soft materials anchored by these interactions.[76,93–96] The project resulted in the generation of fourteen novel Janus cyclohexanes (Figure 2.3), including four *bis*-systems with two alkyl groups and eight *tris*-systems with three alternating alkyl groups directly attached to the cyclohexane. It was anticipated that for the *tris* systems, the alkyl groups should form completely isolated stacks of Janus cyclohexanes from other stacks with the potential to form discotic LCs. The target compounds are illustrated in Figure 2.3.

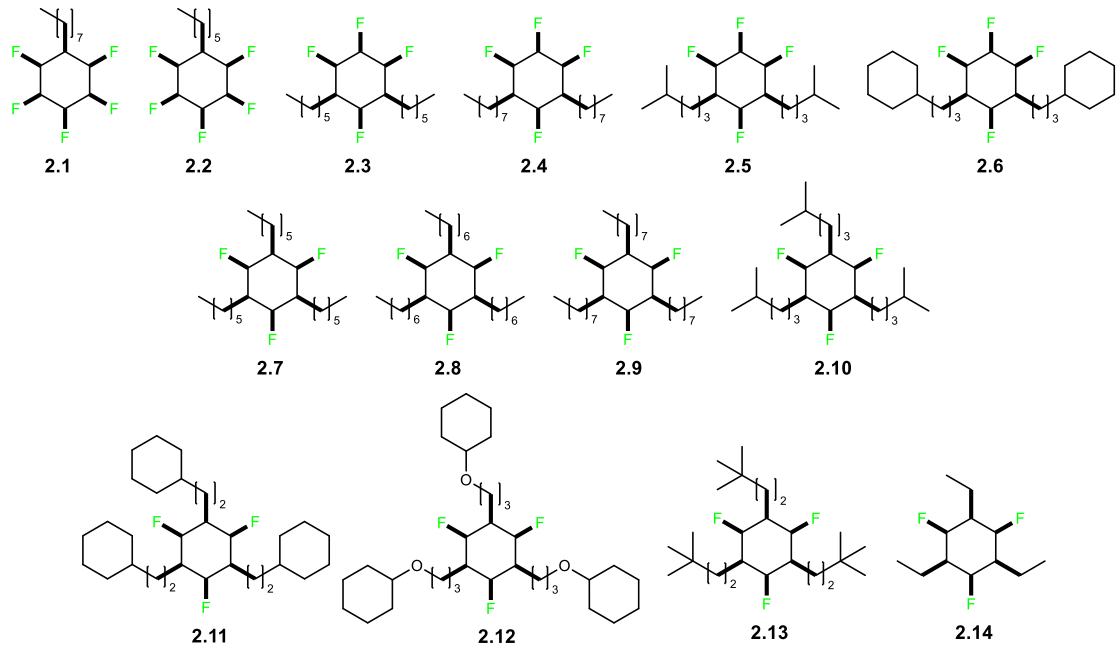

Figure 2.3: Synthetic targets.

2.21 Computational analysis of Janus ring assemblies

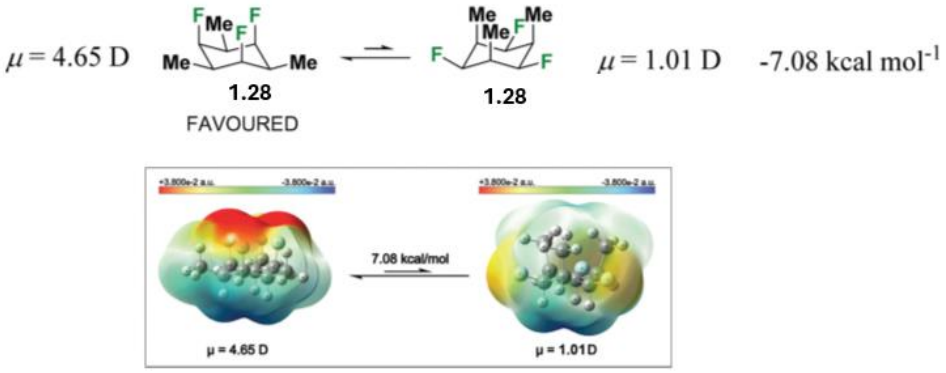

Figure 2.4: Structures optimized at the B3LYPD3/def2-TZVP theory level, with calculated free energy difference and dipole moment between the chair conformations of **1.28**. Bottom image indicates a surface electrostatic potential map for the conformers of the all-*cis* 1,3,5-trialkyl2,4,6-trifluorocyclohexane.[76] (Rodrigo Cormanich and Bruno Piscelli – University of Campinas, Brazil)

Figure 2.4 shows that the most favoured conformation for these 1, 3, 5 alkylated cyclohexane rings is one in which the C-F bonds are axial, favoured by 7.08 kcal mol^{-1}. This is reasonable due to the steric influence of the alkyl groups relative to fluorine which favours an equatorial orientation for the alkyl group.

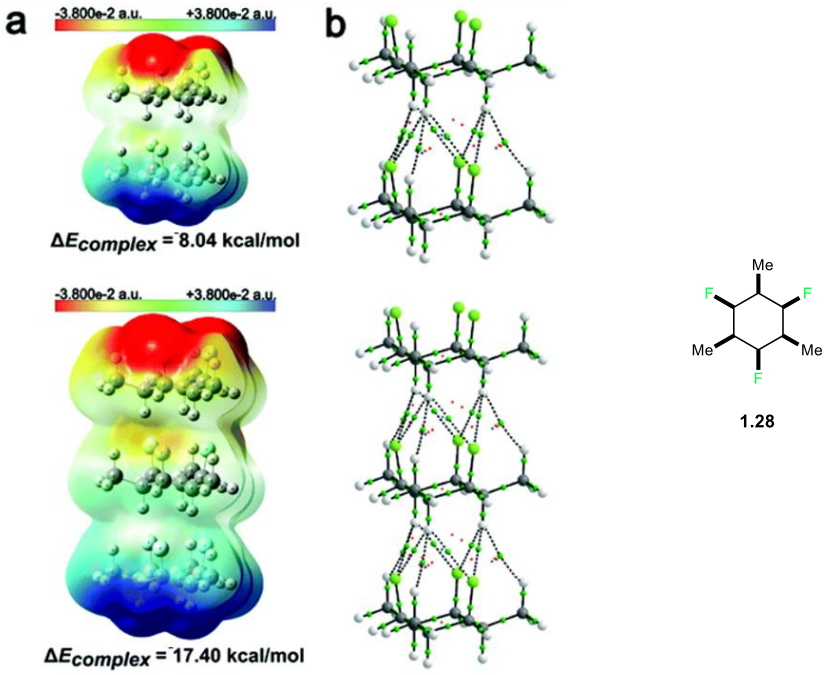

Figure 2.5: (a) Surface electrostatic potential maps for the dimer and trimer arrangements of 1,3,5-trifluoro-2,4,6-trimethylcylcohexane obtained at the PBE0/def2-TZVP theory level. (b) QTAIM molecular graphics obtained from the PBE0/def2-TZVP electron density, with bond critical points (BCPs) represented by green spheres and ring critical points (RCPs) and cage critical points (CCPs) represented by red and blue spheres, respectively. The complexation energies were calculated at B3LYP-D3/def2-TRZVP optimised geometries using the HFLD method and with the aug-cc-pVTZ basis set.[76,97–99] (Rodrigo Cormanich and Bruno Piscelli – University of Campinas, Brazil)

In a collaboration with Dr. Rodrigo Cormanich and Bruno Piscelli of the University of Campinas in Brazil, computational studies were conducted exploring the optimal stacking arrangements of selected Janus cyclohexane rings (Figure 2.5). The experiments explored the energies gained by bringing two or three molecules of the 1,2,3-trifluoro-2,4,6-trimethyl cyclohexane (**1.28**) together in the gas phase. For **1.28**, two molecules come together perfectly one on top of each other and with an energy gain of -8.04 kcal mol^{-1}. This is clearly due to an attractive intermolecular electrostatic interaction between the positive and negative faces of the ring. This value increases to -17.4 kcal mol^{-1} for three molecules forming a trimer. Again, the optimal interaction between the rings involved a perfect stacking one on top of another. Some elements of discrete F···H hydrogen bonding emerged from the theory study too. Hydrogen bonds to oxygen and nitrogen are typically between 2.7 Å – 3.3 Å,[100] with H···F hydrogen bonds typically being ~2.5 Å.[101] A bond critical point (BCP) is the point which lies between two

bonded atoms and identifies the lowest electron density point on the bond path. The bond critical points are highlighted in green. In this case, theory identified BCPs associated with H···F interactions between rings at the distances < 2.7 Å. The ring critical point is a point of minimum electron density on the ring surface, and here, they are highlighted by red spheres. These points estimate a distance consistent with good electrostatic attraction between the rings and again reinforce the idea that such forces promote ring stacking. With these insights from theory, it gave confidence that these *tris*-Janus molecules will self-associate in the solid state forming extended supramolecular assemblies.

2.3 Sonogashira cross-coupling reactions

In order to prepare the target molecules, it was necessary to generate the aromatic precursors for aryl hydrogenation. The initial synthetic route to the monoalkylated cyclohexane **2.1**, envisaged a two-step procedure. This monoalkylated pentafluorocyclohexyl derivative had been synthesized previously[102] utilizing Sonogashira chemistry,[103,104] followed by an exhaustive hydrogenation of both the acetylenes and the aromatic ring using the Zeng catalyst (**1.14**).[62,63,66] Scheme 2.1 summarises the initial route to generate **2.1**. The Sonogashira reaction proved straightforward, however the presence of the acetylene moiety was found to significantly inhibit aryl hydrogenation. In initial reactions, the acetylene was readily reduced to the saturated alkane, however at this point the reaction stopped and did not progress to the cyclohexane even in reactions at 50 bar H_2 and for over 24 hours. It would seem that the reduction of the acetylene 'kills' the catalyst, preventing further hydrogenation of the aromatic ring. However, when the acetylene was hydrogenated under standard conditions (Pd/C and H_2) at atmospheric pressure then the resultant alkyl benzene **2.18** was readily isolated.[105] When **2.18** was submitted to the aryl hydrogenation at pressure, then the reaction progressed reasonably well in this stepwise manner.

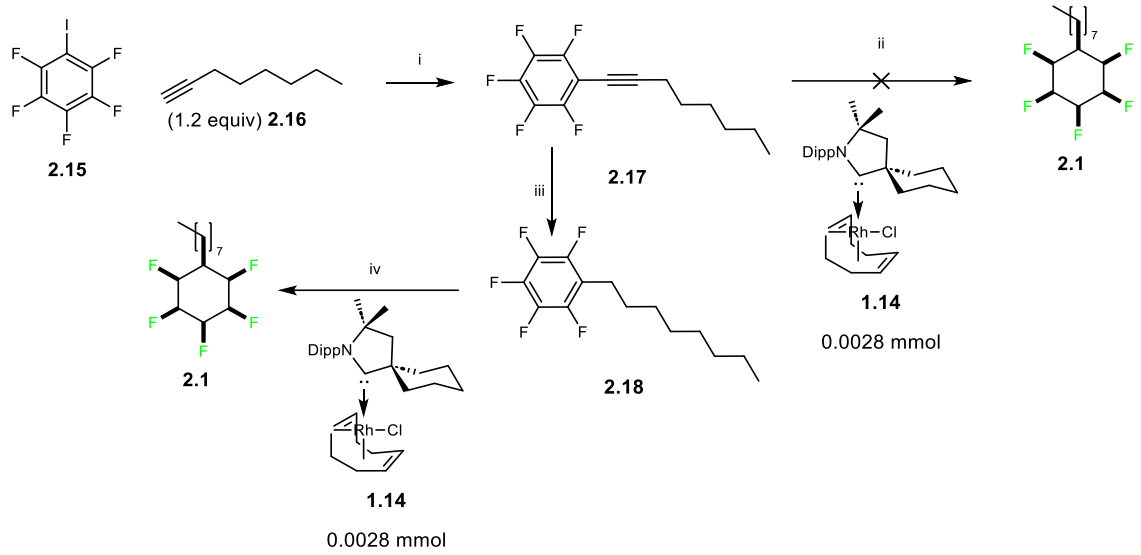

Scheme 2.1: Initial proposed reaction sequence for the generation of Janus target molecules. i: $PdCl_2(PPh_3)_2$ (15 mol%), CuI (15 mol%), DIPA (25 mL), 80 °C, 14 h, 98%. ii: H_2 (50 bar), 4Å molecular sieves (200 mg), hexane (2 mL), 25 °C, 28 h. iii: Pd/C (10% wt eq), hexane (10 mL), H_2 (atmospheric), 24 h, 72%. iv: H_2 (50 bar), 4Å molecular sieves (200 mg), hexane (2 mL), 25 °C, 28 h, quantitative.

The Sonogashira conditions were adapted from Tsuji *et al*., using CuI and $PdCl_2(PPh_3)_2$ as catalysts, and with diisopropylamine as a base and a solvent at 80 °C.[71] The *mono*, *bis*, and *tris* reactions were carried out at 15 mol% of $PdCl_2(PPh_3)_2$ catalyst and copper iodide. This loading was higher than that used by Tsuji, who used 10 mol% of both catalyst and copper iodide.[71] In cases where dimerization side products were formed, the loading of copper iodide was reduced to 2.8 mol%. A general catalytic cycle for a Sonogashira cross coupling is illustrated in (Scheme 2.2). The palladium pre-catalyst is activated under reaction conditions to an active Pd^0 species which participates in oxidative addition (OA) of the aryl halide. Then complex **B** undergoes trans-metallation (TM) with the copper-acetylide to generate complex **C** and this regenerates the copper iodide. Finally, complex **C** undergoes standard reductive elimination (RE) to yield the product and regenerate the catalyst. This copper cycle utilizes the base to form a π-alkyne complex **E**, and the resultant increase in acidity of the terminal proton leads to the formation of the copper acetylide which after deprotonation undergoes the trans-metallation (TM).

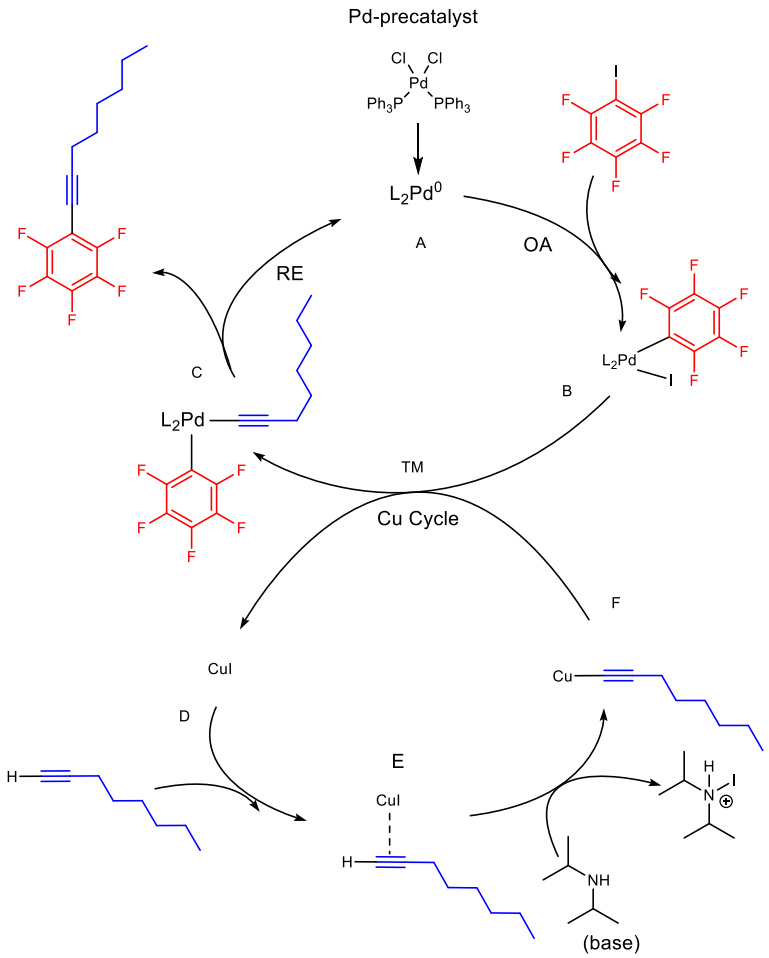

Scheme 2.2: A Representation of the Sonogashira mechanism.

This procedure was then adapted to the *bis*- and *tris*-systems. The Sonogashira cross-coupling reaction was found to work well for all the alkynyl substrates. However, attempts to generate long chain ethers such as compound **2.29** were often met with a decrease in yield. Overall, the Sonogashira cross-coupling reactions gave the desired products ranging from 49% to quantitative yields (Figure 2.6). The lower yielding Sonogashira reactions can be explained by the formation of alkyne dimers. It is known that increased molar equivalents of copper iodide in Sonogashira reactions can lead to lower yields due to promoting such homo couplings. One solution to this problem is slow addition of the copper cycle.

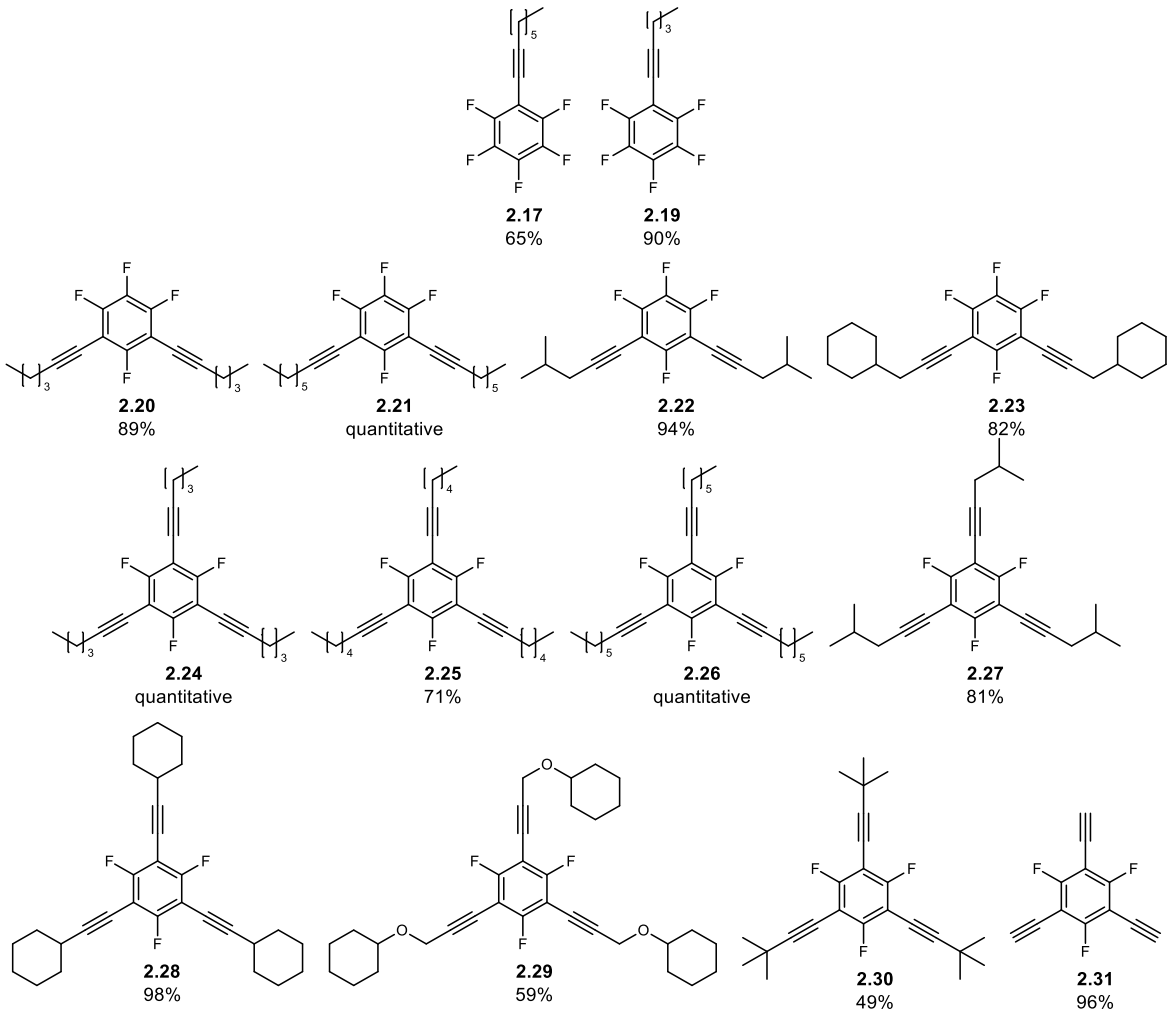

Figure 2.6: Sonogashira cross-coupling reaction with yields.

The Sonogashira cross-coupling reactions with the appropriate aryliodides proceeded efficiently in general. The acetylenes were added in excess; for *mono* addition the acetylene was added at 1.2 eq, and for the *bis* additions they were added at 2.4-2.8 eq; for the *tris* additions the acetylenes were added at 3.6 eq. The initial unreacted acetylene substrates often co-eluted with the cross-coupled products during chromatography. However, products with this contamination were progressed to atmospheric hydrogenation, and the minor components were converted to short aliphatics in the process and were readily separated from the desired alkylated aryl products. This is illustrated in Figure 2.7 for **2.22**, where the product and the contaminating acetylene are clear by ^{1}H NMR.

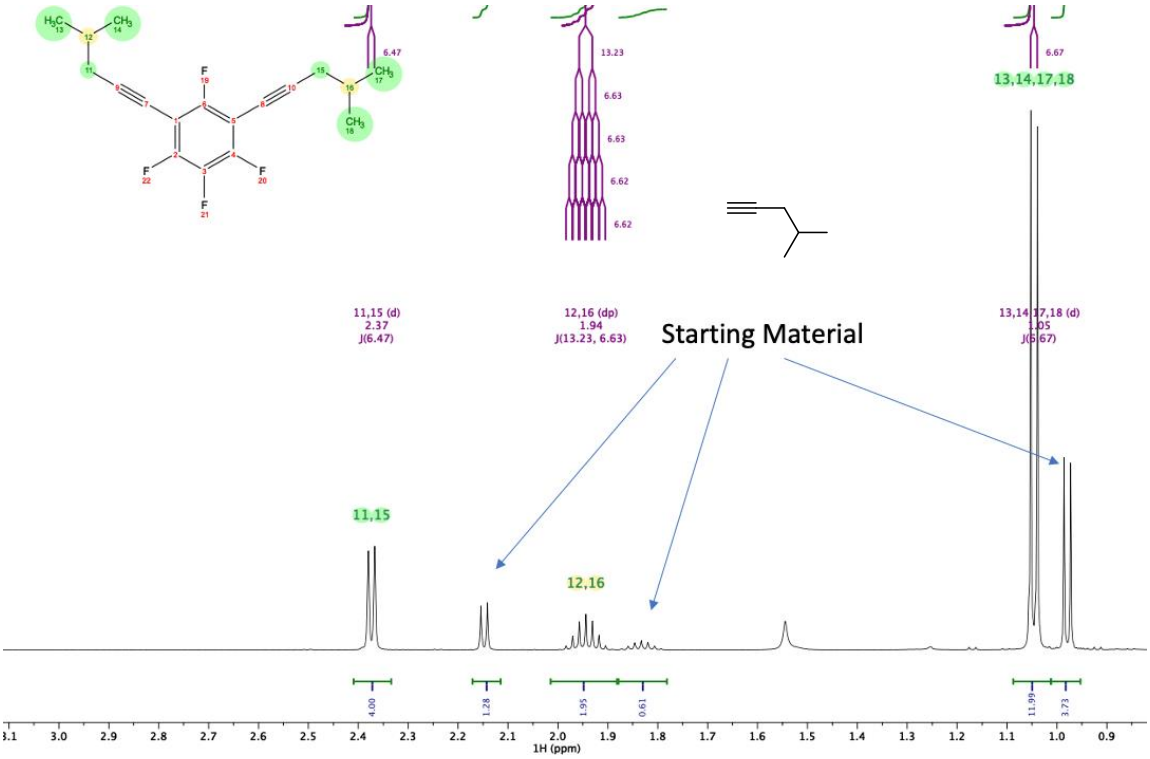

Figure 2.7: ^{1}H NMR of **2.22** contaminated with 4-methyl-1-pentyne.

Compounds **2.29** and **2.31** required synthesis of their early intermediates. Accordingly, alkylation of alcohol **2.32** using propargyl bromide **2.33** was required to generate propargyl ether **2.34** for the synthesis of **2.29**, as illustrated in Scheme 2.3.[106]

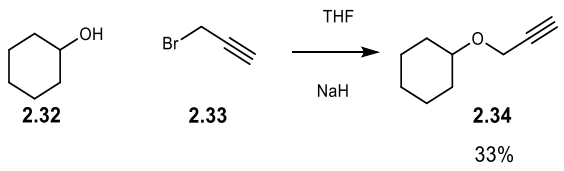

Scheme 2.3: Synthesis of ether **2.29**.

Tris-acetylene **2.31** was generated from silane **2.37** using **2.36**, and this was then deprotected using potassium carbonate (Scheme 2.4). This reaction was carried out in the absence of light as the product was sensitive to polymerization and in DMF instead of MeOH due to solubility.

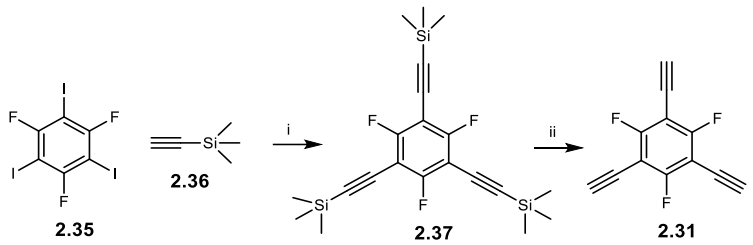

Scheme 2.4: Synthesis of **2.31**. i: $PdCl_2$ (15 mol%), CuI (15 mol%), DIPA (25 mL), 80 °C, 22 h. ii: K_2CO_3 (6 eq), DMF (20 mL), wrapped in tinfoil, r.t., 24 h, 96%.

2.4 Hydrogenation of the aryl acetylenes

The next step towards the target compounds involved hydrogenation of the aryl acetylenes to their corresponding aryl alkyl groups. The *mono*-octynyl **2.17** and hexynyl **2.19** substrates were readily reduced under atmospheric hydrogenation with Palladium on carbon. The *bis*-alkyl systems were also hydrogenated in a straightforward manner, to the *bis*-alkyl aryl products **2.39**, **2.40**, **2.41**, and **2.42**. These reactions utilized 1 eq of alkyne as solutions in either hexane, methanol, or ethyl acetate (10-100 mL) and with 10% palladium on carbon (10% wt eq) as the catalyst. The hydrogenation was then carried out with a H_2 filled balloon. Alternatively, for the more challenging *tris*-alkyl systems, hydrogenations were carried out in a stainless-steel autoclave with a H_2 pressure of 15 bar over 1-4 days (Figure 2.8).

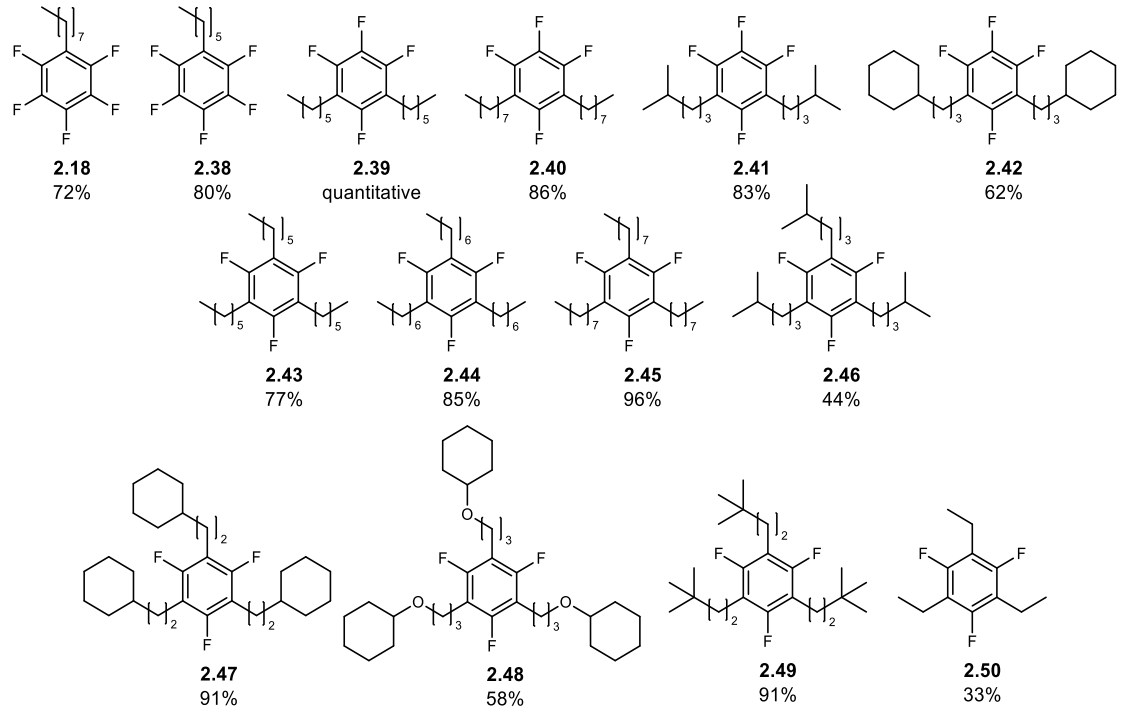

Figure 2.8: Hydrogenated products and their yields.

The *tris*-substituted substrates proved to be less efficient for hydrogenation under the standard conditions using hexane and H_2 at atmospheric pressure. For example, hydrogenations of **2.25**, **2.28**, **2.29**, **2.30**, and **2.31** required optimisation of their reaction conditions. The hydrogenation of **2.25** was initially unsuccessful due to its low solubility in hexane, however, changing the solvent to methanol improved the conversion significantly. Methanol, a protic solvent, improved solubility of the substrate and presumably provides an additional hydrogen source to reduce the acetylenes.[107] Other substrates such as **2.28** and **2.30** were hydrogenated in EtOAc to improve solubility and reaction times were extended to 48 h. Substrates **2.29** and **2.22** proved to be resistant to hydrogenation, with only low conversions at atmospheric H_2. Thus, these two hydrogenations were carried out in an autoclave at 15 bar of H_2 over the course of 2 days. The *tris*-acetylene **2.31** proved particularly sluggish and hydrogenation at atmospheric pressure resulted in only a 33% yield even after 12 days. The yields for the acetylene hydrogenations that were conducted in this study are summarised in Figure 2.8.

2.5 Aryl hydrogenations

Aryl hydrogenations were conducted starting from the general procedure reported by the Glorius group,[62] although many of the substrates in this study required optimization of these reaction conditions. Hydrogenation of the monoalkylated substrate **2.18** to generate cyclohexane **2.1** proceeded efficiently using the reported conditions (4Å molecular sieves, autoclave, H_2 (50 bar), and hexane). Product **2.1** was crystallized from DCM and diethyl ether, and a suitable crystal was submitted to X-ray structure analysis. The resultant structure is shown in Figure 2.9.

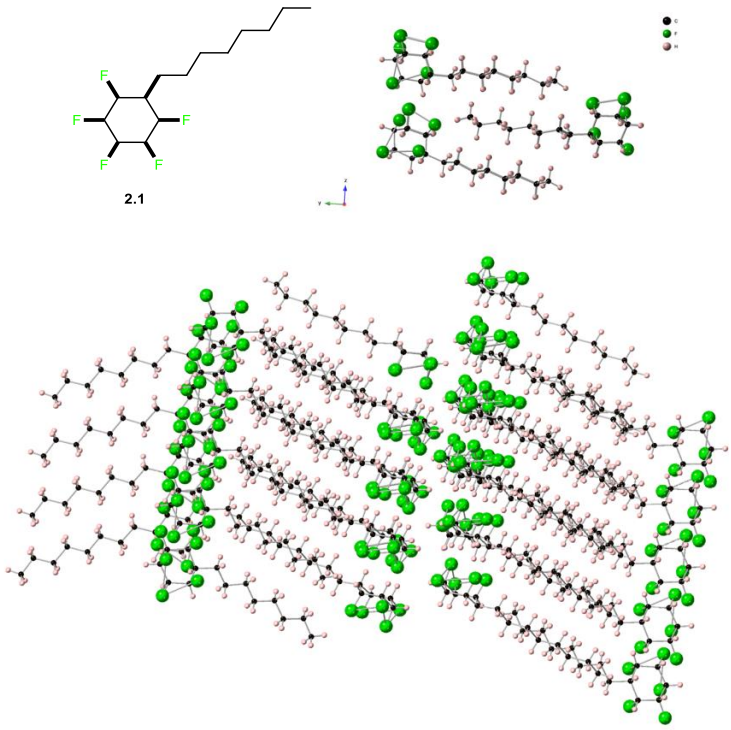

Figure 2.9: Crystal structure and packing of **2.1**.

The crystal structure clearly indicates that the rings stack one on top of each other through electrostatic H···F contacts, and the hydrophobic van der Waals attraction of the alkyl chains is also clear within the structure due to their aggregation. These two structural motifs essentially partition in the solid state.

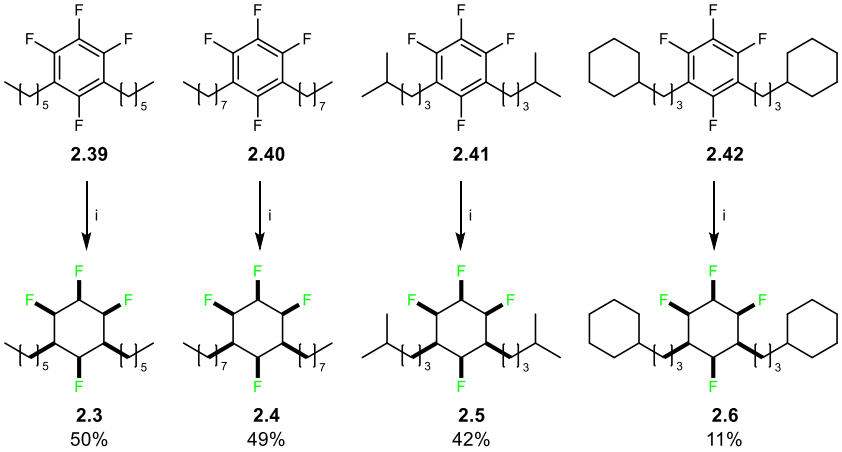

Scheme 2.5: Aryl hydrogenations to *bis*-alkylated Janus products. i: Aryl compound (1 eq), **1.14** (1.6 mol%), silica (200 mg) or 4Å molecular sieves (400 mg), hexane (2 mL), H_2 (50-70 bar), 25-50 °C, 1-10 days.

The next focus was to prepare selected *bis*-alkylated Janus cyclohexanes, and the targets are summarized in Scheme 2.5. The generation of **2.3** was achieved using silica gel rather than molecular sieves as a solid support, as no reaction was observed with sieves. It may have been that there was a poor mixing of the pre-catalyst and the sieves in the sealed autoclave, although this was always difficult to monitor. The other three *bis*-alkyl systems used 4Å molecular sieves but required longer reaction times of between 3-10 days.

The hydrogenation reactions of **2.5** and **2.6** were heated, as these proved to be sluggish, presumably due to the steric bulk of their alkyl groups.

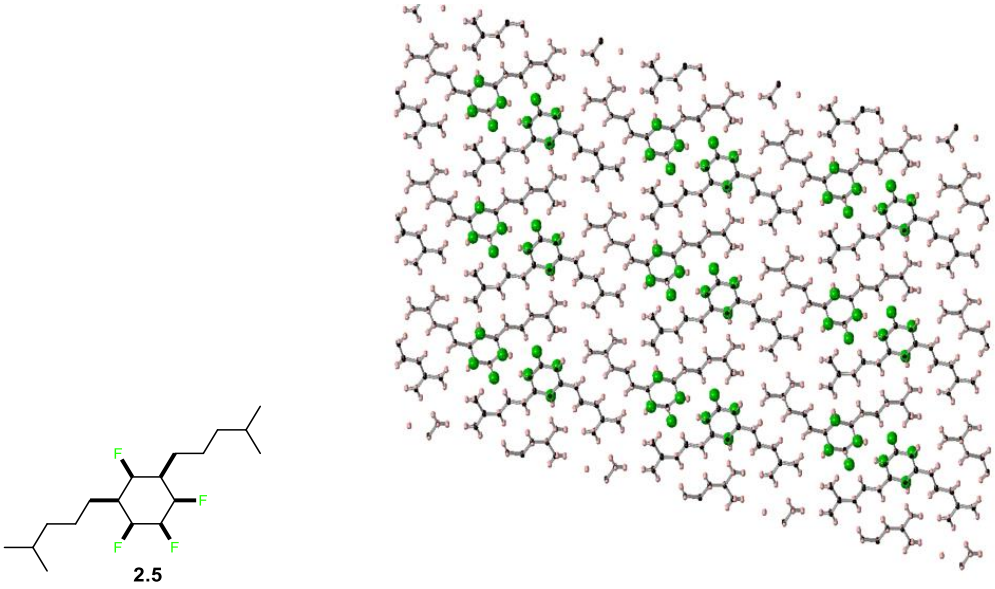

Figure 2.10: Crystal packing of **2.5**.

The crystal structure of *bis*-alkylated cyclohexane **2.5** showed a greater degree of order relative to that of **2.1** (Figure 2.10, Figure 2.11), a result of having two alkyl chains. Figure 2.11 shows how the rings stack one on top of each other, with electrostatic interactions between the fluorine and hydrogen faces. There is only one transverse ring – ring contact between the ring stacks in the solid state as the alkyl chains organize to space the rings from adjacent interactions. Clearly with only two alkyl groups the arrangement is not fully discotic, and a more organised arrangement was anticipated with the 2,4,6-*tris*-alkyl systems.

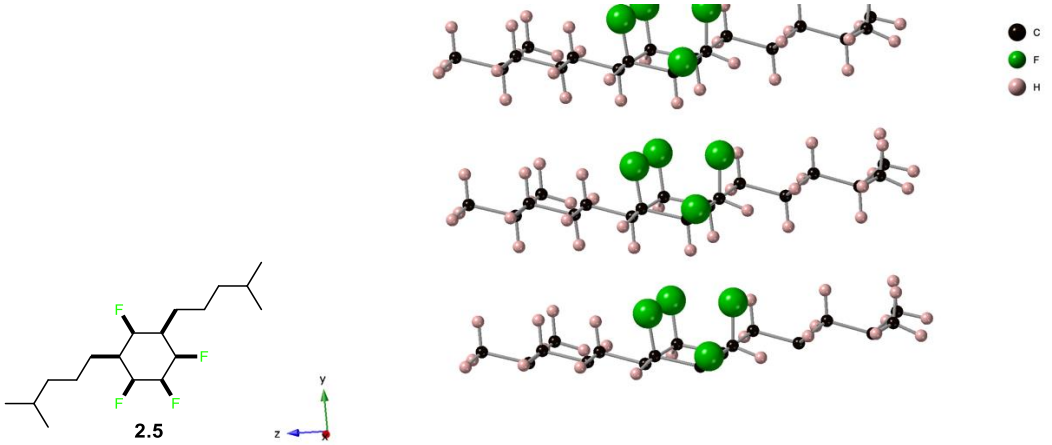

Figure 2.11: Crystal structure of **2.5**.

The *tris*-alkyl cyclohexanes proved to be much more challenging to generate by aryl hydrogenation, most likely due to the three alkyl chains shielding the aromatic ring from the active catalyst. In the first instance a variety of conditions were trialled for the hydrogenation of **2.45** to generate **2.9**. This included exploring silica gel vs molecular sieves and varying temperature and reaction times, as summarised in Table 2.1. The reaction requires the formation of catalyst nanoparticles to proceed, thus the sieves were finely crushed before use (otherwise no aryl-hydrogenation was observed). It was also important to add dry hexane to the catalyst and sonicate for 5-10 min prior to the reaction set up, to ensure solubility. Additionally, the reaction was carried out at 50 °C and at an increased pressure of 70 bar for 72 h. These rather forcing conditions allowed for the formation of product **2.9**, but in only a 19% conversion and subsequent low recovery after chromatography. Modest yields could be achieved by leaving the reaction for extended periods of time, and in the case for **2.45**, the best reaction was left for 10 days, and this allowed a 40% isolated yield of the resultant cyclohexane **2.9**.

Singly substituted Janus rings suffer from defluorination when aryl hydrogenation reaction times are conducted over 24 hours. Interestingly, there was little to no defluorination observed when arene hydrogenations are conducted on these 2,4,6-*tris*-alkylated rings, and it would appear that the alkyl groups are impeding this process in some way. Hydrodefluorination can occur during the formation of the Janus via multiple

pathways as discussed in Chapter 1.41, but it can also occur via acidic or basic HF elimination after the total hydrogenation.

Table 2.1: Reaction optimization for aryl hydrogenation of **2.45** into **2.9**

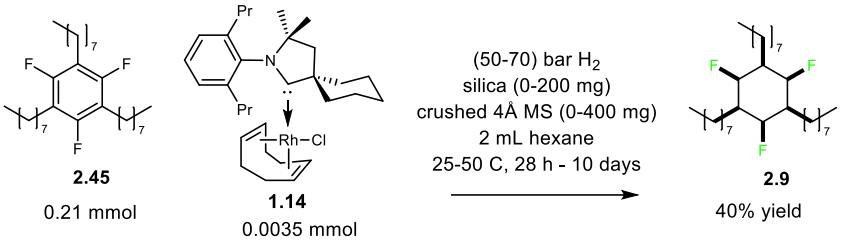

Entry	Pressure (bar)	Silica (mg)	Sieves (mg)	temperature	Reaction length	Conversion into **2.9**
1	50	200	-	25 °C	28 h	0%
2	50	-	200	50 °C	28 h	0%
3	70	200	-	25 °C	28 h	0%
4	70	-	200	50 °C	28 h	0%
5	70	-	400	50 °C	72 h	19%
6	70	-	400	50 °C	10 d	65%

Having explored the aryl hydrogenation of **2.9**, these reaction conditions were then applied to the tri-hexyl **2.7** and tri-heptyl **2.8** substrates which generated the corresponding cyclohexyl products in yields of 41% and 22% respectively. For the remaining *tris*-alkylated systems a mixture of 4Å molecular sieves and silica gel was used in an approximately two to one ratio. This proved to be the optimal method to generate the Janus cyclohexanes with more bulky substituents and it was used for the synthesis of the remaining tri-alkylated targets (Scheme 2.6). It is important to note that the reactivity of the nanoparticle catalyst generated by adsorption of **1.14** on the silica / 4Å sieves mix, deteriorates with exposure to air with the subsequent oxidation of the rhodium, whereas the pre-catalyst (**1.14**) is bench stable for months at a time.[61]

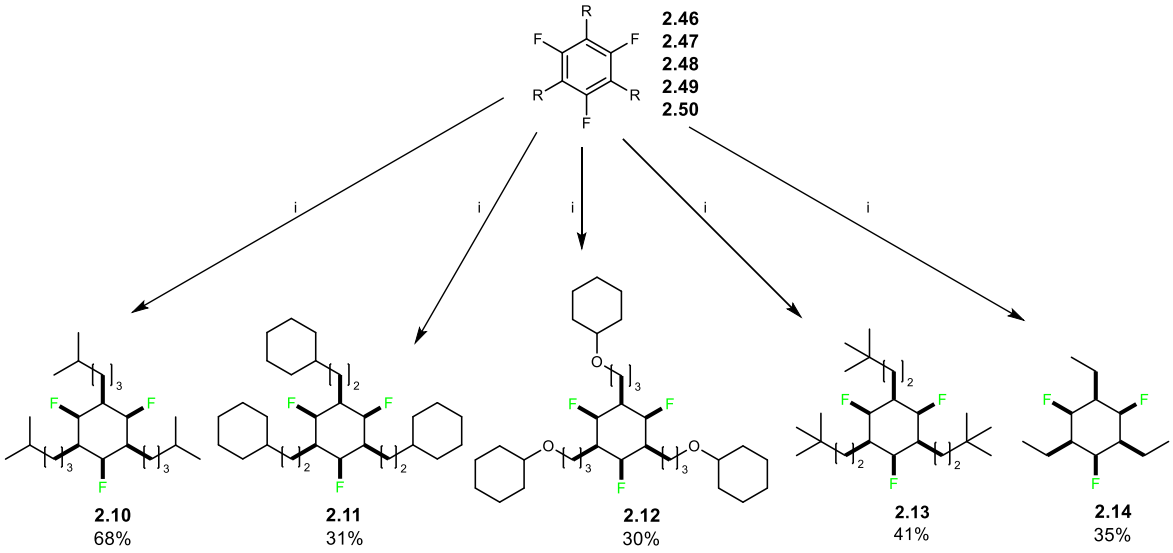

Scheme 2.6: Conditions and yields of Janus cyclohexane products. i: Aryl substrate (0.17-0.78 mmol), Rh(CAAC)-COD **1.14** (1.6mol%), silica (0.4-1.6 g)/4Å mol sieves (0.7-3.2 g) hexane (2-40 mL), H_2 (50 bar), 50 °C, 6-10 d.

A clear discotic columnar stacking could be determined in the solid state from the crystal structure of **2.10**. It can be seen that the cyclohexane rings ordered the stacks and that these stacks are completely insulated from each other (Figure 2.12) and the alkyl chains self-associate. Interestingly, the faces of the Janus rings in adjacent columns are ordered alternately, thus the dipoles of one column cancel out its neighbour. This suggests that this molecule may have ferroelectric and or antiferroelectric properties. Antiferroelectric materials are oriented in an antiparallel direction, which is primarily responsible for macroscopic spontaneous polarization.[108,109] This antiparallel dipolar ordering is observed in these *tris*-Janus compounds.

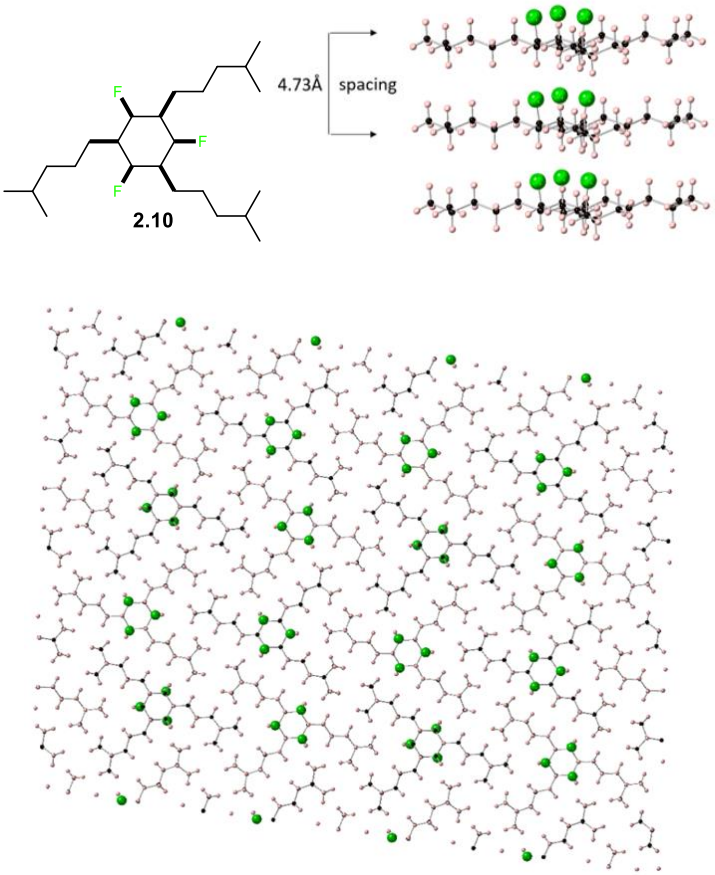

Figure 2.12: Crystal packing of *tris*-alkylated cyclohexane **2.10**.

Intermolecular interactions between the rings in the crystal structure of **2.10** have H···F distances < 2.7 Å and the repeat spacing of the ring systems is 4.73 Å. The ether system, **2.12** has a T-shape packing (Figure 2.13) similar to the *iso*-butyl system **2.10**. The solid-state structures of these *tris*-alkylated cyclohexanes all display clear columnar stacking suggesting that this may be general for this class of compounds.

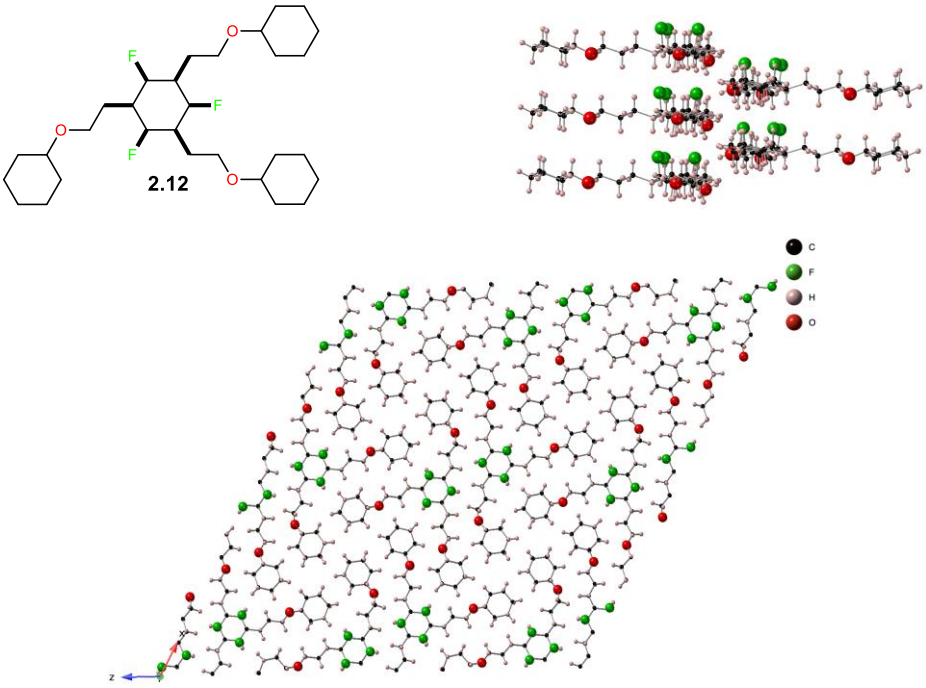

Figure 2.13: X-ray structure and molecular packing of **2.12**.

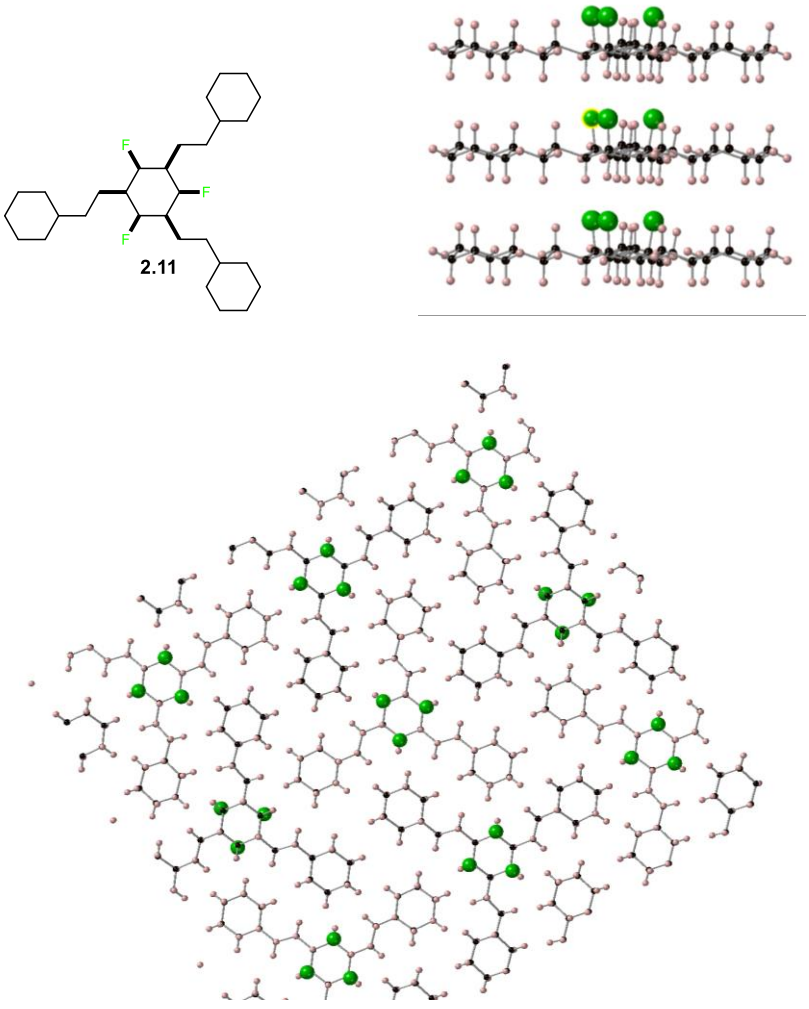

Figure 2.14: Crystal packing of **2.11**.

Interestingly the supramolecular assembly of **2.11** also showed fully insulated columnar stacking (Figure 2.14), however this time the molecules form a Y rather than a T shape arrangement, demonstrating that the alkyl substituents determine the overall organisation of the *tris*-alkylated supramolecular assemblies.

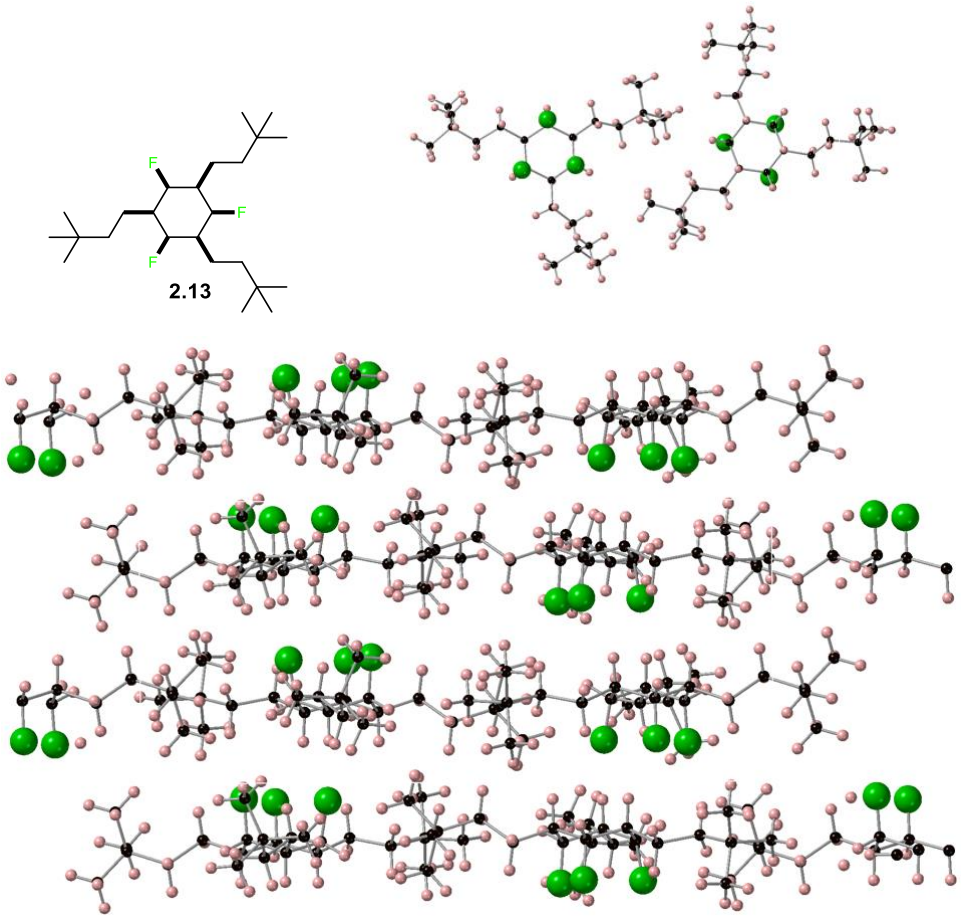

Figure 2.15: X-ray structure and packing of **2.13**.

Compound **2.13** presented differently in terms of its supramolecular assembly relative to the other *tris*-alkylated cyclohexanes that were prepared. The alkyl chains have terminal *tert*-butyl groups. This feature was designed in at the outset to reinforce ring stacking insulation in the solid state and perhaps induce more coherent phase transitions / polymorphism. In the solid state, the structure ordered such that it still possessed isolated Janus ring stacks, but the rings in the stacks are not perfectly aligned as in other cases, and in this case they alternate from side to side. Hence, the structure

possesses a screw axis. It was of interest to determine if these imperfect columns (Figure 2.15) might impart different properties (see DSC analysis). Chiral liquid crystals can form a cholesteric phase in which there are more degrees of order. In this phase the molecules stack directly on top of each other but rotate in a helical fashion, although this is not the case in compound **2.13**, it is interesting to see the similarity in this achiral molecule.

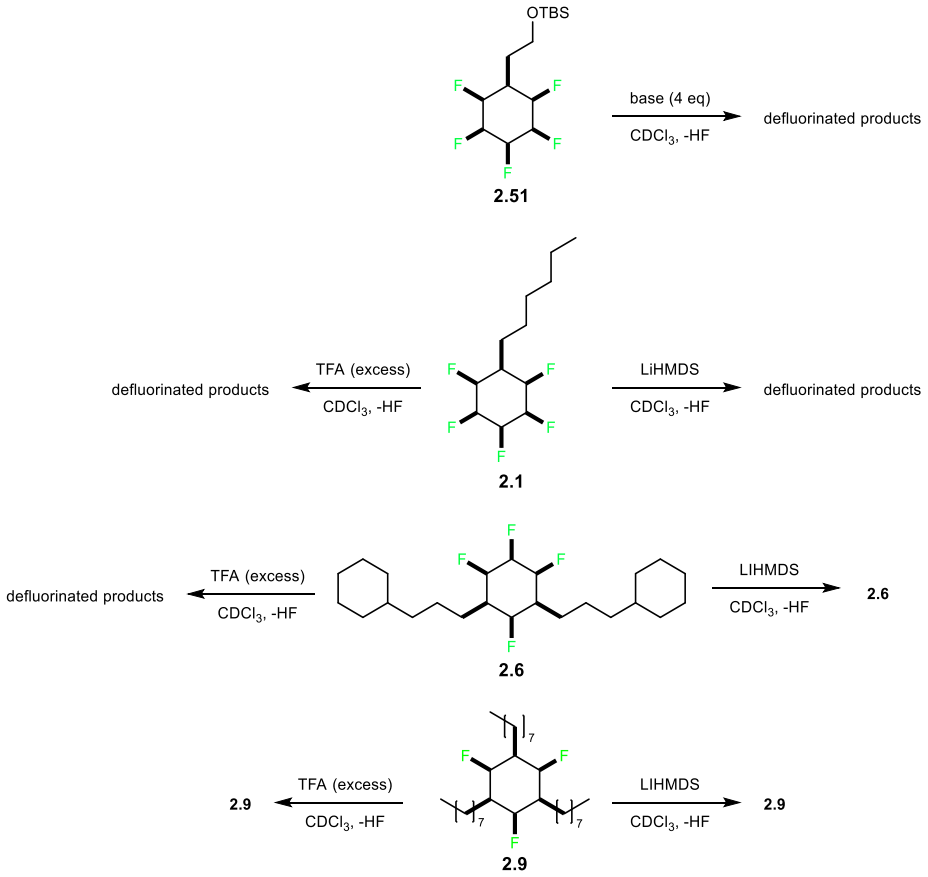

Scheme 2.7: NMR tube experiment on acid / base stability of Janus compounds.

One final test was preformed to determine the chemical stability of these types of molecules compared to the initial pentafluoro-Janus cyclohexanes that have been made previously. Clark[54] had run base stability experiments, as there was a known propensity for base-promoted elimination of HF from the Janus cyclohexanes. The silyl ether **2.51** shown above (Scheme 2.7) was explored and found to be stable in different bases such as pyridine, triethylamine, piperidine, and NaOH up to pK_a = 14.[54] However **2.51** was found to partially degrade with NaOMe (pK_a = 16) and fully degrade with LiHMDS (pK_a

= 26). To determine the stability of these new classes of Janus cyclohexanes they were tested by contact with both a strong acid (TFA, pK_a = 0.23) as well as LiHMDS in NMR tubes. The substrates were loaded into the tube along with $CDCl_3$ as a solvent, then either TFA or LiHMDS was added in large excess and NMR spectra were taken after an hour. The *tris*-alkylated cyclohexane **2.9** was found to be stable in both acidic and basic media for up to an hour. *Bis*-alkylated **2.6** was found to be stable in base but partially degrade in TFA over 1h, leaving 92% of starting material **2.6**. The mono-alkylated cyclohexane **2.1** was partially stable in TFA leaving 85% of starting **2.1** and degraded partially in LiHMDS leaving 87% of starting **2.1** after 1 hour. The ^{19}F NMR profiles related to these outcomes are detailed in the Experimental, Chapter 7, Section 7.21.

2.6 POM and DSC analysis

In order to further characterize the tri-alkylated Janus cyclohexane products, and particularly to explore their potential as candidate OLC materials, selected compounds were analysed by differential scanning calorimetry (DSC) and also by optical polarisation microscopy (POM). In the first instance their melting points were recorded, and it was found that all of the prepared compounds possess relatively high melting points. The lowest melting point was recorded for **2.3** at 100—103 °C, a *bis*-hexyl system, and the highest was recorded for the *tris*-alkylated system **2.13** m.p. at 171—173 °C. The target products **2.7** – **2.13** were then analysed by differential scanning calorimetry (DSC). DSC is a thermal analysis in which a substrate is heated progressively to beyond its melting point and then cooled down again to determine the specific heat capacity of a compound as it progresses through various phase transitions.[110] Often only a melt is observed, but the method will record polymorphic changes in the solid state too and will reveal the number of phase transitions a material undergoes before melting.

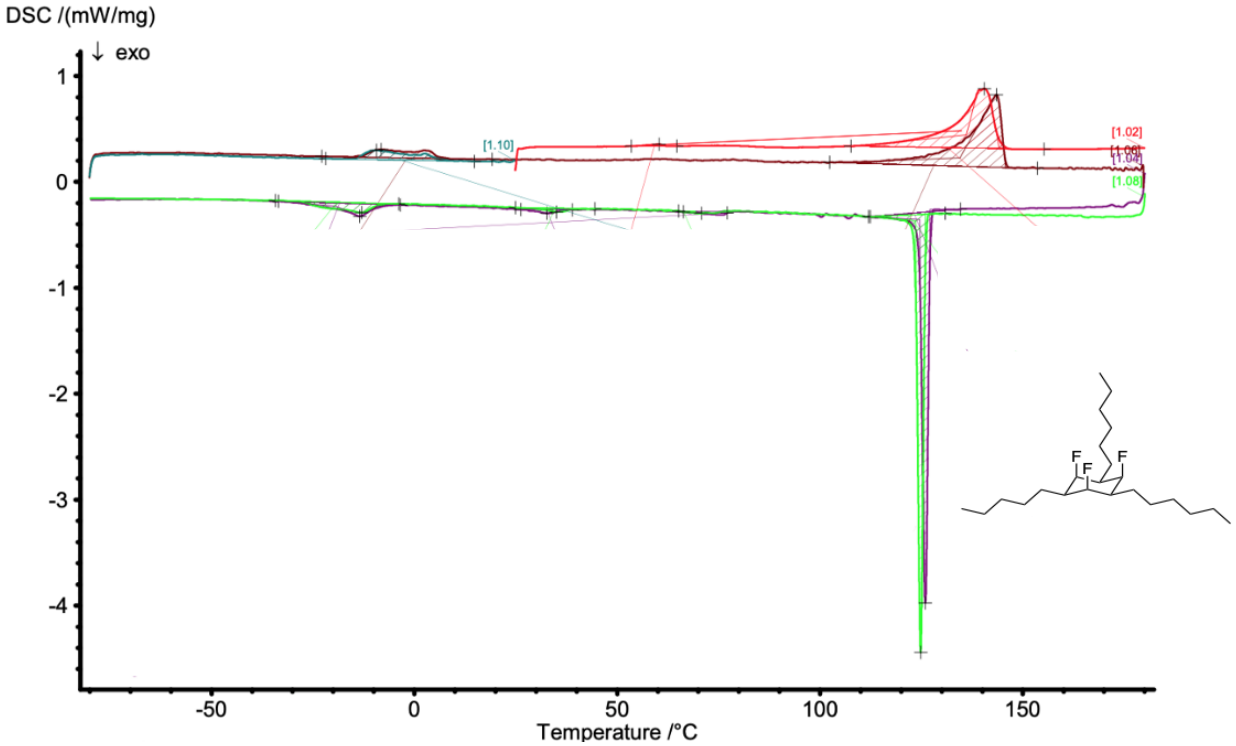

Figure 2.16: DSC temperature profile of cyclohexane **2.7**.

A DSC profile for **2.7** is illustrated in Figure 2.16. It can be seen that on first heating (red trace) there is a single-phase transition followed by the melting point. On cooling (purple and green traces), recrystallization is followed by a glass transition between 70.5 – 69.4 °C. This is then followed by two additional phase transitions at 36.6 – 27.8 °C and -9.1 – -19.4 °C. A second heating cycle (maroon trace) shows the same two transitions with good reproducibility. The second cooling cycle also contained the four transitions with high reproducibility (green). These results show multiple phase transitions, which indicate polymorphism and the possibility for liquid crystallinity. With these preliminary results, we entered a collaboration with Dr. Shigeyuki Yamada and Keigo Yoshida at the Kyoto Institute of Technology. The DSC profiles as well as polarized optical microscopy (POM) images recorded in Tokyo for compounds **2.7** – **2.13** are

shown in Figure 2.17 and Figure 2.18. Figure 2.17 indicates three Janus samples that show normal melting points and no polymorphism.

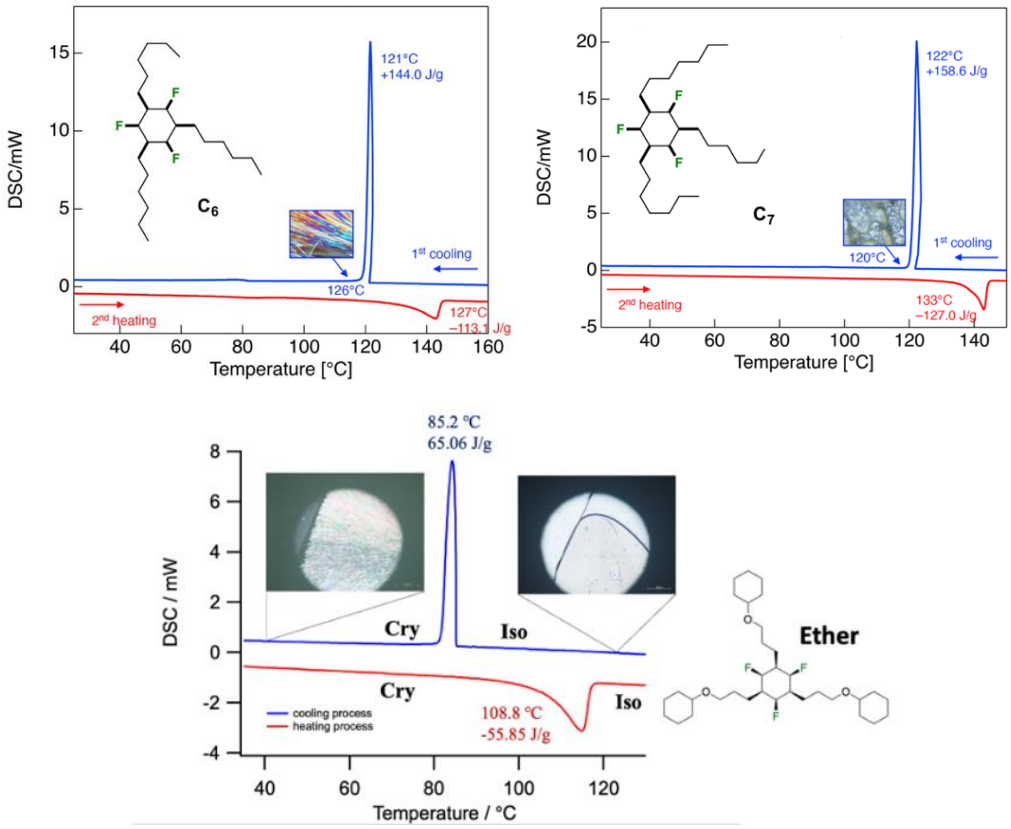

Figure 2.17: DSC and POM analysis of compounds **2.7**, **2.8**, and **2.12**. Red traces are heating, and blue traces are cooling. POM images are shown as insets.

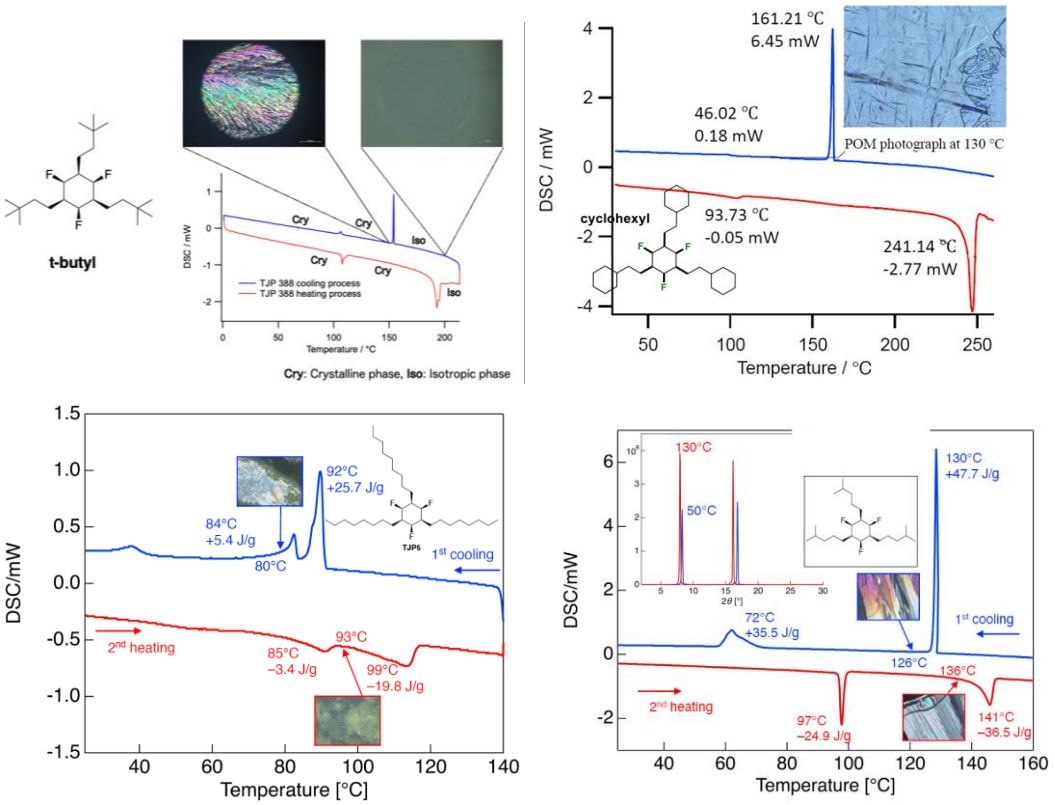

Figure 2.18: DSC and POM analysis of compounds **2.13**, **2.11**, **2.9**, and **2.10**. Red traces are heating, and blue traces are cooling. POM images are shown as insets.

Figure 2.18 shows four *tris*-alkylated Janus compounds **2.9**, **2.10**, **2.11**, **2.13**, that displayed polymorphism. Cyclohexane **2.11** did not have a liquid crystal mesophase (indicated by POM analysis), however a phase transition was observed at 93 °C before melting to the isotropic phase at 241 °C. This first transition can be attributed to a solid-solid transition between two non-LC polymorphs. However, cyclohexanes **2.9** and **2.10** show a mesophase-crystal phase transition. Compound **2.10** showed clear polymorphic behaviour with a distinct transition at 97 °C prior to melting at 141 °C. The POM image of the polymorphic phase of **2.10** exhibits a distinct and well-defined fibrous appearance, which is characteristic of an organized supramolecular structure with high orientation. Similar features are observed in **2.9** and to an extent in **2.13.** Although there are phase transitions in compound **2.11** the POM images in tandem with DSC analysis confirm that it is a crystal-crystal transition, which is a solid-solid transitions between two different crystalline phases. These transitions fall within the desired visual display range (-20 to 250 °C), but no LC phase was observed in the daily use range (0 – 40 °C).[111]

2.7 Conclusions

This Chapter has focussed on the generation and characterization of alkylated Janus face fluorocyclohexanes. Starting from simple commercially available fluoroiodo-arenes, Sonogashira reactions were conducted to attach long (C2-C8) chain acetylene groups in a regiocontrolled manner. These aromatic acetylenes were then hydrogenated under mild conditions to the corresponding alkylated fluoroarenes. The fluoroarenes were then subjected to more forcing aryl hydrogenation conditions using the Zeng catalyst and an adapted protocol as previously reported by Glorius's lab. This offers a robust general approach to this class of *mono*-, *bis*- or *tris*- alkylated Janus cyclohexanes.

This study primarily focused on elucidating the structural characteristics of the alternating 2,4,6-trialkyl motifs attached to the Janus cyclohexanes. The triaxial parallel alignment of C-F bonds confers a pronounced polarity to these cyclic structures, leading to intriguing structural outcomes. Notably, the cyclohexane rings stack in a highly ordered manner dictated by electrostatic interactions and the pendant alkyl chains create an insulating barrier between adjacent Janus ring stacks—an arrangement not observed in mono- or di-alkylated systems.

The DSC and POM analyses indicated that four of these *tris*-alkylated Janus fluorocyclohexanes possess relatively complex polymorphism. The tendency of polar Janus rings to stack together, due to the attraction between their alternating faces, is very promising. This could lead to the creation of well-organized supramolecular structures with unique polar characteristics. This innovative approach opens doors to the design and creation of next-generation soft materials, including polar liquid crystals, which could find applications in various fields, from materials science to advanced technologies. The insights gained from this project pave the way for further exploration of these intriguing molecular systems and their potential for transformative applications in the realm of materials science.

3: JOF-MOFs

3.1 Introduction

Metal organic frameworks (MOFs) are a subset of microporous framework solids and are defined as a class of material with pore diameters of < 20 Å in size. They can adsorb small molecules into their pores and as a consequence they are attracting considerable attention across a range of possible applications.[112] MOFs were first developed in the 1990's with the term being coined in 1995.[113–115] They are three-dimensional connected network structures, made of nodes, usually metal cations, or clusters, linked by organic ligands.[112] The organic ligands are often called 'linkers' or 'struts'. Since their initial synthesis, there have been over 100,000 MOF structures reported in the literature, hence this relatively new field has grown rapidly.[116] Over the last three decades since their initial synthesis, MOFs have found particular applications as drug delivery systems,[117] in surface catalysts,[118] as energy storage materials,[119,120] as gas storage and separation vehicles,[121] and more.[122]

MOFs use functionalised organic struts to coordinate the metal centres and to create organised cages. These struts are often hydrophobic organic molecules with polar head groups such as carboxylic acids and tetrazoles which coordinate with the metal centres to create the cage structures (Figure 3.1).

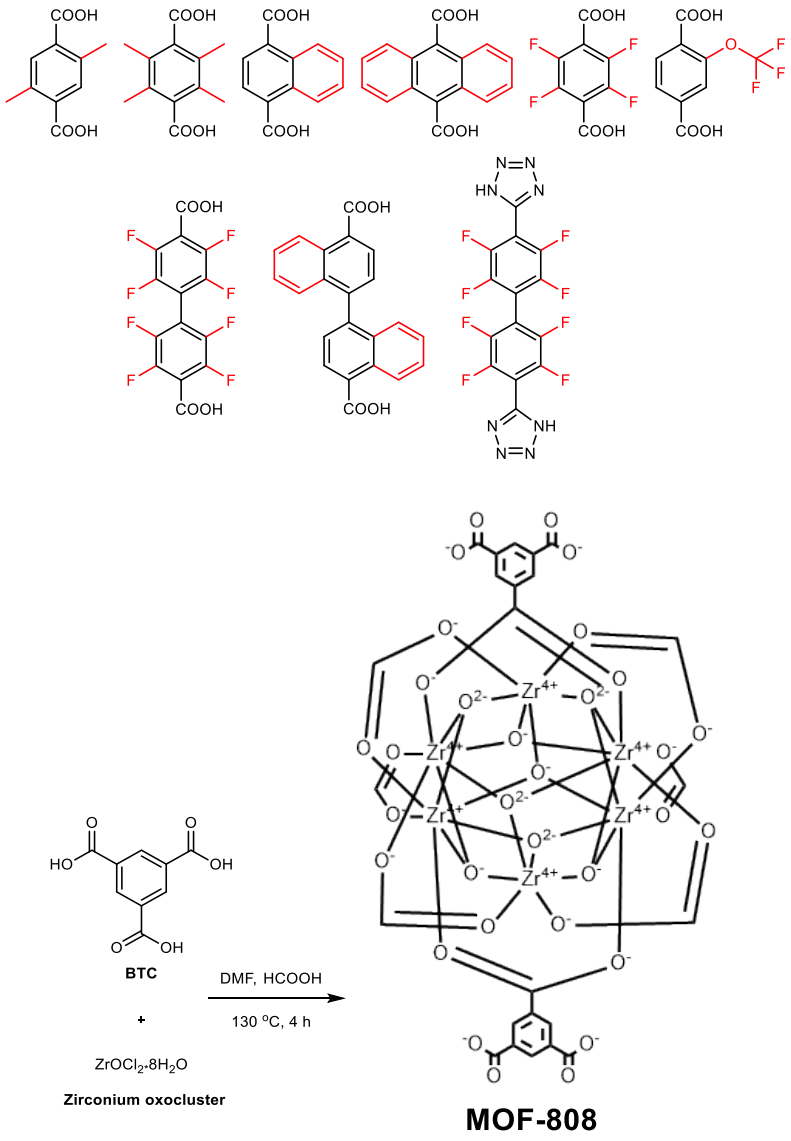

Figure 3.1: Top: Structures of some common organic linkers (struts) used in MOFs (hydrophobic regions in red).[116] Bottom: Formation of MOF-808 using a strut (BTC) and zirconium oxoclusters.[123]

Given the strong electrostatic intermolecular attraction that occurs between opposite faces of Janus cyclohexanes, this project set out to explore supramolecular Janus Organic Framework (JOF) assemblies stabilised by these interactions. Two candidate struts containing the Janus ring motif were designed and synthesised. These compounds were then investigated in a collaboration with Prof. Russell Morris, Dr. Romy Ettlinger, and Russell Main (St Andrews), a group with expertise in MOF synthesis and analysis. The struts were incorporated into coordination complexes / networks using zirconium and copper ions in an effort to create Janus Organic Framework – Metal Organic Framework (JOF-MOF) assemblies. An initial outcome was to examine the

structure and porosity of these materials. MOFs have been widely explored as molecular sieves and selective gas adsorbents.[124] One possible application of such materials might be an ability to scavenge partially fluorinated anaesthetic gases from the environment, on the principle that 'like attracts like' at the molecular level.

3.2 Organic frameworks

There are multiple examples of organic frameworks in the field of porous solids chemistry. Covalent organic frameworks (COFs) are a class of porous materials characterised by a 2D or 3D network of covalently bonded building blocks. They exhibit remarkable structural diversity due to the tuneability of organic substitutions and functionalities, making them suitable for various applications such as energy conversion and storage applications.[125] COFs are known for their high surface area, chemical stability, and precise pore size control. These attributes make them promising candidates for gas storage, catalysis, and separation processes. An example of a COF used in CO_2 storage is illustrated in (Figure 3.2).[126] This COF is known as cCTF-500 and was the first charged covalent triazine framework. It absorbs 133 mg g^{-1} of CO_2 at 1 bar and at 273 K.[126,127] This is impressive, and the compound can still absorb 80 mg g^{-1} of CO_2 at room temperature, 298 K.[126,127] cCTF-500 is synthesized under ionothemal conditions using $ZnCl_2$ as both the reaction medium and catalyst. The methodology was established by Antonietti and Thomas.[128] A mixture of COF monomeric unit (1,1'-bis(4-cyanophenyl)-[4,4'-bipyridine]-1,1'-diium dichloride) and anhydrous $ZnCl_2$ was heated in a sealed ampule at 400 ^oC, 450 ^oC, and 500 ^oC for 48 hours to produce the charged Covalent Triazine Framework (cCTF) scaffold.[126,128] The resulting powders were soaked in HCl (1M) to remove excess $ZnCl_2$, washed with distilled water, THF, and methanol, and then activated under vacuum at 120 ^oC.[126]

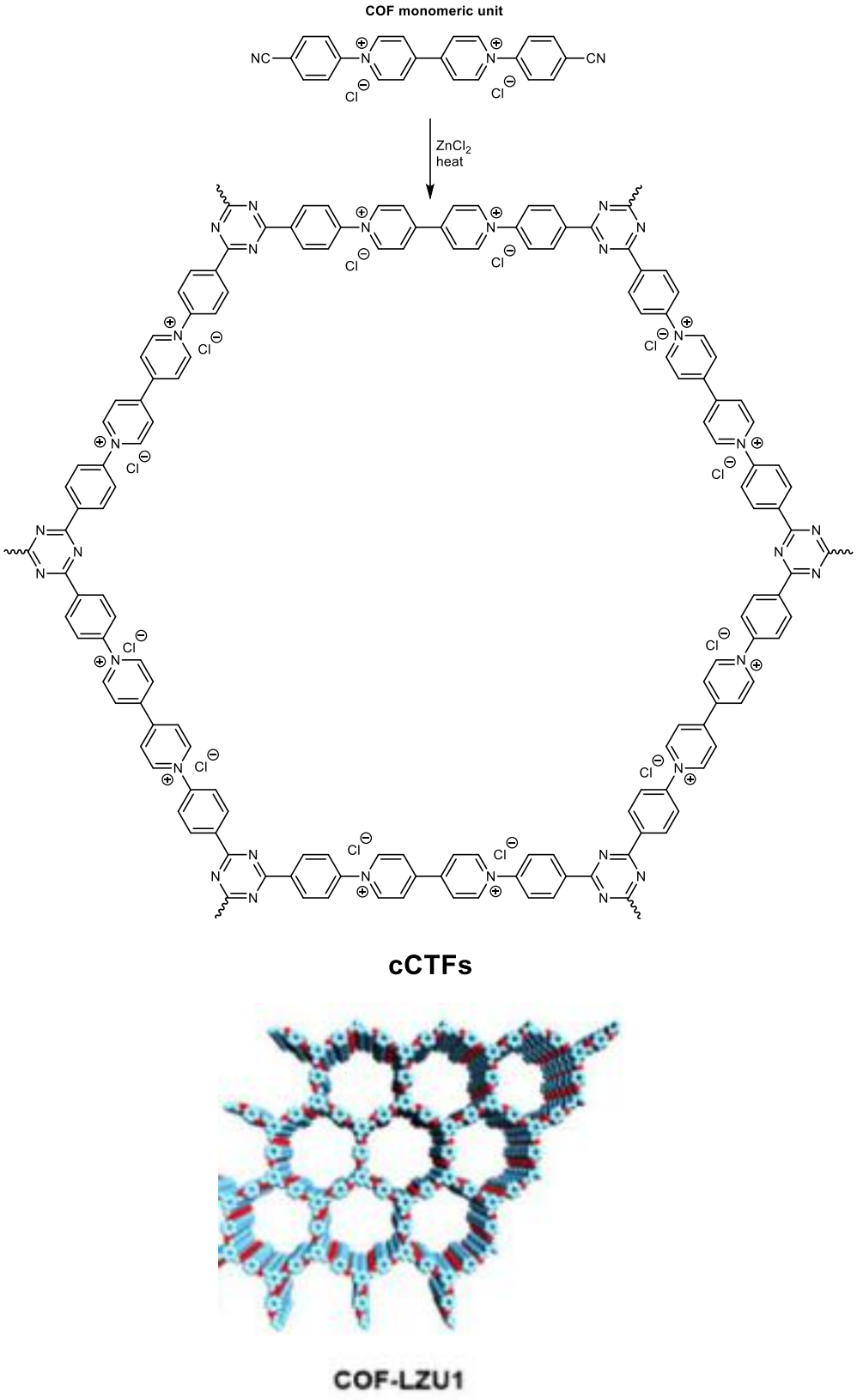

Figure 3.2: Top: COF framework known as cCTF-500 used for carbon dioxide uptake. Bottom: supramolecular framework of COF-LZU1 used in catalysis.[126]

Hydrogen-bonded organic frameworks (HOFs) offer an alternative class of porous materials formed through complementary hydrogen bonding interactions between organic building blocks.[129] Unlike COFs, HOFs rely on non-covalent interactions, primarily hydrogen bonds, to create their porous structures. This class of material has gained attention for their ease of synthesis and tuneability, allowing for the design of specific pore sizes and functionalities. HOFs have shown promise in gas adsorption, sensing, and as hosts for guest molecules.[130] Their dynamic nature and potential for reversable transformations are areas of active research. One example of a HOF used in sensing is illustrated by HOF-20 (Figure 3.3).

HOF-20 is highly efficient at detecting aniline in water through fluorescence.[131–133] It has a BET surface area of 1323 m^2g^{-1}, remaining stable in water.[131] When excited at 315 nm, HOF-20 emits a strong fluorescence at around 370 nm. The fluorescence intensity significantly increases after exposure to aniline, due to the rigidification of the structure caused by hydrogen bonding and π–π stacking interactions between aniline and the host framework.[131]

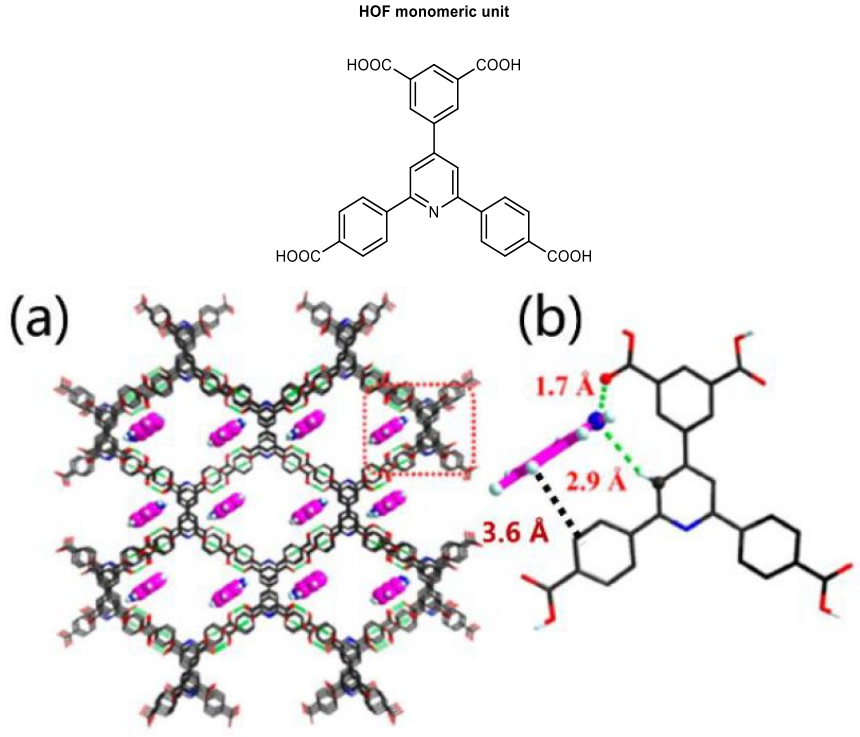

Figure 3.3: Top: HOF monomeric unit.[134] Bottom: (a) Structure of HOF-20 (aniline highlighted in pink is absorbed in the channels of the HOF). (b): Zoomed in section of (a) Hydrogen bonding and π–π stacking interactions between HOF-20 and the adsorbed aniline. Figure taken from Lin *et al*.[131]

The reviewed topology diagrams for COFs, HOFs, and MOFs are outlined below (Figure 3.4).

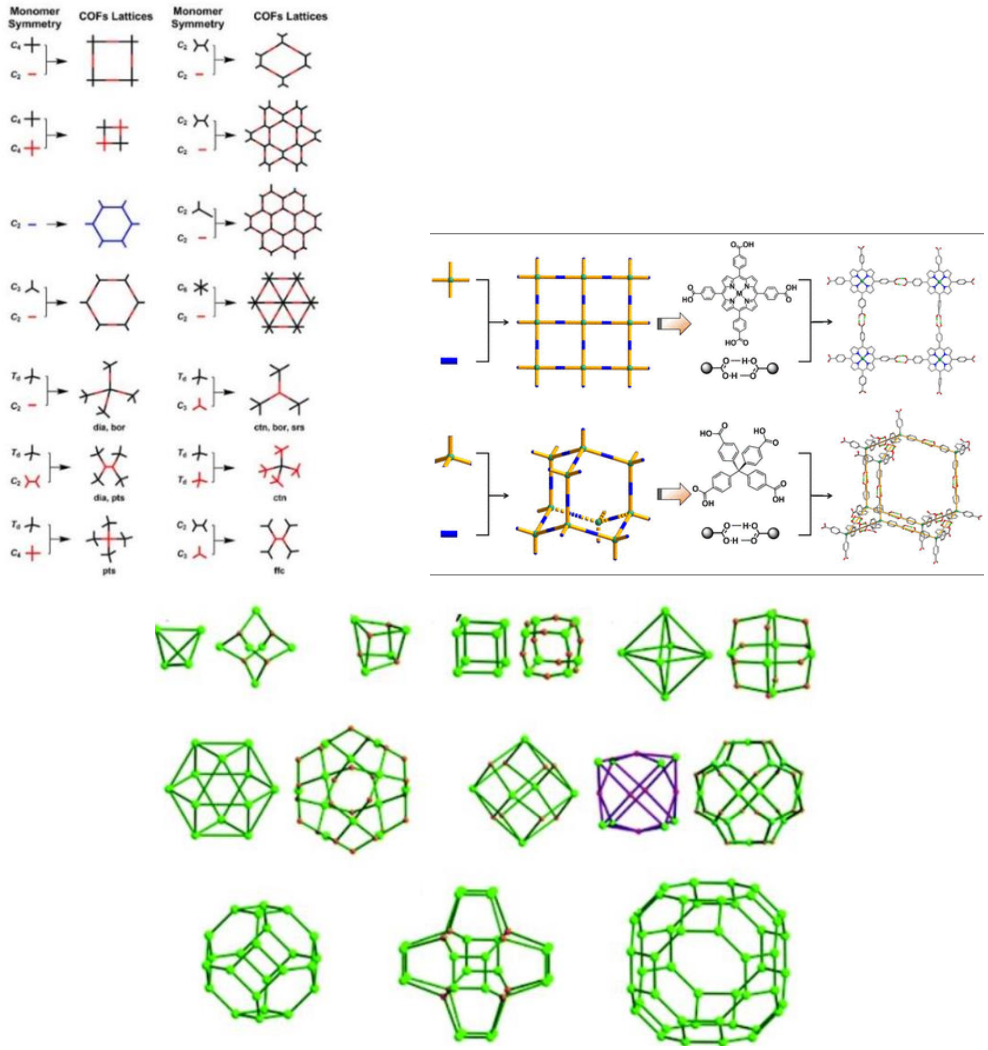

Figure 3.4: Topology diagrams for COFs (top left), HOFs[131] (top right) and MOFs (bottom).[119,125,135–139]

COFs and HOFs can form 2D or 3D frameworks. MOFs on the other hand form 3D frameworks only. There are key differences between the way COFs, HOFs and MOFs coordinate. COFs are composed of light elements like carbon, nitrogen, and oxygen, connected by strong covalent bonds, forming highly stable and porous structures. HOFs, on the other hand, are held together by hydrogen bonds between organic molecules, offering flexible and potentially dynamic frameworks with comparatively lower stability. MOFs consist of metal ions or clusters coordinated to organic ligands through

strong coordination bonds, resulting in highly tuneable structures with diverse functionalities and applications. Each type offers unique properties, with COFs providing robust frameworks, HOFs offering flexibility, and MOFs excelling in tunability and functional diversity.

Janus cyclohexanes are polar with electropositive and electronegative faces that have the ability to form 3D frameworks through self-association.[76] It became a research objective to establish whether this interaction could drive supramolecular assembly when these Janus rings were incorporated into struts, eliminating the need for conventional functional groups like carboxylates or alkynes and nitriles, which have been commonly employed in the construction of COFs or MOFs.[74] With this in mind, Dr. Cihang Yu (St Andrews PhD, 2022) synthesised a first generation of Janus organic frameworks (JOFs).

3.21 First generation JOFs

The interaction energy (~7-8 kcal mol^{-1}) between two isolated Janus cyclohexane rings is in the order of a good hydrogen bond and it has already been shown that functionalised derivatives have a tendency to self-associate and form extended supramolecular assemblies.[76] These intermolecular interactions between the fluorine and hydrogen faces of the rings open up the possibility of linking 3D cores into networks and stabilise porous supramolecular assemblies in a manner characteristic of HOFs, thereby eliminating the need for the more conventional functional groups with hydrogen bonding donors and acceptors which are commonly employed in the construction of HOFs and MOFs.[74] In preliminary work (Dr. Cihang Yu) some candidate core structures were synthesised and their extended supramolecular assembly explored. Selected structures of such cores are shown in Figure 3.5 with Janus rings on the periphery.[74] Additionally, the X-ray structure of **3.2** is illustrated in Figure 3.6 where void volumes are highlighted. Compounds **3.1**, **3.2**, and **3.3** were the first examples of JOFs, and the structures indicated a level of porosity, a feature that was also supported by Brunauer-Emmett-Teller (BET) analysis. BET is a common characterization technique used to assess the specific surface area and void volumes of porous materials.[140] The

technique is based on measuring the adsorption of a low molecular weight gas (often N_2) on the surface of a porous material, at different pressures.

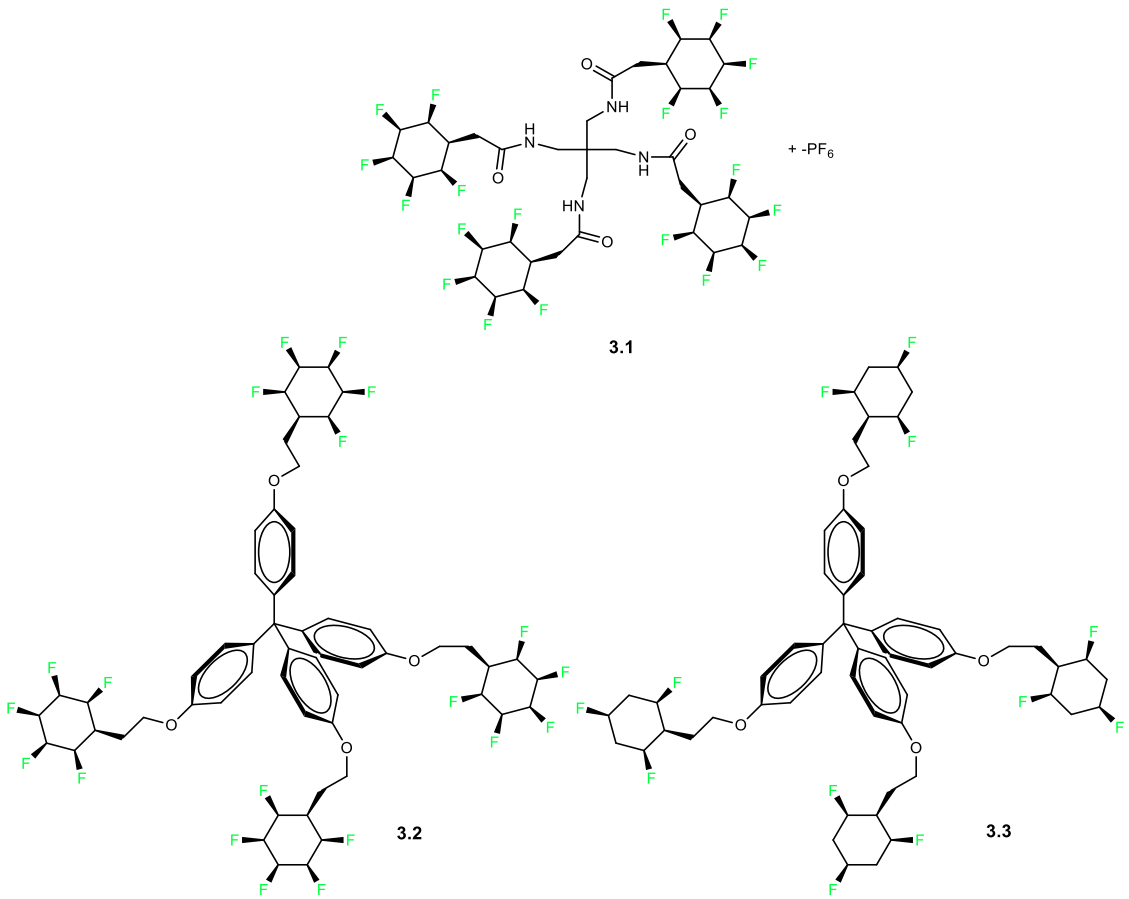

Figure 3.5: The first JOF cores (Dr. Cihang Yu, St Andrews PhD thesis 2022).[74]

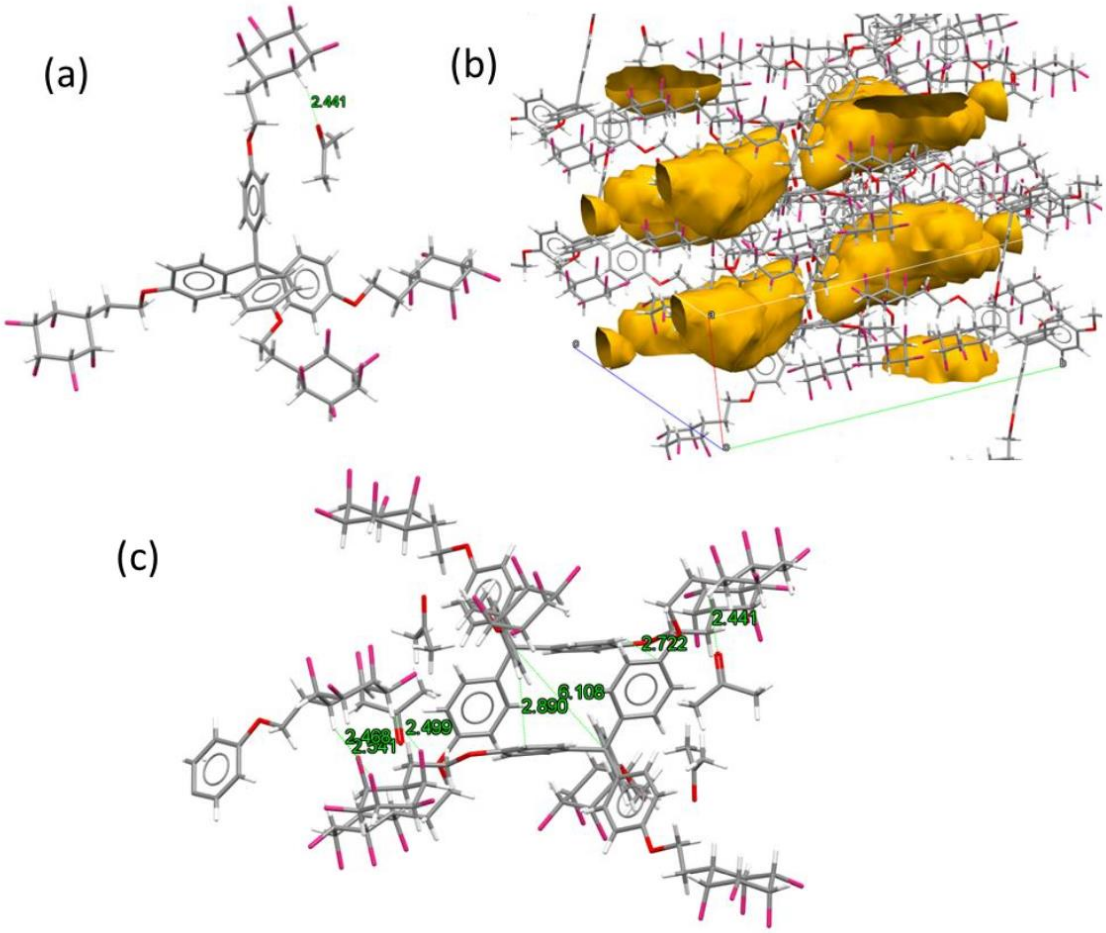

Figure 3.6: X-ray crystal structure of **3.2**, (a) The monomer **3.2** with guest solvent (acetone); (b) Void volume in the crystal structure of **3.2**; (c) The intermolecular contact distance of **3.2**. NOTE: grey for C, white for H, red for O, and pink for F. Crystal structure and images taken from Yu.[74]

The St Andrews group (Dr. Atsushi Tarui) recently developed a different type of organic framework using the tri-fluoro *tert*-butyl (TFTB) group as the centre piece, where there is a single fluorine on each methyl of a *tert*-butyl group. Although this is not a JOF, it combines single fluorines with geminal hydrogens within an organic motif and has some of the polar aliphatic characteristics of Janus cyclohexanes where the TFTB groups were anticipated to self-associate (Figure 3.7). For example, the enantiopure BINOL ether **3.4**, which has two TFTB moieties within each monomeric unit shows a hexagonal clustering of the TFTB units in the solid state. In this case solvent molecules (hexane) fill the resultant porous channels. The crystal structure shows a hexagonal cluster using the TFTB unit.

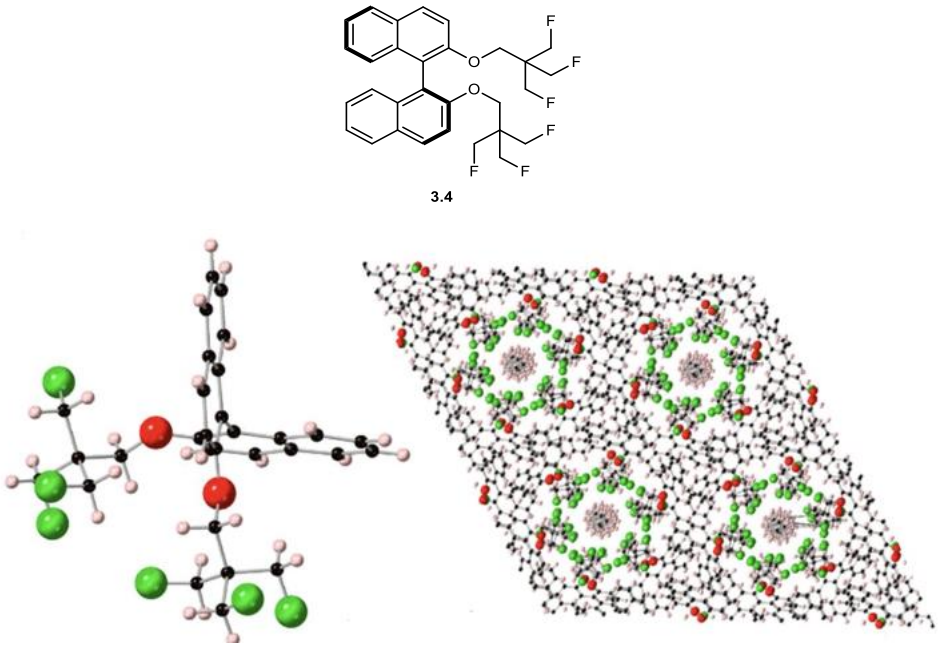

Figure 3.7: Top: BINOL ether **3.4**. Bottom: X-ray structure of **3.4** indicating the hexagonal arrangement of the TFTB groups, which generate solvent (hexane) filled channels. NOTE: black for C, white for H, red for O, and green for F.

3.3 Synthesis of penta- and tri-fluoro JOF-MOF struts

3.31 Initial investigations

The early indications of porosity and supramolecular ordering in the 3D structures highlighted above suggested that, with better design, there may be prospects for generating more porous materials. It therefore became an objective to prepare struts for MOFs that can both coordinate key metal ions (Zr^{4+}, Cu^{2+}) and also self-assemble and interact with one another through their Janus cyclohexyl motifs to make a new class of materials, JOF-MOFs. In order to synthesise JOF-MOFs the project identified the following two targets (Figure 3.8), one with the pentafluoro and one with a trifluoro motif.

Figure 3.8: Target JOF struts.

Attention focused on the development of struts that can self-assemble and interact with one another through Janus rings. The aim was to synthesize a strut that could coordinate to a pre-existing MOF as well as itself *via* the Janus ring, making a JOF-MOF.

For synthesis, the idea was to use MacMillan photoredox chemistry to couple Janus containing alkyl bromides to aryl bromides through Ni catalysis to achieve sp^3-sp^2 coupled products.[141] To explore this, an initial task required to generate the necessary alkyl bromide **3.9** (Scheme 3.1).

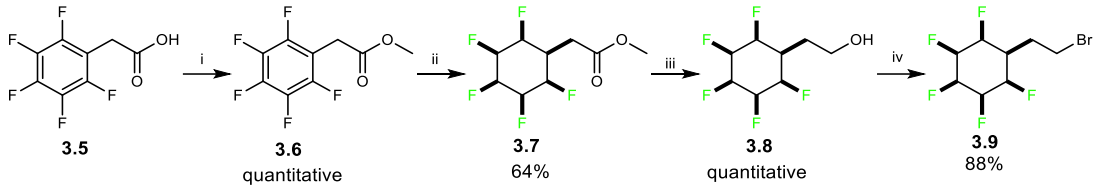

Scheme 3.1: Synthetic route to alkyl bromide **3.9**. i: **3.5** (22.1 mmol), MeOH (40 mL), HCl (2M, 1 mL), reflux, 24 h, quantitative. ii: **3.6** (3.95 mmol), Rh-CAAC-COD-Cl **1.14** (2 mol%), 4Å MS (8 g), hexane (40 mL), H_2 (50 bar), r.t., 1 day, 64%. iii: **3.7** (6.09 mmol), THF (30 mL), DIBALH (3.3 eq), 0 °C-r.t., 16 h, quantitative. iv: **3.8** (5.73 mmol), CH_3CN (30 mL), PPh_3 (12.03 mmol, 2.1 eq), CBr_4 (12.03 mmol, 2.1 eq), r.t., 16 h, 88%.

Compound **3.9** was synthesized from commercially available **3.5**, utilising a straightforward esterification reaction followed by an aryl hydrogenation to Janus cyclohexyl ester product **3.7**. After purification, a DIBAL reduction of the ester to the corresponding alcohol, **3.8**, was conducted. Finally, an Appel bromination was carried out to access **3.9** for photoredox reactions. These reactions were adapted from previous protocols.[35,54]

If successful, this photoredox chemistry offers an attractive strategy to attach the key Janus motif to higher molecular architectures such as drugs scaffolds and JOF struts. The photocatalytic cycles proposed by MacMillan *et al*. [141] during this reaction are shown below (Scheme 3.2). The process is initiated by photo-activation of the Ir^{III} to generate a high energy $*Ir^{III}$ complex. This complex can oxidize bromide, generating bromine radicals which interacts with TTMSS forming a silyl radical, which then abstracts the halogen from alkyl bromide **3.9**. Concurrently aryl bromide, undergoes oxidative addition to Ni^0 and this combines with the alkyl radical to create an alkyl–Ni^{III}

species. Reductive elimination produces the C_{sp}^3–C_{sp}^2 bond and regenerates the Ni catalyst.[141]

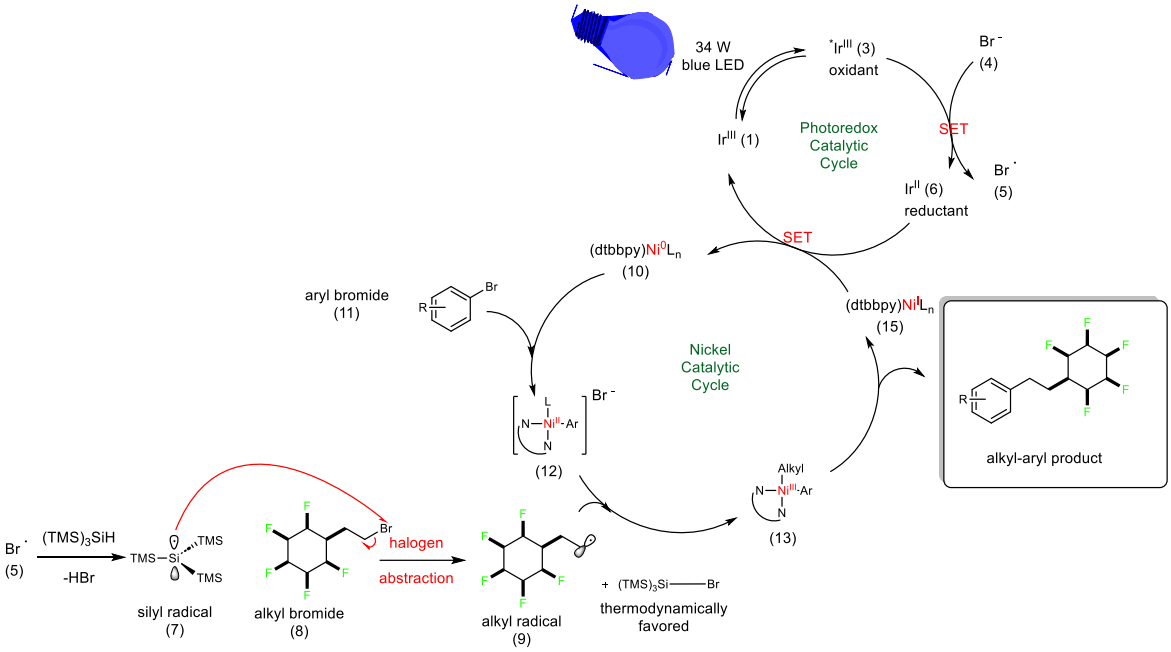

Scheme 3.2: Photocatalytic cycle to alkyl-aryl products.[141]

In order to establish if this methodology was viable with a Janus cyclohexane, an initial photoredox reaction of **3.9** with 1-bromo-4-(trifluoromethyl)benzene was explored. On completion of the reaction, the crude sample revealed a shift in the ^{19}F NMR, indicating the reaction may have proceeded with 82% conversion to the product. The compound was subsequently purified via flash chromatography using a hexane / ethyl acetate gradient and obtained in an 80% yield. The X-ray crystal structure of **3.10** was acquired, which indicated that the Janus rings stack one on top of each other (Scheme 3.3). Additionally, the other two coupled products, **3.11** and **3.12**, were generated and purified in good yields.

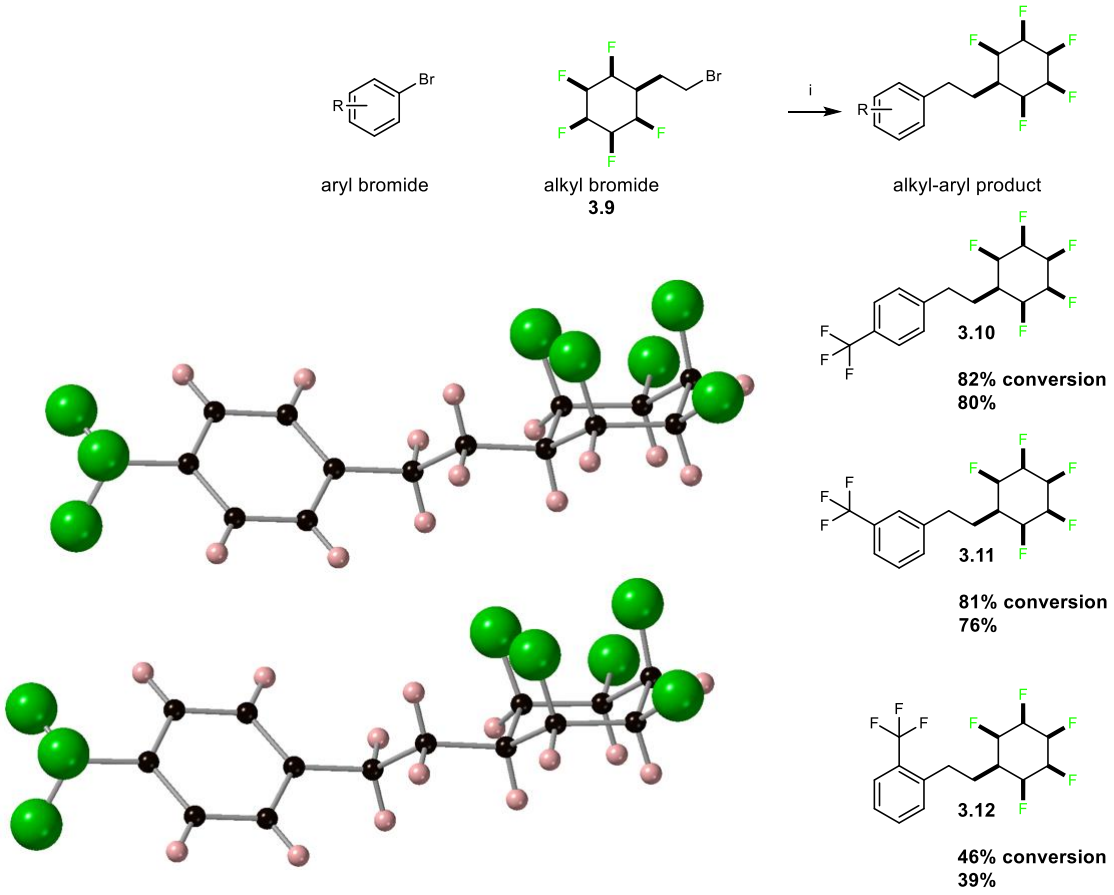

Scheme 3.3: X-ray structure of **3.10**, showing ring stacking. MacMillan photoredox chemistry applied to Janus molecules.[141] i: **3.9** (1.5 eq), $Ir[dF(CF_3)ppy]_2(dtbbpy)PF_6$ (0.01 eq), bromobenzotrifluoride (1 eq), tris(trimethylsilyl)silane (1 eq), anhydrous Na_2CO_3 (2 eq), DME (4 mL), $NiCl_2$•glyme (0.01 eq), 4,4'-di-tert-butyl-2,2'-bipyridine (0.01 eq), 34 W blue LED lamp, 17 h.

The reaction required the use of a 34-Watt blue LED lamp and photoreactor which was custom built. The Ir photocatalyst was taken up in solution with the reagents, however $NiCl_2$•glyme was poorly soluble, and thus this pre-catalyst was dissolved in DME and degassed separately to ensure full dissolution. Although mostly dissolved, the vessel was sonicated until full solubility was reached and then the solution was syringed into the main reaction in a microwave tube. The sealed tube was then placed into the photoreactor. A fan was activated to avoid over-heating and the whole system was then wrapped in tin foil to prevent adventitious light. Once the reaction was finished it was exposed to air and subject to column chromatography.

With the successful synthesis of **3.10 — 3.12** the method was now explored for the preparation of suitable JOF struts. This would entail incorporating a Janus cyclohexane

with a carboxylic acid linker to attach on the metal centre of either Zr-nodes or a pre-existing MOF. Therefore, the immediate target became ester **3.14**.

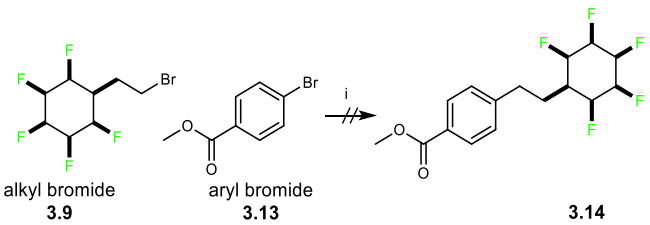

Scheme 3.4: Attempted synthesis of **3.14**. i: **3.9** (1.5 eq), Ir[dF(CF$_3$)ppy]$_2$(dtbbpy)PF$_6$ (0.01 eq), methyl 4-bromobenzoate (1 eq), tris(trimethylsilyl)silane (1 eq), anhydrous sodium carbonate (2 eq), DME (4 mL), NiCl$_2$•glyme (0.01 eq), 4,4'-di-tert-butyl-2,2'-bipyridine (0.01 eq), 34 W blue LED lamp, 17 h.

The reaction in Scheme 3.4 was explored with bromobenzoate ester **3.13**, and it may have progressed to some extent (based on ^{19}F NMR, Figure 3.9), however, due to low conversion and significant purification problems the product could not be isolated. The compound was found to stick to the column until methanol flushes were used resulting in only ~10 mg of **3.14** coming off the column with significant impurities such as the metals used in catalysis.

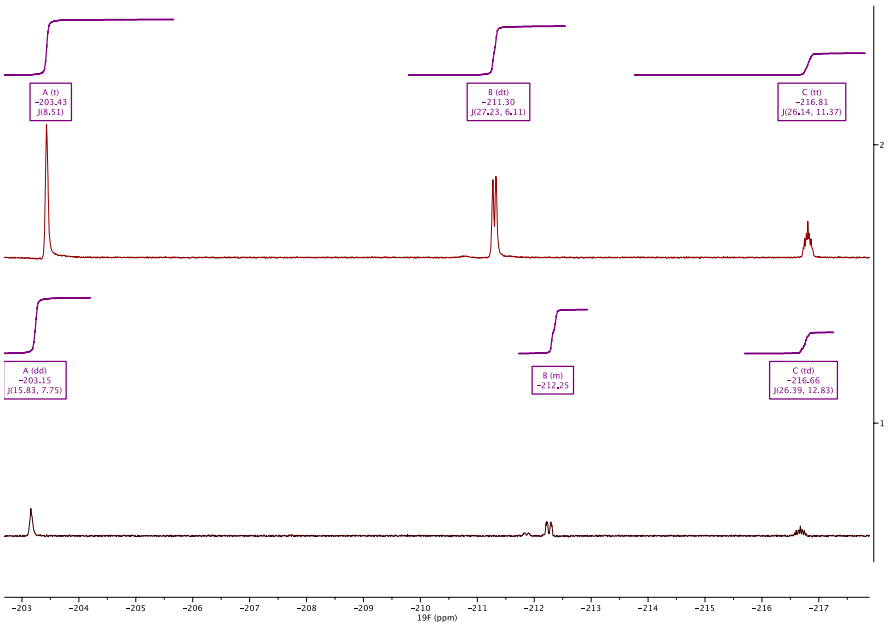

Figure 3.9: Top: ^{19}F NMR of **3.9** (A = *meta* 2F, B = *Ortho* 2F, C = *Para* 1F). Bottom: ^{19}F NMR of reaction mixture (A = *meta* 2F, B = new *Ortho* 2F, C = *Para* 1F. Indicating a new product (peak B) associated with the *ortho*-F (**3.14**).

So, although some progress had been made with this photoredox chemistry for incorporating the Janus cyclohexane motif, it was not pursued further here. Therefore, to simplify our strategy it was decided to try and generate ether linked Janus compounds *via* substitution reactions.

3.32 Synthesis of JOF struts

The Janus carboxylic ester **3.16** was prepared by phenolate substitution of the bromoalkyl Janus substrate, **3.9**, and methyl 4-hydroxybenzoate (**3.15**).[142] This reaction was conducted in DMF at 70 °C and using Cs_2CO_3 as a base. The product was easily purified via column chromatography using a hexane / ethyl acetate gradient. From here ester **3.16** was hydrolysed under acidic conditions, to avoid any HF elimination which can occur under basic conditions.[54] This resulted in a complete conversion to **3.17** which was purified by column chromatography using hexane / ethyl acetate and provided the first candidate JOF strut (Scheme 3.5).

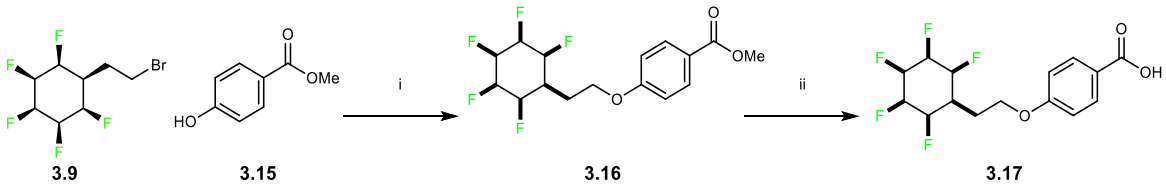

Scheme 3.5: Synthesis of **3.17**. i: **3.9** (1 eq), **3.15** (1 eq), Cs_2CO_3 (1.6 eq), DMF (10 mL), 70 °C, 24 h, 63-87%. ii: **3.16** (1 eq), HCl (6 M, 30 mL), THF (10 mL), 100 °C, 24 h, 90%.

With a synthetic route to **3.17** established, it proved necessary to prepare the compound on a larger scale as 0.5 – 1.0 g was required to explore the synthesis of the Zr and Cu JOF-MOFs. Aryl hydrogenation of **3.6** to **3.7** proved to be the limiting reaction and could not be conducted in greater than ~900 mg scale reactions due to the size of the available autoclaves required to pressurise the H_2 gas. Also, preparation of the Zeng catalyst **1.14** in multi-milligramme amounts is limited by cost. It was found too that carrying out hydrogenations close to a 1 g scale resulted in lower yields of all-*cis* hydrogenated products, presumably due to substrate solubilities and poorer catalysts dispersions with higher catalyst loadings. The aryl hydrogenation of the **3.6** was carried

out in several autoclaves in parallel and after multiple 200 – 950 mg scale reactions ~1.6g of **3.7** was generated. This was then progressed progressively, in small batches, through the DIBAL reduction, bromination, ether formation, and hydrolysis sequence to generate over ~1.1 g of the JOF strut **3.17**. JOF-MOF preparations did prove successful, as discussed in section 3.41 and 3.42, although initial experiments were hampered by the poor solubility of this strut.

It is a feature of pentafluoro Janus cyclohexanes that they have poor solubility in both organic and aqueous solvents. This is due to the five *cis*-fluorines on the cyclohexane ring, although inducing polarity, they retain a hydrophobicity, and have a tendency to self-aggregate rather than dissolve (polar hydrophobicity).[143]

The St Andrews research group recently reported on the gas phase, solution, and solid state conformation of all-*cis* 1,3,5-trifluorocylcohexane **3.18**. In the solution and gas phases the three C-F bonds adopt the all-equatorial conformation (**3.18$_{eq}$**), and it was calculated that this conformation is favoured in the gas phase by 3.55 kcal mol^{-1}.[144] In the solid state however, the three C-F bonds adopt the tri-axial conformation (**3.18$_{ax}$**) despite this being the higher energy structure. This is shown most clearly in the X-ray derived structure in Figure 3.10. In order to rationalise this, it was demonstrated by theory calculations that the energy gained in condensing three molecules of **3.18** together in the gas phase, is very significantly higher (16.7 kcal mol^{-1}) when the polar triaxial conformers (**3.18$_{ax}$**) are brought together. Electrostatic interactions between molecules of **3.18** are much stronger in the more polar triaxial rather than the tri-equatorial conformation.[144] Therefore **3.18** and presumably functionalised derivatives will be more soluble in solution (tri-equatorial conformation) but, they should adopt the polar triaxial conformations in condensed solid phases due to the strong dipole associated with triaxial fluorines.

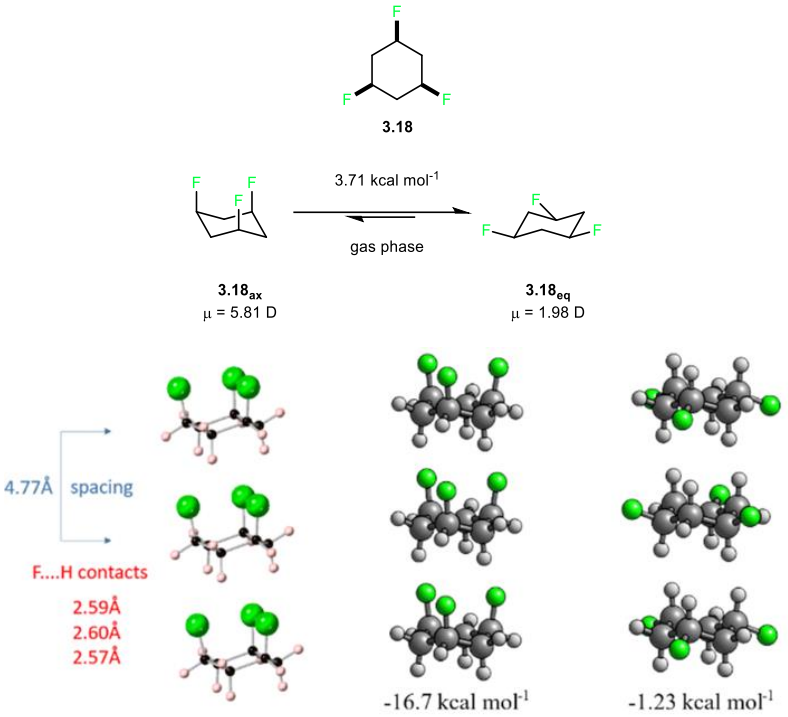

Figure 3.10: Equilibrium energies, X-ray structure (left hand side images – showing three molecules) and computational analysis indicating the energy gained from condensation of tri-axial and tri-equatorial conformers of **3.18** in the gas phase.[144]

It became an objective therefor to prepare alkyl bromide **3.23** such that it could be progressed in a similar manner to carboxylic acid **3.25** as a candidate JOF strut. The synthetic route to the required intermediate alkyl bromide **3.23** is shown in Scheme 3.6.[35,54]

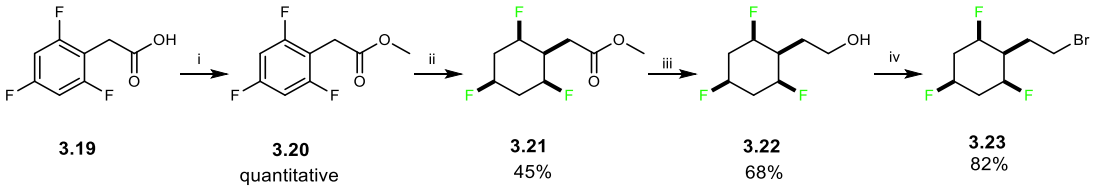

Scheme 3.6: Synthetic route to alkyl bromide **3.23**. i: **3.19** (22.1 mmol), MeOH (40 mL), HCl (2M, 1 mL), reflux, 24 h, quantitative. ii: **3.20** (13.96 mmol), Rh-CAAC-COD-Cl **1.14** (2 mol%), 4Å MS (24 g), silica (6 g), hexane (120 mL), H_2 (50 bar), r.t., 3 days, 45%. iii: **3.21** (6.18 mmol), THF (30 mL), DIBALH (2.2 eq), 0 °C-r.t., 16 h, 68%. iv: **3.22** (4.144 mmol), CH_3CN (40 mL), PPh_3 (8.7 mmol, 2.1 eq), CBr_4 (8.7 mmol, 2.1 eq), r.t., 24 h, 82%.

In order to make sufficient material to progress towards this new class of strut, the aryl hydrogenation reaction, converting **3.20** to **3.21**, was carried out batchwise on a 285 mg scale. The products from ten reactions of this scale were combined for a single work

up and purification. It was notable that defluorinated side products were less obvious here when compared to that found more generally in pentafluoro aryl hydrogenations and thus reactions could be left for up to 3 days with no significant defluorination. After this the DIBAL reaction was undertaken to produce **3.22** in good yields, and an Appel reaction delivered the key intermediate **3.23** in good yields.

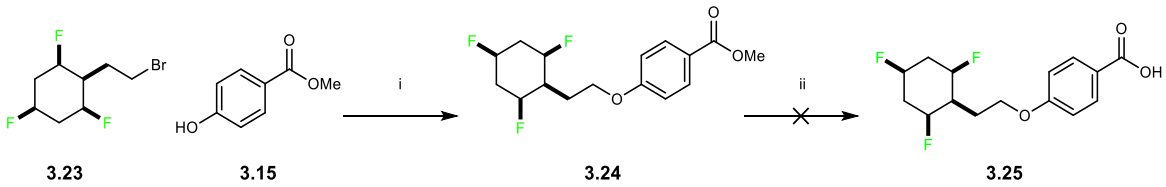

Scheme 3.7: Synthetic route to **3.25** i: **3.23** (1 eq), **3.15** (1.2 eq), Cs_2CO_3 (1.5 eq), DMF (10 mL), 70 °C, 24 h, 72%. ii: **3.24** (1 eq), HCl (6 M, 30 mL), THF (10 mL), 100 °C, 24 h, decomposition.

The alkyl bromide **3.23** was reacted with methyl 4-hydroxybenzoate (**3.15**) in the presence of base, to successfully prepare the trifluoro Janus carboxylic ester **3.24**. However, during initial attempts to hydrolyse **3.24** substantial decomposition was observed (Scheme 3.7).[54]

Table 3.1: Reaction conditions for hydrolysis of **3.24**

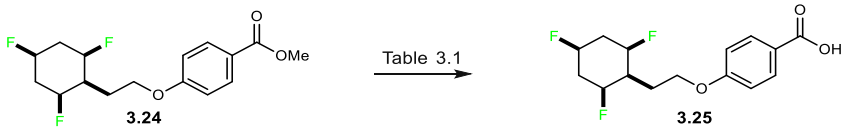

Entry	Reagents	Solvent	Temperature	Reaction length	Yield **3.25**
1	HCl (6 M)	-	100 °C	16 h	-
2	LiOH•H_2O (2.95 eq)	THF	0 °C	3 h	-
3	LiOH•H_2O (3.5 eq)	THF	0 - 20 °C	28 h	-
4	LiOH•H_2O (4 eq)	THF	50 °C	16 h	-
5	NaI (3 eq), TMSCl (3 eq)	MeCN	50 °C	35 h	55%

The trifluoro Janus cyclohexane motif was found to be unstable in the presence of strong acids over 2M HCl. Therefore, a protocol adapted from Kuntz *et al.* involving lithium hydroxide (pK_a = 14.4) in varying equivalents was trialled to attempt to generate

the hydrolysed product **3.25** (Table 3.1).[145] Low equivalents of lithium hydroxide resulted in no reaction, and when this was increased to 4 eq, NMR revealed some product formation (conversions below 20%), however the ester $OC\underline{H}_3$ peak at 3.89 ppm was still present after 24 hours, indicating a low conversion.

Subsequently, conditions were found in a 2022 patent, detailing the use NaI and trimethylsilyl chloride (TMSCl) to convert an ester to a carboxylic ester.[146] After addition of both reagents and once the reaction had gone to completion, the reaction mixture was cooled, and the product silyl ester was hydrolysed by the addition of water, to the corresponding carboxylic acid. After ether extraction and work up it was found that the carboxylic acid was not fully water soluble and therefore it was extracted into sodium bicarbonate solution while the ether layer contained the unreacted ester **3.24**. However, a significant amount of product was also retained in the ether layer. Pure carboxylic acid **3.25** was finally obtained after acidification of the bicarbonate solution and then filtering the product. Lyophilization of the final product was necessary to remove excess water, which resulted in dry and pure **3.25**, although the yield was modest.

Having successfully prepared the two candidate JOF struts in sufficient amounts, each exceeding ~500 mg, the next step was to determine crystal structures to provide insights into their supramolecular packing arrangements. Crystals were obtained (Figure 3.11) using a two-phase solvent system for crystallization. An inner reservoir of acetone in which the material was dissolved in was placed in and exposed to an outer layer of methanol. The methanol was left to slowly diffuse into the acetone solution, to help with the formation of crystals. Suitable crystals were then submitted for X-ray diffraction.

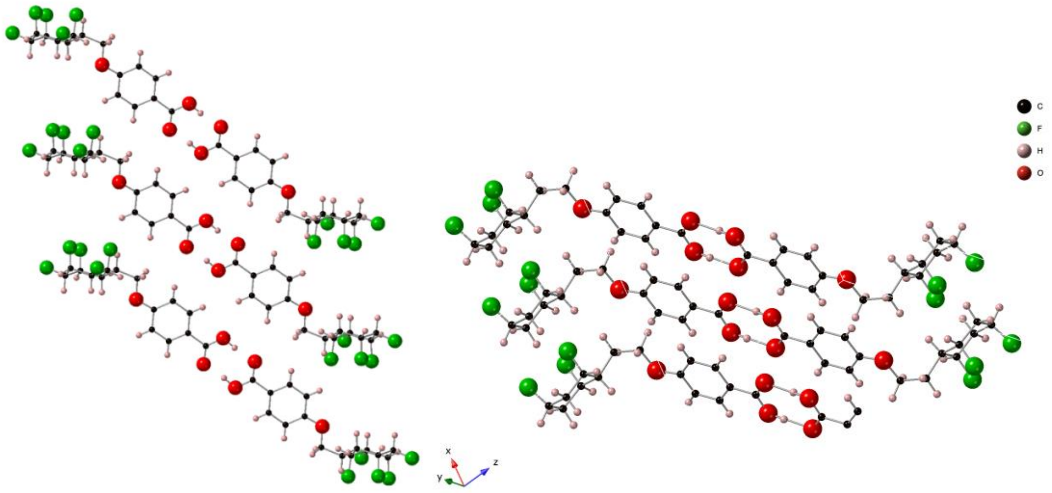

Figure 3.11: Crystal structure of pentafluoro JOF strut **3.17** (left)and trifluoro JOF strut **3.25** (right).

The two X-ray structures clearly show the Janus rings stacking one on top of the other, as well as head-to-head hydrogen bonding between the carboxylic acid groups. Interestingly, these pentafluoro Janus systems stack directly on top of each other. They are not off-set as previously observed in other Janus cyclohexane systems. The shortest intermolecular H···F contact distance of 4.96 Å in the pentafluoro system **3.17**, is actually rather long relative to other systems. The carboxylic acid hydrogen bonding, H···O, distance is 1.63 Å which is typical for a hydrogen bond of this type.[147] The trifluoro system **3.25**, had the shortest H···F distance of 2.39 Å which is significantly closer than the pentafluoro system, **3.17** and the hydrogen bonding distance of the carboxylic acids, H···O, was slightly longer at 1.65 Å. Finally, in both crystal structures it should be noted that the paired Janus ring stacks, are oriented in opposite directions.

These two JOF struts were then progressed for the preparation of JOF-MOF assemblies (Dr. Romy Ettlinger and Russell Main). Specifically, there was a focus on complexing carboxylic acids **3.17** and **3.25** with zirconium nodes $Zr_6O_4(OH)_4(C_2O_2H_3)_6$ for the target JOF-MOFs.

3.4 JOF-MOF synthesis and analysis

3.41 Preliminary JOF-MOF synthesis

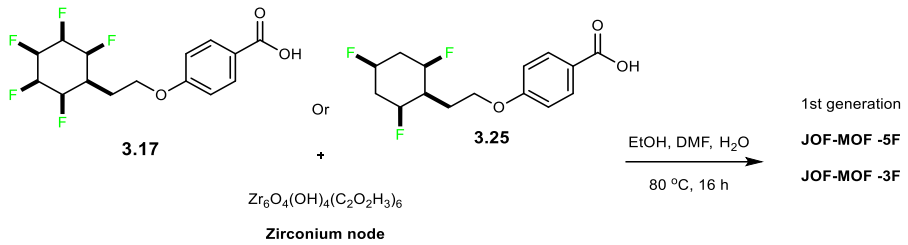

Scheme 3.8: Synthesis of 1st generation JOF-MOFs.

The basic procedure for MOF synthesis is to combine the sturt (organic linker) and metal salt in a solution, and then heat until the MOF products precipitate. Once the precipitate is filtered and washed, it is then dried.

Premade Zr nodes ($Zr_6O_4(OH)_4(OAc)_6$), were used to attempt an initial synthesis of a JOF-MOF (Scheme 3.8). These Zr nodes are water soluble and react very quickly with carboxylate linkers. For the synthesis of the JOF-MOF, the strut (~30 mg) **3.17** or **3.25**, was dissolved in EtOH (7 mL) and DMF (2 mL). $Zr_6O_4(OH)_4(OAc)_6$ (50 mg) was then dissolved in H_2O (1 mL) and the resultant solutions were then mixed and heated at 80 °C and left overnight in a glass vial. The resultant precipitate was found to be constituted of nanoparticles in which IR suggests good short-range order. As IR only shows first range order, the clear peaks indicated that the JOF-MOF looks qualitatively as it should. However, powder X-ray diffraction (PXRD) suggested these particles were very small and / or not very crystalline. Scanning electron microscopy (SEM) images revealed that the nanoparticles were clumped together (Figure 3.12 and Figure 3.13). The observed gaps between the particles are not pores in the material, as these would be too small to see by SEM (JEOL JSM-IT800 microscope) but are an artifact of solids “clumping together” as the nanoparticles dried. The powdered samples were prepared by depositing one drop of the nanoparticle suspension onto a copper tape. The images show the new 1st generation JOF-MOF product formed from the reaction between the Zr-nodes and the JOF-linkers. This reaction resulted in small, monodispersed particles, which appear as agglomerated larger blocks. Therefore, the images display only the

external surface and morphology of the particles, not their interior. To obtain interior imaging one would need transmission electron microscopy (TEM) and these 1st generation JOF-MOFs using the Zr-nodes were not analysed due to time constraints. These initial results indicated that more syntheses should be attempted as there is some evidence of the presence of a novel JOF-MOF. BET experiments (N_2 adsorption) were then conducted to assess the porosity of the new materials.

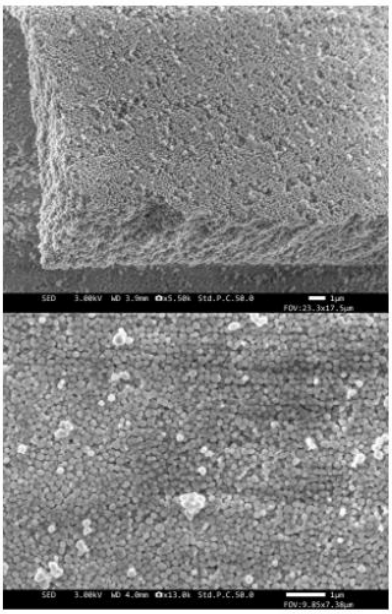

→ 189 ± 32 nm

Figure 3.12: SEM image of 1st generation JOF-MOF -5F indicating porosity.

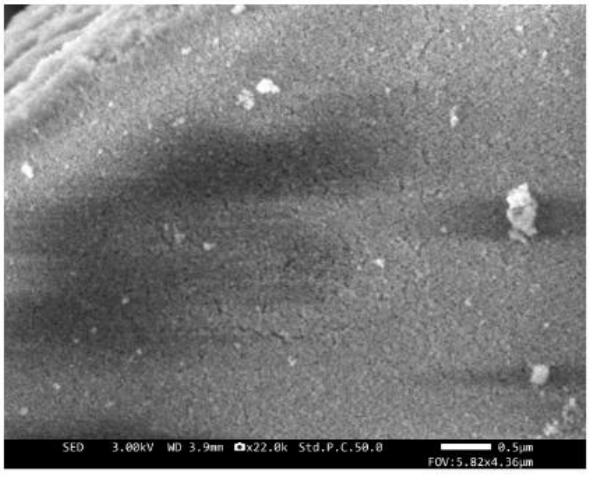

→ 25 ± 4 nm

Figure 3.13: SEM image of 1st generation JOF-MOF -3F indicating porosity.

In an effort to improve the particle size and crystallinity of the JOF-MOF products, the conditions were modified by changing the concentrations of the reagents used in the reaction and exploring the reaction temperature. The reaction did not take place at room temperature, and ZrO_2 forms when the reactions were conducted above 120 °C, confirmed via PXRD analysis.

Ostwald ripening is a method in which the already formed JOF-MOF crystals are left in solution for prolonged periods of time and whereby the crystals ripen and grow. This phenomenon occurs in systems where smaller particles dissolve and redeposit onto larger particles. Therefore, in the context of MOF synthesis, Ostwald ripening can influence the growth and size distribution of MOF crystals over time. The process is governed by the principle that smaller particles have higher surface energies compared to larger ones. This higher energy makes them less stable and more soluble. As the smaller MOF particles dissolve, the ions, or molecules in solution can migrate and attach to larger MOF particles causing the larger particles to grow at the expense of the smaller ones. Adjusting parameters such as temperature, concentration, and the presence of modulators or inhibitors can help control the rate of Ostwald ripening, and consequently, the final characteristics of the MOF. Three different solutions were used to explore Ostwald ripening of the JOF-MOFs: water, DMF, and a water / DMF mixture. Solutions were left to mature for several weeks. Additionally, a seed solution with premade nanoparticles was used. However, in this event there was little success in improving the quality of the product JOF-MOFs.

The porosity of the single crystals of the two JOF struts **3.17** and **3.25** were evaluated using N_2 adsorption isotherms. These were recorded on a Micrometrics Tristar ii Surface Area and Porosity instrument. In each case the samples were added to a frit tube and activated *in vacuo* (150 °C, ~3 x 10 – 5 mbar, 16 h) prior to the measurement to ensure no solvent was still in the pores of the sample. The values were compared to the two 1^{st} generation JOF-MOFs (1^{st} gen JOF-MOF -5F and 1^{st} gen JOF-MOF -3F) and it was observed that there was an increase in porosity of new JOF-MOFs relative to the initial JOF struts. The synthetic pentafluoro JOF strut, **3.17**, has a porosity of 10 m^2g^{-1} and the

trifluoro JOF strut, **3.25**, has a porosity of 9 m^2g^{-1}. So, these were essentially similar. When the 1st generation JOF-MOFs were formed there is a clear increase in porosity by approximately 100% (Figure 3.14).

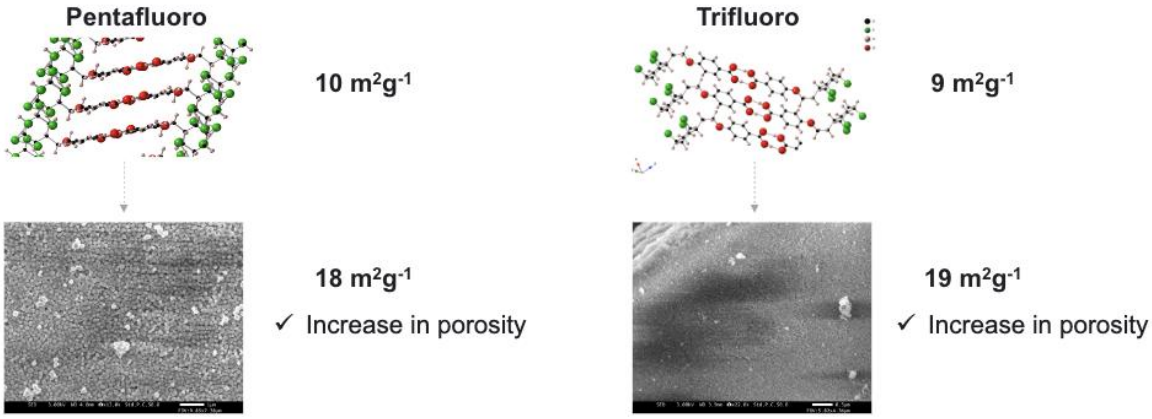

Figure 3.14: BET gas uptake volumes of the struts and then the 1st generation JOF-MOF materials.

3.42 New strategy: Strut replacement from MOF-808

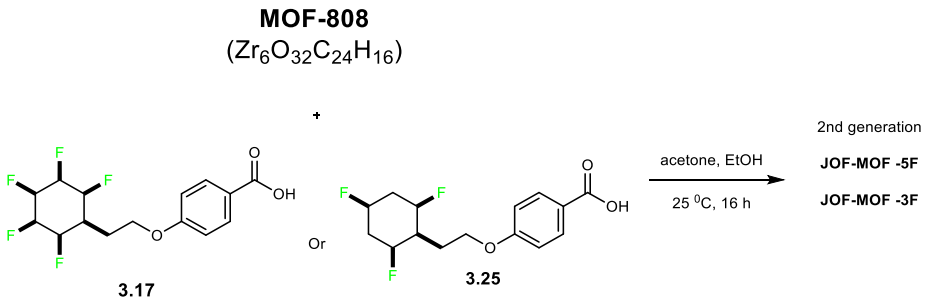

Scheme 3.9: Post-synthetic modification of MOF-808 to produce 2nd generation JOF-MOFs.

A new approach to a JOF-MOF synthesis set out to replace struts in MOF-808 with the new struts to make a more uniform JOF-MOF (Scheme 3.9). The approach began with the synthesis of Zr_6-oxoclusters (denoted as Zr-nodes, $Zr_6O_4(OH)_4(C_2O_2H_3)_6$) using the approach of Dai *et al.*[148] Accordingly a solution of the Zr-nodes (0.6 g) in water (2.5 mL) and formic acid (1.5 mL) was stirred at 25 °C. Subsequently, 1,3,5-BTC (150 mg) was added, and the mixture continued to stir for 24 h. The resultant white precipitate was separated by centrifugation (14500 rpm, 15 min) and washed with water (1x) and ethanol (2x). The resultant MOF-808 was redispersed in EtOH to a concentration of 15.3 mg/mL.

For the post-synthetic strut exchange, MOF-808 (15 mg, 1 mL) was re-dispersed in a stock-solution, containing **3.17** (11 mg) or **3.25** (15 mg) in acetone (1 mL). The mixture was left to exchange overnight at 25 °C. The resultant solid was separated via centrifugation and washed with acetone. The two isolated 2nd generation JOF-MOFs were partially dried for analysis and redispersed in EtOH. This redispersion turned out to be less favourable when compared to pure MOF-808. This is an indication that the nanoparticles have been modified, producing 2nd generation JOF-MOFs.

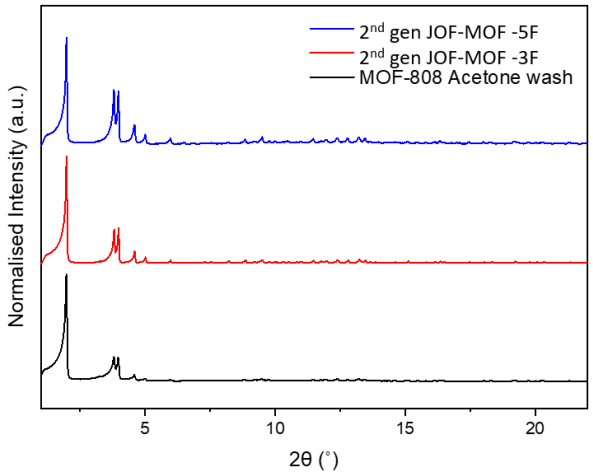

Figure 3.15: PXRD patterns (Mo radiation) of pristine MOF-808 (black trace) and the two JOF-MOFs: 2nd generation JOF-MOF -5F (blue trace) and 2nd generation JOF-MOF -3F (red trace).

The PXRD pattern of the strut modified MOF powders, compared with a reference sample of MOF-808 are illustrated in (Figure 3.15). The compounds were subject to only an acetone wash and show no sign of crystalline impurity or crystallinity loss. This is a sign that the new compounds are pure JOF-MOFs and not some kind of impurity. There is a decrease in relative intensity of the first peak of the two 2nd generation JOF-MOFs (blue and red). This decrease in intensity can attributed to molecules in the pore of the new JOF-MOF. This is shown in Figure 3.15 via the second set of peaks being larger in the blue and red spectra than in the black. This is because the spectra are normalized on the first peak.

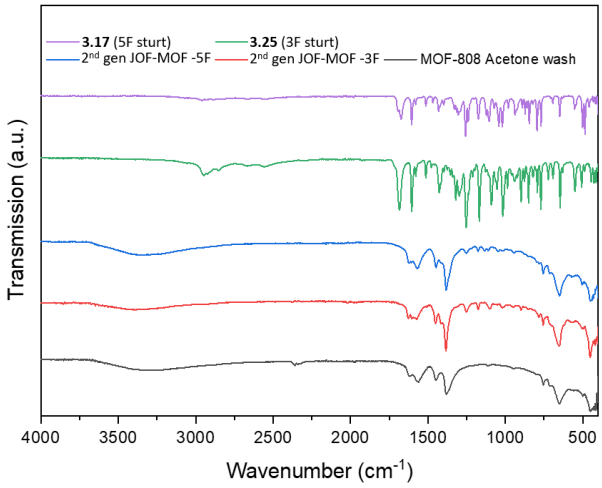

Figure 3.16: FTIR spectra of **3.17** (-5F strut), **3.25** (-3F strut), pristine MOF-808, and the 2nd generation JOF-MOFs.

FTIR shows the presence of additional low intensity bands in the region 800 cm^{-1} – 1250 cm^{-1} of **3.25** and **3.17** in the respective samples alongside the MOF bands (Figure 3.16). The bands associated with the carboxylic acid group of the Janus struts at 1680 cm^{-1} will shift to the carboxylate range (1610cm^{-1} - 1550cm^{-1}) within these MOFs and are not distinguishable from the dominating carboxylate stretches associated with the 1,3,5-benzene-tricarboxylate struts. The absence of the struts free carboxylic acid group peaks at 1680 cm^{-1} in both the -5F and -3F JOF-MOF indicate their exchange into the JOF-MOF.

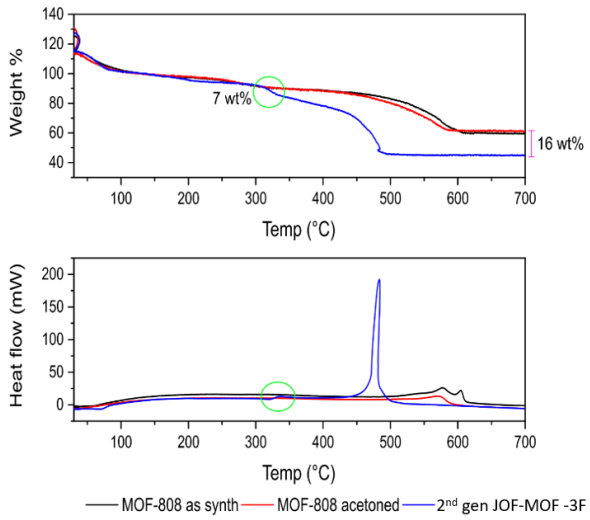

Figure 3.17: TGA data of pristine and modified MOF-808 with **3.25** forming a 2nd generation JOF-MOF -3F (heating rate of 5°C/min).

Thermogravimetric analysis (TGA) for the 2nd generation JOF-MOF -3F shows that in total there was 16 wt% loading of the JOF into the new JOF-MOF (Figure 3.17). A new mass loss can be observed at 340 °C corresponding to 7 wt% and the remaining 9 wt% occurs along with the JOF-MOF decomposition at 450 °C. The decomposition can be seen via the large peak in the bottom graph (Figure 3.17). Compared to the pristine MOF-808 sample and MOF-808 after acetone wash, the JOF-MOF decomposition temperature at 450 °C is lower by around 100 °C (from ~550 °C). The top graphs shows when the 2nd generation JOF-MOF -3F begins to decompose via the green circle, the full decomposition does not occur until 450 °C. The bottom graph indicates this as well but as a measure of heat flow, therefor once there is a spike the compounds have decomposed.

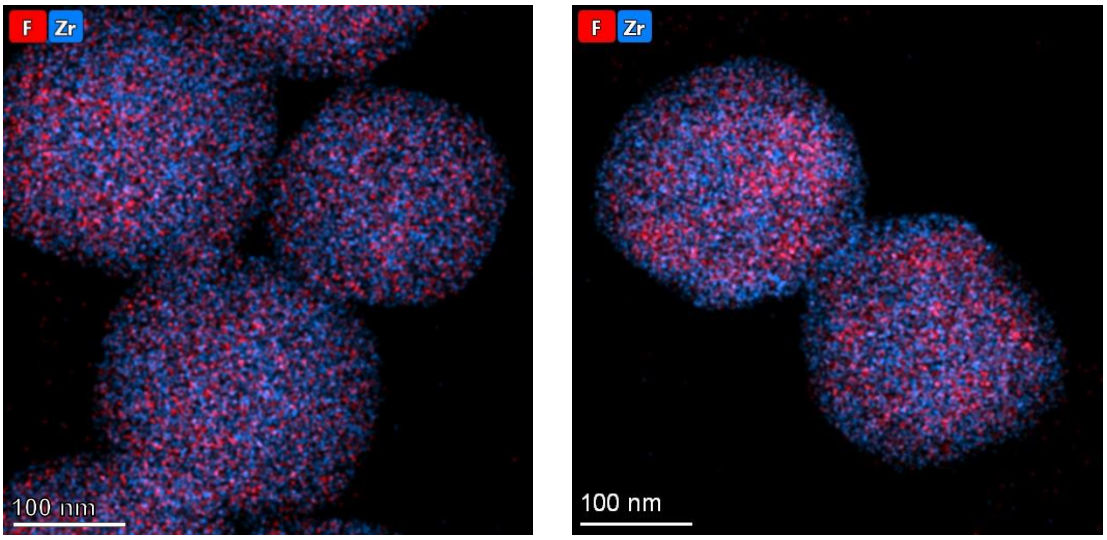

Figure 3.18: TEM analysis results of 2nd generation JOF-MOFs. Left: overlay of the elemental composition map of F (red) and Zr (blue) of 2nd generation JOF-MOF -3F. Right: overlay of the elemental composition map of F (red) and Zr (blue) of 2nd generation JOF-MOF -5F.

Finally, samples of the JOF-MOFs were investigated by transmission electron microscopy (TEM) to explore the presence of fluorine in the JOF-MOF-nanoparticles. MOF materials often tend to be highly electron beam sensitive, however, TEM analysis revealed that the new JOF-MOF nanoparticles were significantly more beam stable than pristine MOF-808 samples, and TEM images could be obtained (Figure 3.18). TEM images of MOF-808 do exist, but the MOFs are prone to shrinking due to the large pore

sizes of the MOF. The electron beam will react with the sample shrinking the overall MOF. However, with the 2nd generation JOF-MOFs the functionalization of the compound is more stable, and the pores are less susceptible to collapsing and therefor the molecule does not shrink, and good TEM images were acquired. In the case of 2nd generation JOF-MOF -3F an elemental map of fluorine (red) was recorded. Fluorine is uniformly distributed throughout the modified MOF nanoparticles suggesting that the Janus struts (**3.25**) are bound within the internal pores of the MOF as well as in the external surface. For the 2nd generation JOF-MOF -5F the elemental map of fluorine (red) reveals its presence mainly inside the pores of the modified nanoparticles but only very little on the external surface. This is due to the solubility of the penta-F vs the tri-F JOF-MOF. Compound **3.17** tended to detach from the JOF-MOF during washes which may indicate why the surface of 2nd generation JOF-MOF -5F did not have fluorine present in the TEM image. Collectively these analytical techniques indicate that the JOF struts, can be successfully exchanged into MOF-808, an outcome which provides a first step towards the syntheses of JOF-MOFs.

3.5 Conclusions

The synthesise of the two novel JOF struts **3.17** and **3.25** was achieved. The structure and packing arrangements were confirmed by single crystal X-ray structure analysis. These molecules possess carboxylic acid linkers on one end and either the traditional pentafluoro Janus ring or trifluorinated Janus ring on the other. These two aspects allow for this JOF strut to connect to metal centres through the carboxylic acid groups to generate JOF-MOFs anticipating that the cyclohexane interactions might provide a further degree of supramolecular assembly through interactions of the H-F faces of the Janus rings.

The preliminary findings using a de-nova synthesis shared by our collaborators have shown a promising increase in porosity, with the 1st generation JOF-MOF molecules exhibiting approximately twice the porosity compared to their counterparts when the JOF struts were isolated single crystals.

The 2nd generation JOF-MOFs were developed via exchange synthesis using premade MOF-808. This resulted in multiple bits of analysis confirming the new class of organic frameworks. While these findings represent early results, they open the door for further experimentation to improve porosity enhancements. These materials are the first examples of JOF-MOF type suprastructures. Such materials should have unique characteristics and applications.

4: Janus cyclohexanes, a candidate motif for memory storage

4.1 Introduction

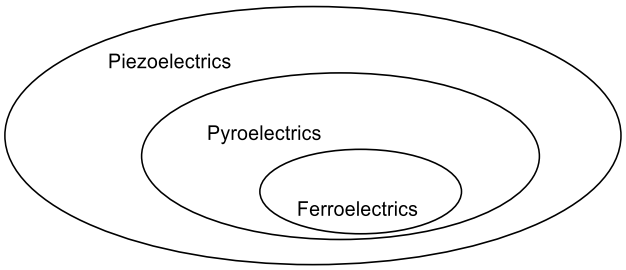

Figure 4.1: The three subsets of electronics

Computers store memory by simplifying data into binary 1's and 0's. Computer memory that can retain its information even when the computer itself is switched off needs to be non-volitile.[149] Non-volatile in this instance refers to the device being able to maintain and store the information when no power is applied to the device. Ferroelectric random-access memory (RAM) has emerged as a dominant memory storage technology where information is stored as ferroelectric polarization.[149] Ferroelectricity occurs in materials that possess a spontaneous electric polarization that can be reversed by the application of an electric field and maintained in the new polarization.[150] Ferroelectric materials are a subcategory of pyroelectric materials which themselves are a subset of piezoelectric materials (Figure 4.1). Piezoelectricity is the phenomenon whereby an applied stress results in the development of an electric charge across a material or conversely where application of an electric field results in a strain and physical distortion of a material. Only polar, non-centrosymmetric, crystals are able to exhibit these properties. The polarization types of these compounds are illustrated in Figure 4.2, and in the case of ferroelectrics there is the formation of a hysteresis loop. A hysteresis loop in the context of polarization in an electric field represents the relationship between the electric field applied to a ferroelectric material and its resulting polarization, illustrating how the polarization varies with the field and shows different paths for increasing and decreasing fields due to the material's history.

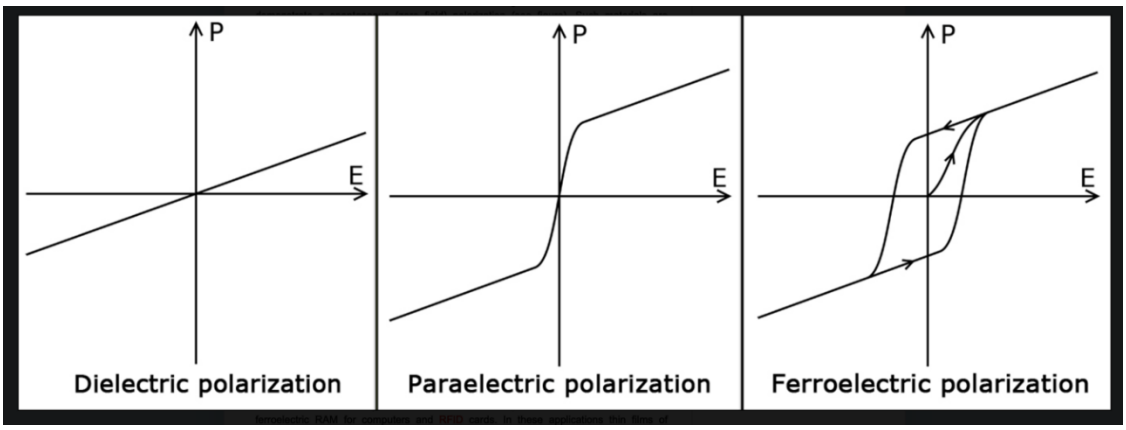

Figure 4.2: Polarization types where P is the polarization and E is the applied electric field.

The hysteresis loop shown in the case of ferroelectric materials is caused from the direction of the spontaneous polarization being reversed by the applied electric field. To be a ferroelectric material, it must exhibit a permanent spontaneously generated electric polarisation, with the direction of polarization being able to flip responding to the direction of the applied electric field. This is demonstrated above in the polarisation-electric field hysteresis loop. Figure 4.3 maps each position A – D where the polarisation changes to generate this hysteresis loop.[151] Under a positive electric field applied in a given direction, the dipoles of the ferroelectric are directed in the same direction leading to a macroscopic saturation polarisation (P_S) at position A. When the electric field is removed entirely (position B), the majority of dipoles remain parallel to each other, giving rise to a remanent polarisation (P_r). Then the electric field is applied negatively, and the dipoles gradually reorientate to the point (position C) that they cancel each other out and an equal number of oppositely directed dipoles is present. At position C, the electric field results in zero net polarisation and is called the coercive field (E_C). Position D corresponds to a negative saturation polarisation ($-P_S$). The maximum negative saturation polarisation is then reached, and the diploes are aligned to the direction of the applied negative electric field. Finally, the area enclosed by the *P-E* hysteresis loop yields a measure of the energy required to achieve switching. The ability to switch between 0 and 1 logical states allows for applications in memory storage technologies.[151]

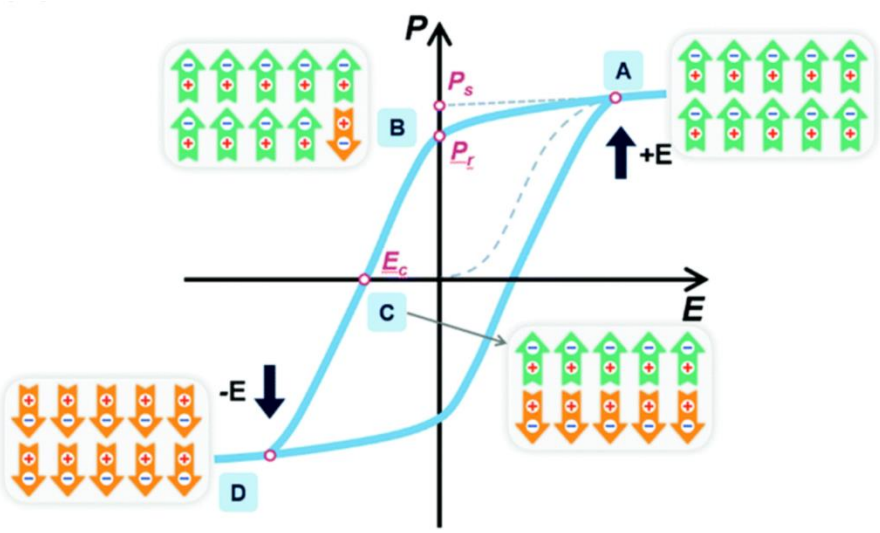

Figure 4.3: Representation of a hysteresis loop for polarisation (P) verses electric field (E) from Liu *et al*.[151]

Typical ferroelectric materials are often inorganic compounds and oxide-based ceramics, such as $BaTiO_3$, $PbTiO_3$, or $PbZr/TiO_3$.[151] These materials contain toxic metals and require high processing temperatures.[151,152] The development of organic ferroelectric materials offers new and desirable features as an alternative to conventional inorganic ferroelectrics.[151] Organic ferroelectrics can be cast onto films and other devices more easily than traditional inorganics with low-cost, and they are more environmentally compatible in their synthesis processes.[152] However, to date, there has been little research into organic ferroelectrics. Supramolecular chemistry has proven an effective method for designing high-performance ferroelectrics in the solid-state.[151,152] Ferroelectricity in these materials arises from molecular dipoles and the changing of the direction of these dipoles by an applied electric field. Some organic ferroelectrics that have been studied are illustrated in Figure 4.4.

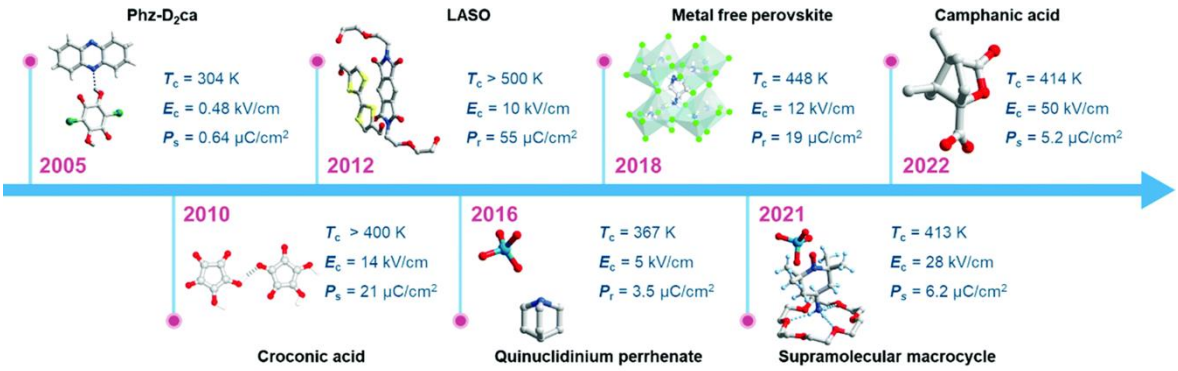

Figure 4.4: Historical timeline for the development of organic ferroelectrics from Liu *et al*.[151,153–159]

Ferroelectric materials with usable properties are judged to possess several important characteristics.[160,161] They should have a high spontaneous polarisation (P_s), a high saturation polarisation (P_{sat}) and a high dielectric constant (ε_r), as well as low dielectric loss, and a Curie temperature (T_c) near or above room temperature. The Curie temperature (T_c) is the point where materials lose their permanent magnetic/electric properties, whereby the dielectric loss is the amount of electromagnetic energy a dielectric material dissipates. Polyvinylidene difluoride (PVDF)-based ferroelectric polymers were the first-generation of organic ferroelectric materials and they have been known for over 20 years.[151] In general the useful organic ferroelectrics have been polymers[151] and the number of ferroelectric materials derived from low molecular weight organics is few. Some of these, developed since 2005, are shown in Figure 4.4.[151,153–159] In this arena, weak intermolecular interactions such as halogen bonding are judged to be able to strongly influence the property of ferroelectric materials, and in the context of this research, electrostatic interactions between Janus cyclohexanes may offer a route into ordering ferroelectric materials such that they can act as memory storage devices.[162]

Dr. Peer Kirsch (Merck & University of Darmstadt) has been developing organic ferroelectric materials for memory storage devices, exploring conductance switching in liquid crystal-inspired self-assembled monolayer junctions to achieve this goal.[163] This involved the development of a ferroelectric tunnel junction (FTJ).[163] Such a device is based on a self-assembled monolayer (SAM) made of small functional molecules, that

order similarly to liquid crystals.[163] The SAM itself has a diameter of ~3.4 nm and requires to be highly uniform.[163] The structure of the SAM components give functionality to the FTJ via a conformationally flexible dipole that can be reversibly reorientated in an electric field. This allows for the SAM to act as an electrically switchable tunnel barrier.[163] Kirsch *et al.*'s materials are built on stacks of Al/Al_2O_3-/SAM/Pb/Ag.[163] The SAM precursor possess a dipole, and hence a switch for in-memory and neuromorphic computing architectures. A neuromorphic computing architecture is a computing design that emulates the neural structure and functioning of the human brain, using specialized hardware components like artificial neurons and synapses to achieve efficient, parallel, and adaptive information processing.[163–165] The dipole of these molecules is created by the orientated polarity of the 2,3-difluoro aryl motif in the organic framework of the SAM precursor.

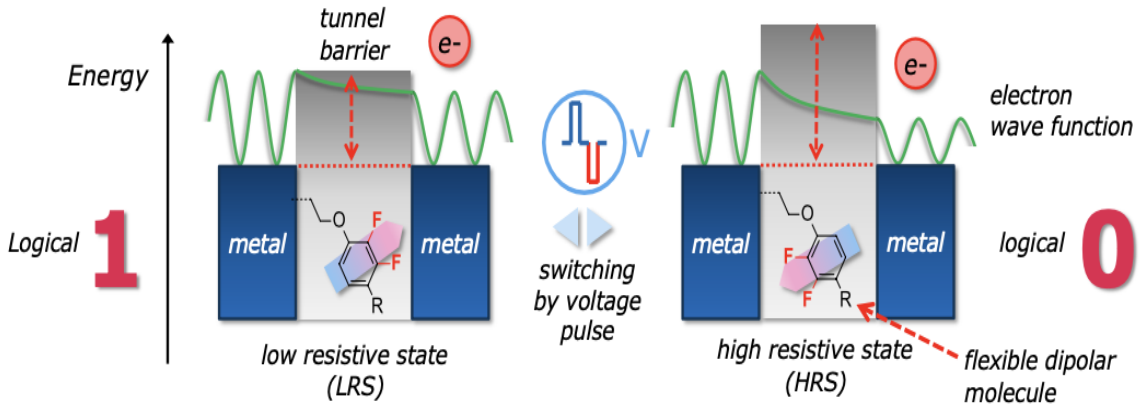

Figure 4.5: Organic memory storage device. Diagram illustrates a logical 1 state, and a logical 0 state where switching occurs by voltage pulse. Figure taken from Kirsch *et al.*[163]

When an electric field is applied, the molecules align their dipole moments in response. This alignment remains stable even after the external field is removed, "holding" an orientated dipole (Figure 4.5). Application of a voltage pulse then causes the molecule to rotate, effectively reversing its dipole orientation. The original orientation of the dipole can be designated as representing a logical 0 state, and the reversed orientation as a logical 1 state, or vice versa, depending on the convention adopted. This binary system of dipole orientations provides a fundamental mechanism for encoding information, where each molecule's state represents a unique bit of data. This

prototype represents a significant advance in organic ferroelectrics, achieving high-density data storage.

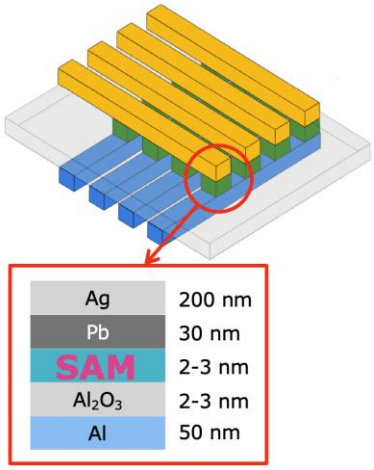

Figure 4.6: Crossbar array for memory storage taken from Kirsch *et al.*[163]

In order to construct a memory storage system, these molecules, often referred to as Self-Assembled Monolayer (SAM) precursors due to their ability to form organized layers through self-assembly, are arranged in a crossbar array structure consisting of perpendicular sets of parallel lines, allowing for dense molecular packing at the intersections of the grid as illustrated in Figure 4.6. By organizing the SAM precursors in such a fashion, it is possible to create a matrix of 'bits' where each intersection point in the array can independently hold a logical 1 or a logical 0 state. This configuration enables the storage of multiple bits of information, facilitating the construction of a memory device capable of storing and retrieving digital data. Through the careful manipulation of the electric field applied to these molecules, information can be written, stored, and read back by observing the orientation of the molecular dipoles at each point in the array, thereby realizing a compact and efficient memory storage system.[163]

4.2 Types of memory storage

The molecular memory storage systems anticipated here represent a new approach. Current memory storage uses a wide range of technologies, each with unique

mechanisms for storing and retrieving digital data. Typically, the main technology adopts solid-state drives (SSDs) and traditional hard disk drives (HDDs), as well as volatile and non-volatile memory types like Dynamic Random Access Memory (DRAM) and flash memory.[166–169]

SSDs use interconnected flash memory chips, which can retain information without power, meaning they are non-volatile. They provide advantages in terms of access, speed, and resistance to physical shock. The key principle involves using floating-gate transistors that trap electrons, thereby representing bits of data as either charged (logical 1) or uncharged (logical 0) states.[169]

HDDs, by contrast, employ a magnetic storage mechanism where data is stored on rotating disks with read / write heads floating above to read or modify the magnetic orientation that encode data.[167]

For system memory, DRAM is preferred, relying on cells composed of a capacitor and transistor to store bits. DRAM is volatile, meaning it can lose information and requires periodic refresh cycles to maintain the stored data.[168]

Flash memory, which is used in both USB drives and SSDs, stores data in an array of memory cells in a non-volatile manner, such that it does not require power to save data.[166]

The current selection between these memory storage technologies is driven by the consideration of speed, capacity, durability, and energy consumption, which directly influence the performance and efficiency of computing system extending from handheld devices to expansive data centres.

4.3 Aim: Organic SAM memory storage project

The appeal of using organic molecules for memory storage lies in their potential for enabling the production of flexible, lightweight, biodegradable electronics. Additionally,

the molecular-level control of properties offers pathways to devices with high storage densities and lower power consumption. The problems with the current technology include the usage of energy, the robustness of stored information over longer times, and its ability to resist corruption through tampering.[170] In this vein Dr. Peer Kirsch has begun to develop organic molecules to be used in conductance switching in liquid crystal-inspired SAM junctions.[163]

The initial SAM-based memory devices were composed of a liquid crystal like molecule **4.1** (Figure 4.7), designed to be inert during operation,[163] with no bond breaking, change in redox state, or electronic excitation when the memory device is in operation. These factors are necessary to minimize degradation and increase longevity of the resulting device.[163] Using this SAM precursor, a long chain terminated phosphonic acid was used to link to an alumina oxide layer above an aluminium surface. This was sandwiched between the top electrode, made of lead and silver (Figure 4.7).

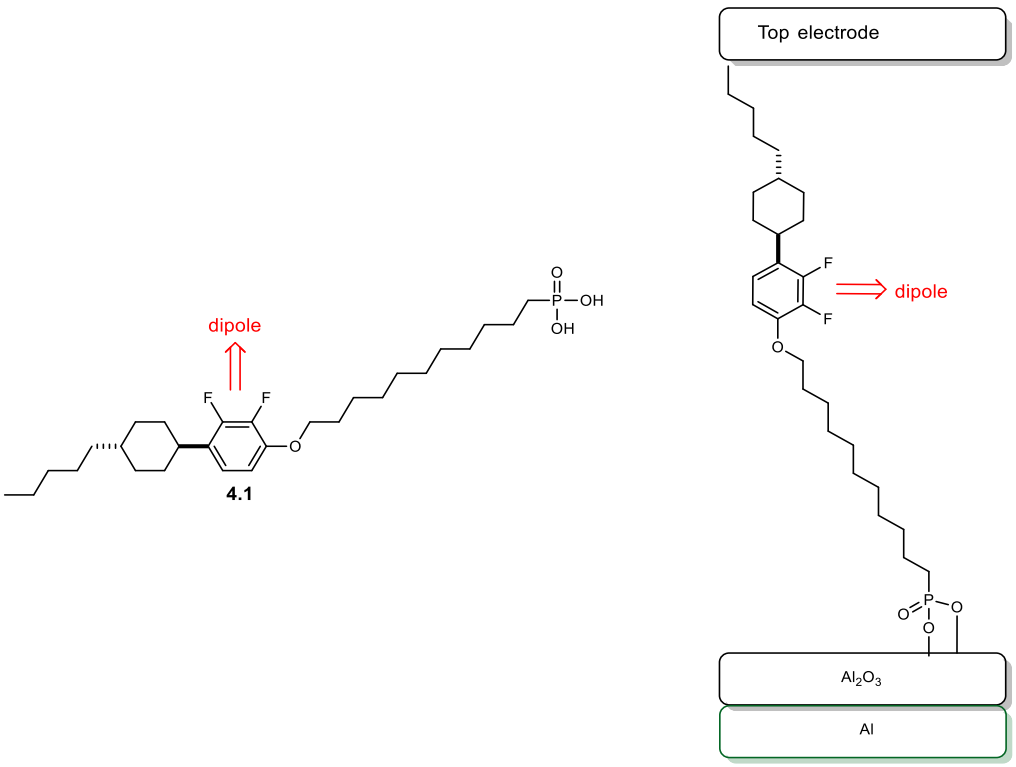

Figure 4.7: Left: First-generation SAM. Right: Image of SAM memory storage device highlighting the organic SAM and its dipole in red.

Initial results led to a requirement for a better understanding of the microscopic charge transport mechanism including the asymmetric nature of the partial rectification.[163] The rectification is the process by which an electrical device allows current to flow more easily in one direction than the other, this results in the magnitude of current for positive and negative applied voltages. Future applications could include resistive memories as well as components for neuromorphic and in-memory computing. With all this in mind, in this project the synthesis of two SAM memory storage precursors was initiated utilizing the Janus cyclohexane motif with its large molecular dipole.

4.4 Synthesis of Janus containing long chain phosphonic acid

4.41 Initial approaches

The Janus cyclohexane motif has a molecular dipole of ~6 Debye and presented an option to explore as a novel polar motif in the context of comparing its properties relative to the 2,3-difluoroaryl motif in **4.1**. The key attributes required for such a SAM precursor are a phosphonic acid attached to the Janus cyclohexane by a long hydrocarbon chain. With these structural requirements in mind **4.7** became a synthetic target and the proposed route is outlined in Scheme 4.1.

The route envisioned an Arbusov reaction on dibromodecane **4.3**, and then a phenolate substitution. Finally, the Janus cyclohexane will be introduced as an ether using a Zheng/Glorius aryl hydrogenation.

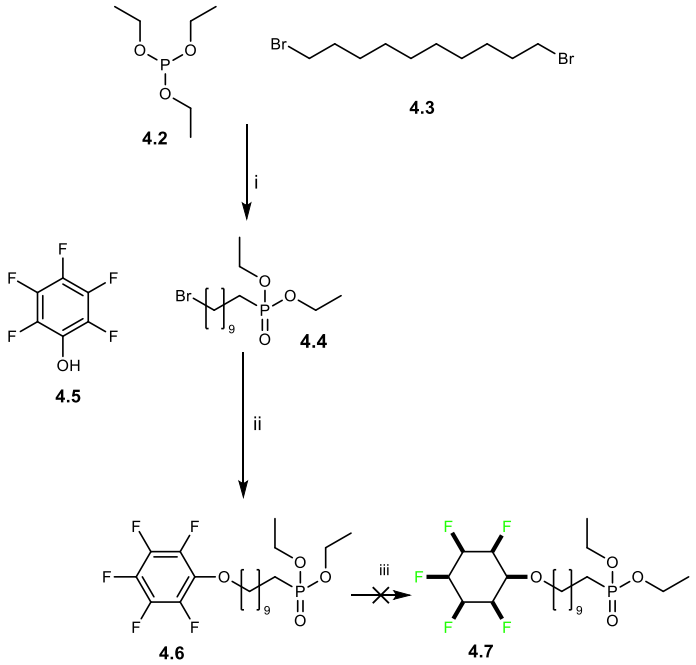

Scheme 4.1: Initial route to **4.7**. i: **4.2** (0.88 eq) and **4.3** (1 eq), 140 °C, 24 h, 80%. ii: Pentafluorophenol (1 eq), potassium carbonate (3 eq), acetonitrile (30 mL), **4.4** (1.2 eq), 90 °C, 18 h, 47%. iii: **4.6** (2.18 mmol), Rh-CAAC-COD-Cl **1.14** (2 mol%), 4Å MS (8 g), silica (4 g), hexane (40 mL), H_2 (50 bar), 50 °C, 2 d, starting material recovered.

The initial Arbuzov reaction had already been reported in literature.[171–173] This worked well, efficiently generating **4.4** which could be purified in a satisfactory manner in 80% yield, higher than that previously reported.[171–173]

Triethyl phosphite **4.2** was loaded at less than one equivalent to prevent double addition. The compound was purified via column chromatography in 50% ethyl acetate in hexane. Great care was taken to ensure that **4.4** was as pure as possible with no double addition or starting materials present and in the event, purification required a second column using the same conditions. The ^{1}H NMR is clearly consistent with **4.4** (Figure 4.8).[173]

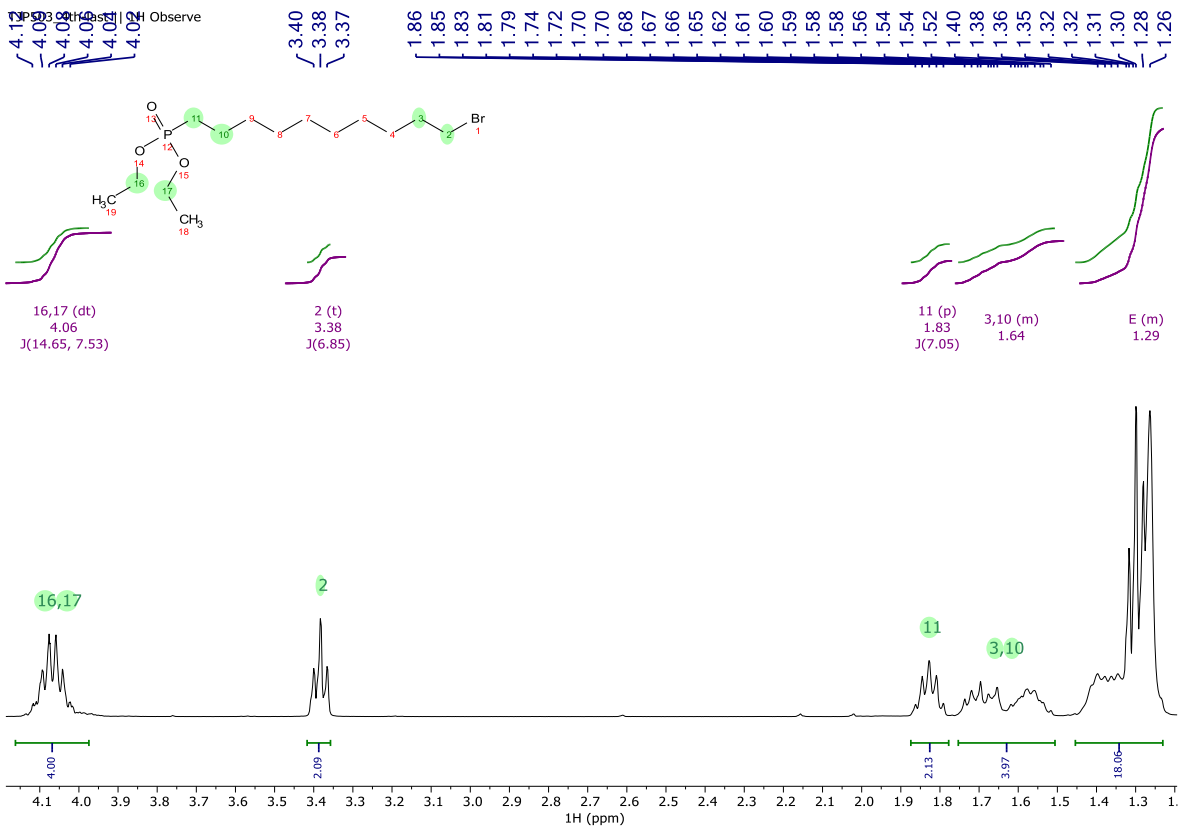

Figure 4.8: ^{1}H NMR of phosphonate **4.4**. The signals are assigned; ~4.1 ppm (H16 & H17); at ~3.4 ppm (H2); at ~1.8 ppm (H11); at ~1.6 ppm (H3 & H10); at ~1.3 ppm (H4-9, H18-19).

For the next step a phenolate substitution was conducted with potassium carbonate in acetonitrile, to generate **4.6**. The protocol was adapted from the literature involving deactivated aryl oxide nucleophiles.[174,175]

The substitution reaction to generate **4.6** was achieved in 47% yield. The reaction proved to be straight forward, and purification was achieved via a 1 – 50 % gradient of ethyl acetate in hexane, and the pure product was isolated.

Finally, the aryl hydrogenation was addressed. However, this reaction was unsuccessful. The reaction was attempted for 2 days although extended reaction times are known to promote dehydrofluorination. In the event the compound had not reacted at all, most likely due to the double substitution preventing the catalyst from coming into contact with the aromatic ring, or perhaps the polar phosphonate aggregating on the catalyst.

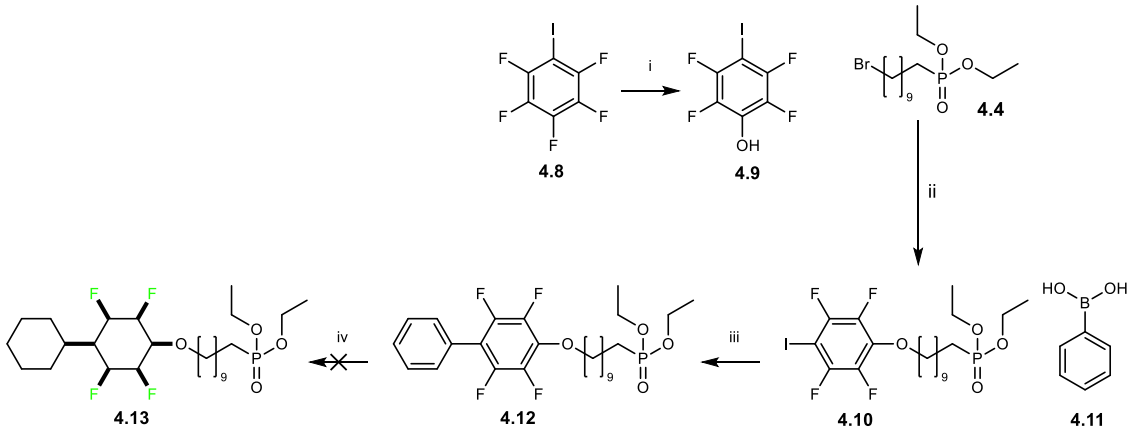

Scheme 4.2: Second approach to **4.13**. i: KOH (50 mmol, 2.5 eq), *tert*-Butanol (40 mL), iodopentafluorobenzene **4.8** (20 mmol, 1 eq), 90 °C, overnight, 67%. ii: NaI (1 eq), **4.4** (1.2 eq), acetone (10 mL), **4.9** (1 eq), K_2CO_3 (3 eq), toluene (20 mL), 88 °C, 16h, 25%. iii: **4.10** (1 eq), **4.11** (1.3 eq), K_2CO_3 (2 eq), tetrakis(triphenylphosphine)palladium(0) (8 mol%), THF/H_2O (3:1, 16 mL), 75 °C, 17 h, 79%. iv: **4.12** (0.19 mmol), Rh-CAAC-COD-Cl **1.14** (2 mol%), 4Å MS (800 mg), silica (400 mg), hexane (40 mL), H_2 (50 bar), 50 °C, 3 d, failed.

A new target, compound **4.13** was chosen as it had an accessible synthetic route (Scheme 4.2) whilst possessing the key facets envisaged for a SAM precursor. A new aspect involved generating **4.9** from **4.8** through an S_NAr reaction. This reaction[176,177] used *tert*-butanol as a solvent and the source of the nucleophile, with potassium hydroxide as a base. The reaction resulted in a purified *para / meta* product ratio of 10.3 : 1 (**4.9**). This high *para* selectivity was of interest and is investigated more fully for a range of substrates in Chapter 5. The *tert*-butyl ether intermediate was then conveniently deprotected to phenol (**4.9**) with concentrated HCl as illustrated in Scheme 4.3.

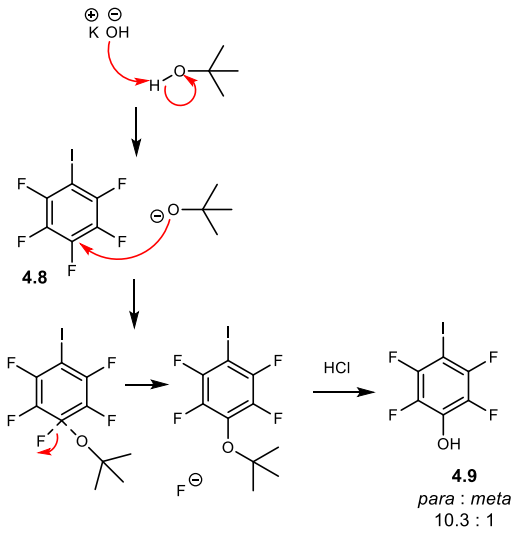

Scheme 4.3 S_NAr reaction and acidic deprotection to **4.9**.[178]

The Finkelstein reaction, developed in 1910 to promote substitution reactions, was adapted here for the reaction to generate **4.10** in step ii.[179,180] The substitution reaction was accelerated with NaI to generate an alkyliodide *in-situ*. The presence of the alkyliodide is supported by ^{1}H NMR where the terminal CH_2 group of phosphonate **4.4** shifts upfield from ~3.4 ppm, to ~3.2 ppm indicating the halogen exchange (Figure 4.9). Starting alkylbromide **4.4**, was still present in the reaction mixture, perhaps consistent with the relatively low yield of the reaction (~25%).

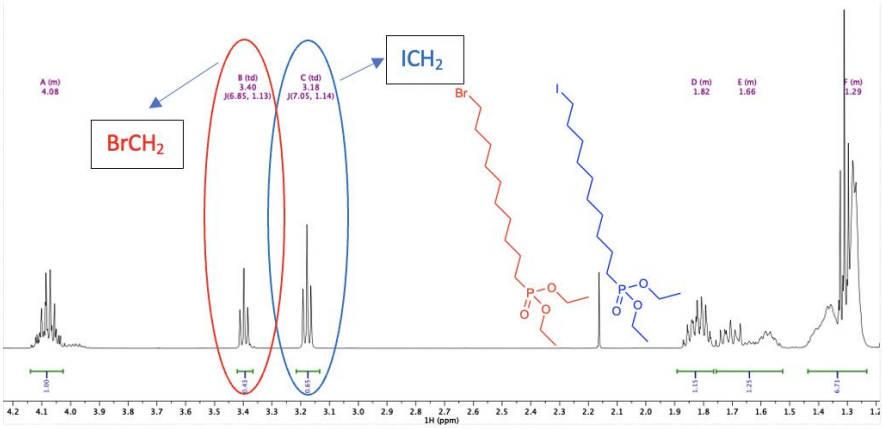

Figure 4.9: ^{1}H NMR of **4.4$_{iodide}$**, Finkelstein reaction Indicating the presence of the -CH_2I intermediate.

The next intermediate **4.12** was generated *via* a Suzuki cross-coupling reaction (Scheme 4.4). The palladium pre-catalyst provides the active Pd(0) species which undergoes

oxidative addition (OA) with **1** to develop complex **B**. Complex **C** then undergoes trans-metallation (TM) where the aryl ring of organoboron species **D** cross couples with the palladium(II) in complex **C** giving complex **E**. Finally, complex **E** undergoes a reductive elimination (RE) which yields the product and regenerates the catalyst in the cycle.[181–183] Product **4.12** was obtained in good yield and was purified in a straightforward manner by column chromatography.

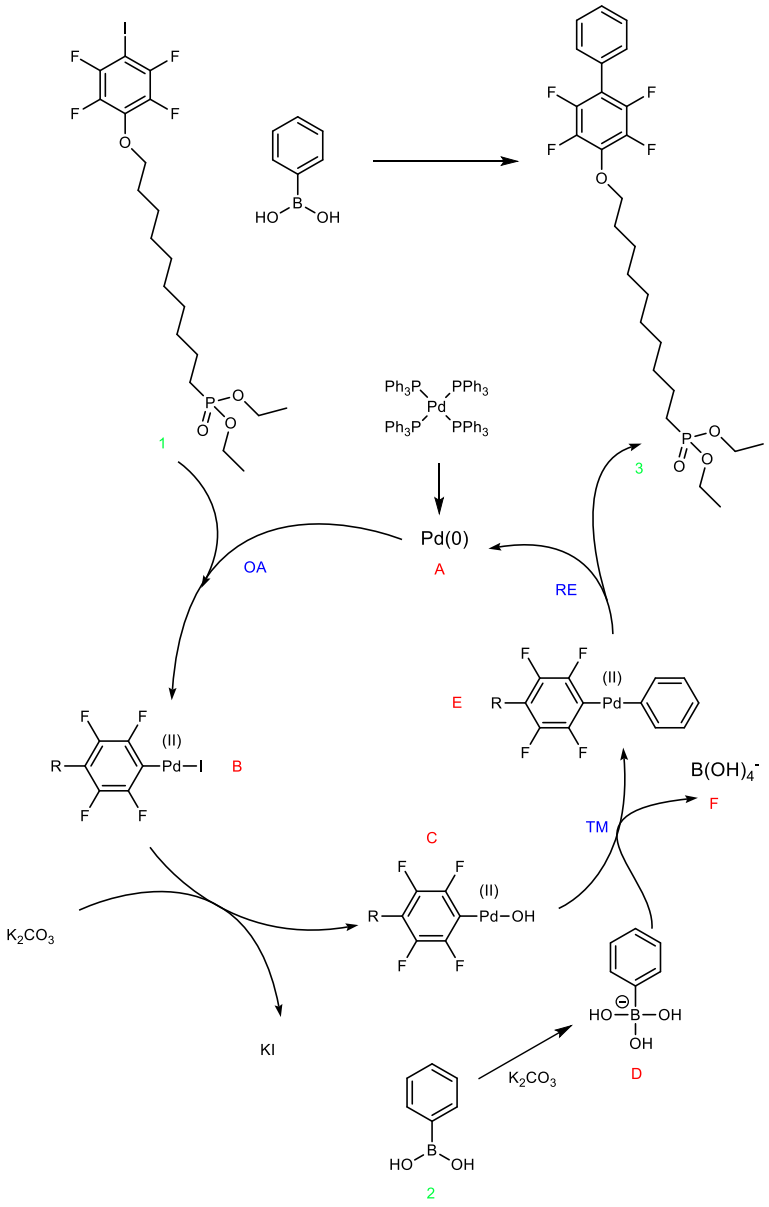

Scheme 4.4: Suzuki cross-coupling mechanism.

Despite numerous attempts and the application of various conditions, the total aryl hydrogenation reaction consistently failed to progress. This is perhaps due to the aryl ring directly attached to the fluorinated aromatic ring. The two aryl rings align inversely planar. Therefore, there may be a steric problem in locating these rings on the surface of the catalyst. Again, there was no obvious defluorination, but rather just recovery of the starting material **4.12** and the aryl hydrogenation did not progress.

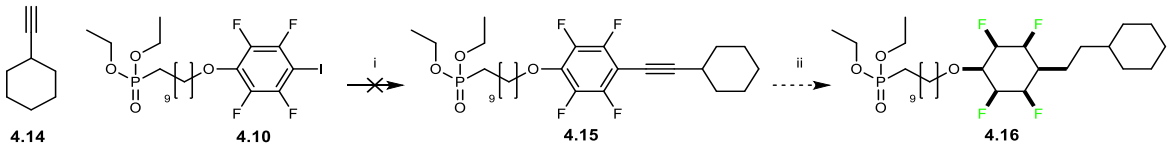

Scheme 4.5: Third approach to SAM precursor **4.16**. i: **4.10** (1 eq), **4.14** (2.4 eq), bis(triphenylphosphine)Pd(II) (10 mol%), Cu(I)I (6 mol%), DIPA (40 mL), THF (10 mL), 21 h, failed. ii: not attempted.

From here it was decided to explore Sonogashira chemistry to attach the cyclohexane ring by cross-coupling with acetylenecyclohexane **4.14**. This would put a distance between the rings and may be more amenable to an aryl hydrogenation (Scheme 4.5).[103] However, in the event the phosphonate group proved to interfere with the Sonogashira reaction resulting in the decomposition of the starting material when the reaction was attempted. This is assumed as the ^{31}P NMR showed multiple peaks after the reaction was worked up.

4.42 Synthesis of Janus SAM precursors

It became important at this stage to re-investigate the reaction for the preparation of **4.8** to **4.9**. Phenol **4.9** is generated by deprotection of *tert*-butyl ether **4.18** with treatment of conc. HCl. However, choosing not to remove the *tert*-butyl group would allow it to be used as a substituent to direct a second S_NAr reaction involving a different alkoxide to achieve a *para*-substituted product. This procedure for generating **4.19** from **4.17** was adapted from Gheong and Wakefield.[184] Subsequently, it was found that the *tert*-butyl group can be removed using trifluoroacetic acid (TFA) particularly as conc. HCl proved to be ineffective for this reaction when attempted initially. The resulting product was then reacted with phosphonate **4.4** to generate ether **4.23**, and this product was

then subjected to an aryl hydrogenation. This new route proved to be successful and is summarised in Scheme 4.6.

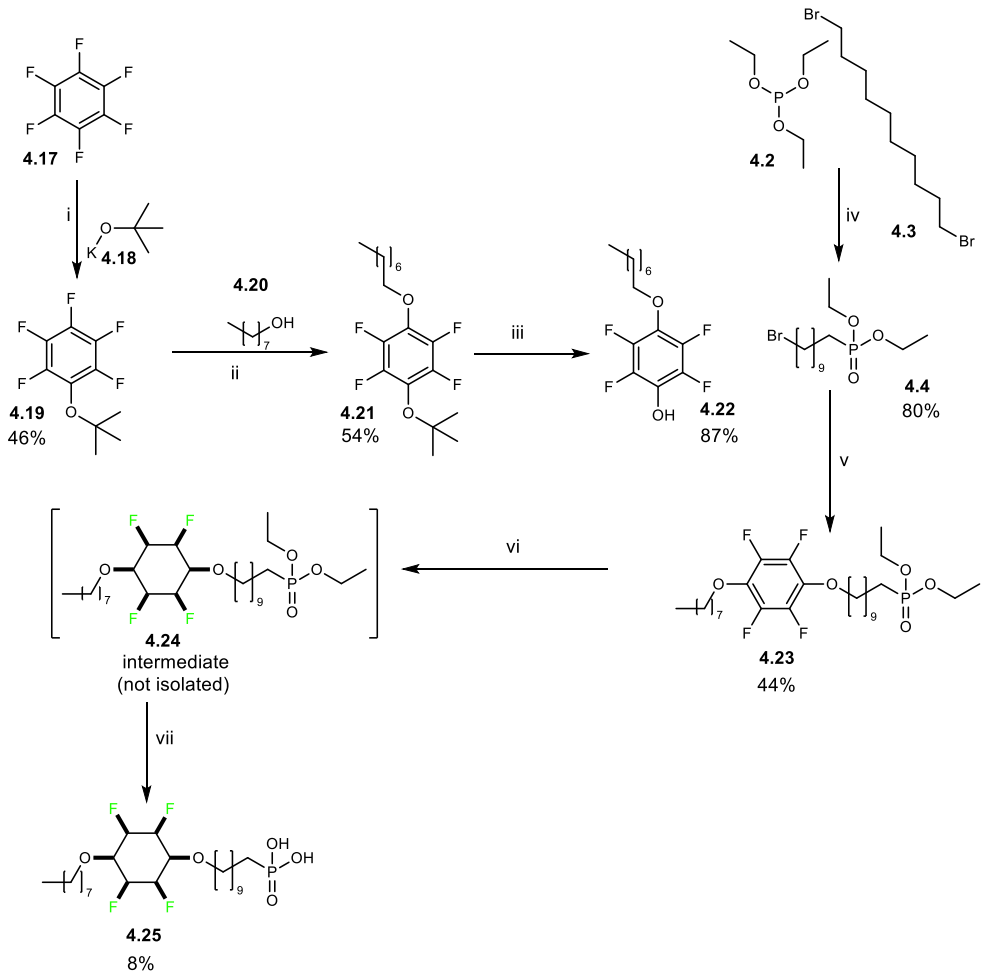

Scheme 4.6: Successful route to SAM precursor **4.25**. i: *tert*-BuOK (43.2 mmol), hexafluorobenzene **4.17** (43.2 mmol), THF (150 mL), -8 °C, 2 h, 46%. ii: KOH (20.8 mmol), 1-octanol **4.20** (10.9 mmol), **4.19** (8.32 mmol), 90 °C, 22 h, 54%. iii: **4.21** (4.5 mmol), TFA (4.5 mL), DCM (50 mL), r.t., 23 h, 87%. iv: **4.2** (0.88 eq) and **4.3** (1 eq), 140 °C, 24 h, 80%. v: K_2CO_3 (10.2 mmol), **4.22** (3.4 mmol), **4.4** (4.1 mmol), acetonitrile (50 mL), 90 °C, 23 h, 44%. vi: **4.23** (1.23 mmol), Rh-CAAC-COD-Cl **1.14** (2 mol%), 4Å MS (8 g), silica (4 g), hexane (40 mL), H_2 (50 bar), 50 °C, 2 d. vii: TMSBr (3.12 mmol), **4.24** (1.04 mmol), DCM (100 mL), r.t., 24 h, 8%.

This final reaction sequence involved two S_NAr reactions (steps i and ii) as well as deprotection of the *tert*-butyl group. In the event target **4.24** was prepared however it proved challenging to purify. Regular column chromatography with ethyl acetate / hexane, or DCM / hexane, or DCM /methanol in hexane all resulted in the product sticking to the silica gel until a methanol flush released it. Recrystallization was attempted in three solvents (DCM, methanol, and acetone) but this again proved

unsuccessful. In the end purification was overcome by acidic hydrolysis of the phosphonate ester to generate phosphonic acid **4.25**. The product was purified by reverse phase, flash column chromatography (0—100% acetonitrile in water) yielding the target compound in a modest yield (8%).

The successful synthesis of **4.25** led us to develop an additional compound for assessment. Analogue **4.31**, replaced the terminal C_8 alkyl chain with a cyclohexane methylene group. The synthesis of this second target is illustrated in Scheme 4.7.

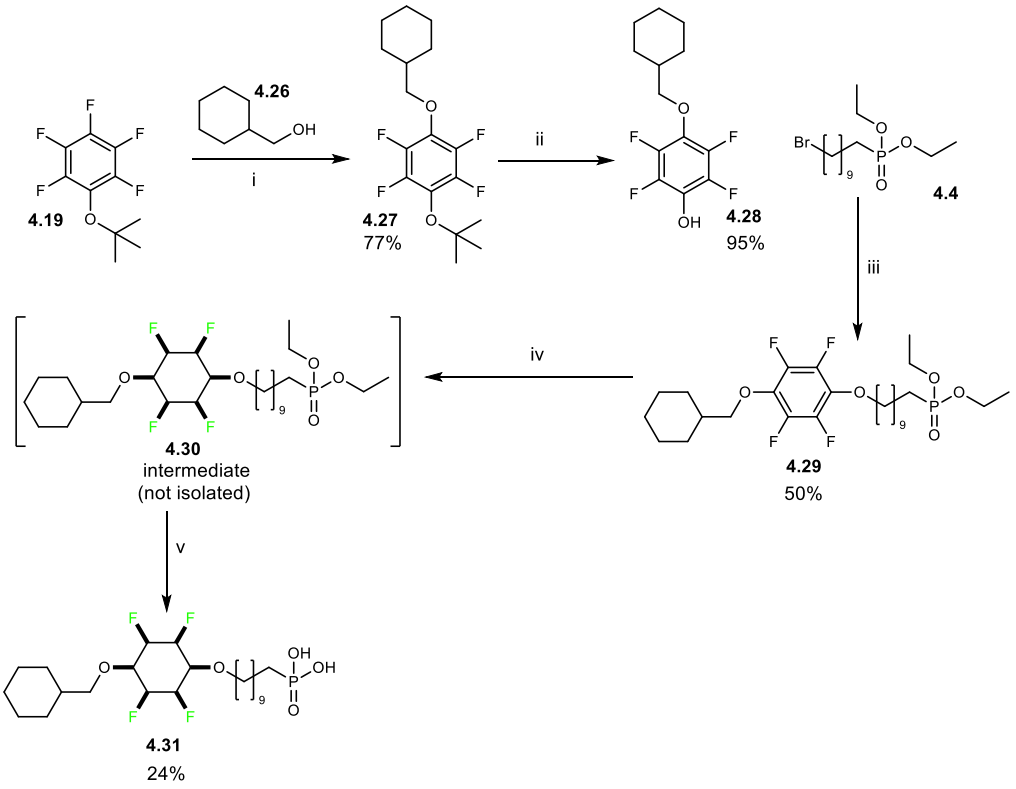

Scheme 4.7: Synthetic route SAM precursor **4.31**. i: KOH (63.4 mmol), cyclohexanemethanol **4.26** (31.7 mmol), **4.19** (25 mmol), 90 °C, 22 h, 77%. ii: **4.27** (3.71 mmol), TFA (3.7 mL), DCM (50 mL), r.t., 23 h, 95%. iii: K_2CO_3 (10.8 mmol), **4.28** (3.6 mmol), **4.4** (4.3 mmol), acetonitrile (50 mL), 90 °C, 23 h, 50%. iv: **4.29** (1.62 mmol), Rh-CAAC-COD-Cl **1.14** (2 mol%), 4Å MS (8 g), silica (4 g), hexane (40 mL), H_2 (50 bar), 50 °C, 2 d. v: TMSBr (3.21 mmol), **4.30** (1.07 mmol), DCM (100 mL), r.t., 24 h, 24%.

With phosphonic acids **4.25** and **4.31** in hand, these compounds were sent to Dr. Peer Kirsch's lab for his team to assemble into organic memory storage devices as illustrated below (Figure 4.10).

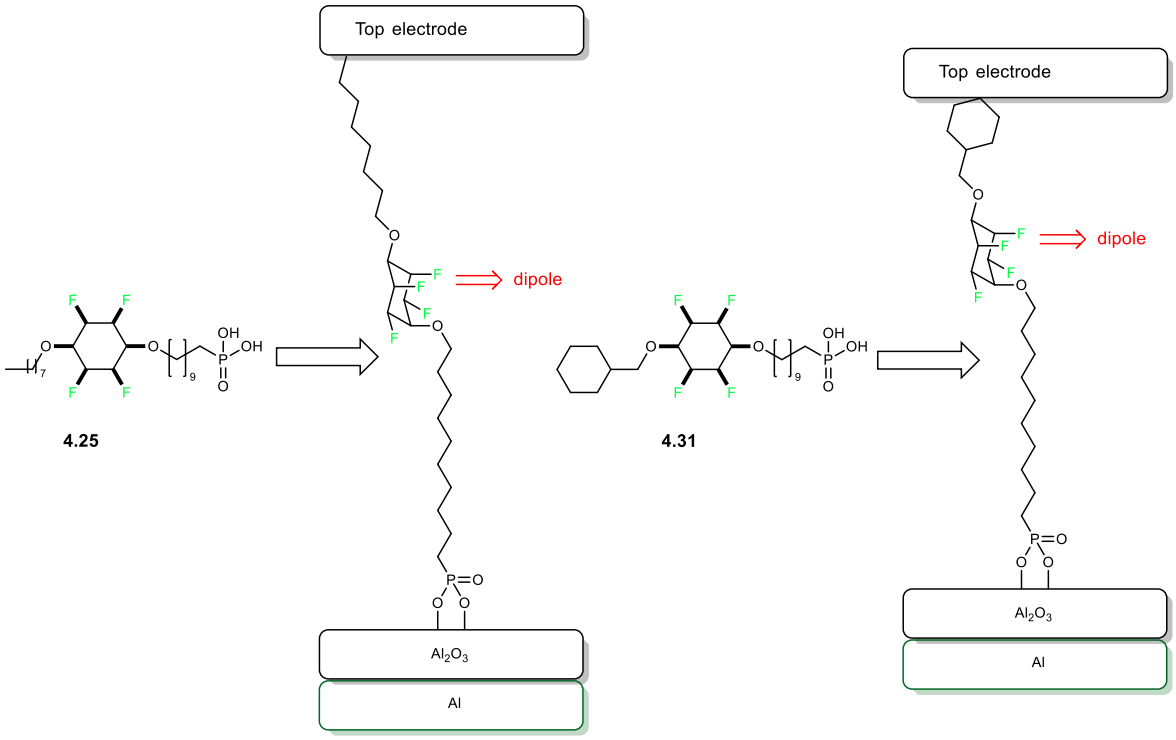

Figure 4.10: Graphic of **4.25** and **4.31** in a memory storage device.

4.5 SAM fabrication

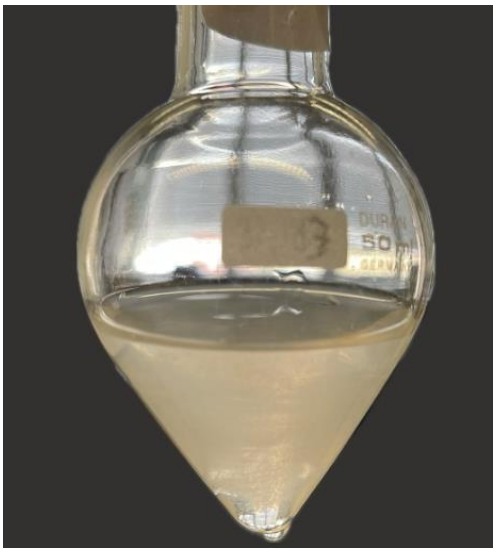

Figure 4.11: 4.25 partially dissolved in methanol.

The solubility of **4.25** and **4.31** was tested in various solvents, including tetrahydrofuran (THF), methanol, and hexafluoroisopropanol (HFIP), with THF ultimately selected as the

most appropriate solvent (Figure 4.11). The THF solution was filtered through a 0.2 µm PTFE membrane to remove undissolved particles and impurities.

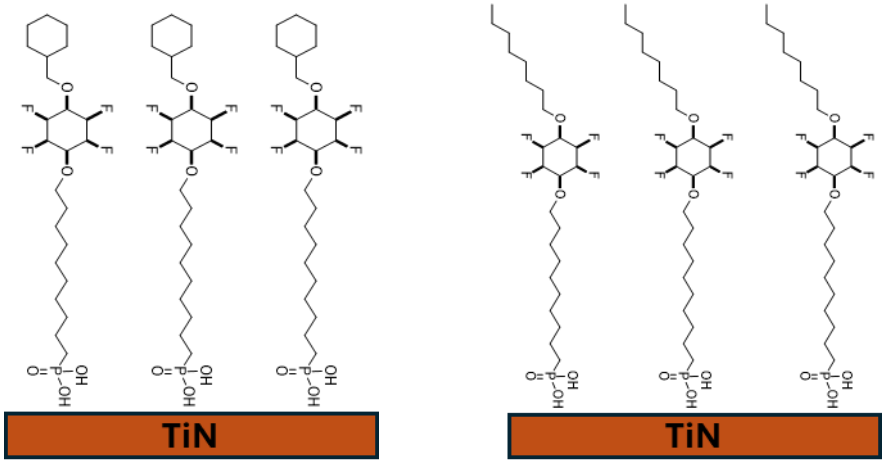

Figure 4.12: 4.31 and **4.25** SAM on TiN surface.

Self-assembled monolayers (SAMs) of **4.25** and **4.31** were successfully formed on a TiN, substrate with **4.25** on four chips and **4.31** on two chips (Figure 4.12). The water contact angle on uncoated TiN was 68.43 ± 0.47°. This angle increased to 97.87 ± 1.57° for the **4.31** coated surface and to 95.17 ± 1.42° for the **4.25** coated surface. In order to explore lipophilicity, the contact angle with diiodomethane was measured. Diiodomethane is commonly used as a reference 'oil' for wetting surfaces due to its high hydrophobicity and low volatility.[185] In this case the contact angle also increased. These changes clearly indicated successful surface coatings with the long chain phosphonic acids **4.25** and **4.31**. highly fluorinated surfaces have a very low surface energy, which results in low wettability and therefor contact angles above 100°.[186] The water contact angles are lower than that expected for a hydrocarbon coated surface (~113°)[187] perhaps suggesting some exposure of the Janus rings to the surface and a lack of order in the SAM assembly.

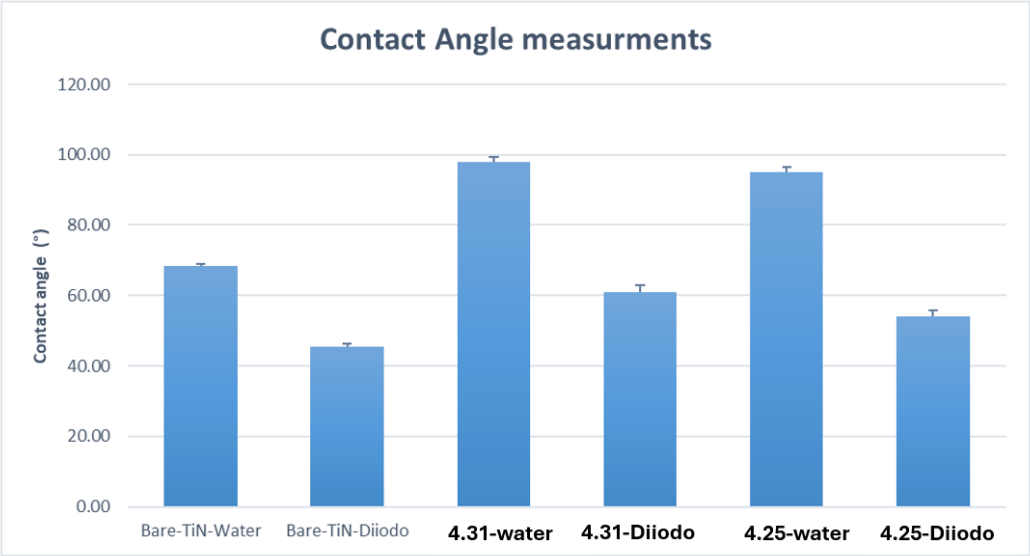

Figure 4.13: 4.31 and **4.25** SAM contact angles in two solvents.

Tapping mode images showed surface inhomogeneities and some particles, which are likely due to insoluble nanoparticle assemblies or perhaps multilayers. These issues were perhaps reflected in scratching thickness measurements, with **4.25** and **4.31** showing thicknesses of 2.85 ± 1.0 nm and 2.95 ± 2.0 nm, respectively, which were about 10-20% higher than expected.

For electrical (current density-voltage) experiments the voltage range applied across the SAMs was varied between +2 V to -2 V. However, there was consistent breakdown in the current densities measured for both SAMs across these ranges. This was interpreted by our collaborators as likely due to imperfections or defects within the SAM monolayer, such as disordered regions or incomplete coverage, which creates weak points. Essentially both substrates failed to survive the electrical current and this compromised further development towards their use in memory storage devices. More soluble compounds designed to create more cohesive SAMs may be required to make progress here. It may be that the 3,6-diether arrangement with their *ax/eq* and then *eq/ax* equilibrium are just not a good design for stable SAMs.

4.6 Summary

Although this aspect of the project did not progress so well, chemistry was developed to a new class of 3,6-dialkyl ether Janus cyclohexanes. These were accessed through *para* selective S_NAr reactions, and this stimulated a fuller investigation which is discussed in the next chapter.

5: Preparation of the Janus cyclohexane 3,6-diether motif

5.1 Introduction

In Janus cyclohexanes it is the co-alignment of axial C-F bonds which contribute most significantly to their polarity. Interconversion of the chair conformers of these cyclohexanes results in the equatorial and axial C-F bonds switching, and polarity of the cyclohexane is retained to the same face. In order to add substituents to these rings for functional purposes, all-*cis* pentafluorocyclohexanes have been prepared with the 'sixth' fluorine replaced with an alkyl or ether substituent as discussed in Chapter 3. In another variant, all-*cis* 1,3,5-trifluoro-2,4,6-trialkyl cyclohexanes have been prepared as discussed in Chapter 2. The preference for the alkyl substituents to adopt an equatorial arrangement promotes a chair conformation with triaxial C-F bonds, an arrangement where a large molecular dipole is retained as demonstrated by Figure 1.21. In this chapter the synthesis of all-*cis* 1,2,4,5-tetrafluoro-3,6-dialkyl ethers is explored, essentially replacing two of the C-F bonds with alkyl ethers and retaining the all *cis*-configuration. This class of products was prepared by *para* directed S_NAr reactions on pentafluorophenol alkyl ethers and particularly the *tert*-butyl ether. The route is such that products are prepared with either similar (equivalent) or different (non-equivalent) alkoxide ether substituents in the *para* positions of the aromatic ring. Aryl hydrogenations then delivered the final Janus 3,6-diether products (Scheme 5.1).

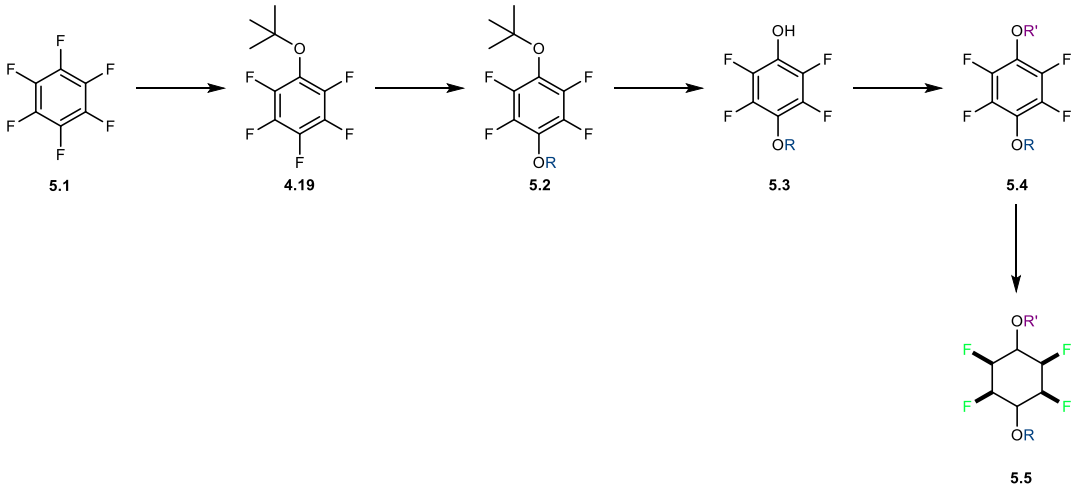

Scheme 5.1: General synthesis route to all-cis 3,6-diethyl ethers.

Initially a systematic investigation was undertaken to better understand the *para* selectivity arising from nucleophilic aromatic substitution (S_NAr) on pentafluorophenol alkyl ethers, developing from Chapter 4. S_NAr reactions have been regularly used from the organic chemist's tool kit, dating back over a century with an initial publication by Dr. Arthur Lapworth in 1903. Lapworth described reactions involving the displacement of halogen atoms in aromatic systems by nucleophiles.[188] The concept and mechanism of S_NAr continued to evolve and became more refined throughout the 20th century.[189] A generally accepted mechanism for S_NAr reactions is illustrated in Scheme 5.2 for an alkoxide nucleophile on an aromatic ring with electron withdrawing groups eg NO_2. Fluoride is generally a good leaving group in S_NAr chemistry as F is highly electronegative, polarizing the C-F bond and increasing the carbon's electrophilicity and susceptibility to nucleophilic attack.

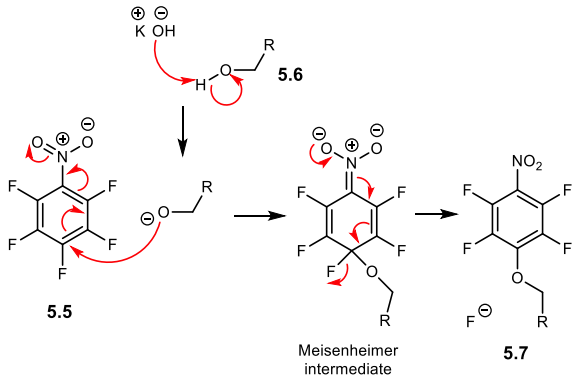

Scheme 5.2: S_NAr addition-elimination mechanism.

The reactivity of halogens as in S_NAr reactions follows a clear order, with aryl fluorides being the most reactive, followed by aryl chlorides then aryl bromides and finally aryl iodides being the least reactive. This sequence is primarily influenced by the polarity of the C-X bond on the aromatic ring. The more electronegative the halogen, the more electropositive the C-X carbon and therefore it is more susceptible to attack by a nucleophile. Consequently, fluorine facilitates S_NAr reactions most effectively and aryl fluorides are widely used in this context.[190] Moreover, the presence of an electron-withdrawing group (EWG) on the aryl ring further enhances S_NAr reaction rates, particularly at *ortho* and *para* positions to the fluorine. EWGs, by their nature, stabilize

the negative charge on the intermediate 'Meisenheimer' complex that forms during the reaction process. This stabilization lowers the energy barrier for the reaction, thereby increasing the rate. The combined effect of the halogen electronegativity and the presence of EWGs on the aryl ring are key factors that govern the mechanism, selectivity and efficiency of S_NAr reactions. Perfluorinated aromatic rings are certainly more reactive toward nucleophiles relative to their non-fluorinated or partially fluorinated counterparts, however without conjugated groups such as -NO_2, -CN etc, generally hard nucleophiles and higher temperatures are required for such transformations and these reactions are considered to be much more concerted in nature. Common nucleophiles include hydroxide, alkoxide, amide, and other anionic species in polar aprotic solvents.

Therefore, the mechanisms of S_NAr reactions range from stepwise addition-elimination reactions involving Meisenheimer intermediates[189] to concerted one step processes.[191] This spectrum of nucleophilic aromatic substitution chemistry has been reviewed widely recently.[192,193] The reaction shown in Scheme 5.2 represents a classical two-step addition-elimination pathway whereas the reaction in scheme 5.3 represents a concerted pathway. The concerted S_NAr reactions tend to occur when there are no strong activating substituents,[194–196] and various computations suggest that some of these reactions progress through a concerted nucleophilic attack and leaving group coordination often as four-centred transition states.[178,193]

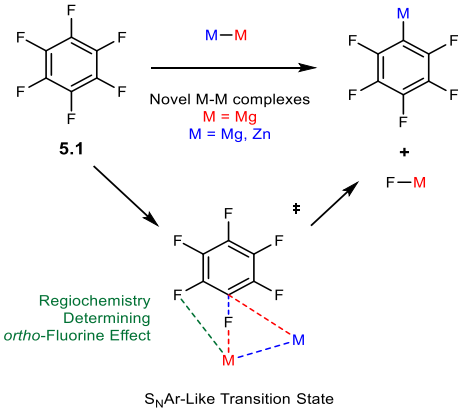

Scheme 5.3: Concerted nucleophilic aromatic substitution reaction (cS_NAr).[191]

S_NAr reactions of perfluorinated aryl rings benefit from the strong electronegativity of fluorine, but this is countered by some mesomeric donor ability from the fluorine lone pairs, and therefore fluorine substituents display ambiguous characteristics.

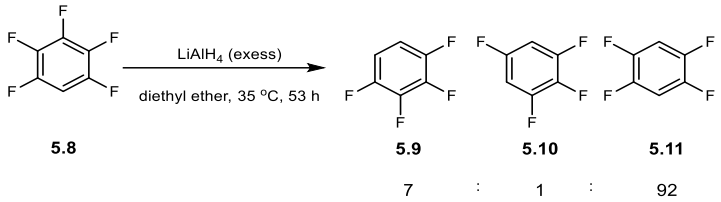

Scheme 5.4: Early hydride addition on pentaflurorobenzene.[197]

Scheme 5.4 illustrates an early example of a *para*-directed S_NAr on pentafluorobenzene **5.8**, with hydride as a nucleophile, as reported by Brooke, Burdon, and Tatlow.[197] This reaction resulted in predominant *para* selectivity with only minor *ortho* or *meta* directed products to the aryl hydrogen.[197] There are also examples of *ortho*- and *meta*-substituted product outcomes however these tend to be on lesser fluorinated aryls.[198]

A regiospecific *para* selectivity in a pentafluoroaryl is also exemplified by Paleta *et al.,* in 2010 with phenyl as a substituent using **5.12** as a substrate (Scheme 5.5).[199] These reactions were sluggish taking 3 days to obtain high yields, and larger more bulky substrates only produced lower yields of ~38%.[199] Paleta also discussed reactions with thiol and amine nucleophiles to **5.12**, all of which displayed exclusive *para* selectivity to the phenyl group.

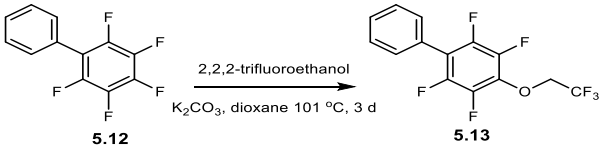

Scheme 5.5: S_NAr of **5.12** to *para* product **5.13** in 97% yield.[199]

Paleta went on to calculate the regioselectivity of S_NAr products using Hammett constants. Specifically looking at pentafluoro aryls with different substituents. They calculated that the methoxy substituent in **5.14** would result in a much more ambiguous outcome (16 : 52 : 36, *ortho* : *para* : *meta*) relative to -H and -Ph,[199] attributed to the

mesomeric donor ability of the methoxyl group. The negative Hammett constant (σ_p) of -0.28 indicates destabilisation of a negative charge (Scheme 5.6).

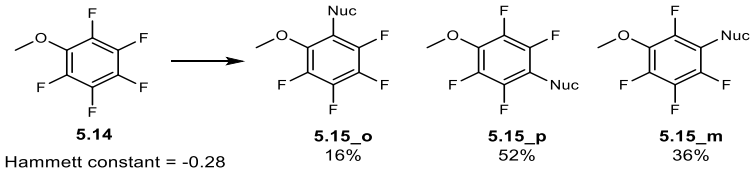

Scheme 5.6: Calculated regioselectivity S_NAr of **5.14**.[199]

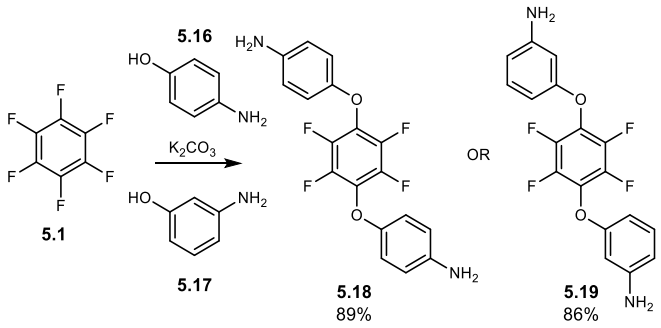

Scheme 5.7: S_NAr reaction of hexafluorobenzene into *para* products.[200]

Some examples appear in the literature in synthesis protocols indicating *para* selectivity with pentafluoroaryl ether substrates. For instance, Avdeev *et al.* were able to prepare **5.18** and **5.19** from hexafluorobenzene (**5.1**), and although good yields (86-89%) were reported, there was no indication of the level, if any, of a *meta* product formation (Scheme 5.7).[200] Another report prepared **5.20** in 45% yield and reported the *para* ether **5.21** as a minor over-addition product in 17% yield.[201] However, again there was no comment on any *meta* / *para* selectivity of **5.21** when compared to **5.20** (Scheme 5.8).

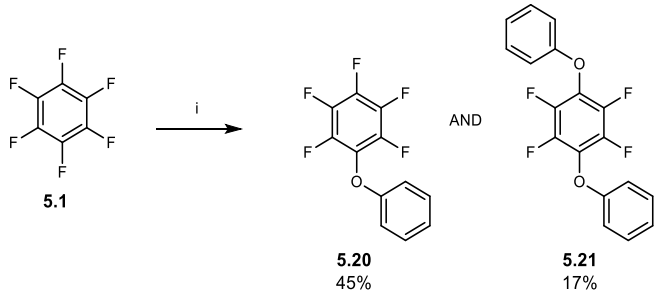

Scheme 5.8: S_NAr reaction of hexafluorobenzene into mono and *para* product. i: **5.1** (1 eq), sodium phenoxide (1 eq), MeCN (10 mL), 50 °C, 4 h.[201]

Our observations in Chapter 4 indicated *para* selectivity in the generation of intermediates **4.21** and **4.27**, but it was notable that there were also significant levels of *meta* products too, therefore it became a focus to explore factors influencing *meta / para* ratios. A study was undertaken exploring the addition of nucleophiles to a series of pentafluorophenol alkyl ethers. One example from Chapter 4 involved a reaction of **4.19** with 1-octanol (**4.20**) and this resulted in a 54% yield of the *para* product **4.21**. However, the product ratio was determined before purification to be 5.62 : 1 of *para* to *meta* (Scheme 5.9).

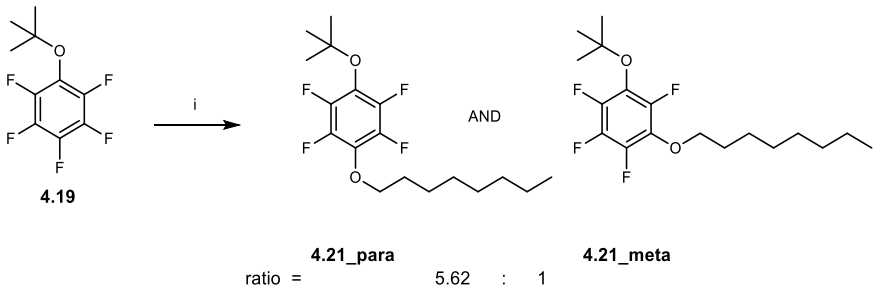

Scheme 5.9: i: KOH (21 mmol), 1-octanol **4.20** (11 mmol), **4.19** (8.32 mmol), 90 °C, 22 h, 54%.

5.2 Experimental S_NAr study

A series of experimental studies was conducted to explore these trends and particularly the influence of OMe vs the O^{t}Bu substituents as directing groups.

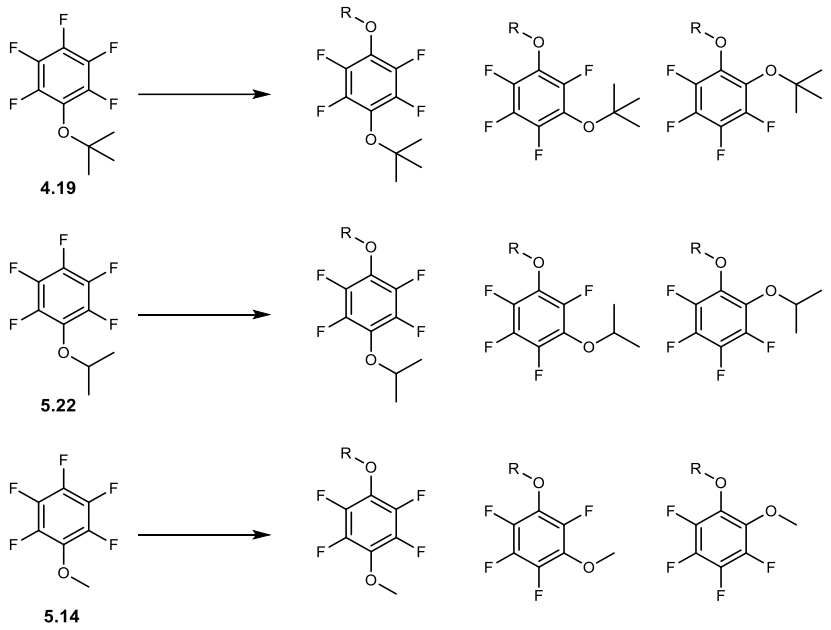

Scheme 5.10: The reaction schemes to determine S_NAr selectivity.

A set of experiments were designed which explored the reaction of *tert*-butyl **4.19**, *iso*-propyl **5.22** and methyl **5.14** ethers with three different nucleophiles, in order to determine the resultant *para* / *meta* ratios (Scheme 5.10). It was necessary at the outset to be able to interpret the nature of the substrates and the products by ^{19}F NMR to confidently identify the *ortho*, *meta*, and *para* products in reaction mixtures. The ^{19}F NMR of ether substrates **5.14**, **5.22**, and **4.19** are assigned in Figure 5.1.

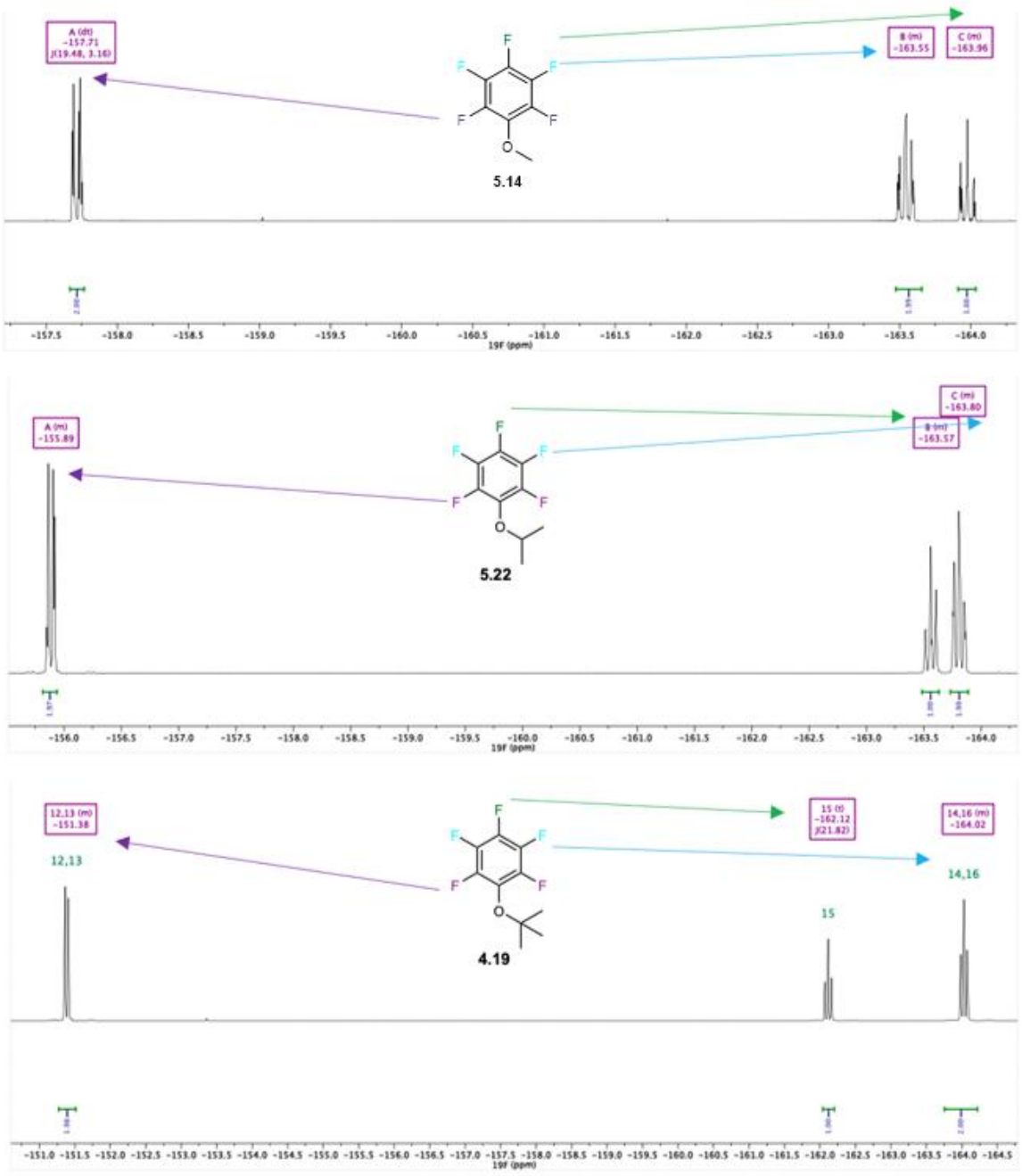

Figure 5.1: ^{19}F NMR spectra of aryl ethers **5.14**, **5.22** and **4.19** and their assignments.

Interestingly the signal for the *para* fluorine of pentafluoroanisole (**5.14**) is up-field of the *meta* fluorines relative the *iso*propyl and *tert*-butyl ethers, perhaps indicative of an increased donor ability on the methoxyl ether oxygen due to the best stereoelectronic overlap of the oxygen lone pair with the aromatic ring system. In this respect it is notable that the corresponding fluorine in the *tert*-butyl ether **4.19** is significantly downfield shifted.

Reactions were carried out in triplicate and followed by ^{19}F NMR every 30 min over 2.5 hours. Additionally, to avoid double addition or other side products the nucleophiles were loaded at half an equivalent, therefore the maximum conversion was 50%. Sodium hydride was used as a base.[195] The ^{19}F NMR of a reaction product of *tert*-butyl-ether **4.19** and isopropanol is shown in Figure 5.2. The *meta* and *para* products are clearly identifiable at a ratio of 4.3 ± 0.10 : 1.

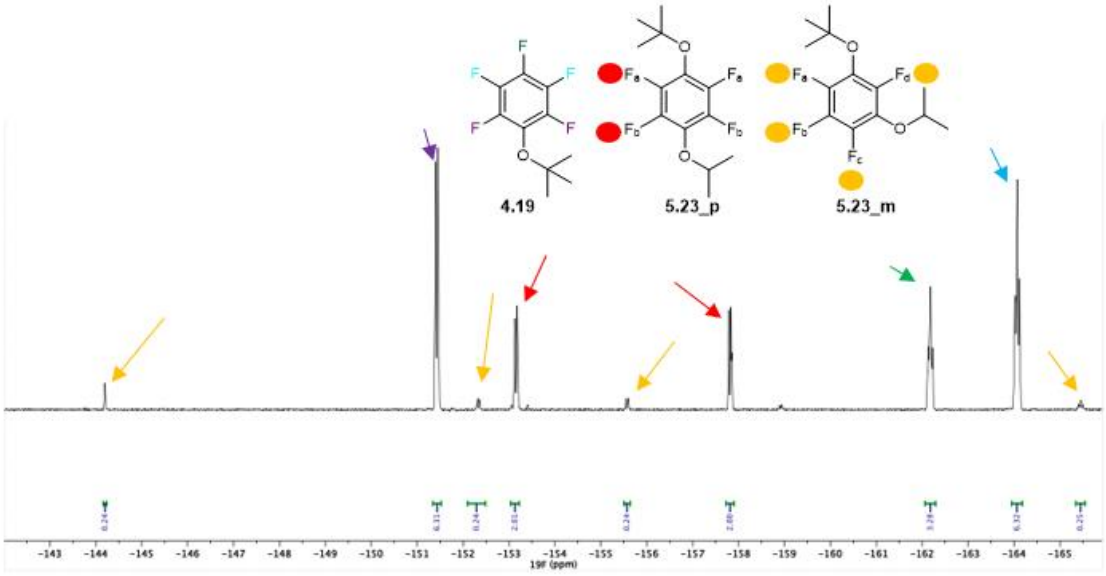

Figure 5.2: ^{19}F NMR of the reaction mixture after 2.5 hours showing starting ether (**4.19**) and the *meta* (**5.23_m**) and *para* (**5.23_p**).

The ratios were calculated by dividing the integral of the *para* over that of the *meta* product. To determine the percentage conversion, the integrals of both the *para* and *meta* products were summed and then divided by the total integral of all observed peaks. This method provided a clear quantitative measure of product distribution and the overall efficiency of the reactions.

Table 5.1: Substrate (1.0 eq), nucleophile (0.5 eq), NaH (0.75 eq), THF (3 mL), 2.5 hours, 50 °C

Substrate	Nucleophile	*para* : *meta* ratio average	Conversion after 2.5 hours	Reaction number
C_6F_5-OMe	MeOH	(0.55 : 1.27) ± 0.017 : 1[a]	23%	**5.24**
C_6F_5-OMe	IPA	(0.49 : 1.34) ± 0.18 : 1[a]	13%	**5.25**
C_6F_5-OMe	^{tert}BuOH	(0.28 : 1.81) ± 0.071 : 1[a]	34%	**5.26**
C_6F_5-O*i*Pr	MeOH	1.8 ± 0.034 : 1	25%	**5.27**
C_6F_5-O*i*Pr	IPA	1.7 ± 0.022 : 1	19%	**5.28**
C_6F_5-O*i*Pr	^{tert}BuOH	2.4 ± 0.40 : 1	3%	**5.29**
C_6F_5-O*t*Bu	MeOH	3.7 ± 0.12 : 1	28%	**5.30**
C_6F_5-O*t*Bu	IPA	4.3 ± 0.10 : 1	33%	**5.23**
C_6F_5-O*t*Bu	^{tert}BuOH	7.1 ± 0.29 : 1	24%	**5.31**

[a] (*ortho* : *para*) : *meta* ratio. Maximum conversion of 50%.

Table 5.1 presents the average product ratio for a series of reactions, derived from three separate experiments under the same reaction conditions. In overview, these experiments indicate that the *para* products are more favoured, and the *tert*-butyl ether showed the largest orientation effect. It is noteworthy that the *iso*-propyl and methoxyether substrates had similarly lower (*ortho* + *para*) / *meta* ratio outcomes, across different solvents (~2:1). In the case of pentafluoroanisole (**5.14**) some *ortho* product is also generated at a low level. The level of *ortho* product diminishes as the nucleophile increases in steric bulk. This is consistent with a minimum steric hindrance which better facilitates some nucleophilic attack at the *ortho* position. These outcomes underscore the role that both steric and stereoelectronic factors play in determining product distributions and offer a strategy to manipulate selectivity through careful choice of the ether substituent.

Tert-butyl ether **4.19** gave the highest *para / meta* ratio and it was selected to further investigate the effect, if any, that the nucleophile had on the reaction selectivity. Prior to this the conditions were optimized to obtain the highest *para* selectivity and were adapted from Chen *et al.*[176] and Desper *et al.*[177] using chemistry developed in Chapter 4. This involved *tert*-butyl ether **4.19** (1.0 eq), nucleophile (1.3 eq), KOH (2.5 eq) for 24 h at 90 °C. These conditions were then applied in exploring the role of the nucleophile, and the outcomes are summarised in Table 5.2.

5.21 Nucleophile scope

Chapter 2 explored the synthesis of polar 1,2,3-all *cis* trifluorocyclohexanes designed to form supramolecular stacks. These structures were notable for having three linear alkyl chains radiating from the centre of the molecule, and embodying a negative dielectric characteristic, with a dipole oriented perpendicular to the molecular plane. In this Chapter a new goal emerged to generate linear 3,6-ether linked Janus cyclohexanes for supramolecular assemblies. This new class of molecules may be predisposed to polymorphism due to the inherent *ax/eq* to *eq/ax* interconversions, although this design may be less amenable to stable packing arrangements. The LC layer in a typical LC display is made by mixing several compounds together to form a cocktail of components but with a primary component. It is anticipated that these linear 3,6-ether systems could contribute to these cocktails as negative or positive dielectrics if they possess appropriate phase behaviours.

With this in mind 3,6-diether products emerged as attractive targets and thus reactions that maximised *para* outcomes were most desirable. In the first instance nucleophiles such as **5.34**, **5.39**, and **5.40** were explored. It should be noted that these three reactions required a solvent, in this case THF, as the nucleophilic alcohols are all solids.[202,203] Other nucleophiles such as phenol (**5.38**) were also explored. When phenol was reacted with the *tert*-butoxypentafluorobenzene (**4.19**) the reaction resulted in a low yield but with good *para* / *meta* ratio of 5.90 / 1. This can be compared to a 17% yield for the double addition on hexafluorobenzene (**5.1**) as reported by Kilickiran *et al.*[201] To better understand the nucleophile effects, primary alcohols such as methanol (**5.32**), hexanol

(**5.35**), and octanol (**4.20**); secondary alcohols such as *iso*-propanol (**5.33**), cyclohexanol (**5.36**), and L-menthol (**5.40**); and then the tertiary alcohol *tert*-butanol (**5.37**) were all used. The results from these reactions are summarised in Table 5.2.

Table 5.2: 4.19 (1.0 eq), nucleophile (1.3 eq), KOH (2.5 eq), 24 hours, 90 °C.

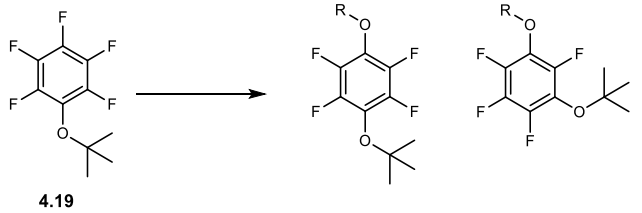

4.19

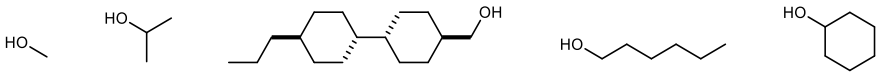

5.32 5.33 5.34 5.35 5.36

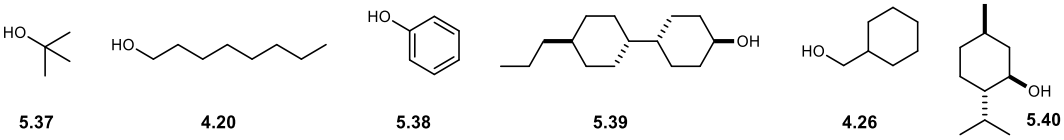

5.37 4.20 5.38 5.39 4.26 5.40

Nucleophile	Average *para:meta* ratio	Conversion of starting material	Product number
Methanol (**5.32**)	1.88:1[a]	100%	**5.41**
iso-propanol (**5.33**)	3.50:1	92%	**5.42**
5.34	4.38:1[b]	86%	**5.43**
1-hexanol (**5.35**)	4.52:1	100%	**5.44**
Cyclohexanol (**5.36**)	5.37:1	100%	**5.45**
tert-butanol (**5.37**)	5.61:1	31%	**5.46**
1-octanol (**4.20**)	5.62:1	100%	**4.21**
Phenol (**5.38**)	5.90:1	89%	**5.47**
5.39	6.1:1[b]	100%	**5.48**
Cyclohexanemethanol (**4.26**)	7.01:1	100%	**4.27**
L-menthol (**5.40**)	7.32:1[b]	100%	**5.49**

[a] (*ortho* + *para*) : *meta* ratio = (0.55 + 1.33) : 1. [b] THF (10 mL) was used as a solvent at 75 °C.

Unlike the ether substituents on the pentafluoroaryl substrate, no obvious tendency emerged relating the steric influence of the nucleophile to an increased *para* selectivity. For example, cyclohexanemethanol **4.26,** a primary alcohol gave one of the highest regioselectivities, and 1-octanol and *tert*-butanol have identical outcomes.

5.3 Computational study (Dr. Rodrigo Cormanich, University of Campinas)

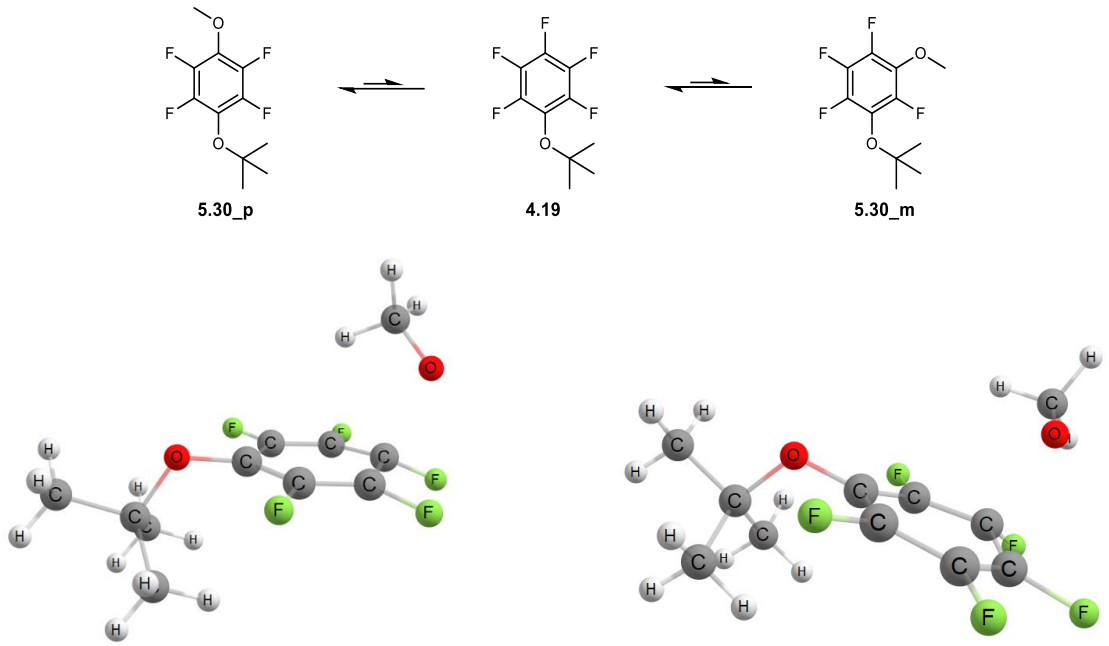

Scheme 5.11: Top: S_NAr reactions between **4.19** and methoxide. Bottom Left: Computed trajectory for *para* attack. Bottom Right: Computed trajectory for *meta* attack.

A computational study carried out by Dr Rodrigo Cormanich at the University of Campinas, Brazil, explored a nucleophile (methoxide) reacting with *tert*-butyl ether **4.19** (Scheme 5.11). The energy difference between the nucleophile attacking the *para* and *meta* positions was evaluated.

5.31 Kinetic considerations

It proved difficult to locate transition states (TSs) in each case for *meta* and *para* formation. After using a variety of different methods (~15), two theory levels did find transition states, and in each case only a low barrier (1.3 – 2.1 kcal mol^{-1}) was found above the ground state energy of the starting ether **4.19**. The reaction is highly

exothermic (by 17.8 kcal mol^{-1}) overall with a more stable ground state *para* over *meta* product, by 2.9 kcal mol^{-1}. However, the *para* / *meta* ratio appears to be determined kinetically as the *meta* TS is a little higher (by 0.8 kcal mol^{-1}) than that of the *para* TS (Figure 5.3).

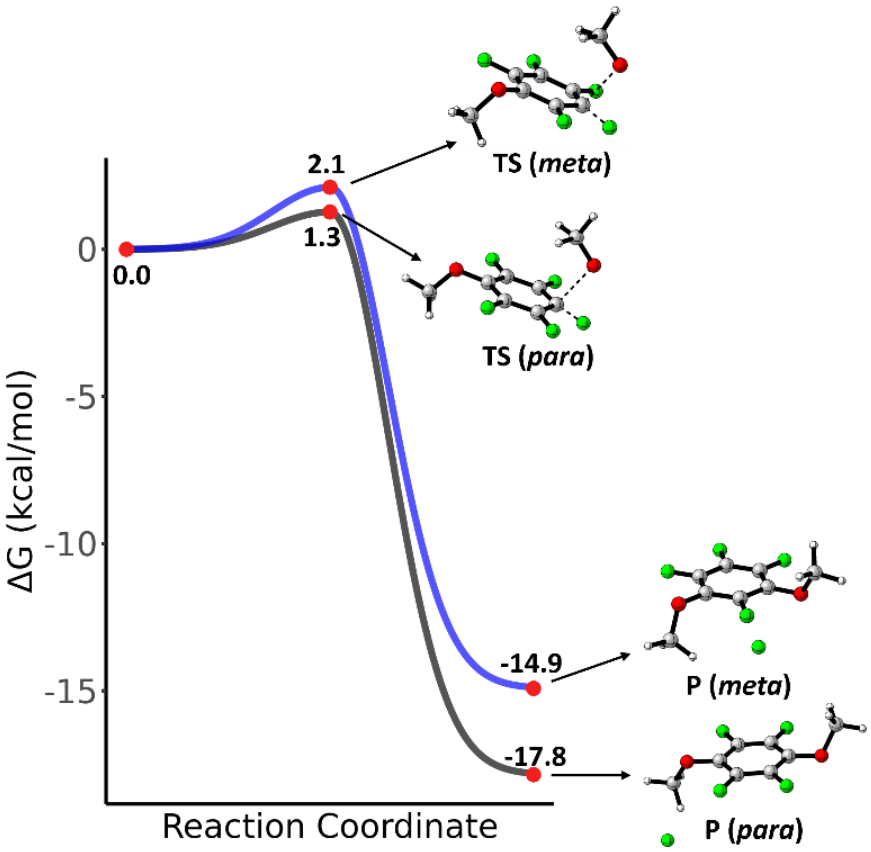

Figure 5.3: Intrinsic reaction coordinate barrier calculated for *para* and *meta* attack (**5.24**). Comparison of reaction energy profiles for *meta* and *para* approaches calculated at M06-2X/6-311+G**.

Additionally, the presence of a Mesenheimer intermediate was not obvious. Several of the methods explored did find a plateauing of the reaction profile but this never progressed to a distinct energy minimum. This is illustrated for the reaction profile in Figure 5.4. Thus, it is concluded that these reactions fit the concerted S_NAr reaction profiles as discussed above.[178,204]

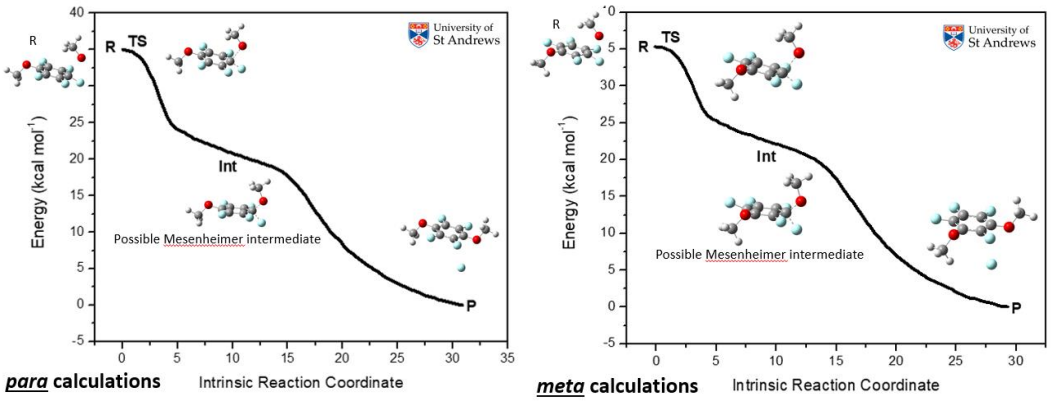

Figure 5.4: Intrinsic reaction coordinate barrier calculated for *para* and *meta* attack. Left: *para* calculations showing R (staring reagent), TS (transition state), Int (possible Mesenheimer complex), and P (product). Right *meta* calculations showing R (starting reagent), TS (transition state), Int (possible Mesenheimer complex), and P (product).

These initial computational studies helped to reinforce the *para* preference in S_NAr reactions of ether substituted pentafluoroaryl rings. Experimentally the highest selectivity occurs with the O-*tert*-butyl group **4.19**. O-*tert*-Butyl group adopts a perpendicular conformation relative to the aryl ring due to unfavourable sterics in the planar orientation, and this reduces the donor potential of the oxygen lone pairs (Figure 5.5). This tendency will be less for the -OMe group as the barrier to achieving a planar orientation will be lower.

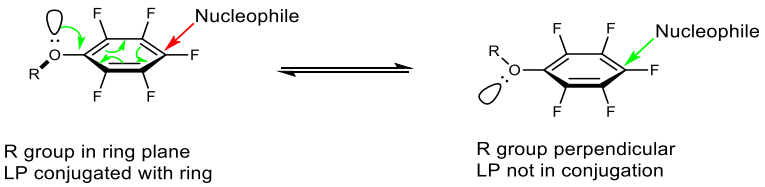

Figure 5.5: Diagram showing the conjugation of the lone pair on the perfluoro aryl ether compound with respect to nucleophilic attack.

5.32 Thermodynamic considerations

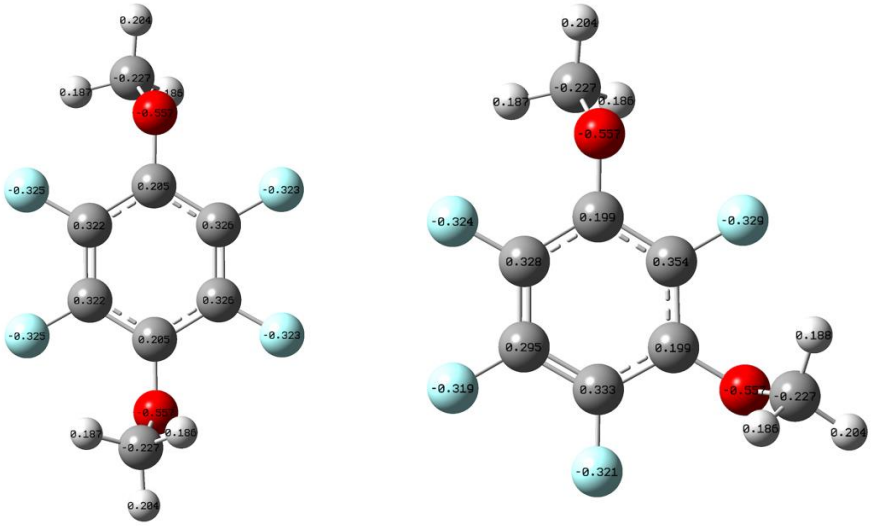

Figure 5.6: Ground state NBO charges for the Left: *para* and Right: *meta* 3,6 dimethoxy ethers **5.24_p** and **5.24_m** aromatic rings.

In the ground state the *para* product has the lower energy. The *para* product appears to be more stable as it allows for greater separation between the most positively charged carbon atoms in the ring, when compared to the *meta* product. Specifically, in the *meta* product, carbons 4, 5, and 6 are adjacent (Figure 5.6), leading to increased electrostatic repulsion in this isomer. This is minimised in the *para* product where there are only ever two electropositive carbons adjacent to each other. Figure 5.6 shows the charges of the different atoms of both the *meta* and *para* products. The carbons attached to the fluorine show values of ~+0.3 which is about one third of a full carbocation. The carbons bonded to the oxygen are only ~+0.2, less. This observation suggests a general principle: *para* derivatives of aromatic rings with attached electronegative atoms or groups tend to be more stable due to reduced electrostatic repulsions between the carbon atoms in the ring. This effect is exemplified below in Figure 5.7.

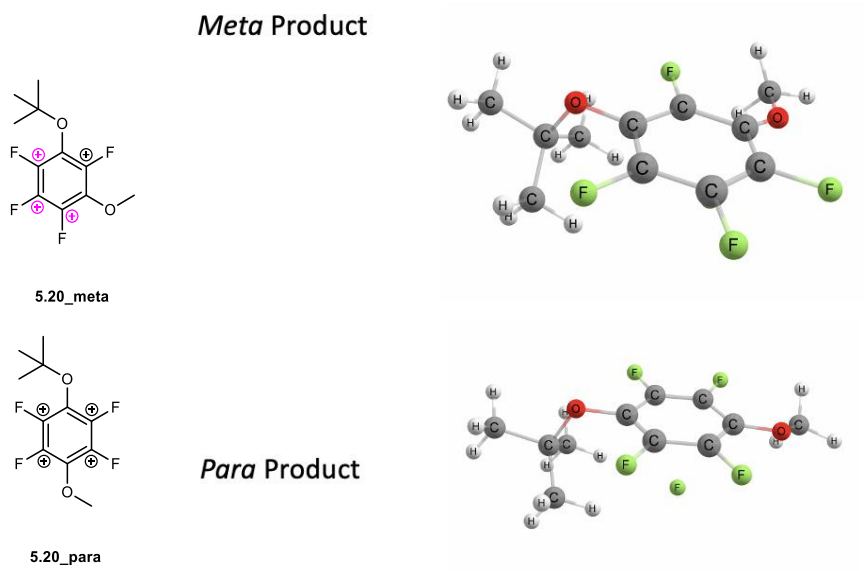

Figure 5.7: *Meta* and *para* product indicating the arrangements of electropositive carbons.

5.4 Synthesis of all-*cis* 3,6-Janus cyclohexanes

Chapter 2 explored dielectric properties as a characteristic feature of liquid crystals, and a desire for target compounds to form supramolecular stacks. These structures were notable for having three linear alkyl chains radiating from the centre of the molecule, embodying a negative dielectric characteristic, where the molecular dipole is oriented perpendicular to the molecular plane. This orientation influences how the molecule interacts with electric fields, an important factor in the functionality of liquid crystal materials.

During our collaboration with Dr. Yamada, we found that some of these targets possessed polymorphism; to show that it is actually a polycrystalline material, it is necessary to show different diffraction patterns. This can be done using variable-temperature powder X-ray diffraction measurements. However, the tri-fluoro tri-alkyl Janus molecules discussed in Chapter 2 did not possess this level of liquid crystallinity. It became apparent that leveraging more traditional methodologies in liquid crystal chemistry could offer significant advantages. These conventional strategies have a proven track record for successfully producing materials with the desired properties and functionalities. In this context, the 3,6-Janus motif emerged as promising compounds. This motif is expected to yield linear molecules that might also exhibit a negative dielectric anisotropy, similar to our original targets but potentially easier to

work with due to their structural simplicity and alignment with conventional liquid crystal design principles. However, if the molecule aligns parallel to its dipole, this will result in a positive dielectric anisotropy with applications in visual displays (IPS displays). A number of Janus 3,6-diether cyclohexanes were identified as targets in this context.

5.41 'Equivalent' 3,6-Janus molecules

An initial investigation into preparing 'equivalent' Janus 3,6-diether systems was undertaken. Accordingly, hexafluorobenzene was treated with sodium ethoxide to generate 1,4-diethoxy-2,3,5,6-tetrafluorobenzene (**5.50**) as illustrated in Scheme 5.12. This resulted in a 3.3 / 1 ratio of *para* to *meta* ratio of products similar to expectation. Aryl hydrogenation was then carried out to obtain the Janus 3,6-diether **5.51** as a mixture of *para* / *meta* regioisomers, however, the *para* product could be separated from the *meta* during purification to give a single isomer.

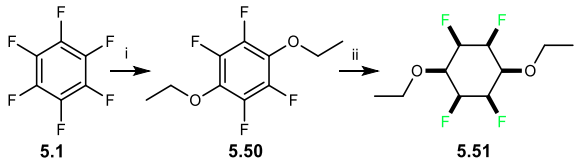

Scheme 5.12: Synthesis of 'equivalent' 3,6-diether **5.51**. i: EtONa (26 mmol), hexafluorobenzene **5.1** (8.67 mmol), THF (25 mL), r.t., 24 h, 37%. ii: **5.50** (0.42 mmol), Rh-CAAC-COD-Cl **1.14** (1.6 mol%), silica (1 g), hexane (40 mL), H_2 (50 bar), r.t., 1 day, 43%.

A suitable crystal of **5.51** was submitted to X-ray structure analysis and the resultant structure is shown in Figure 5.8. The structure shows an axial and an equatorial OEt group as expected on the cyclohexane, and this confers a less ordered stacking of these molecules relative to other Janus cyclohexyl systems.

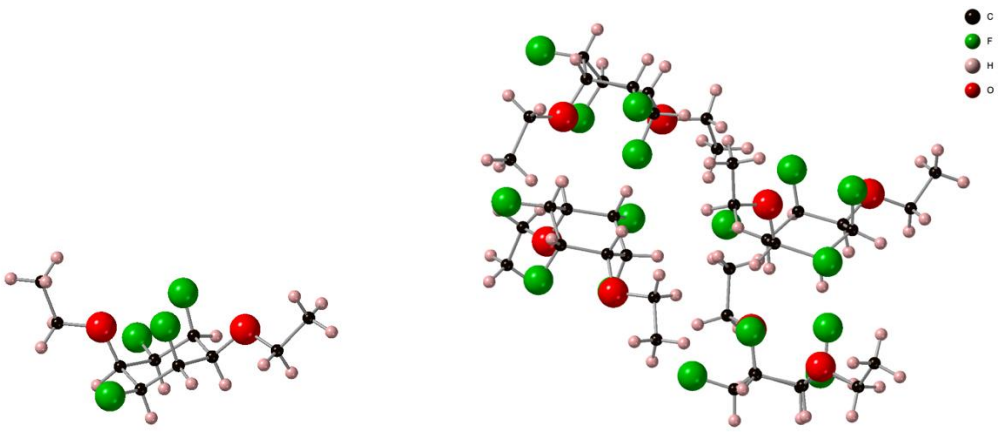

Figure 5.8: X-Ray structure of **5.51**. Left: isolated cyclohexane molecule. Right: Four molecules showing the molecular packing.

The *ax* / *eq* OEt groups clearly disrupts the level of columnar packing relative to that observed for the 1,3,5-trifluorocyclohecanes prepared in Chapter 2. The H···F interaction lengths varied here. Interestingly the shortest H···F interaction between any pair of molecules is 2.308 Å, shorter than the shortest contacts the tri fluoro systems, which were much more uniform at ~ 2.7 Å.

After the successful synthesis of **5.51** another 'equivalent' Janus 3,6-diether was prepared with a particular focus on potential for liquid crystallinity. With this in mind, alcohol **5.34** was explored as a motif found in commercial LC materials such as **5.52** and **5.53** (Figure 5.9).[44,205,206]

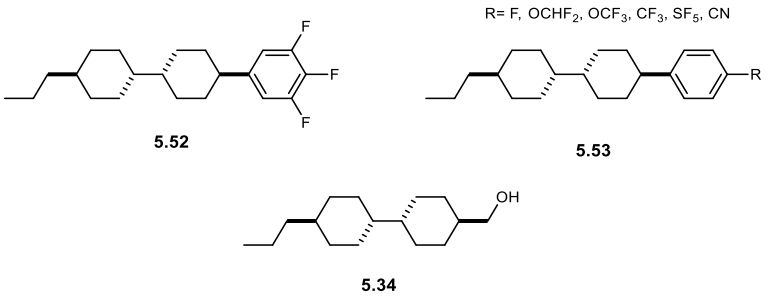

Figure 5.9: Some fluorinated LCs with the bis-cyclohexyl motif and alcohol **5.34**.[44]

Accordingly alcohol **5.34** was treated under the developed conditions and this generated **5.54** (1.4 : 1 *para* : *meta*) in a rather modest yield after purification as illustrated in Scheme 5.13.

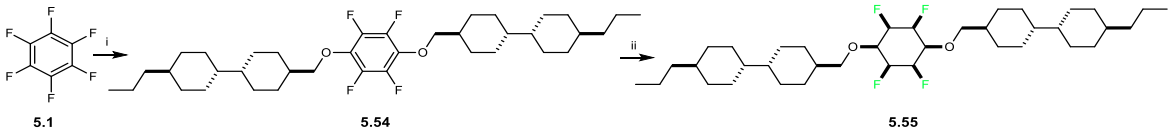

Scheme 5.13: Synthesis of Janus 3,6-diether **5.55**. i: KOH (10.83 mmol), **5.34** (13 mmol), THF (10 mL), hexafluorobenzene **5.1** (4.33 mmol), 65-90°C, 24 h, 12%. ii: **5.54** (0.482 mmol), Rh-CAAC-COD-Cl **1.14** (2 mol%), 4 Å MS (1 g), silica (500 mg), hexane (20 mL), H_2 (50 bar), r.t., 5 days, 4%.

Aryl hydrogenation of **5.54** was then carried out. The reaction time was extended to 5 days but without heating to minimise any defluorination. Although the synthesis of **5.55** was successful, this product could only be isolated in poor yield. In the event ~13 mgs of product **5.55** was obtained, and this proved insufficient for DSC or POM analysis. The compound was confirmed via NMR (^{1}H, ^{19}F, and ^{13}C) as well as HRMS details of which are provided in the Experimental.

5.42 'Non-equivalent' Janus 3,6-diethers

The route to the S_NAr products synthesised in Section 5.21 offered an approach to 'non-equivalent' Janus 3,6-dialkyl ether cyclohexanes. Of the six non-equivalent diethers prepared here, only the *bis* ether **5.56** retained the *tert*-butyl group in the final product. The approach is shown in Scheme 5.14 for diether **5.56**. The other ethers were developed further to 'non-equivalent' ethers after removal of the *tert*-butyl ether to generate a phenol.

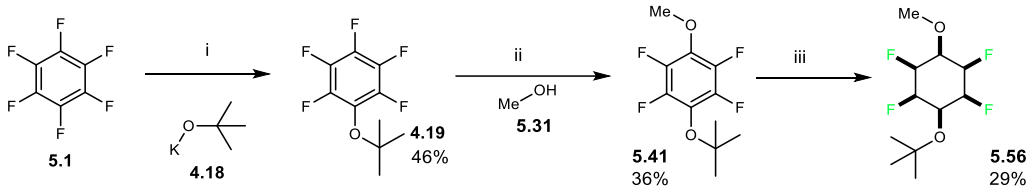

Scheme 5.14: Route to **5.56**. i: ^{tert}BuOK (**4.18**) (43.2 mmol), hexafluorobenzene **5.1** (43.2 mmol), THF (150 mL), -8 °C, 2 h, 46%. ii: potassium hydroxide (10.4 mmol), methanol (5.46 mmol), **4.19** (4.16 mmol), 90 °C, 22 h, 36%. iii: **5.41** (1.43 mmol), Rh-CAAC-COD-Cl **1.14** (1.6 mol%), 4 Å MS (8 g), silica (4 g), hexane (40 mL), H_2 (50 bar), r.t., 2 days, 29%.

For example the 'non-equivalent' diether **5.59**, was prepared from *tert*-butyl ether **4.19** as illustrated in Scheme 5.15.

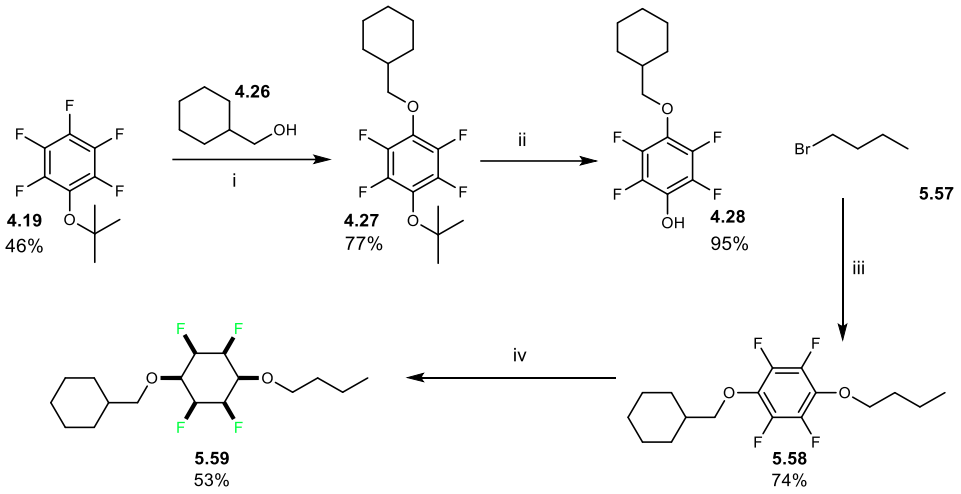

Scheme 5.15: Route to **5.59**. i: KOH (63.4 mmol), cyclohexanemethanol **4.26** (31.7 mmol), **4.19** (24.98 mmol), 90 °C, 22 h, 77%. ii: **4.27** (3.71 mmol), TFA (3.7 mL), DCM (50 mL), r.t., 23 h, 95%. iii: K_2CO_3 (10.78 mmol), **4.28** (3.59 mmol), **5.57** (4.31 mmol), acetonitrile (50 mL), 90 °C, 23 h, 74%. iv: **5.58** (1.85 mmol), Rh-CAAC-COD-Cl **1.14** (2 mol%), 4Å MS (8 g), silica (2 g), hexane (40 mL), H_2 (50 bar), r.t., 4 days, 53%.

These reactions worked well. The aryl hydrogenation to generate **5.59** was achieved in a 53% yield, which is high for this type of reaction. The purification was also straightforward using 60% DCM in hexane as the solvent system for column chromatography. The *meta* product was not observed in the final compound. Compound **5.59** was obtained as a white solid, a crystal of which was submitted for X-ray structure analysis and the structure is shown in Figure 5.12. The molecular packing arrangement between the rings was similar to that found for diethyl ether **5.51** with the cyclohexane ring lying equatorial, and the *n*-butyl group lying axial.

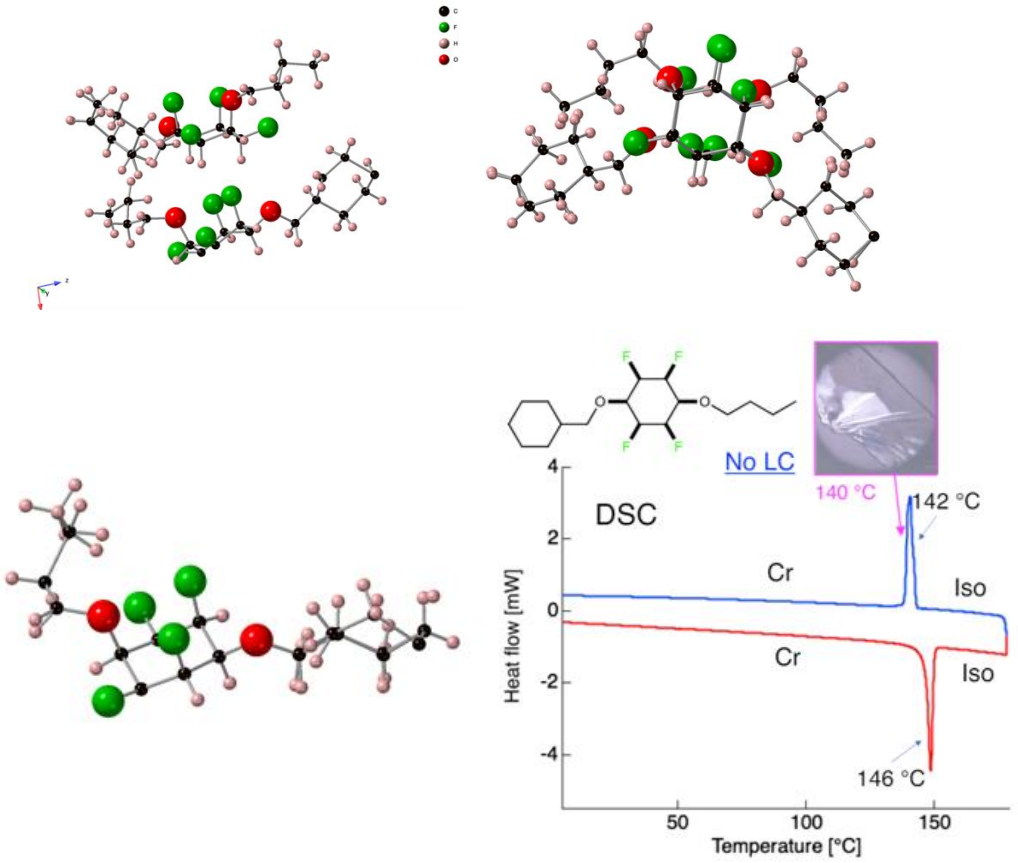

Figure 5.12: Crystal structure of **5.59** and DSC profile. Top Left and Right: Two molecules showing the molecular packing from different trajectories. Bottom Left: single molecule of **5.59**. NOTE: black for C, white for H, red for O, and green for F. Bottom Right: DSC and POM image of **5.59**.

Diether **5.59** stacks in a similar manner to **5.51** (see Figure 5.8) where the ether chains do not overlap each other, and the rings rotate in a spiral pattern progressing down a given column stack. The closest H···F contact at 2.405 Å is within the van der Waals contact distance (2.47 Å) indicating a stabilising contact. DSC analysis did not reveal any evidence of polymorphism and only showed a melting point of 146 °C.

L-Menthol **5.40** was explored as a nucleophile to generate **5.49**. Our collaborators in Kyoto were interested in such an enantiopure compound as a candidate chiral LC.

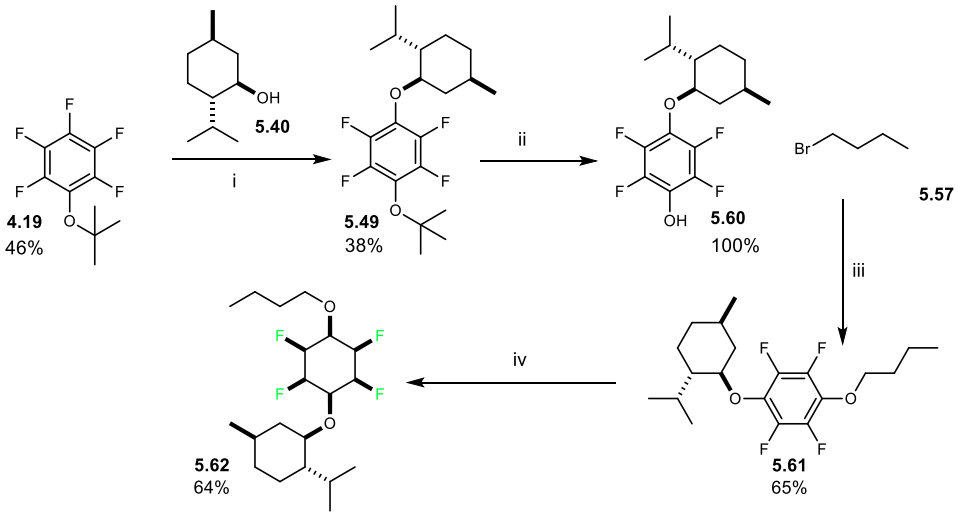

Scheme 5.16: Route to **5.62**. i: KOH (10.41 mmol), L-menthol **5.40** (10.41 mmol), **4.19** (4.164 mmol), THF (10 mL), 75 °C, 24 h, 38%. ii: **5.49** (2.529 mmol), TFA (2.6 mL), DCM (50 mL), r.t., 48 h, quantitative. iii: K_2CO_3 (18.63 mmol), **5.60** (6.21 mmol), **5.57** (8.07 mmol), acetonitrile (20 mL), THF (10 mL), 75 °C, 24 h, 65%. iv: **5.60** (1.063 mmol), Rh-CAAC-COD-Cl **1.14** (1.8 mol%), 4Å MS (8 g), silica (4 g), hexane (40 mL), H_2 (50 bar), r.t., 4 days, 64%.

The synthesis towards target compound **5.62** is shown in Scheme 5.16, following a similar route to that for **5.59**.

An X-ray structure of **5.62** was again solved and is presented in Figure 5.13. The rings of **5.62** stack directly one on top of each other but are off centred and the ether oxygens eclipse fluorines, not oxygens in the adjacent rings. This helical type stacking is common in the cholesteric phases associated with chiral liquid crystals.[207] The axial alkyl ether is again the *n*-butyl group. The more sterically bulky L-menthol moiety lies equatorial, with its ring approximately perpendicular to the Janus ring. This would mean the long axis of the molecule as well as the dipole would be parallel. Potentially yielding a positive dielectric anisotropy. The closest H···F interaction length was 2.285 Å which is the shortest contact length of any system evaluated so far and indicates a meaningful contact.

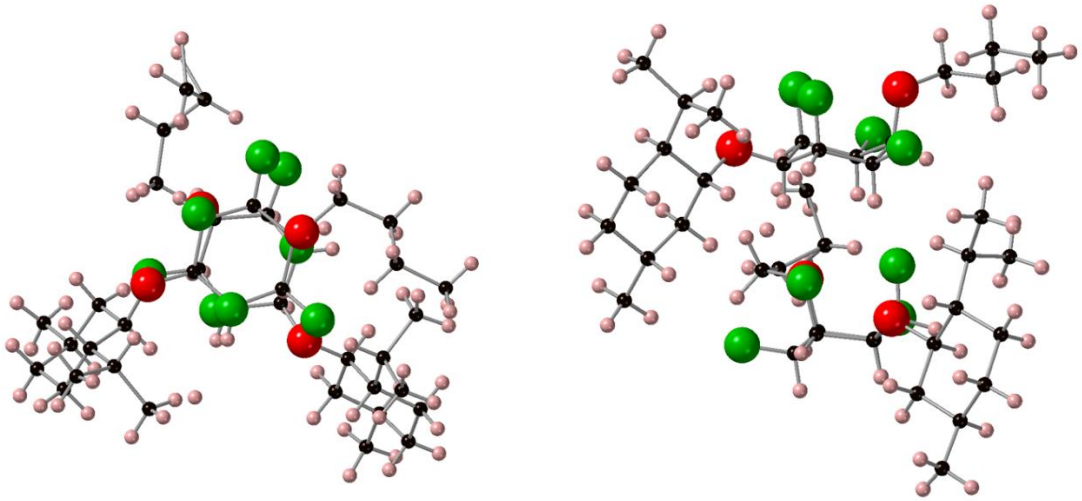

Figure 5.13: Crystal structure of **5.62**. Left: top view of molecules stacking on top of each other with a helical rotation. Right: two units from a different trajectory. NOTE: black for C, white for H, red for O, and green for F.

The DSC profile of **5.62** recorded in Kyoto, indicates that there are three polymorphic phases (Figure 5.14). A glass phase, a crystal phase, and an iso liquid (melt) phase. These phases indicate that the compound possesses polymorphism and potentially some liquid crystallinity.

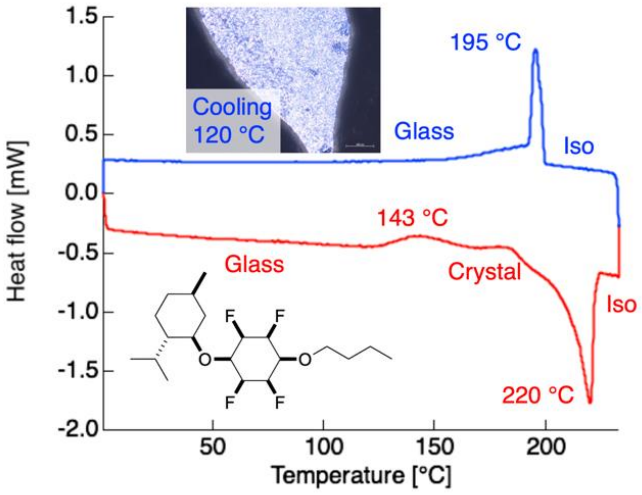

Figure 5.14: DSC and POM image of compound **5.62**. The blue DSC profile right to left shows the 1st cooling stage from above the melting point. The 2nd heating stage (red) to above the melting point. The POM image (inset) is taken at 120 °C (glass phase).

The next two targets were prepared from **5.43**, containing the *bis*-cyclohexyl LC motif discussed earlier. The idea was to cap each with either an n-butyl or methyl ether to assess the impact of the length on the resultant polymorphism.

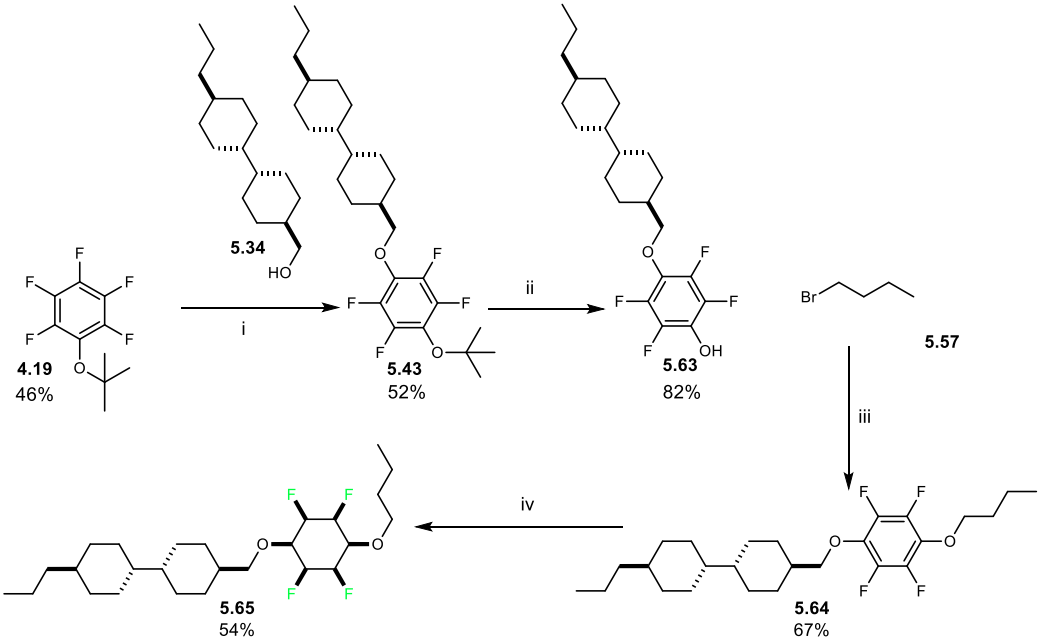

Scheme 5.17: Route to butyl ether **5.65**. i: KOH (10.4 mmol), alcohol **5.34** (5.413 mmol), **4.19** (4.16 mmol), THF (10 mL), 75 °C, 24 h, 52%. ii: **5.43** (1.45 mmol), TFA (1.45 mL), DCM (50 mL), r.t., 23 h, 82%. iii: K_2CO_3 (2.37 mmol), **5.63** (0.79 mmol), **5.57** (0.95 mmol), acetonitrile (20 mL), THF (10 mL), 85 °C, 23 h, 67%. iv: **5.64** (1.2 mmol), Rh-CAAC-COD-Cl **1.14** (2 mol%), 4Å MS (8 g), silica (4 g), hexane (40 mL), H_2 (50 bar), r.t., 5 days, 54%.

The synthesis of the butyl ether **5.65** and methyl ether **5.68** are summarised in Scheme 5.17 and Scheme 5.18 respectively. The *meta* product was found to co-elute on purification of both of these compounds. This resulted in **5.65** containing 12% *meta* product, and **5.68** containing 15% *meta* product.

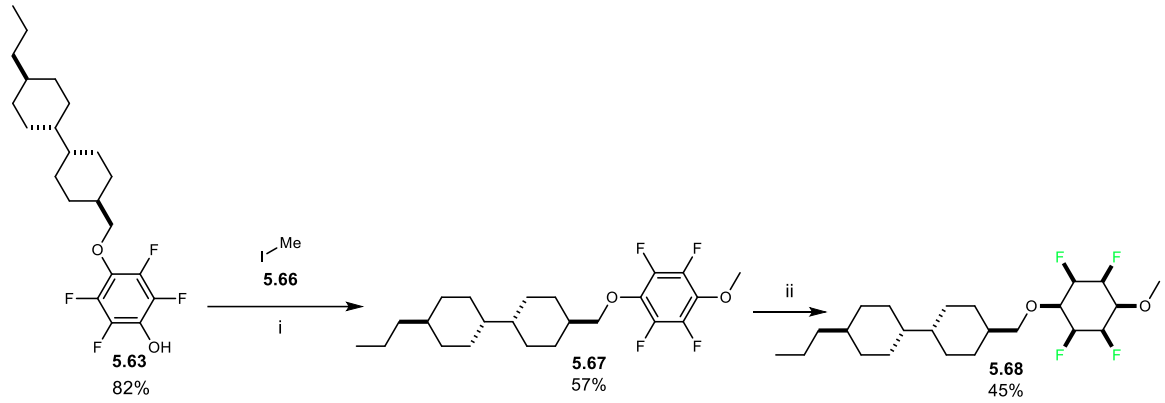

Scheme 5.18: Route to methyl ether **5.68**. i: K_2CO_3 (3.5 mmol), **5.63** (1.17 mmol), **5.66** (1.4 mmol), acetonitrile (50 mL), 90 °C, 23 h, 57%. ii: **5.67** (0.264 mmol), Rh-CAAC-COD-Cl **1.14** (2 mol%), 4Å MS (1 g), silica (250 g), hexane (20 mL), H_2 (50 bar), r.t., 5 days, 45%.

The ethers **5.65** and **5.68** were subjected to DSC and POM analyses. They both exhibited distinct polymorphic behaviour, indicative of their ability to exist in multiple crystalline forms (Figure 5.15). In particular, the butyl ether **5.65** possesses a glass phase, two crystalline phases, as well as a liquid phase. These two crystalline phases are interesting as this has yet to be observed with other Janus LC type molecules. This polymorphism is encouraging, offering potential LC applications.

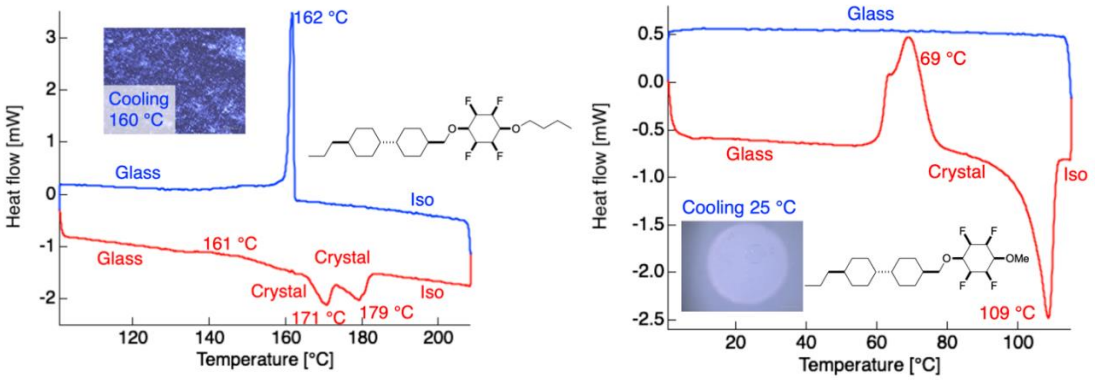

Figure 5.15: DSC profiles and POM images of **5.65** and **5.68**. The 1st cooling stage (blue) from above the melting point then the 2nd heating stage (red) until its melting point. The POM image for **5.65** at 160 °C shows the crystalline phase transitioning into the glass phase. Right: DSC profile and POM image at 25 °C of **5.68**.

Due to the rich polymorphic behaviour of these bis cyclohexyl containing Janus ethers, an additional target was prepared removing a CH_2 spacer. This should make the molecule less flexible and more compact. A butyl ether was used as a cap as this seemed

to increase the level of polymorphism, eg comparing **5.65** with **5.68**. The route is outlined in Scheme 5.19.

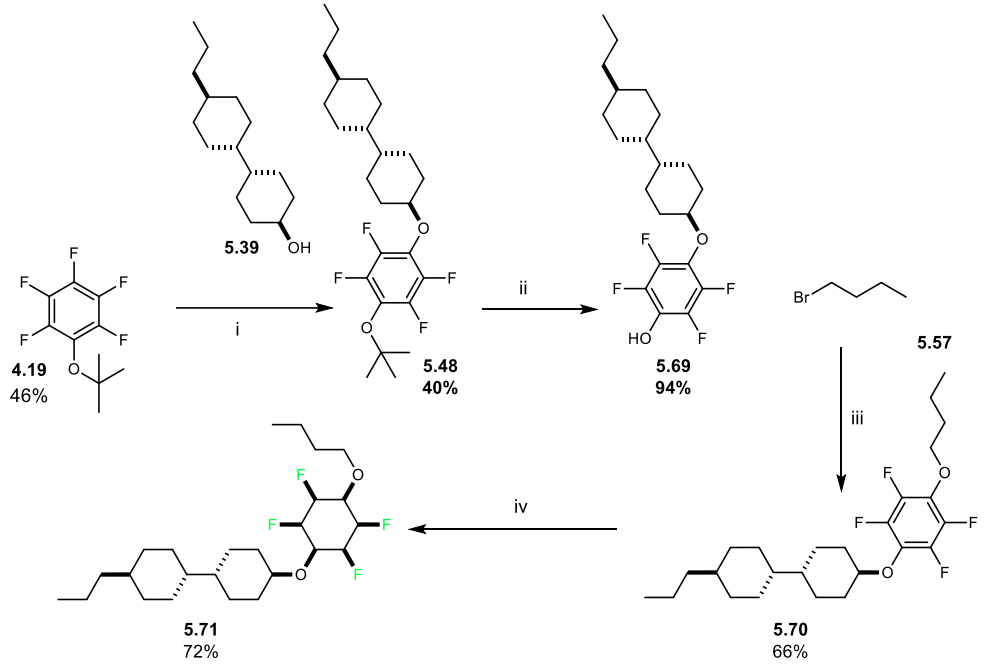

Scheme 5.19: Route to **5.71**. i: KOH (10.4 mmol), alcohol **5.39** (5.413 mmol), **4.19** (4.16 mmol), THF (10 mL), 75 °C, 24 h, 40%. ii: **5.48** (1.57 mmol), TFA (1.57 mL), DCM (50 mL), r.t., 23 h, 94%. iii: K_2CO_3 (4.26 mmol), **5.69** (1.42 mmol), **5.57** (2.13 mmol), acetonitrile (50 mL), THF (10 mL), 85 °C, 23 h, 66%. iv: **5.70** (0.877 mmol), Rh-CAAC-COD-Cl **1.14** (2 mol%), 4Å MS (1 g), silica (500 mg), hexane (20 mL), H_2 (50 bar), r.t., 3 d, 72%.

It is notable that the aryl hydrogenation progressed well in this case, resulting in a yield of 72%. TGA, DSC, and POM analysis are summarised in Figure 5.16. The purified **5.71** only possessed 6% *meta* product after purification.

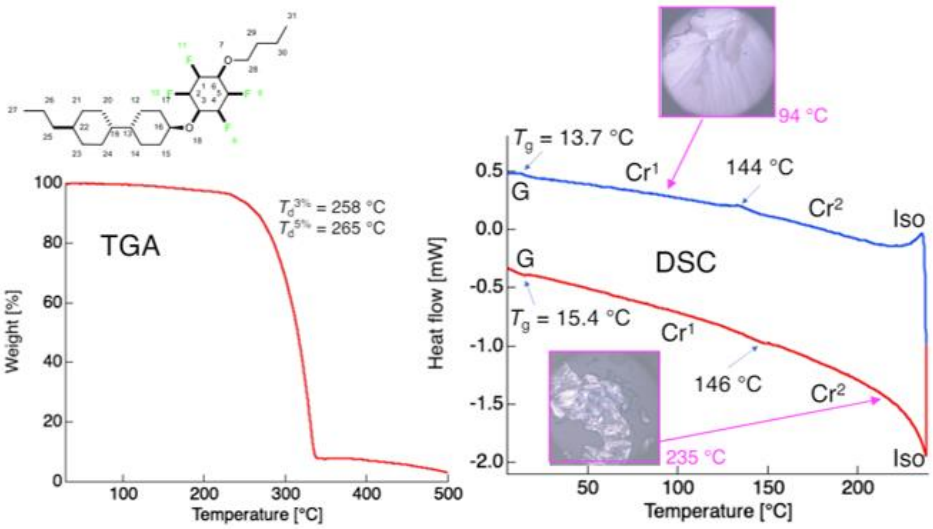

Figure 5.16: The TGA, DSC and POM image of **5.71**. Left: TGA indicating the melting point was close to the thermal decomposition temperature at 3% and 5% weight loss. Right: The DSC and POM image of **5.71**. These results show in blue the 1st cooling stage going from above the melting point of the materials to a low temperature, then in red the 2nd heating stage as the material goes to above its melting point.

This dialkyl ether has a particularly high melting point where it decomposes above 260 °C. The DSC profile indicates a significant level of polymorphism with four clear phases. Thermogravimetric analysis (TGA)[208] explores changes in mass as a sample is heated. This allows an insight into decomposition temperature, thermal stability, moisture content, and composition.[209,210] The TGA indicated that the melting point of **5.71** was close to the thermal decomposition temperature (T_d) when T_d involved 3% and 5% weight loss ($T_d^{3\%}$ =258 °C and $T_d^{5\%}$ = 265 °C).

5.5 Conformational equilibrium between *ax/eq* and *eq/ax* Janus 3,6-diethers

It is clear that these Janus 3,6-dialkyl ethers adopt chair conformations and this dictates an axial and an equatorial ether bond within each ring.

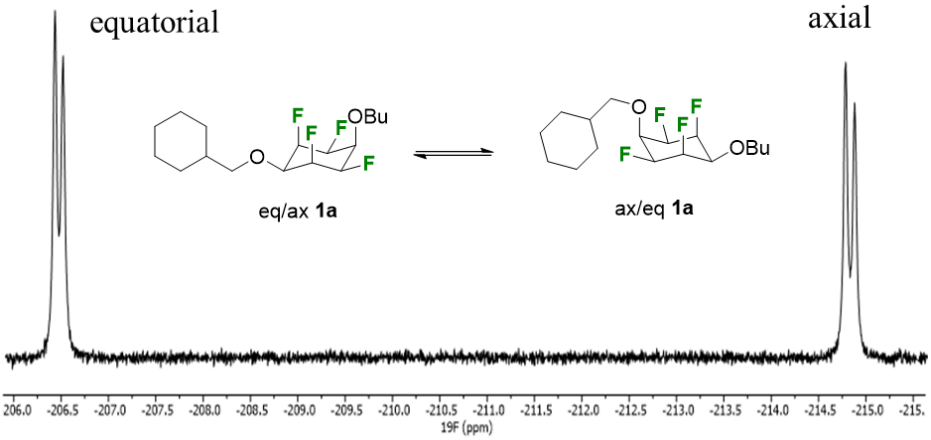

Figure 5.10: ^{19}F NMR of equatorial vs axial Janus 3,6-diether **5.59**.

^{19}F NMR analysis indicates that these compounds adopt mixed ratios of presumably the *ax/eq* and *eq/ax* chair conformers in solution, where either of the ether substituents can occupy the axial or equatorial orientation (Figure 5.10). These have recently been termed 'thermodynamically disfavoured cyclohexanes',[211] where within interconverting chair conformations, non-equivalent substituents switch between axial and equatorial orientations. The pathway and energy barrier to this interconversion was explored theoretically for the tetrafluoro dimethyl ether and it was compared to the all-*cis*-hexafluorocyclohexane (**1.13**) and to cyclohexane itself, to act as a point of reference. Calculations were carried out at the M06-2X/def2-TZVP theory level. This work was carried out by Prof Rodrigo Cormanich and Bruno Piscelli at the University of Campinas, Brazil. The resultant interconversion pathways and barriers are illustrated below in Figure 5.11.

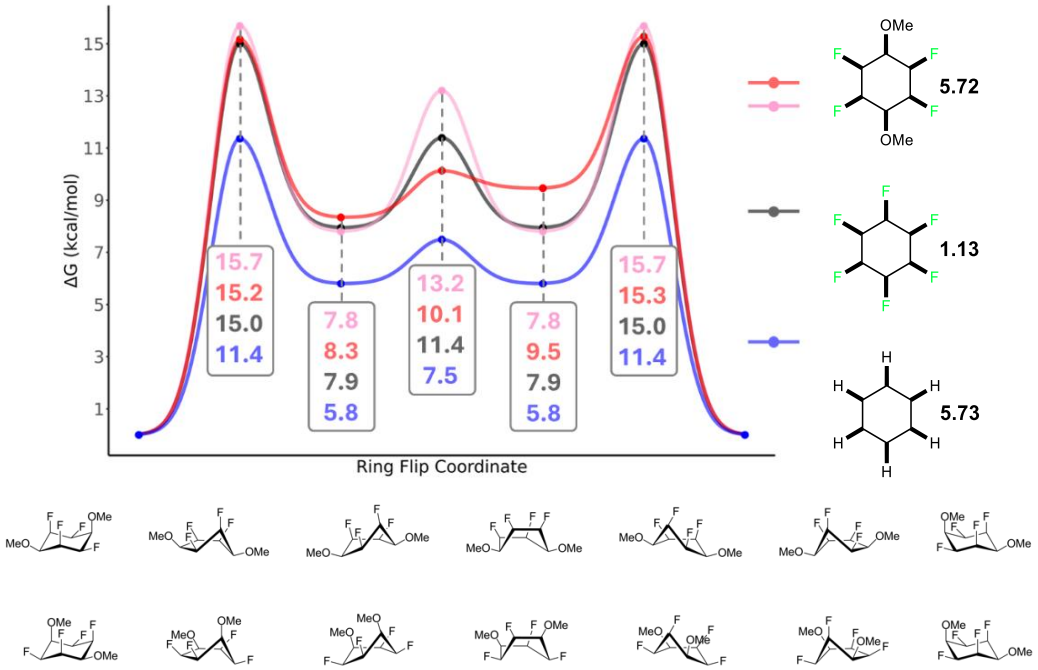

Figure 5.11: Comparative cyclohexyl interconversion energy profiles for **5.72**, **1.13**, and cyclohexane (**5.73**) showing the relative energies of intermediates. Energy values in kcal mol^{-1}.

The ring interconversion barrier for **1.13** has been reported previously using different theory levels.[70,75] The values here for the transition states and also the twist boat intermediates are similar to those reported in previous studies for both **1.13** and for cyclohexane (**5.73**). It is notable that the barriers to interconversion for the Janus 3,6-dimethoxy ether **5.72** is almost identical to **1.13**, although there is now an asymmetry to the profile relative to the two other cyclohexanes studied here. This reflects the two possible boat / twist boat structures where either two C-O bonds or two C-F bonds adopt equatorial orientations at the apical carbons. This analysis revealed that these rings are able to interconvert relatively straightforwardly with a barrier to inversion of only ~4-5 kcal mol^{-1} above cyclohexane.

5.6 Pentafluoro alkyl ether Janus compound

As a final experiment to better understand the supramolecular assembly of compounds **5.65** and **5.68** a simplified pentafluoro system was sought after.

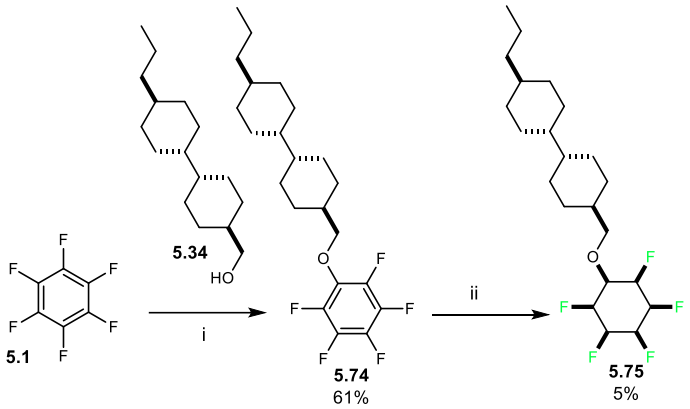

Scheme 5.20: Synthesis of **5.75**. i: KOH (13 mmol) alcohol **5.34** (13 mmol), **5.1** (8.66 mmol), THF (15 mL), 75 °C, 23 h, 61%. ii: **5.74** (1.2 mmol), Rh-CAAC-COD-Cl **1.14** (2 mol%), 4Å MS (1 g), silica (500 mg), hexane (20 mL), H_2 (50 bar), r.t., 24 h, 5%.

The target **5.75** was easily prepared through a two-step synthesis (Scheme 5.20). The aryl hydrogenation was conducted for only a 24-hour period as longer reactions times result in defluorination. The shorter reaction time however compromised the yield of **5.75**. For chromatography the compound proved to be insoluble in most solvents, requiring sonication to prepare a solution, and then material was lost on the column, precipitating during purification. However, a sample of the purified product was characterized, and a crystal structure was obtained (Figure 5.17). Notably the cyclohexane rings stacked directly on top of each other, typical of monosubstituted Janus cyclohexanes.

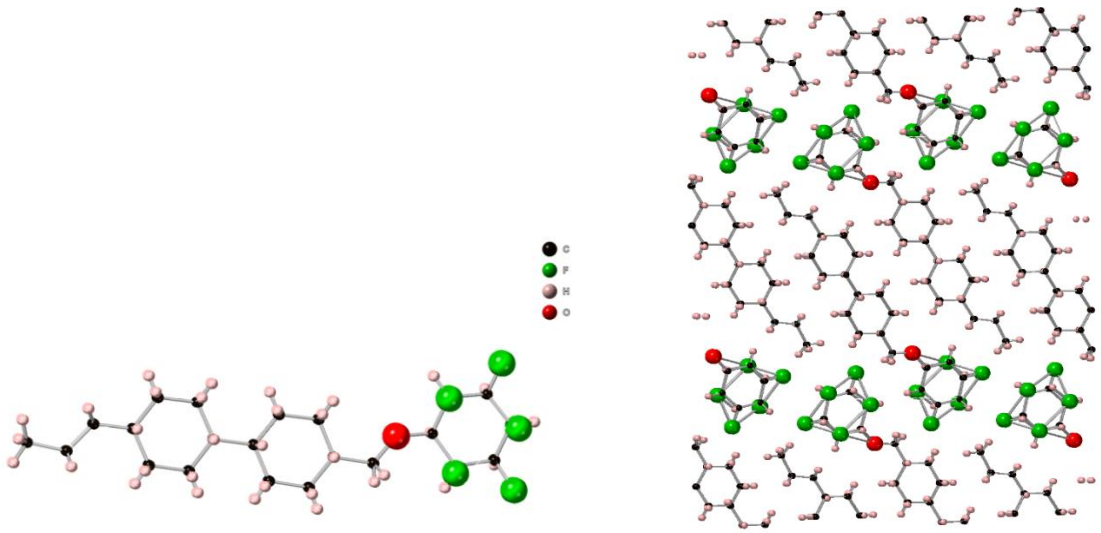

Figure 5.17: Crystal structure of **5.75**. Left: single molecule. Right: molecular packing. NOTE: black for C, white for H, red for O, and green for F.

The Janus rings are not isolated here, they instead stack next to each other with the LC group acting as a spacer (Figure 5.17). The closest H···F interaction length was 2.366 Å which is similar to the 3,6-diether systems prepared previously, such as **5.62**. This compound was subject to DSC, POM images, and TGA in Kyoto.

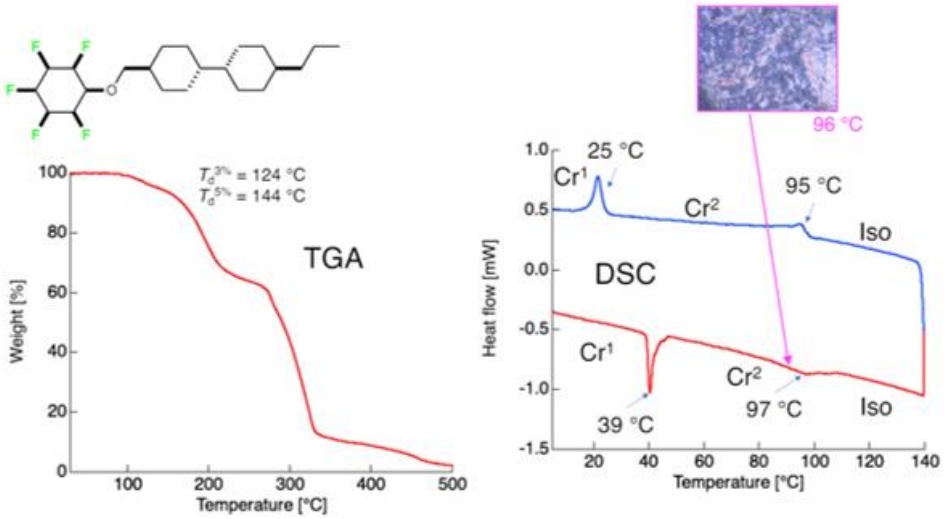

Figure 5.18: The TGA, DSC and POM image for **5.75**. Left: TGA showing decomposition temperatures at 3% or 5% weight loss at 124 °C and 144 °C respectively. Right: The DSC and POM image of **5.75**.

The DSC along with the POM images indicate the presence of two crystalline phases as well as an isotropic liquid phase (Figure 5.15). This is similar to compound **5.65** but is missing the amorphous glass phase. Interestingly however, **5.75** possess a 'plastic crystal' phase in which only the orientation order is broken and only the positional order is present. A plastic crystal is a type of solid where the molecules maintain their positional order, meaning they are arranged in a regular lattice, but have rotational freedom, meaning they can rotate more freely within their lattice positions.[212] This phase is characterized by having some of the fluid-like properties of a liquid, such as the ability to rotate or reorient, while still maintaining the long-range positional order of a crystalline solid. In other words, in a plastic crystal phase, the molecules are organized in a structured pattern but can rotate or reorient themselves within their fixed positions, unlike in a conventional crystal where both positional and orientational orders are maintained.[212] This is the first example in our series possessing such a phase.

TGA indicated that the melting point (97 °C) was not close to the thermal decomposition of the molecule. Additionally, the decomposition temperate at a weight loss of 3% was 124 °C whereby at a weight loss of 5% occurred at 144 °C.

It is clear that monosubstituted ether **5.75** is more highly ordered in the solid state than the *bis*-ether systems **5.65** and **5.68**.

5.7 Dielectric anisotropy Investigation

The selected compounds in Figure 5.19 were explored in dielectric measurements. This was carried out in a collaboration with Professor Taiju Takahashi at Kyoto University.

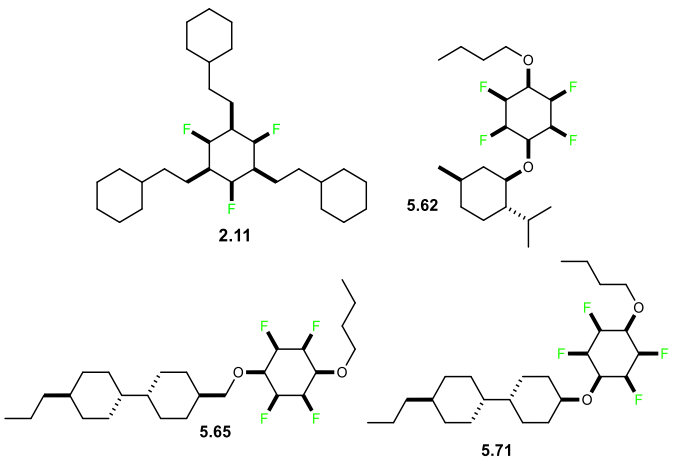

Figure 5.19: Janus ring containing compounds investigated for dielectric anisotropy.

The compounds were prepared as mixtures with the mother LC mixture known as ZLI-4792 (Figure 5.20) and were mixed with the candidate molecules at 3 wt%, 5 wt%, 7 wt%, and 10 wt% concentrations. The cell was 10 μm thick and the alignment treatment was carried out both horizontally and vertically. The dielectric anisotropy along the short molecular axis (ε_n) is subtracted from the dielectric anisotropy along the long molecular axis (ε_p) to acquire the dielectric anisotropy constant ($\Delta\varepsilon$). The resulting dielectric constants for compound **5.62** are discussed below.

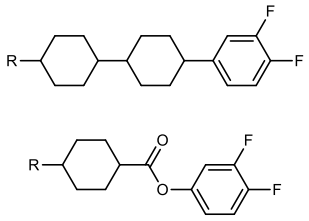

Figure 5.20: Primary components of the mixed Liquid Crystal ZLI-4792.[213]

The dielectric constant of compound **5.62** could be measured between 3 and 5 weight % but when this increased to 7 and 10 weight %, measurements failed as the material become horizontally aligned even if a vertically alignment material is used. The calculated results for **5.62** are outlined below.

$$\Delta\varepsilon = \varepsilon_p - \varepsilon_n$$

2.98 wt% → ε_p = 8.6, ε_n = 3.8 → $\Delta\varepsilon$ = +4.8

5.06 wt% → ε_p = 8.5, ε_n = 3.8 → $\Delta\varepsilon$ = +4.7

7.00 wt% → failed

9.85 wt% → failed

VA and TN LC displays require strong negative dielectric anisotropy. This is due to the need of the LC to have a dipole perpendicular to the main axis of the molecule. However, if a compound possesses a positive dielectric constant, it could be used in in-plane switching visual displays. Such compounds have the dipole of the LC parallel with the long axis of the molecule. At ~3 and ~5 weight% the chiral **5.62** possessed a positive dielectric anisotropy of ~+4.8. The relatively high positive dielectric anisotropy of **5.62**, actually meets the key requirement for use in in-plane switching visual displays, a mode that possess liquid crystals with strong positive dielectric anisotropy,[214] suggesting that the molecule polarity aligns with the long molecular axis. This can be seen in the compound's crystal structure (Figure 5.13). However, as the dielectric constant did not increase with larger concentrations the dielectric constant of compound **5.62** by itself is negligible.

Compound **5.65** was found to have poor compatibility with the LC matrix. When mixing the material with the host cocktail LCs (ZLI-4792), and injecting into vertically aligned treatment empty cells, vertical alignment was not achieved. Specifically, when the mixed LCs are heated above the isotropic phase (melting) temperature, they become transparent. However, upon cooling to the nematic-isotropic (NI) point, precipitation occurred, causing the host LC to align around the precipitate, thus preventing vertical alignment. Additionally, some materials did not dissolve in the host LC, forming large clumps. Most materials caused the LC to solidify into a gel-like state, even at a concentration of 1 wt%. Specifically, **5.71** did not dissolve into the matrix. For **2.11**, even when the liquid crystal was heated above the isotropic (melting) phase, it did not become transparent.

5.8 Conclusions

Nucleophilic aromatic substitution reactions of pentafluoro aryls were investigated in this Chapter. It was demonstrated that there is a preference for *para* over *meta* product formation. This was attributed to a kinetic effect, where computation indicated a more stable *para* transition state. Experimentally the *tert*-butyl ether **4.19** was the most *para* directing of a series of pentafluoroaryl ethers. As a consequence, *tert*-butyl ether **4.19** was explored as a starting material for synthesis to develop the first examples of Janus 3,6-dialkyl ether cyclohexanes. The synthesis approach allowed control for the preparation of both 'equivalent' and 'non-equivalent' diether targets, and products were investigated for properties relevant to their development as organic liquid crystals.

Upon investigation, it was found that these linear Janus ring containing compounds do display diverse polymorphic characteristics, more so than the trialkyl compounds developed in Chapter 2. These results give a clear indication that the linear compounds have the best prospects for the development of Janus containing LCs.

The negative dielectric anisotropic ($-\Delta\varepsilon$) properties of selected compounds were investigated. In the event none possessed $-\Delta\varepsilon$, however, the menthol derived and

optically pure **5.62** possessed positive dielectric anisotropy (+$\Delta\varepsilon$). This suggested that it, or a derivative, could be a candidate for in-plane switching type visual displays, but it would have to be able to mix with the ZLI-4792 matrix at higher concentrations.

6: Conclusions

In this thesis, synthesis approaches to novel materials containing Janus-face fluorocyclohexanes have been developed.

Chapter 2 outlined a journey in generating Janus-faced fluorocyclohexanes, starting from accessible fluoroarenes and long-chain acetylenes. Utilizing Sonogashira reactions, *bis*- and *tris*- aromatic acetylenes were generated, which were then reduced to fluoroarenes and subsequently to cyclohexanes by aryl hydrogenations, based on an adapted protocol from the Glorius group. This work led to a new synthesis method for selectively alkylating cyclohexanes, resulting in molecules with triaxial C-F bonds and a distinct polar character. These molecules, display an intriguing assembly behaviour due to electrostatic attractions, and they offer potential for creating ordered supramolecular assemblies with unique polar properties.

In Chapter 3, the synthesis of two struts were prepared and structurally characterised to investigate the first preparation of a JOF-MOF. These molecules, featuring carboxylic acid linkers and either traditional pentafluoro or trifluoro Janus faces, enable a new approach to supramolecular assemblies through the interactions with MOF metal centres and the H-F faces of Janus rings. Early results have shown a promising increase in the porosity of these first generation JOF-MOF molecules, suggesting significant potential for the development of a new class of porous material.

Chapter 4 focused on developing Janus cyclohexanes but with a 3,6-dialkyl ether linkage. These may have potential in various applications and were investigated here in the context of their dielectric anisotropic properties. This design aligned with characteristics found in many organic liquid crystals. The synthesized compounds exhibited a strong dipole perpendicular to the main axis of the molecule and include a phosphonic acid group for self-assembly on Al_2O_3 layers of memory storage devices.

Lastly, Chapter 5 explored nucleophilic aromatic substitution reactions of pentafluoro aryls, exploring the preference for *para* products. Investigations into the directing capabilities of different ether substituents led to the development of a synthesis of Janus 3,6-di alkyl ether cyclohexanes, exploiting the directing influence of the *tert*-butyl ether moiety. These linearly substituted Janus cyclohexanes demonstrated a high degree of polymorphism suggesting their potential for the development of LCs. This exploration into 3,6-dialkyl ethers opens new possibilities for the application of Janus molecules in technology.

In conclusion, the work presented in this thesis advances the synthetic methodologies for Janus-face fluorocyclohexanes and highlights their potential impact in fields ranging from materials science to liquid crystal technology, offering exciting new avenues for future research and innovation.

7: Experimental

7.1 Analytical Instrumentation supporting synthesis

Unless otherwise noted, all reactions were carried out under an atmosphere of argon in oven-dried glassware. Reaction temperatures are reported as the temperature of the bath surrounding the vessel unless otherwise stated. Dry hexane was obtained from SPS in house (4Å), and dry methanol from Sigma-Aldrich.

Hydrogenation reactions at elevated pressure were carried out in stainless steel autoclaves using hydrogen gas. Commercially available chemicals were obtained from Acros, Alfa Aeser, Fluorochem, Sigma Aldrich, TCI (UK) and used as received unless otherwise stated. Degassing methodology achieved by bubbling nitrogen through the reagents via syringe for 20-40 min.

Analytical thin layer chromatography was performed on pre-coated aluminium plates (Kieselgel 60 F254 silica) and visualisation was achieved using ultraviolet light (254 nm) and/or staining with aqueous $KMnO_4$ solution followed by heating. Flash column chromatography was performed in glass columns fitted with porosity 3 sintered discs over Kieselgel 60 silica using the solvent system stated. Automated chromatography was performed on a Biotage Selekt 2 system with a UV/Vis detector using the method stated and cartridges filled with Kieselgel 60 silica.

Melting points were recorded on an Electrothermal 9100 melting point apparatus and (dec) refers to decomposition.

IR were recorded on a Shimadzu IRAffinity-1 Fourier transform IR spectrophotometer fitted with a Specac Quest ATR accessory (diamond puck). Spectra were recorded of either thin films or solids, with characteristic absorption wavenumbers (ν_{max}) reported in cm^{-1}.

^{1}H, $^{13}C\{^{1}H\}$, and $^{19}F\{^{1}H\}$ NMR spectra were acquired on either a Bruker AVII 400 with a BBFO probe (^{1}H 400 MHz; $^{13}C\{^{1}H\}$ 101 MHz; $^{19}F\{^{1}H\}$ 376 MHz), a Bruker AVIII-HD 500 with a SmartProbe BBFO+ probe (^{1}H 500 MHz, $^{13}C\{^{1}H\}$ 126 MHz, $^{19}F\{^{1}H\}$ 470 MHz) or a Bruker AVIII 500 with a CryoProbe Prodigy BBO probe (^{1}H 500 MHz, $^{13}C\{^{1}H\}$ 126 MHz, $^{19}F\{^{1}H\}$ 470 MHz) in the deuterated solvent stated. All chemical shifts are quoted in parts per million (ppm) relative to the residual solvent peak. All coupling constants, J, are quoted in Hz. Multiplicities are indicated as s (singlet), d (doublet), t (triplet), q (quartet), m (multiplet), and multiples thereof. The abbreviation Ar denotes aromatic and app denotes apparent. NMR peak assignments were confirmed using 2D ^{1}H correlated spectroscopy (COSY), 2D ^{1}H nuclear Overhauser effect spectroscopy (NOESY), 2D ^{1}H–^{13}C heteronuclear multiple-bond correlation spectroscopy (HMBC), and 2D ^{1}H–^{13}C heteronuclear single quantum coherence (HSQC) where necessary.

Mass spectrometry (m/z) data were acquired by either electrospray ionisation (ESI), chemical ionisation (CI), electron impact (EI), atmospheric solids analysis probe (ASAP), atmospheric pressure chemical ionization (APCI), matrix-assisted laser desorption/ionization (MALDI), Atmospheric pressure photoionization (APPI), fast atom bombardment (FAB) or nanospray ionisation (NSI).

7.2 Synthetic procedure and characterisation of molecules

Zeng catalyst 1.14

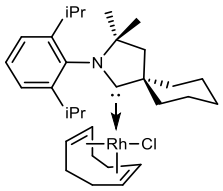

Rhodium-COD-chloride precursor (151 mg, 0.31 mmol), carbene salt (150 mg, 0.42 mmol) and KHMDS (236 mg, 1.18 mmol) were added to a schlenk tube under an argon atmosphere. Dry THF (9 mL) was added dropwise over 10 min to the solids at -78 °C. The suspension was stirred for 10 min at -78 °C, after which the cooling bath was removed, and the reaction mixture was allowed to warm up to r.t.. The yield was found to decrease when the reaction was stirred for longer periods at -78 °C. After stirring for 16 h at r.t., the suspension was filtered, concentrated, adsorbed on silica gel and

purified twice by column chromatography (pentane/diethyl ether = 9:1 and pentane/diethyl ether = 19:1). Traces of other solvents were found to prevent separation of the desired complex and the Rhodium-COD-chloride precursor. The second chromatography was necessary to remove traces of Rhodium-COD-chloride precursor. After evaporation of the solvents, the complex was precipitated from a concentrated solution in dichloromethane with pentane to yield the desired Zeng complex as yellow powder with spectroscopic data in accordance with the literature.[61] Yield 45% (78.1 mg, 0.14 mmol).

^{1}H NMR (500 MHz, $CDCl_3$) δ : 7.49–7.41 (m, 2H), 7.17 (dd, *J* = 1.6, 7.5 Hz, 1H), 5.27 (m, 1H), 4.64 (m, 1H), 3.92 (dt, *J* = 13.2, 6.8 Hz, 1H), 3.49–3.44 (m, 1H), 2.94–2.88 (m, 2H), 2.65–2.49 (m, 3H), 2.31–2.28 (m, 2H), 2.16–2.12 (m, 1H), 2.04–1.94 (m, 5H), 1.81–1.76 (m, 8H), 1.60–1.52 (m, 18H), 1.48 (s, 3H), 1.46–1.31 (m, 6H), 1.29-1.24 (m, 14H), 1.22 (s, 3H), 0.98 (d, *J* = 6.7 Hz, 3H); ^{13}C NMR (126 MHz, $CDCl_3$) δ : 148.4, 146.4, 136.6, 129.6, 126.4, 125.1, 104.2 (d, *J* = 3.0 Hz), 100.7 (d, *J* = 11.5 Hz), 77.5, 65.2, 64.7 (d, *J* = 3.4 Hz), 53.3, 41.8, 39.3, 34.3.

7.21 Experimental for Chapter 2

General Procedure 1 Sonogashira reactions

1,3,5-Trifluoro-2,4,6-triiodobenzene (1 eq), appropriate acetylene (3.6 eq), palladium catalyst (0.15 eq), and copper (I) iodide (0.15 eq) were added to a RBF. Diisopropylamine (20 — 34 mL) was then added and the reaction was heated to 80 °C for 24 h. The reaction mixture was then cooled to r.t. and slowly passed through a pad of silica gel with elusion of ethyl acetate. The solvent was removed under reduced pressure to give the crude product, which was purified by flash silica column chromatography.

General Procedure 2 Pd/C reactions

A solution of alkyne (1 eq) was dissolved in either hexane, methanol, or ethyl acetate (10—100 mL) and 10% palladium on carbon catalyst (10% wt eq) was added to the suspension. The hydrogenation was then carried out at either atmospheric pressure of H_2 gas from a balloon, or, the hydrogenation was carried out in a stainless steel autoclave with H_2 pressure at 15 bar. The reaction was carried out for 1 — 4 d. The reaction mixture was then slowly passed through a pad of celite with elusion of ethyl acetate. The solvent was removed under reduced pressure to give the crude product, which was purified by flash silica column chromatography.

General Procedure 3 Aryl hydrogenations

Rhodium-CAAC-COD-Cl catalyst (**1.14**) (1.6 — 2 mol%) was added to an oven dried 9 mL screw-cap vial or a 50 mL glass cylinder equipped with a stirring bar and activated 4 Å molecular sieves (0.2 — 3.2 g) and/or silica (0.2 — 1.6 g). Hexane (2 — 40 mL) and aromatic substrate (1 eq) were added under argon atmosphere. The glass vial/cylinder was placed in a 150 mL stainless steel autoclave under argon atmosphere. The autoclave was pressurized and depressurized with hydrogen gas three times before the indicated pressure was set (50 — 70 bar). The reaction mixture was stirred at 25 — 50 °C for 1 — 10 d. After the autoclave was carefully depressurized, the mixture was filtered through a sinter funnel and washed with 10% methanol in DCM. The solvent was removed under reduced pressure to give the crude product, which was purified by flash silica column chromatography.

1,2,3,4,5-Pentafluoro-6-(octynyl)benzene 2.17

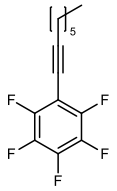

1,2,3,4,5-Pentafluoro-6-iodobenzene (0.330 mL, 2.50 mmol), 1-octyne (0.440 mL, 3.00 mmol), palladium catalyst (263 mg, 0.380 mmol), and copper (I) iodide (71.4 mg, 0.380 mmol) were all added to a 100 ml RBF. Diisopropylamine (25.0 mL) was then added, and the reaction mixture was heated to 80 ˚C under argon and stirred for 22 h. The reaction mixture was then cooled to r.t. and slowly passed through a pad of silica gel with an elusion of ethyl acetate. The solvent was removed via concentration in vacuo at 0 mbar and for 3 h and then purified via column chromatography (pentane) to afford **2.17** as a colourless oil (65%, 0.230 g, 0.820 mmol).

IR ν_{max} (film): 2930, 2860, 2247, 1518, 1468 cm^{-1}; ^{1}H NMR (500 MHz, $CDCl_3$) δ : 2.49 (t, *J* = 7.1 Hz, 2H, C≡CC$\underline{H}_2$), 1.63 (app. quint., *J* = 7.2 Hz, 2H, C≡CCH$_2$C$\underline{H}_2$), 1.39-1.24 (m, 6H, C≡CCH$_2$CH$_2$C$\underline{H}_2$C$\underline{H}_2$C$\underline{H}_2$), 0.90 (m, 3H, C$\underline{H}_3$); $^{19}F\{^{1}H\}$ (376 MHz, $CDCl_3$) δ : -137.3 (m, 2F, *ortho*-F), -154.5 (t, *J* = 20.8 Hz, 1F, *para*-F), -162.5 (td, *J* = 21.9 and 6.7 Hz, 2F, *meta*-F); ^{13}C NMR (126 MHz, $CDCl_3$) δ : 147.6 – 138.9 (m, Ar-CF), 104.3 (Ar-$\underline{C}$C≡C), 65.4 (C≡C$\underline{C}$CH$_2$), 64.8 ($\underline{C}$≡CCH$_2$), 31.4 ($\underline{C}$H$_2$CH$_2$CH$_3$), 28.5 ($\underline{C}$H$_2$CH$_2$CH$_2$CH$_3$), 22.7 (C≡CCH$_2$$\underline{C}H_2$), 19.9 ($\underline{C}H_2CH_3$), 19.4 (C≡C$\underline{C}H_2$), 14.2 ($\underline{C}H_3$); HRMS (EI) $C_{14}H_{13}F_5$ [M] found 276.093, requires 276.094.

1,2,3,4,5-Pentafluoro-6-octylbenzene 2.18

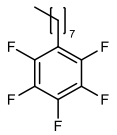

Following General Procedure **2**, **2.17** (100 mg, 0.370 mmol), 10% palladium on carbon catalyst (10.0 mg, 10% wt eq), and hexane (10.0 mL), under atmospheric H_2 for 24 h gave, after purification by flash silica chromatography (hexane) **2.18** (72%, 70.0 mg, 0.260 mmol) was isolated as a colourless oil.

IR ν_{max} (film): 2956, 2924, 2854, 1654, 1485 cm^{-1}; ^{1}H NMR (500 MHz, $CDCl_3$) δ : 2.68 (t, *J* = 7.63 Hz, 2H, $C\underline{H}_2$), 1.56 (q, *J* = 7.8, 7.4 Hz, 2H, $CH_2C\underline{H}_2$), 1.31—1.25 (m, 17H, $CH_2CH_2C\underline{H}_2C\underline{H}_2C\underline{H}_2C\underline{H}_2C\underline{H}_2CH_3$), 0.88 (t, *J* = 6.9 Hz, 3H, $C\underline{H}_3$); $^{19}F\{^{1}H\}$ NMR (470 MHz, $CDCl_3$) δ : -144.5 – 144.6 (m, 2F, *ortho*-F), -158.5 (t, *J* = 20.8 Hz, 1F, *para*-F), -163.2 (td, *J* = 22.1, 8.0 Hz, 2F, *meta*-F); ^{13}C NMR (126 MHz, $CDCl_3$) δ : 146.0 – 140.4 (m, Ar-$\underline{C}$F), 138.4 (Ar-$\underline{C}CH_2$), 124.2 ($\underline{C}H_2CH_2CH_3$), 115.6 ($\underline{C}H_2CH_2CH_2CH_2CH_2CH_2CH_3$), 31.9 ($\underline{C}H_2CH_2CH_2CH_2CH_2CH_3$), 29.7 ($\underline{C}H_2CH_2CH_2CH_3$), 29.3 ($\underline{C}H_2CH_2CH_2CH_2CH_3$), 22.7 (Ar-$\underline{C}H_2$), 22.3 ($\underline{C}H_2CH_3$), 14.1 ($\underline{C}H_3$); HRMS (EI) $C_{14}H_{17}F_5$ [M] found 280.125, requires 280.125.

All-*cis* 1,2,3,4,5-pentafluoro-6-octylcyclohexane 2.1

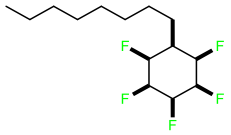

Following General Procedure **3**, **2.18** (46.7 mg, 0.170 mmol), Rh-CAAC-COD-Cl (1.60 mg, 0.003 mmol), 4Å molecular sieves (200 mg), and hexane (2.00 mL) for 24 h, r.t., and at 50 bar H_2 gave, after purification by flash silica chromatography (60:40 diethyl ether:pentane) **2.1** (>99%, 72.0 mg, 0.250 mmol) was isolated as a white crystal. m.p. 138—140 °C.

IR ν_{max} (solid): 2920, 1506 cm^{-1}; ^{1}H NMR (500 MHz, $CDCl_3$) δ : 5.37—5.24 (m, 1H, *para*-$\underline{H}$F), 4.92 (apparent d, *J* = 48.7 Hz, 2H, *ortho*-$\underline{H}$F), 4.4 (apparent dt, *J* = 41.1, 26.7 Hz, 2H, *meta*-$\underline{H}$F), 1.86—1.77 (m, 1H, ring-$\underline{H}$C), 1.29—1.18 (m, 14H, chain-C$\underline{H}_2$), 0.86 (t, *J* = 7.1 Hz, 3H, C$\underline{H}_3$); $^{19}F\{^{1}H\}$ NMR (470 MHz, $CDCl_3$) δ : -203.3 (dt, *J* = 11.6, 7.8 Hz, 2F, *meta*-F), -212.1 (ddd, *J* = 26.7, 7.3, 4.5 Hz, 2F, *ortho*-F), -216.7 (tt, 26.6, 11.3 Hz, 1F, *para*-F); ^{13}C NMR (126 MHz, $CDCl_3$) δ : 88.2 – 85.5 (m, 5x $\underline{C}$F), 38.6 (ring-$\underline{C}$H), 34.3 ($\underline{C}H_2CH_2CH_3$), 32.0 ($CHCH_2CH_2\underline{C}H_2$), 29.8 ($CHCH_2CH_2\underline{C}H_2\underline{C}H_2$), 29.5 ($\underline{C}H_2CH_2CH_2CH_3$), 26.3 ($CH\underline{C}H_2$), 22.5 ($CHCH_2\underline{C}H_2$), 15.4 ($\underline{C}H_2CH_3$), 14.2 ($\underline{C}H_3$); HRMS ($ESI^+$) $C_{14}H_{23}F_5$ [M+Na] found 309.161, requires 309.162.

1,2,3,4,5-Pentafluoro-6-(hexynyl)benzene 2.19

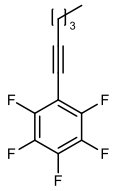

Following General Procedure **1**, pentafluoroiodobenzene (5.34 mL, 20.0 mmol), 1-hexyne (2.76 mL, 24.0 mmol), bis(triphenylphosphine)palladium(II) chloride (526 mg, 0.750 mmol), copper (I) iodide (107 mg, 0.560 mmol), DIPA (40.0 mL) and THF (48.0 mL) for 21 h gave, after purification by flash silica chromatography (0-5% EtOAc in hexane) the title compound (90%, 4.46 g, 18.0 mmol) as a clear oil.

IR ν_{max} (solid): 2937, 2249, 1494 cm^{-1}; ^{1}H NMR (500 MHz, $CDCl_3$) δ : 2.50 (t, *J* = 7.1 Hz, 2H, C≡CC$\underline{H}_2$), 1.70 – 1.57 (m, 2H, C≡CCH$_2$C$\underline{H}_2$), 1.53 – 1.44 (m, 2H, C≡CCH$_2$CH$_2$C$\underline{H}_2$), 0.95 (t, *J* = 7.3 Hz, 3H, C$\underline{H}_3$); $^{19}F\{^{1}H\}$ NMR (470 MHz, $CDCl_3$) δ : -137.2 – -137.4 (m, 2F, *ortho*-F), -154.5 (t, *J* = 20.6 Hz, 1F, *para*-F), -162.4 – -162.7 (m, 2F, *meta*-F); ^{13}C NMR (126 MHz, $CDCl_3$) δ : 147.6 (br d, ^{1}J = 256.7 Hz, *ortho*-C$\underline{F}$), 141.0 (br d, ^{1}J = 255.6 Hz, *para*-C$\underline{F}$), 137.7 (br d, ^{1}J = 250.5 Hz, *meta*-C$\underline{F}$), 104.3 (Ar-C$\underline{C}$C≡C), 65.4 (Ar-CC≡C$\underline{C}$), 64.8 (Ar-C$\underline{C}$≡C), 30.4 (C≡CCH$_2$C$\underline{H}_2$), 22.0 (C≡CCH$_2$CH$_2$C$\underline{H}_2$), 19.3 (C≡C$\underline{C}$H$_2$), 13.7 (C$\underline{H}_3$); HRMS (EI) $C_{12}H_9F_5$ [M] found 248.062, requires 248.062.

1,2,3,5-Tetrafluoro-4,6-di(hexynyl)benzene 2.20

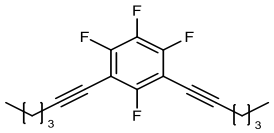

1,2,3,5-Tetrafluoro-4,6-diiodobenzene (1.01 g, 2.50 mmol), 1-hexyne (0.690 mL, 6.00 mmol), palladium catalyst (263 mg, 0.380 mmol), and copper (I) iodide (71.0 mg, 0.380 mmol) were all added to a 100 mL RBF. Diisopropylamine (25.0 mL) was then added, and the reaction mixture was heated to 80 °C under argon and stirred for 22 h. The reaction mixture was then cooled to r.t. and slowly passed through a pad of silica gel, 3 cm tall, eluting with ethyl acetate. The solvent was removed via concentration in vacuo and the purified via column chromatography (pentane), care was taken to separate hexyne from final product to afford **2.20** as an oil (89%, 0.660 g, 2.12 mmol).

IR ν_{max} (film): 2958, 2933, 2243, 1627, 1500 cm^{-1}; ^{1}H NMR (500 MHz, $CDCl_3$) δ : 2.48 (t, *J* = 7.0 Hz, 4H, C≡CC$\underline{H_2}$), 1.61 (p, *J* = 7.1 Hz, 4H, C≡CCH$_2$C$\underline{H_2}$), 1.54 – 1.44 (m, 4H, C$\underline{H_2}$CH$_3$), 0.95 (t, *J* = 7.3 Hz, 6H, C$\underline{H_3}$); $^{19}F\{^{1}H\}$ NMR (470 MHz, $CDCl_3$) δ : -110.5 (d, *J* = 10.1 Hz, 1F, *iso*-F), -130.4 (d, *J* = 21.6 Hz, 2F), -164.5 (td, *J* = 21.6, 10.1 Hz, 1F); ^{13}C NMR (126 MHz, $CDCl_3$) δ : 159.6 – 157.6 (m, Ar-$\underline{C}$F), 151.9 – 149.9 (m, Ar-$\underline{C}$F, 2C), 138.3 – 136.4 (m, Ar-$\underline{C}$F), 102.7 (Ar-$\underline{C}$C), 100.4 (C≡$\underline{C}$CH$_2$), 65.5 ($\underline{C}$≡CCH$_2$), 30.5 ($\underline{C}$H$_2$CH$_2$CH$_3$), 22.0 ($\underline{C}$H$_2$CH$_3$), 19.3 (C≡C$\underline{C}$H$_2$), 13.7 ($\underline{C}$H$_3$); HRMS (ESI^-) calculated for $C_{18}H_{18}F_4$ [M-H] found 309.126, requires 309.127.

1,2,3,5-Tetrafluoro-4,6-(dioctynyl)benzene 2.21

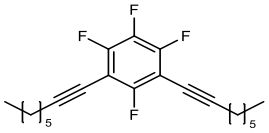

1,2,3,5-Tetrafluoro-4,6-diiodobenzene (1.01 g, 2.50 mmol), 1-octyne (0.890 mL, 6.00 mmol), palladium catalyst (263 mg, 0.380 mmol), and copper (I) iodide (71.0 mg, 0.380 mmol) were all added to a 100 ml RBF. Diisopropylamine (25.0 mL) was then added, and the reaction mixture was heated to 80 ˚C under argon and stirred for 22 h. The reaction mixture was then cooled to r.t. and slowly passed through a pad of silica gel, 3 cm tall, with an elusion of ethyl acetate. The solvent was removed via concentration in vacuo and the purified via column chromatography (pentane), care was taken to separate octyne from final product to afford **2.21** as an oil (>99%, 0.950 g, 2.60 mmol).

IR ν_{max} (film): 2953, 2929, 2245, 1647, 1616, 1489, 1480 cm^{-1}; ^{1}H NMR (500 MHz, $CDCl_3$) δ : 2.47 (t, *J* = 7.1 Hz, 4H, C≡CC$\underline{H_2}$), 1.62 (tt, *J* = 14.8, 7.2 Hz, 4H, C≡CCH$_2$C$\underline{H_2}$), 1.56 – 1.32 (m, 12H, C≡CCH$_2$CH$_2$C$\underline{H_2}$C$\underline{H_2}$C$\underline{H_2}$), 0.94 – 0.85 (m, 6 H, C$\underline{H_3}$); $^{19}F\{^{1}H\}$ NMR (470 MHz, $CDCl_3$) δ : -110.5 (d, *J* = 10.0 Hz, 1F, *iso*-F), -130.4 (d, *J* = 21.6 Hz, 2F), -164.5 (td, *J* = 21.6, 10.1 Hz, 1F); ^{13}C NMR (126 MHz, $CDCl_3$) δ : 157.6 – 153.4 (m, Ar-$\underline{C}$F), 151.9 – 150.3 (m, 2C, Ar-$\underline{C}$F), 150.9 – 148.5 (m, Ar-$\underline{C}$F), 102.7 (Ar-$\underline{C}$≡CC), 65.6 C (C≡$\underline{C}$ CH$_2$), 65.4 ($\underline{C}$≡CCH$_2$), 31.4 ($\underline{C}$H$_2$CH$_2$CH$_3$), 28.6 ($\underline{C}$H$_2$CH$_2$CH$_2$CH$_3$), 28.4 ($\underline{C}$H$_2$CH$_2$CH$_2$CH$_2$CH$_3$), 22.7 ($\underline{C}$H$_2$CH$_3$), 19.6 (C≡C$\underline{C}$H$_2$), 14.2 ($\underline{C}$H$_3$); HRMS (EI) $C_{22}H_{26}F_4$ [M] found 366.197, requires 366.197.

1,2,3,5-Tetrafluoro-4,6-bis(4-methylpentynyl)benzene 2.22

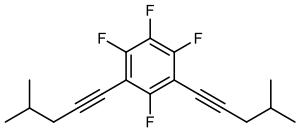

1,2,3,5-Tetrafluoro-4,6-diiodobenzene (1.01 g, 2.50 mmol), 4-methyl-1-pentyne (0.700 mL, 6.00 mmol), palladium catalyst (267 mg, 0.380 mmol), and copper (I) iodide (78.0 mg, 0.380 mmol) were all added to a 100 ml RBF. Diisopropylamine (25.0 mL) was then added, and the reaction mixture was heated to 80 ˚C under argon and stirred for 22 h. The reaction mixture was then cooled to r.t. and slowly passed through a pad of silica gel, 3 cm tall, with an elusion of ethyl acetate. The solvent was removed via concentration in vacuo and the purified via column chromatography (pentane), care was taken to separate starting alkyne from final product to afford **2.22** as an oil (94%, 0.730 g, 2.360 mmol).

IR ν_{max} (film): 2958, 2927, 2243, 1629, 1480 cm^{-1}; ^{1}H NMR (500 MHz, $CDCl_3$) δ : 2.37 (d, *J* = 6.5 Hz, 4H, C≡CC<u>H</u>$_2$), 1.94 (tsept, *J* = 13.2, 6.6 Hz, 2H, C<u>H</u>), 1.05 (d, *J* = 6.7 Hz, 12H, C<u>H</u>$_3$); $^{19}F\{^{1}H\}$ NMR (470 MHz, $CDCl_3$) δ : -110.4 (d, *J* = 10.1 Hz, 1F, *iso*-F), -130.4 (d, *J* = 21.6 Hz, 2F), -164.5 (td, *J* = 21.7, 10.2 Hz, 1F); ^{13}C NMR (126 MHz, $CDCl_3$) δ : 160.0 – 157.7 (m, Ar-<u>C</u>F), 152.0 – 149.9 (m, Ar-<u>C</u>F, 2C), 138.7. – 136.6 (Ar-<u>C</u>F), 101.7 – 101.5 (m, Ar-<u>C</u>C), 66.4 (<u>C</u>≡CCH$_2$), 66.2 (C≡<u>C</u>CH$_2$), 28.7 (<u>C</u>H), 28.1 (<u>C</u>H$_2$CH), 22.1 (<u>C</u>H$_3$); HRMS (EI) $C_{18}H_{18}F_4$ [M] found 310.129, requires 310.134.

((Perfluoro-1,3-phenylene)bis(propyne-3,1-diyl))dicyclohexane 2.23

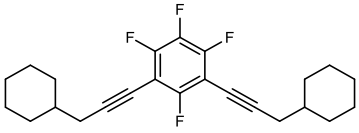

1,2,3,5-tetrafluoro-4,6-diiodobenzene (1.01 g, 2.50 mmol), 3-cyclohexyl-1-propyne (1.00 mL, 7.00 mmol), palladium catalyst (263 mg, 0.380 mmol), and copper (I) iodide (71.4 mg, 0.380 mmol) were all added to a 100 ml RBF. Diisopropylamine (24.0 mL) was then added and the reaction mixture was heated to 80 °C under argon and stirred for 24 h. The reaction mixture was then cooled to r.t. and slowly passed through a pad of silica gel with an elusion of ethyl acetate. The solvent was removed via concentration

in vacuo and the purified via flash chromatography (hexane) to afford the clear oil product in 82% yield. (0.808 g, 2.07 mmol). With spectral data in accordance with the literature.[71]

IR ν_{max} (neat): 2922, 2850, 2243, 1627, 1479 cm^{-1}; ^{1}H NMR (500 MHz, $CDCl_3$) δ : 2.37 (d, *J* = 6.6 Hz, 4H, C≡CC<u>H</u>$_2$), 1.62 – 1.56 (m, 2H, ring-C<u>H</u>), 1.32 – 0.95 (m, 16H, ring-C<u>H</u>$_2$); $^{19}F\{^{1}H\}$ NMR (500 MHz, $CDCl_3$) δ : -110.3 (d, *J* = 10.1 Hz, 1F, *iso*-Ar-<u>F</u>), -130.4 (d, *J* = 21.7 Hz, 2F, Ar-<u>F</u>), -164.5 (td, *J* = 21.7, 10.1 Hz, 1F, Ar-<u>F</u>); ^{13}C NMR (500 MHz, $CDCl_3$) δ : 157.7 – 149.7 (m, Ar-<u>C</u>F), 101.6 – 101.5 (m, Ar-<u>C</u>C), 66.3 (Ar-C<u>C</u>≡C), 66.1 (Ar-CC≡<u>C</u>), 37.2 (*ortho*-ring-<u>C</u>H$_2$), 32.7 (ring-<u>C</u>H), 27.5 (*para*-ring-<u>C</u>H$_2$), 27.0 (*meta*-ring-<u>C</u>H$_2$), 26.1 (C≡C<u>C</u>H$_2$).

1,3,5-Trifluoro-2,4,6-tri-1-hexynylbenzene 2.24

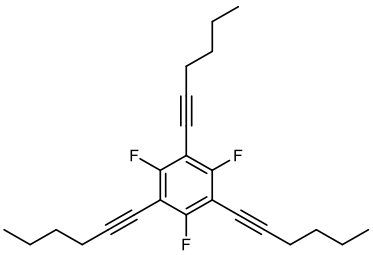

Following General Procedure **1**, 1,3,5-trifluoro-2,4,6-triiodobenzene (1.27 g, 2.50 mmol), 1-hexyne (1.03 mL, 9.00 mmol), bis(triphenylphosphine)palladium(II) chloride (263 mg, 0.380 mmol), copper (I) iodide (71.4 mg, 0.380 mmol), and DIPA (21.0 mL) for 24 h gave, after purification by flash silica chromatography (hexane) **2.24** (99%, 1.18 g, 2.50 mmol) was isolated as a yellow oil.

IR ν_{max} (film): 2958, 2933, 2872, 2243, 1604, 1323, 760 cm^{-1}; ^{1}H NMR (500 MHz, $CDCl_3$) δ : 2.47 (t, *J* = 7.1 Hz, 6H, C≡CC<u>H</u>$_2$), 1.60 (app. p, *J* = 7.0 Hz, 6H, C≡CCH$_2$C<u>H</u>$_2$), 1.55 — 1.44 (m, 6H, C≡CCH$_2$CH$_2$C<u>H</u>$_2$), 0.94 (t, *J* = 7.3 Hz, 9H, C<u>H</u>$_3$); $^{19}F\{^{1}H\}$ NMR (470 MHz, $CDCl_3$) δ : -103.9 (s, 3F); ^{13}C NMR (126 MHz, $CDCl_3$) δ : 162.2 (br dt, ^{1}J = 257.6, ^{2}J = 7.6 Hz, Ar-<u>C</u>F), 101.6 – 101.3 (m, Ar-<u>C</u>C), 65.9 (C≡<u>C</u>CH$_2$), 65.4 (<u>C</u>≡CCH$_2$), 30.4 (<u>C</u>H$_2$CH$_2$CH$_3$), 21.9 (<u>C</u>H$_2$CH$_3$), 19.2 (C≡C<u>C</u>H$_2$), 13.6 (<u>C</u>H$_3$).

1,3,5-Trifluoro-2,4,6-tri(heptynyl)benzene 2.25

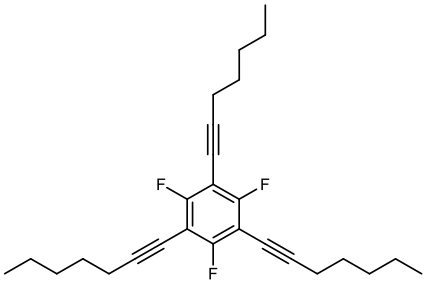

Following General Procedure **1**, 1,3,5-trifluoro-2,4,6-triiodobenzene (1.27 g, 2.50 mmol), 1-heptyne (1.18 mL, 9.00 mmol), bis(triphenylphosphine)palladium(II) chloride (263 mg, 0.380 mmol), copper (I) iodide (71.4 mg, 0.380 mmol), and DIPA (34.0 mL) for 24 h gave, after purification by flash silica chromatography (hexane) **2.25** (71%, 74.0 mg, 1.78 mmol) was isolated as a yellow oil.

IR ν_{max} (film): 2956, 2931, 2860, 2243, 1606, 1460, 1039 cm^{-1}; ^{1}H NMR (400 MHz, $CDCl_3$) δ : 2.46 (t, *J* = 7.0 Hz, 6H, C≡CC<u>H</u>$_2$), 1.62 (app. p, *J* = 7.1 Hz, 6H, C≡CCH$_2$C<u>H</u>$_2$), 1.52 – 1.41 (m, 12H, C<u>H</u>$_2$C<u>H</u>$_2$CH$_3$), 0.92 (t, *J* = 7.2 Hz, 9H, C<u>H</u>$_3$); $^{19}F\{^{1}H\}$ NMR (376 MHz, $CDCl_3$) δ : -103.9 (s, 3F); ^{13}C NMR (101 MHz, $CDCl_3$) δ : 163.7 – 161.2 (m, Ar-<u>C</u>F), 101.5 (Ar-<u>C</u>C≡C), 66.0 (Ar-CC≡<u>C</u>), 65.4 (Ar-C<u>C</u>≡C), 31.1 (<u>C</u>H$_2$CH$_2$CH$_3$), 28.1 (<u>C</u>H$_2$CH$_2$CH$_2$CH$_3$), 22.3 (<u>C</u>H$_2$CH$_3$), 19.8 (Ar-CC≡C<u>C</u>H$_2$), 14.1 (<u>C</u>H$_3$); HRMS (ESI^-) $C_{27}H_{33}F_3$ [M-H] found 413.245, requires 413.245.

1,3,5-Trifluoro-2,4,6-(trioctynyl)benzene 2.26

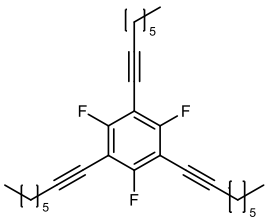

Following General Procedure **1**, 1,3,5-trifluoro-2,4,6-triiodobenzene (1.27 g, 2.50 mmol), 1-octyne (1.33 mL, 9.00 mmol), bis(triphenylphosphine)palladium(II) chloride (263 mg, 0.380 mmol), copper (I) iodide (71.4 mg, 0.380 mmol), and DIPA (21.0 mL) for 24 h gave, after purification by flash silica chromatography (hexane) **2.26** (99%, 1.18 g, 2.50 mmol) was isolated as a yellow oil.

IR ν_{max} (film): 2927, 2858, 2243, 1606, 1450 cm^{-1}; ^{1}H NMR (500 MHz, $CDCl_3$) δ : 2.46 (t, *J* = 7.0 Hz, 6H, C≡CC<u>H</u>$_2$), 1.61 (tt, *J* = 14.8, 7.2 Hz, 6H, C≡CCH$_2$C<u>H</u>$_2$), 1.49 – 1.29 (m, 18H, long chain hydrogens), 0.90 (t, *J* = 7.2 Hz, 9H C<u>H</u>$_3$); $^{19}F\{^{1}H\}$ NMR (470 MHz, $CDCl_3$) δ : -103.9 (s, 3F); ^{13}C NMR (126 MHz, $CDCl_3$) δ : 164.0 – 162.2 (m, Ar-<u>C</u>F), 101.5 (Ar-<u>C</u>C), 66.0 (C≡<u>C</u>CH$_2$), 65.4 (<u>C</u>≡CCH$_2$), 31.4 (<u>C</u>H$_2$CH$_2$CH$_3$), 28.6 (<u>C</u>H$_2$CH$_2$CH$_2$CH$_3$), 28.4 (C≡CCH$_2$<u>C</u>H$_2$), 22.7 (<u>C</u>H$_2$CH$_3$), 19.6 (C≡C<u>C</u>H$_2$), 14.2 (CH$_3$); HRMS (ESI^+) $C_{30}H_{39}F_3$ [M+Cl] found 491.269, requires 491.269.

1,3,5-Trifluoro-2,4,6-tris(4-methylpentynyl)benzene 2.27

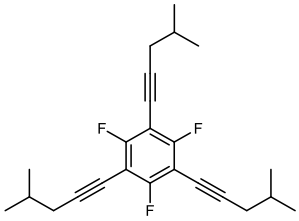

Following General Procedure **1**, 1,3,5-trifluoro-2,4,6-triiodobenzene (1.27 g, 2.50 mmol), 4-methyl-1-pentyne (1.06 mL, 9.00 mmol), bis(triphenylphosphine)palladium(II) chloride (263 mg, 0.380 mmol), copper (I) iodide (71.4 mg, 0.380 mmol), and DIPA (21.0 mL) for 24 h gave, after purification by flash silica chromatography (hexane) **2.27** (81%, 76.0 mg, 2.00 mmol) was isolated as a yellow oil.

IR ν_{max} (film): 2960, 2929, 2872, 2243, 1606, 1460 cm^{-1}; ^{1}H NMR (500 MHz, $CDCl_3$) δ : 2.36 (d, *J* = 6.4 Hz, 6H, C≡CC<u>H</u>$_2$), 1.93 (app. hept, *J* = 6.6 Hz, 3H, C<u>H</u>), 1.04 (d, *J* = 6.7 Hz, 18H, C<u>H</u>$_3$); $^{19}F\{^{1}H\}$ NMR (470 MHz, $CDCl_3$) δ : -103.8 (s, 3F); ^{13}C NMR (126 MHz, $CDCl_3$) δ : 142.4 – 138.6 (m, Ar-<u>C</u>F), 100.4 (Ar-<u>C</u>C), 66.9 (<u>C</u>≡CCH$_2$), 29.0 (C≡<u>C</u>CH$_2$), 28.5 (<u>C</u>H), 28.1 (<u>C</u>H$_2$CH), 22.1 (<u>C</u>H$_3$); HRMS (EI) $C_{24}H_{27}F_3$ [M] found 372.204, requires 372.207.

((2,4,6-Trifluorobenzene-1,3,5-triyl)tris(ethyne-2,1-diyl)tricyclohexane 2.28

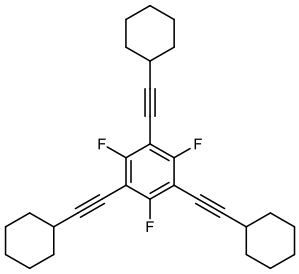

Following General Procedure **1**, 1,3,5-trifluoro-2,4,6-triiodobenzene (1.27 g, 2.50 mmol), ethynylcyclohexane (1.20 mL, 9.00 mmol), bis(triphenylphosphine)palladium(II) chloride (263 mg, 0.380 mmol), copper (I) iodide (71.4 mg, 0.380 mmol), and DIPA (24.0 mL) for 24 h gave, after purification by flash silica chromatography (hexane) **2.28** (98%, 1.11 g, 2.46 mmol) was isolated as a yellow oil.

IR ν_{max} (film): 2927, 2235, 1600, 1442, 1410 cm^{-1}; ^{1}H NMR (400 MHz, $CDCl_3$) δ : 2.70 (apparent tt, J = 8.2, 3.7 Hz, 3H, Ar-CC≡CC<u>H</u>), 1.81 — 1.67 (m, 12H, alkyl-*ortho*-C<u>H</u>$_2$), 1.46 – 1.29 (m, 18H, alkyl-*meta*, *para*-C<u>H</u>$_2$); $^{19}F\{^{1}H\}$ NMR (376 MHz, $CDCl_3$) δ : -103.7 (s, 3F); ^{13}C NMR (101 MHz, $CDCl_3$) δ : 162.0 (br dt, $^{1}J_{CF}$ = 258.5 Hz, $^{2}J_{CF}$ = 7.6 Hz, Ar-<u>C</u>F), 117.6 (Ar-<u>C</u>C≡C), 105.2 (Ar-CC≡<u>C</u>), 66.2 (Ar-C<u>C</u>≡C), 32.3 (alkyl-<u>C</u>H), 29.9 (alkyl-*meta*-<u>C</u>H$_2$), 26.0 (alkyl-*para*-<u>C</u>H$_2$), 24.7 (alkyl-*ortho*-<u>C</u>H$_2$); HRMS (EI) $C_{30}H_{33}F_3$ [M] found 450.249, requires 450.253.

(((2,4,6-Trifluorobenzene-1,3,5-triyl)tris(propyne-3,1-diyl))tris(oxy))tricyclohexane 2.29

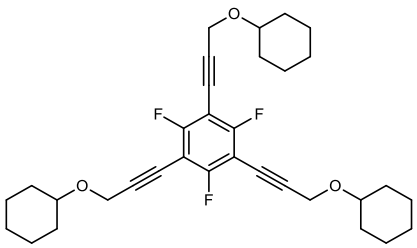

Following General Procedure **1**, 1,3,5-trifluoro-2,4,6-triiodobenzene (1.65 g, 3.24 mmol), (prop-2-yn-1-yloxy)cyclohexane (1.61 g, 11.7 mmol), bis(triphenylphosphine)palladium(II) chloride (341 mg, 0.490 mmol), copper (I) iodide (92.6 mg, 0.490 mmol), and DIPA (30.0 mL) for 24 h gave, after purification by flash silica

chromatography (0-20% Et_2O in hexane) **2.29** (59%, 1.04 g, 1.93 mmol) was isolated as a yellow oil.

IR ν_{max} (film): 2929, 2160, 1606, 1456, 1082 cm^{-1}; ^1H NMR (500 MHz, $CDCl_3$) δ: 4.44 (s, 6H, C≡CC$\underline{H}_2$), 3.55 (tt, *J* = 8.9, 4.0 Hz, 3H, cyclo-C$\underline{H}$), 1.97—1.95 (m, 6H, *ortho*), 1.77—1.75 (m, 6H, *meta*), 1.56—1.53 (m, 3H, *para*), 1.37—1.21 (m, 15H, cyclo-H); $^{19}F\{^1H\}$ NMR (470 MHz, $CDCl_3$) δ : -100.2 (3F, C$\underline{F}$); ^{13}C NMR (126 MHz, $CDCl_3$) δ: 162.9 (br d, $^1J_{CF}$ = 269.3 Hz, 3C, Ar-$\underline{C}$F), 97.4 (3C, Ar-$\underline{C}$C), 77.1 (3C, cyclo-$\underline{C}$H), 70.6 (C≡$\underline{C}$CH$_2$), 55.8 ($\underline{C}$≡CCH$_2$), 31.9 (3C, C≡C$\underline{C}$H$_2$), 25.9 (6C, cyclo-*ortho*-$\underline{C}$H$_2$), 24.2 (3C, cyclo-*para*-$\underline{C}$H$_2$), 22.8 (6C, cyclo-*meta*-$\underline{C}$H$_2$); HRMS (ESI^+) $C_{33}H_{39}F_3O_3$ [M+Na] found 563.274, requires 563.275.

1,3,5-Tris(3,3-dimethylbutynyl)-2,4,6-trifluorobenzene 2.30

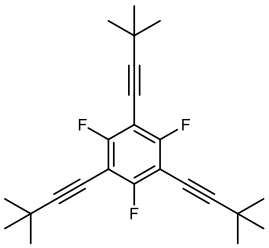

Following General Procedure **1**, 1,3,5-trifluoro-2,4,6-triiodobenzene (1.27 g, 2.50 mmol), 3,3-dimethyl-1-butyne (1.12 mL, 9.00 mmol), bis(triphenylphosphine)palladium(II) chloride (263 mg, 0.380 mmol), copper (I) iodide (71.4 mg, 0.380 mmol), and DIPA (48.0 mL) for 24 h gave, after purification by flash silica chromatography (hexane) **2.30** (49%, 458 mg, 1.23 mmol) as a white solid. m.p. = 229—230 °C.

IR ν_{max} (solid): 2528, 2206, 1640, 1516 cm^{-1}; ^1H NMR (500 MHz, $CDCl_3$) δ : 1.32 (s, 27H, C$\underline{H}_3$); $^{19}F\{^1H\}$ NMR (470 MHz, $CDCl_3$) δ : -103.8 (s, 3F); ^{13}C NMR (126 MHz, $CDCl_3$) δ : 161.8 (br d, $^1J_{CF}$ = 257.3 Hz, 3C, Ar-$\underline{C}$F), 109.2 (3C, Ar-$\underline{C}$C≡C), 64.6 (6C, Ar-C$\underline{C}$≡$\underline{C}$C), 30.8 (9C, $\underline{C}$H$_3$), 28.6 (3C, Ar-CC≡C$\underline{C}$); HRMS (ESI^+) $C_{24}H_{27}F_3$ [M+H] found 373.213, requires 373.218.

2(Propynyloxy)cyclohexane 2.34

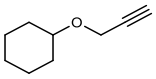

NaH (2.40 g, 60.0 mmol, 60 wt% in mineral oil) was slowly added into a solution of cyclohexanol (5.00 mL, 48.0 mmol) in 100 ml THF at 0 °C. After stirring for 5 min at 0 °C, propargyl bromide (80 wt% in toluene, 4.50 mL, 48.0 mmol) was added to the mixture and the solution was left to warm to r.t.. After 3 h the reaction was quenched with saturated aqueous NH_4Cl (30.0 mL), followed by extraction with Et_2O (3 x 20.0 mL). The combined organic layers were washed with brine (25.0 mL) then the combined organic layers were dried over anhydrous $MgSO_4$, filtered, and concentrated *in vacuo*. The resulting yellow liquid was purified by flash chromatography (0—5% diethyl ether in hexane, silica gel) yielding title compound as a yellow oil with spectroscopic data in accordance with the literature,[106] (33%, 2.20 g, 15.9 mmol).

^{1}H NMR (500 MHz, $CDCl_3$) δ: 4.17 (d, *J* = 2.4 Hz, 2H, C≡CC$\underline{H}_2$), 3.46 (dp, *J* = 8.8, 3.7 Hz, 1H, cyclo-C$\underline{H}$), 2.38 (t, *J* = 2.4 Hz, 1H, $\underline{H}$C≡C), 1.93 – 1.88 (m, 2H), 1.74 – 1.73 (m, 2H), 1.55 – 1.53 (m, 1H), 1.33 – 1.19 (m, 5H); ^{13}C NMR (126 MHz, $CDCl_3$) δ: 80.7 (HC≡$\underline{C}$CH$_2$), 76.7 (H$\underline{C}$≡CCH$_2$), 73.7 (cyclo-$\underline{C}$H), 55.0 (HC≡C$\underline{C}$H$_2$), 32.0 (2C, *ortho*-$\underline{C}$H$_2$), 25.8 (*para*-$\underline{C}$H$_2$), 24.2 (2C, *meta*-$\underline{C}$H$_2$).

((2,4,6-Trifluorobenzene-1,3,5-triyl)tris(ethyne-2,1-diyl))tris(trimethylsilane) 2.37

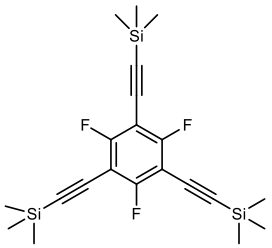

1,3,5-trifluoro-2,4,6-triiodobenzene (0.637 g, 1.25 mmol), ethynyltrimethylsilane (0.620 mL, 442 mg, 4.50 mmol), palladium catalyst (132 mg, 0.190 mmol), and copper (I) iodide (357 mg, 0.190 mmol) were all added to a 100 ml RBF. Diisopropylamine (25.0 mL) was then added, and the reaction mixture was heated to 80 ˚C under argon and stirred for 22 h. The reaction mixture was then cooled to r.t. and slowly passed through a pad of silica gel, 3 cm tall, with an elusion of ethyl acetate. The solvent was removed

via concentration in vacuo and the purified via flash chromatography (hexane), very slowly and care was taken to separate starting alkyne from final product to afford the brown oil product in 83% yield. (0.436 g, 1.04 mmol).

^{1}H NMR (500 MHz, $CDCl_3$) δ : 0.26 (s, 27H); ^{19}F{^{1}H} NMR (500 MHz, $CDCl_3$) δ : -99.3 (s, 3F); ^{13}C NMR (500 MHz, $CDCl_3$) δ : 164.0 — 162.0 (m, Ar-F), 88.6 (Ar), 86.0, -0.4 (CH_3).

1,3,5-Triethynyl-2,4,6-trifluorobenzene 2.31

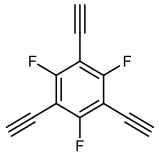

Silane protected compound (405 mg, 0.950 mmol) and potassium carbonate (787 mg, 5.67 mmol, 6 eq) were dissolved in the minimum amount of DMF (20.0 mL) and left to stir under argon for 24 h. The mixture was then diluted with ethyl acetate (10.0 mL) and water (10.0 mL) the organic layer was extracted with ethyl acetate (2 x 10.0 mL) and the organic layers were combined. The organic layer was concentrated *in vacuo* to give the crude product, which was purified by flash column chromatography (SiO_2, 0-50% EtOAc in hexane) to give **2.31** as a brown oil (96%, 186 mg, 0.910 mmol).

^{1}H NMR (500 MHz, $CDCl_3$) δ : 3.53 (s, 3H); ^{19}F{^{1}H} NMR (500 MHz, $CDCl_3$) δ : -97.9 – -98.9 (m, 3F); ^{13}C NMR (500 MHz, $CDCl_3$) δ : 163.4 – 162.2 (m, 3C, Ar-CF), 99.4 (3C, Ar-CC≡C), 89.9 (3C, Ar-CC≡C), 88.4 (3C, C≡CH).

1,2,3,4,5-Pentafluoro-6-hexylbenzene 2.38

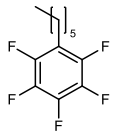

Following General Procedure **2**, **2.19** (2.10 g, 8.46 mmol), 10% palladium on carbon catalyst (210 mg, 10% wt eq), and EtOAc (150 mL), under atmospheric H_2 for 48 h gave, after purification by flash chromatography (0—5% EtOAC in hexane), **2.38** (80%, 1.71 g, 6.77 mmol) as a clear oil.

IR νmax (solid): 2935, 1496, 987 cm^{-1}; ^{1}H NMR (500 MHz, $CDCl_3$) δ : 2.50 (t, *J* = 7.1 Hz, 2H, Ar-CC$\underline{H}_2$), 1.62 (tt, *J* = 14.5, 7.1 Hz, 2H, Ar-CCH$_2$C$\underline{H}_2$), 1.56 – 1.22 (m, 6H, C$\underline{H}_2$C$\underline{H}_2$C$\underline{H}_2$CH$_3$), 0.96 (t, *J* = 7.3 Hz, 3H, C$\underline{H}_3$); $^{19}F\{^{1}H\}$ NMR (470 MHz, $CDCl_3$) δ : -137.2 – -137.3 (m, 2F, *ortho*-F), -154.5 (t, *J* = 20.7 Hz, 1F, *para*-F), -162.5 (td, *J* = 21.9, 7.7 Hz, 2F, *meta*-F); ^{13}C NMR (126 MHz, $CDCl_3$) δ : 147.7 (br d, $^{1}J_{CF}$ = 256.2 Hz, *meta*-$\underline{C}$F), 142.8 – 140.4 (m, *para*-$\underline{C}$F), 112.2 – 109.5 (m, *ortho*-$\underline{C}$F), 104.3 (Ar-$\underline{C}$CH$_2$), 30.5 ($\underline{C}$H$_2$CH$_2$CH$_3$), 30.3 ($\underline{C}$H$_2$CH$_2$CH$_2$CH$_2$CH$_3$), 29.9 ($\underline{C}$H$_2$CH$_2$CH$_2$CH$_3$), 22.0 (Ar-C$\underline{C}$H$_2$), 19.6 ($\underline{C}$H$_2$CH$_3$), 13.7 ($\underline{C}$H$_3$); HRMS (EI) $C_{12}H_9F_5$ [M] found 248.062, requires 248.062.

1,2,3,5-Tetrafluoro-4,6-dihexylbenzene 2.39

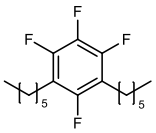

Following General Procedure **2**, **2.20** (118 mg, 0.380 mmol), 10% palladium on carbon catalyst (13.0 mg, 10% wt eq), and hexane (10.0 mL), under atmospheric H_2 for 24 h gave, after purification by flash silica chromatography (hexane) **2.39** (99%, 120 mg, 0.380 mmol) was isolated as a colourless oil.

IR ν_{max} (film): 2956, 2927, 2858, 1647, 1490, 1467 cm^{-1}; ^{1}H NMR (500 MHz, $CDCl_3$) δ : 2.62 (t, *J* = 7.6 Hz, 4H, Ar-C$\underline{H}_2$), 1.55 (app. q, *J* = 7.7 Hz, 4H, Ar-CH$_2$C$\underline{H}_2$), 1.29 – 1.13 (m, 12H, remaining chain-C$\underline{H}_2$), 0.88 — 0.86 (m, 6H, C$\underline{H}_3$); $^{19}F\{^{1}H\}$ NMR (470 MHz, $CDCl_3$) δ : -126.1 (d, *J* = 11.4 Hz, 1F, *iso*-F), -142.2 (d, *J* = 21.7 Hz, 2F), -166.8 (td, *J* = 21.8, 11.5 Hz, 1F); ^{13}C NMR (126 MHz, $CDCl_3$) δ : 153.8 (br dtd, $^{1}J_{CF}$ = 241.5 Hz, $^{3}J_{CF}$ = 9.7 Hz, $^{4}J_{CF}$ = 3.4 Hz, Ar-$\underline{C}$F), 147.5 (br ddt, $^{1}J_{CF}$ = 244.5 Hz, $^{2}J_{CF}$ = 11.3 Hz, $^{3}J_{CF}$ = 5.6 Hz, Ar-$\underline{C}$F), 136.9 (br dtd, $^{1}J_{CF}$ = 246.2 Hz, $^{2}J_{CF}$ = 16.3 Hz, $^{4}J_{CF}$ = 4.8 Hz, Ar-$\underline{C}$F), 114.6 (br dd, $^{2}J_{CF}$ = 22.2, 16.3 Hz, Ar-$\underline{C}$CH$_2$), 31.5 ($\underline{C}$H$_2$CH$_2$CH$_3$), 29.5 ($\underline{C}$H$_2$CH$_2$CH$_2$CH$_2$CH$_3$), 28.9 ($\underline{C}$H$_2$CH$_2$CH$_2$CH$_3$), 22.6 (Ar-C$\underline{C}$H$_2$), 22.4 ($\underline{C}$H$_2$CH$_3$), 14.0 ($\underline{C}$H$_3$); MS (ESI^-) $C_{18}H_{18}F_4$ [M-2H] found 316.2, requires 316.2.

1,2,3,5-Tetrafluoro-4,6-(dioctyl)benzene 2.40

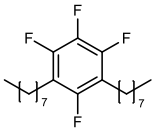

Following General Procedure **2**, **2.21** (100 mg, 0.270 mmol), 10% palladium on carbon catalyst (10.0 mg, 10% wt eq), and hexane (10.0 mL), under atmospheric H_2 for 24 h gave, after purification by flash silica chromatography (hexane) **2.40** (86%, 83.0 mg, 0.220 mmol) was isolated as a colourless oil.

IR ν_{max} (film): 2956, 2924, 2854, 1645, 1517, 1465 cm^{-1}; ^1H NMR (500 MHz, $CDCl_3$) δ : 2.62 (t, *J* = 7.6 Hz, 4H, Ar-CC$\underline{H}_2$), 1.53 – 1.44 (m, 4H, Ar-CCH$_2$C$\underline{H}_2$), 1.28 – 1.12 (m, 20H, Ar-CCH$_2$CH$_2$C$\underline{H}_2$C$\underline{H}_2$C$\underline{H}_2$C$\underline{H}_2$C$\underline{H}_2$), 0.88 (t, *J* = 7.0 Hz, 6H, C$\underline{H}_3$); $^{19}F\{^1H\}$ NMR (470 MHz, $CDCl_3$) δ : -126.0 (d, *J* = 11.4 Hz, 1F, *iso*-F), -142.2 (d, *J* = 22.2 Hz, 2F), -166.8 (td, *J* = 21.7, 11.5 Hz, 1F); ^{13}C NMR (126 MHz, $CDCl_3$) δ : 155.0 – 153.1 (m, Ar-$\underline{C}$F), 148.6 – 146.1 (m, Ar-$\underline{C}$F), 137.0 (br d, $^1J_{CF}$ = 151.1 Hz, Ar-$\underline{C}$F), 114.8 (Ar-$\underline{C}$CH$_2$), 32.0 ($\underline{C}$H$_2$CH$_2$CH$_3$), 29.6 (remaining C), 22.8 (Ar-$\underline{C}$H$_2$), 22.5 ($\underline{C}$H$_2$CH$_3$), 14.3 ($\underline{C}$H$_3$); HRMS (EI) $C_{22}H_{34}F_4$ [M] found 374.260, requires 374.260.

1,2,3,5-Tetrafluoro-4,6-bis(4-methylpentyl)benzene 2.41

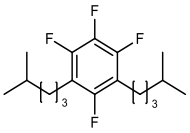

Following General Procedure **2**, **2.22** (675 mg, 2.18 mmol), 10% palladium on carbon catalyst (68.0 mg, 10% wt eq), and hexane (30.0 mL), under 15 bar H_2 for 24 h gave, after purification by flash silica chromatography (hexane) **2.41** (83%, 580 mg, 1.82 mmol) was isolated as a colourless oil.

IR ν_{max} (film): 2954, 2926, 2854, 1645, 1490, 1467 cm^{-1}; ^1H NMR (500 MHz, $CDCl_3$) δ : 2.61 (t, *J* = 7.6 Hz, 4H, Ar-C$\underline{H}_2$), 1.55 – 1.42 (m, 6H, C$\underline{H}_2$CH$_2$C$\underline{H}$), 0.88 – 0.87 (m, 16H, C$\underline{H}_3$ and CHC$\underline{H}_2$); $^{19}F\{^1H\}$ NMR (376 MHz, $CDCl_3$) δ : -126.0 (d, *J* = 11.4 Hz, 1F, *iso*-F), -142.1 (d, *J* = 21.7 Hz, 2F), -166.2 (td, *J* = 21.8, 11.5 Hz, 1F); ^{13}C NMR (126 MHz, $CDCl_3$) δ : 158.7

— 155.5 (m, Ar-CF), 150.9 – 146.9 (m, Ar-CF, 2C), 140.0 – 137.4 (m, Ar-CF), 129.6 (Ar-$\underline{C}CH_2$), 101.7 ($\underline{C}H_2CH$), 32.1 ($\underline{C}H$), 28.7 ($\underline{C}H_2CH_2CH$), 28.1 (Ar-$C\underline{C}H_2$), 22.1 ($\underline{C}H_3$).

((Perfluoro-1,3-phenylene)bis(propane-3,1-diyl))dicyclohexane 2.42

A 250 ml RBF was charged with alkyne **2.23** (808 mg, 2.10 mmol) dissolved in ethyl acetate (100 mL) and 15% palladium on carbon catalyst (121 mg, 15% wt equivalent) was then added. Hydrogenation was carried out at 3 bar of hydrogen for 5 d. The reaction mixture was then filtered through a silica gel pad, which was washed with ethyl acetate, and the filtrate was concentrated under reduced pressure to yield **2.42** (62%, 514 mg, 1.30 mmol) as a pale-yellow oil. With spectroscopic data in accordance with the literature.[105]

IR ν_{max} (film): 2920, 2850, 1645, 1500, 1448 cm^{-1}; ^1H NMR (500 MHz, $CDCl_3$) δ : 2.59 (t, *J* = 7.6 Hz, 4H, Ar-C$\underline{H}_2$), 1.55 – 1.42 (m, 4H, Ar-$CH_2C\underline{H}_2$), 1.32 — 1.19 (m, 22H, ring-H), 0.88 – 0.85 (m, 4H, Ar-$CH_2CH_2C\underline{H}_2$); $^{19}F\{^1H\}$ NMR (500 MHz, $CDCl_3$) δ : -125.93 (d, *J* = 11.3 Hz, 1F, *iso*-F), -142.12 (dd, *J* = 21.9, 1.4 Hz, 2F), -166.78 (td, *J* = 23.7, 11.5 Hz, 1F, conjugated-F); ^{13}C NMR (500 MHz, $CDCl_3$): δ : 155.0 – 151.5 (Ar-*iso*-CF), 146.5 – 144.2 (2C, Ar-CF), 114.6 –111.9 (Ar-conjugated-CF), 96.0 (Ar-$\underline{C}CH_2$), 37.4 (Ar-$CH_2CH_2\underline{C}H_2$), 37.3 (ring-*ortho*-$\underline{C}H_2$), 33.4 (ring-CH), 26.7 (Ar-$CH_2\underline{C}H_2$), 26.4 (ring-*meta*,*para*-$\underline{C}H_2$), 22.6 (Ar-$\underline{C}H_2$).

1,3,5-Trifluoro-2,4,6-trihexylbenzene 2.43

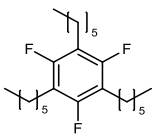

Following General Procedure **2**, **2.24** (391 mg, 1.05 mmol), 10% palladium on carbon catalyst (39.0 mg, 10% wt eq), and hexane (20.0 mL), under atmospheric H_2 for 24 h gave, after purification by flash silica chromatography (hexane) **2.43** (77%, 310 mg, 0.810 mmol) was isolated as a colourless oil.

IR ν_{max} (film): 2956, 2890, 2856, 1622, 1450 cm^{-1}; ^{1}H NMR (500 MHz, $CDCl_3$) δ : 2.60 (t, *J* = 7.6 Hz, 6H, Ar-C$\underline{H}_2$), 1.54 (tt, *J* = 7.5, 5.8 Hz, 6H, Ar-$CH_2C\underline{H}_2$), 1.39 – 1.26 (m, 22H, $C\underline{H}_2C\underline{H}_2C\underline{H}_2CH_3$), 0.90 (td, *J* = 6.9, 1.8 Hz, 9H, C$\underline{H}_3$); $^{19}F\{^{1}H\}$ NMR (470 MHz, $CDCl_3$) δ : -124.1 (s, 3F); ^{13}C NMR (126 MHz, $CDCl_3$) δ : 157.8 – 154.3 (Ar-$\underline{C}$F), 113.1 (Ar-$\underline{C}$C), 32.1 ($\underline{C}H_2CH_2CH_3$), 29.9 ($\underline{C}H_2CH_2CH_2CH_2CH_3$), 29.5 ($\underline{C}H_2CH_2CH_2CH_3$), 22.9 (Ar-C$\underline{C}H_2$), 22.7 ($\underline{C}H_2CH_3$), 14.2 ($\underline{C}H_3$); HRMS ($ESI^+$) $C_{24}H_{39}F_3$ [M+Ca] found 424.374, requires 424.378.

1,3,5-Trifluoro-2,4,6-triheptylbenzene 2.44

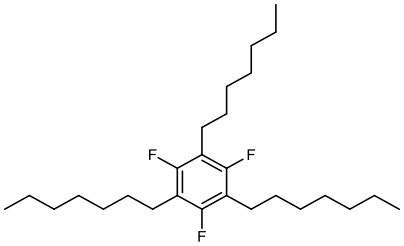

Following General Procedure **2**, **2.25** (720 mg, 1.74 mmol), 10% palladium on carbon catalyst (108 mg, 15% wt eq), and methanol (100 mL), under atmospheric H_2 for 3 d gave, after purification by flash silica chromatography (hexane) **2.44** (85%, 631 mg, 1.48 mmol) was isolated as a colourless oil.

IR ν_{max} (film): 2956, 2920, 2854, 1622, 1458 cm^{-1}; ^{1}H NMR (500 MHz, $CDCl_3$) δ : 2.57 (t, *J* = 7.6 Hz, 6H, Ar-C$\underline{H}_2$), 1.55 – 1.49 (m, 6H, Ar-$CH_2C\underline{H}_2$), 1.32 – 1.25 (m, 24H, $C\underline{H}_2C\underline{H}_2C\underline{H}_2C\underline{H}_2CH_3$), 0.87 (t, *J* = 7.0 Hz, 9H, C$\underline{H}_3$); $^{19}F\{^{1}H\}$ NMR (470 MHz, $CDCl_3$) δ : -124.1 (s, 3F); ^{13}C NMR (126 MHz, $CDCl_3$) δ : 157.5 (br d, $^{1}J_{CF}$ = 241.9 Hz, Ar-$\underline{C}$F), 113.1 (Ar-$\underline{C}CH_2$), 32.0 ($\underline{C}H_2CH_2CH_3$), 29.8 (Ar-$CH_2\underline{C}H_2$), 29.3 (Ar-$CH_2CH_2\underline{C}H_2\underline{C}H_2$), 22.8 (Ar-C$\underline{C}H_2$), 22.4 ($\underline{C}H_2CH_3$), 14.3 ($\underline{C}H_3$); HRMS ($ESI^-$) $C_{27}H_{45}F_3$ [M]+1 found 438.368, requires 438.367.

1,3,5-Trifluoro-2,4,6-trioctylbenzene 2.45

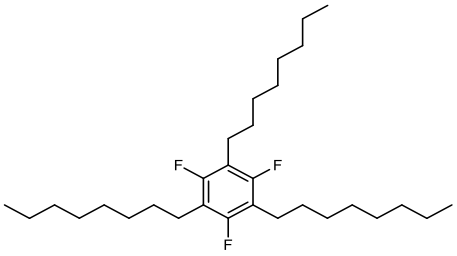

Following General Procedure **2**, **2.26** (871 mg, 1.90 mmol), 10% palladium on carbon catalyst (89.0 mg, 10% wt eq), and hexane (100 mL), under atmospheric H_2 for 24 h gave, after purification by flash silica chromatography (hexane) **2.45** (99%, 936 mg, 1.90 mmol) was isolated as a colourless oil.

IR ν_{max} (film): 2956, 2875, 2852, 1622, 1458 cm^{-1}; ^1H NMR (500 MHz, $CDCl_3$) δ : 2.57 (t, *J* = 7.6 Hz, 6H, Ar-C$\underline{H}_2$), 1.52 (m, 6H, Ar-$CH_2C\underline{H}_2$), 1.27 — 1.13 (m, 35H, long chain hydrogens), 0.87 (m, 9H, C$\underline{H}_3$); $^{19}F\{^1H\}$ NMR (376 MHz, $CDCl_3$) δ : -124.07 (s, 3F); ^{13}C NMR (126 MHz, $CDCl_3$) δ : 157.5 (br dt, $^1J_{CF}$ = 241.9 Hz, $^3J_{CF}$ = 12.2 Hz, Ar-$\underline{C}$F), 113.1 –112.4 (m, Ar-$\underline{C}$C), 32.1 ($\underline{C}H_2CH_2CH_3$), 29.9 (Ar-$CCH_2\underline{C}H_2$), 29.6 (Ar-$CH_2CH_2\underline{C}H_2CH_2$), 29.5 (Ar-$CH_2CH_2CH_2\underline{C}H_2$), 29.4 (Ar-$CH_2CH_2CH_2CH_2\underline{C}H_2$), 22.7 (Ar-$C\underline{C}H_2$), 22.33 ($\underline{C}H_2CH_3$), 14.14 ($\underline{C}H_3$); MS (EI) $C_{30}H_{51}F_3$ [M] found 468.3, requires 468.3.

1,3,5-Trifluoro-2,4,6-tris(4-methylpentyl)benzene 2.46

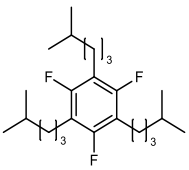

Following General Procedure **2**, **2.27** (724 mg, 1.94 mmol), 10% palladium on carbon catalyst (109 mg, 15% wt eq), and hexane (40.0 mL), under atmospheric H_2 for 24 h gave, after purification by flash silica chromatography (hexane) **2.46** (89%, 660 mg, 1.72 mmol) was isolated as a colourless oil.

IR ν_{max} (film): 2954, 2927, 2870, 1622, 1462, 1384 cm^{-1}; ^1H NMR (500 MHz, $CDCl_3$) δ : 2.57 (t, *J* = 7.6 Hz, 6H, Ar-C$\underline{H}_2$), 1.54 (tq, *J* = 14.1, 6.7 Hz, 6H, Ar-$CH_2C\underline{H}_2$), 1.40 – 1.23 (m, 6H, Ar-$CH_2CH_2C\underline{H}_2$), 1.15 (q, *J* = 6.5 Hz, 3H, C$\underline{H}$), 0.87 (app. dd, *J* = 6.6, 2.9 Hz, 18H, C$\underline{H}_3$);

$^{19}F\{^{1}H\}$ NMR (470 MHz, $CDCl_3$) δ : -124.0 (s, 3F); ^{13}C NMR (126 MHz, $CDCl_3$) δ : 157.5 (br dt, $^{1}J_{CF}$ = 242.0 Hz, $^{3}J_{CF}$ = 12.2 Hz, Ar-CF), 113.4 – 112.3 (m, Ar-CC), 39.2 (CH_2CH), 38.6 (CH), 30.1 (CH_2CH_2CH), 27.9 (Ar-CCH_2), 22.7 (CH_3); MS (ESI$^+$) $C_{24}H_{39}F_3$ [M+H] found 396.3, requires 396.3.

((2,4,6-Trifluorobenzene-1,3,5-triyl)tris(ethane-2,1-diyl))tricyclohexane 2.47

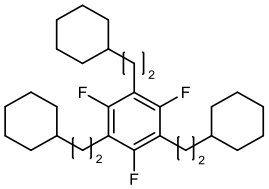

Following General Procedure **2**, **2.28** (1.09 g, 2.42 mmol), 10% palladium on carbon catalyst (162 mg, 15% wt eq), and ethyl acetate (100 mL), under atmospheric H_2 for 2 d gave, after purification by flash silica chromatography (hexane) **2.47** (91%, 1.02 g, 2.20 mmol) was isolated as a colourless oil.

IR ν_{max} (film): 2990, 1622, 1450, 1446 cm^{-1}. ^{1}H NMR (500 MHz, $CDCl_3$) δ : 2.58 (t, *J* = 8.1 Hz, 6H, Ar-CCH_2), 1.40 (dt, *J* = 10.4, 6.7 Hz, 6H, Ar-CCH_2CH_2), 1.29-0.82 (m, 33H, cyclic-H); $^{19}F\{^{1}H\}$ NMR (470 MHz, $CDCl_3$) δ: -124.7 (s, 3F); ^{13}C NMR (126 MHz, $CDCl_3$) δ : 157.5 (br dd, $^{1}J_{CF}$ = 243.1 Hz, $^{3}J_{CF}$ =14.0 Hz, Ar-CF), 113.6 (br d, $^{2}J_{CF}$ = 21.6 Hz, Ar-CCH_2), 37.8 (cyclo-CH), 33.5 (cyclo-ortho-CH_2), 27.4 (Ar-CCH_2), 26.9 (Ar-CCH_2CH_2), 26.6 (cyclo-meta,CH_2), 20.0 (cyclo-para-CH_2); HRMS (ESI$^+$) $C_{30}H_{45}F_3$ [M+H] found 474.367, requires 474.361.

(((2,4,6-Trifluorobenzene-1,3,5-triyl)tris(propane-3,1-diyl))tris(oxy))tricyclohexane 2.48

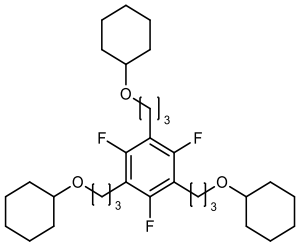

Following General Procedure **2**, **2.29** (1.04 g, 1.90 mmol), 10% palladium on carbon catalyst (124 mg, 15% wt eq), and methanol (40.0 mL), under 15 bar H_2 for 3 d gave,

after purification by flash silica chromatography (0—70% Et_2O in hexane) **2.48** (49%, 410 mg, 0.740 mmol) was isolated as a colourless oil.

IR ν_{max} (film): 2989, 1558, 1506, 1072 cm^{-1}; ^1H NMR (500 MHz, $CDCl_3$) δ : 3.44 (t, *J* = 6.5 Hz, 6H, OCH_2), 3.19 (tt, *J* = 8.8, 3.9 Hz, 3H, OCH), 2.67 (t, *J* = 7.3 Hz, 6H, Ar-CH_2), 1.90—1.85 (m, 6H, $CH_2C\underline{H}_2CH_2$), 1.80 (apparent p, *J* = 6.6 Hz, 6H, *ortho*-C<u>H</u>H), 1.73—1.71 (m, 6H, *ortho* CH<u>H</u>), 1.30—0.87 (m, 18H, remaining cyclo-H); $^{19}F\{^1H\}$ NMR (470 MHz, $CDCl_3$) δ : -122.8 (br s, 3xCF); ^{13}C NMR (126 MHz, $CDCl_3$) δ : 160.8 (br d, $^1J_{CF}$ = 267.0 Hz, 3xCF), 122.0 (br s, 3xAr-<u>C</u>HCH_2), 77.7 (3C, OCH), 67.2 (OCH_2), 32.5 (6C, *ortho*-CH_2), 30.2 (3C, Ar-$CH_2\underline{C}H_2$), 26.0 (3C, Ar-CH_2), 24.4 (3C, *para*-CH_2), 19.3 (6C, *meta*-CH_2); HRMS (ESI^-) $C_{33}H_{51}F_3O_3$ [M-H] found 553.387, requires 553.387.

1,3,5-Tris(3,3-dimethylbutyl)-2,4,6-trifluorobenzene 2.49

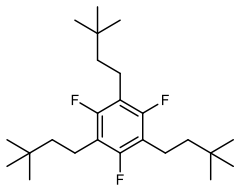

Following General Procedure **2**, **2.30** (458 mg, 1.23 mmol), 10% palladium on carbon catalyst (45.8 mg, 10% wt eq), and ethyl acetate (40.0 mL), under atmospheric H_2 for 48 h gave, after purification by flash silica chromatography (0—10% Et_2O in hexane) **2.49** (91%, 429 mg, 1.11 mmol) as a white crystalline solid. m.p. 90—91 °C

IR ν_{max} (solid): 2366, 1653, 1508 cm^{-1}; ^1H NMR (500 MHz, $CDCl_3$) δ : 2.56—2.53 (m, 6H, Ar-C<u>C</u>H_2), 1.42—1.38 (m, 6H, Ar-$CCH_2C\underline{H}_2$), 0.96 (s, 27H, C<u>H</u>$_3$); $^{19}F\{^1H\}$ NMR (470 MHz, $CDCl_3$) δ : -125.9 (s, 3F); ^{13}C NMR (126 MHz, $CDCl_3$) δ : 157.2 (br d, $^1J_{CF}$ = 229.5 Hz, Ar-<u>C</u>F), 113.9 (Ar-<u>C</u>CH_2), 44.1 (Ar-$CCH_2\underline{C}H_2$), 30.8 (Ar-C<u>C</u>H_2), 29.2 (<u>C</u>H_3), 18.0 (<u>C</u>).

1,3,5-Triethyl-2,4,6-trifluorobenzene 2.50

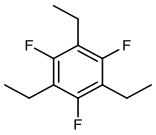

A 250 ml RBF was charged with alkyne **2.31** (186 mg, 0.910 mmol) dissolved in ethyl acetate (100 mL) and 15% palladium on carbon catalyst (28.5 mg, 15% wt equivalent) was then added. Hydrogenation was carried out at 3 bar of hydrogen for 7 d. The reaction mixture was then filtered through a silica gel pad, which was washed with ethyl acetate, and the filtrate was concentrated under reduced pressure to yield the product as a colourless oil 33%. (64.8 mg, 0.290 mmol).

IR ν_{max} (film): 2920, 1622, 1456 cm^{-1}; ^{1}H NMR (500 MHz, $CDCl_3$) δ: 2.63 (q, *J* = 7.2 Hz, 6H, C$\underline{H}_2$), 1.17 (t, *J* = 2.5 Hz, 9H, C$\underline{H}_3$); $^{19}F\{^{1}H\}$ NMR (470 MHz, $CDCl_3$) δ: -125.8 (s, 3F, C$\underline{F}$); ^{13}C NMR (126 MHz, $CDCl_3$) δ: 157.1 (br d, $^{1}J_{CF}$ = 242.1 Hz, 3xAr-$\underline{C}$F), 114.5 (3C, Ar-$\underline{C}$C), 29.7 (3C, $\underline{C}H_2$), 14.4 (3C, $\underline{C}H_3$); MS (ESI^+) $C_{12}H_{15}F_3$ [M+H] found 217.1, requires 217.1.

All *cis*-pentafluoro-6-hexylcyclohexane 2.2

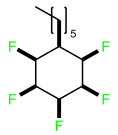

Following General Procedure **3**, **2.38** (990 mg, 3.92 mmol), Rh-CAAC-COD-Cl (38.0 mg, 0.067 mmol, 1.7 mol%), 4Å molecular sieves (10.0 g), silica (5.00 g), and hexane (75.0 mL) at r.t., for 1 d and at 50 bar H_2 gave, after purification by recrystallization in acetone (washed with ice cold methanol) the title compound (29%, 291mg, 1.13 mmol) was obtained as a white crystal. m.p. 131—132 °C.

IR ν_{max} (solid): 2926, 1398 cm^{-1}; ^{1}H NMR (400 MHz, $CDCl_3$) δ : 5.33 (d, *J* = 52.3 Hz, 1H *para*-$\underline{H}$F), 4.94 (d, *J* = 49.0 Hz, 2H, *ortho*-$\underline{H}$F), 4.42 (dt, *J* = 41.4, 26.6 Hz, 2H, *meta*-$\underline{H}$F), 1.87 (q, *J* = 7.6 Hz, 1H, ring-$\underline{H}$C), 1.70 – 1.22 (m, 13H, chain-C$\underline{H}_2$), 0.93 – 0.86 (m, 3H, C$\underline{H}_3$); $^{19}F\{^{1}H\}$ NMR (470 MHz, $CDCl_3$) δ : -203.1 (dt, *J* = 12.0, 7.8, 4.4 Hz, 2F, *meta*-F), -212.1 (ddd, *J* = 26.8, 7.7, 4.5 Hz, 2F, *ortho*-F), -216.7 (tt, *J* = 26.8, 11.4 Hz, 1F, *para*-F); ^{13}C NMR (126 MHz, $CDCl_3$) δ : 87.3 – 85.5 (m, 5x $\underline{C}$F), 38.7 (ring-$\underline{C}$H), 31.7 ($CHCH_2CH_2\underline{C}H_2$),

29.2 (<u>C</u>$H_2CH_2CH_3$), 26.6 ($CHCH_2$<u>C</u>H_2), 26.3 – 25.7 (m, CH<u>C</u>H_2), 22.7 (<u>C</u>H_2CH_3), 14.2 (<u>C</u>H_3); HRMS (EI) $C_{12}H_{19}F_5$ [M] found 258.139, requires 258.140.

All *cis*-tetrafluoro-4,6-dihexylcyclohexane 2.3

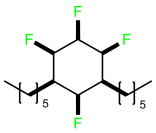

Following General Procedure **3**, **2.39** (56.2 mg, 0.180 mmol), Rh-CAAC-COD-Cl (2.00 mg, 0.004 mmol), silica gel (200 mg), and hexane (2.00 mL) for 24 h, r.t., and at 50 bar H_2 gave, after purification by flash silica chromatography (25—42% diethyl ether in hexane) **2.3** (50%, 32.0 mg, 0.090 mmol) was isolated as a white crystalline solid. m.p. 100—103 °C.

IR ν_{max} (solid): 3300, 1508 cm^{-1}; ^{1}H NMR (500 MHz, $CDCl_3$) δ : 4.96 (apparent d, J = 43.9 Hz, 2H, ring 1,3C-<u>H</u>F), 4.59 (apparent d, J = 47.7 Hz, 1H, ring 2C-<u>H</u>F), 4.48—4.29 (m, 1H, ring 5C-<u>H</u>F), 1.81 (apparent q, J = 7.7 Hz, 2H, ring 4,6C-<u>H</u>C), 1.36—1.25 (m, 20H, chain-C<u>H</u>$_2$), 0.89 (t, J = 6.6 Hz, 6H, C<u>H</u>$_3$); ^{19}F{^{1}H} NMR (376 MHz, $CDCl_3$) δ : -198.1 (t, *J* = 13.0 Hz, 1F), -205.1 (t, *J* = 19.7 Hz, 1F, *iso*-F), -212.1 (dd, *J* = 19.7, 13.0 Hz, 2F); ^{13}C NMR (126 MHz, $CDCl_3$) δ : 88.9 – 85.4 (m, 1,2,3,5-<u>C</u>HF), 37.5 (4,6-<u>C</u>HC), 32.1 (<u>C</u>$H_2CH_2CH_3$), 29.8 (<u>C</u>$H_2CH_2CH_2CH_3$), 26.7 (ring-<u>C</u>H_2), 22.9 (ring-CH_2<u>C</u>H_2), 19.4 (<u>C</u>H_2CH_3), 14.4 (<u>C</u>H_3); HRMS (ESI^+) $C_{18}H_{32}F_4$ [M+Na] found 347.233, requires 347.234.

All *cis*-tetrafluoro-4,6-dioctylcyclohexane 2.4

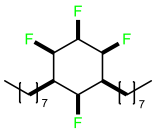

Following General Procedure **3**, **2.40** (75.8 mg, 0.210 mmol), Rh-CAAC-COD-Cl (2.00 mg, 0.004 mmol), 4Å molecular sieves (400 mg), and hexane (2.00 mL) for 10 d, r.t., and at 50 bar H_2 gave, after purification by flash silica chromatography (25—42% diethyl ether in hexane) **2.4** (49%, 42.0 mg, 0.111 mmol) was isolated as a white crystalline solid, m.p. 117—120 °C.

IR ν_{max} (solid): 2920, 1506 cm^{-1}; ^{1}H NMR (500 MHz, $CDCl_3$) δ : 4.96 (apparent dd, J = 49.8, 6.9 Hz, 2H, ring 1,3C-HF), 4.59 (apparent d, J = 47.3 Hz, 1H, ring 2C-HF), 4.39 (apparent dt, J = 42.0, 28.5 Hz, 1H, ring 5C-HF), 1.80 (q, J = 7.7 Hz, 2H, ring 4,6C-HC), 1.32—1.25 (m, 28H, long chain hydrogens), 0.88 (t, J = 6.9 Hz, 6H, CH_3); $^{19}F\{^{1}H\}$ NMR (470 MHz, $CDCl_3$) δ : -198.1 (t, J = 13.0 Hz, 1F), -205.1 (t, J = 19.7 Hz, 1F, *iso*-F), -212.1 (dd, J = 19.7, 13.0 Hz, 2F); ^{13}C NMR (126 MHz, $CDCl_3$) δ : 89.3 (br s, 3,5-CHF), 88.5 (br s, 1-CHF), 87.8 (br s, 4-CHF), 42.4 (2,6-$CHCH_2$), 32.0 ($CH_2CH_2CH_3$), 30.0 ($CH_2CH_2CH_2CH_3$), 29.6 ($CHCH_2CH_2CH_2$), 29.4 ($CH_2CH_2CH_2CH_2CH_3$), 26.9 ($CHCH_2$), 26.8 ($CHCH_2CH_2$), 22.8 (CH_2CH_3), 14.3 (CH_3); HRMS (ESI^+) $C_{22}H_{40}F_4$ [M+Na] found 403.296, requires 403.295.

All *cis*-tetrafluoro-4,6-bis(4-methylpentyl)cyclohexane 2.5

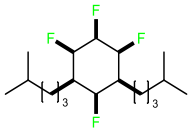

Following General Procedure **3**, **2.41** (80.0 mg, 0.250 mmol), Rh-CAAC-COD-Cl (2.00 mg, 0.004 mmol), 4Å molecular sieves (400 mg), and hexane (2.00 mL) for 3 d, 50 °C, and at 70 bar H_2 gave, after purification by flash silica chromatography (25—42% diethyl ether in hexane) **2.5** (42%, 34.3 mg, 0.110 mmol) was isolated as a white crystalline solid, m.p. 111—119 °C.

IR ν_{max} (solid): 3184, 2848, 1521 cm^{-1}; ^{1}H NMR (500 MHz, $CDCl_3$) δ : 4.97 (apparent dd, *J* = 49.8, 7.0 Hz, 2H, ring1,3C-HF), 4.59 (apparent d, *J* = 49.4 Hz, 1H, ring 2C-HF), 4.40 (apparent dtt, *J* = 41.8, 28.5, 2.9 Hz, 1H, ring 5C-HF), 2.17 – 2.15 (m, 1H, ring 4,6C-CHC), 1.79 (q, *J* = 7.6 Hz, 2H, CH), 1.58 – 1.48 (m, 6H, ring-CHHCH_2), 1.43 (dq, *J* = 15.1, 7.5 Hz, 2H, ring-CHH), 1.23 (q, *J* = 7.6 Hz, 4H, CH_2CH), 0.89 (d, *J* = 6.6 Hz, 12H, CH_3); $^{19}F\{^{1}H\}$ NMR (470 MHz, $CDCl_3$) δ : -198.1 (t, *J* = 13.1 Hz, 1F), -205.0 (t, *J* = 19.7 Hz, 1F, *iso*-F), -212.1 (dd, *J* = 19.6, 13.0 Hz, 2F); ^{13}C NMR (126 MHz, $CDCl_3$) δ : 88.5 – 87.2 (m, 1,2,3,5-CHF), 55.1 (4,6-$CHCH_2$), 38.9 (CH_2CH), 28.0 ($CH_2CH_2CH_2CH$), 27.0 (CH), 24.5 (CH_2CH_2CH), 22.7 (CH_3); HRMS (ESI^+) $C_{18}H_{32}F_4$ [M+Na] found 347.233, requires 347.234.

All *cis*-(tetrafluorocyclohexane-1,3-diyl)bis(propane-3,1-diyl))dicyclohexane 2.6

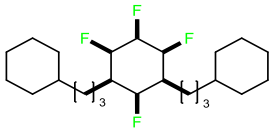

Rhodium-CAAC-COD-Cl (2.00 mg, 0.004 mmol) was added to an oven- dried 9 mL screw-cap vial or 50 mL glass cylinder equipped with a stirring bar and crushed 4Å molecular sieves (400 mg). Hexane (2.00 mL) and **2.42** (83.7 mg, 0.210 mmol) were added under argon atmosphere. The dry hexane and catalyst were sonicated for ~5 min before being placed in a 150 mL stainless steel autoclave under argon atmosphere. The autoclave was pressurized and depressurized with hydrogen gas three times before the indicated pressure was set (69 bar). The reaction mixture was stirred at 35 °C for 7 d. After the autoclave was carefully depressurized, the mixture was filtered through sinter funnel and washed with 10% methanol in DCM (1 mL / 9 mL) until all product could be collected into a sample vile that can then have the crude mixture directly submitted to column chromatography (Pure hexane then 2:8 diethyl ether) to yield the white crystal product 11% (9.10 mg, 0.020 mmol), m.p. = 185—190 °C.

IR ν_{max} (solid): 3303, 3020, cm^{-1}; ^{1}H NMR (500 MHz, $CDCl_3$) δ : 5.01-4.89 (m, 1H, ring-HF), 4.64-4.28 (m, 3H, ring-HF iso & 2,4), 1.78 (apparent q, *J* = 7.5 Hz, 2H, ring-HCH_2), 1.71-0.79 (m, 34H, remaining H); $^{19}F\{^{1}H\}$ NMR (376 MHz, $CDCl_3$) δ : -198.1 (t, *J* = 12.9 Hz, 1F), -205.7 (t, *J* = 19.7 Hz, 1F, *iso*-F), -212.02 (dd, *J* = 19.7, 12.0 Hz, 2F); ^{13}C NMR (126 MHz, $CDCl_3$) δ : 107.1 – 103.8 (m, ring-CF), 53.4 (ring-CCH_2), 37.5 (ring-$CCH_2CH_2CH_2$), 37.3 (ring-CH), 33.4 (ring-*ortho*-CH_2), 27.0 (ring-CCH_2), 26.7 (ring-*meta*-CH_2), 26.4 (ring-*para*-CH_2), 23.8 (ring-CCH_2CH_2); HRMS (ESI^+) $C_{24}H_{40}F_4$ [M+Na] found 427.295, requires 427.296.

All *cis*-trifluoro-2,4,6-trihexylcyclohexane 2.7

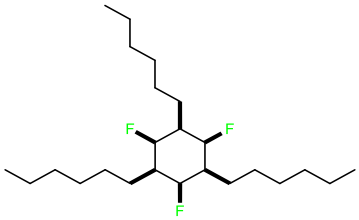

Following General Procedure **3**, **2.43** (87.3 mg, 0.230 mmol), Rh-CAAC-COD-Cl (2.00 mg, 0.004 mmol), 4Å molecular sieves (400 mg), and hexane (2.0 mL) for 7 d, 50 °C, and at 70 bar H_2 gave, after purification by flash silica chromatography (25—42% diethyl ether in hexane) **2.7** (41%, 36.5 mg, 0.090 mmol) was isolated as a white crystalline solid, m.p. 121—127 °C.

IR ν_{max} (solid): 2900, 1506 cm^{-1}; ^{1}H NMR (500 MHz, $CDCl_3$) δ : 4.69 – 4.60 (m, 3H, ring-HF), 1.75 (q, *J* = 7.6 Hz, 3H, ring-HCH_2) 1.41 (q, *J* = 7.4 Hz, 6H, ring-CH_2), 1.37 – 1.20 (m, 18H, long chain hydrogens), 0.93 – 0.81 (m, 9H, CH_3); $^{19}F\{^{1}H\}$ NMR (470 MHz, $CDCl_3$) δ : -205.3 (s, 3F); ^{13}C NMR (126 MHz, $CDCl_3$) δ : 90.8 (Br d, $^{1}J_{CF}$ = 191.6 Hz. CHF), 66.2 ($CHCH_2$), 31.8 ($CH_2CH_2CH_3$), 29.4 ($CH_2CH_2CH_2CH_3$), 27.6 ($CH_2CH_2CH_2CH_2CH_2CH_3$), 26.7 ($CH_2CH_2CH_2CH_2CH_3$), 22.6 (CH_2CH_3), 14.1 (CH_3); HRMS (ESI^+) $C_{24}H_{45}F_3$ [M+Na] found 413.336, requires 414.337.

All *cis*-1,3,5-trifluoro-2,4,6-triheptylcyclohexane 2.8

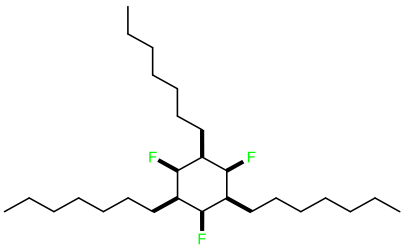

Following General Procedure **3**, **2.44** (90.7 mg, 0.210 mmol), Rh-CAAC-COD-Cl (2.00 mg, 0.004 mmol), 4Å molecular sieves (400 mg), and hexane (2.00 mL) for 7 d, 50 °C, and at 70 bar H_2 gave, after purification by flash silica chromatography (25—42% diethyl ether in hexane) **2.8** (22%, 19.7 mg, 0.050 mmol) was isolated as a white crystalline solid, m.p. 125—130 °C.

IR ν_{max} (solid): 2920, 1440 cm^{-1}; ^{1}H NMR (500 MHz, $CDCl_3$) δ : 4.70-4.59 (m, 3H, ring-HF), 1.75 (apparent q, *J* = 7.1 Hz, 3H, ring-HCH_2), 1.43-1.25 (m, 36H, alkyl-H), 0.89 (t, *J* = 6.9 Hz, 9H, CH_3); $^{19}F\{^{1}H\}$ NMR (470 MHz, $CDCl_3$) δ : -205.3 (s, 3F); ^{13}C NMR (126 MHz, $CDCl_3$) δ : 102.1 – 98.8 (m, ring-CF), 40.0 (ring-CCH_2), 29.7 ($CH_2CH_2CH_3$), 29.2 ($CH_2CH_2CH_2CH_2CH_3$), 26.8 ($CH_2CH_2CH_2CH_2CH_2CH_2CH_3$), 22.7 ($CH_2CH_3$), 14.1 ($CH_3$); HRMS ($ESI^+$) $C_{27}H_{51}F_3$ [M+Na] found 455.383, requires 455.384.

All *cis*-trifluoro-2,4,6-trioctylcyclohexane 2.9

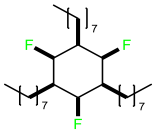

Following General Procedure **3**, **2.45** (33.6 mg, 0.072 mmol), Rh-CAAC-COD-Cl (1.6 mg, 0.0028 mmol), 4Å molecular sieves (400 mg), and hexane (2 mL) for 10 d, 50 °C, and at 70 bar H_2 gave, after purification by flash silica chromatography (25—42% diethyl ether in hexane) **2.9** (40%, 13.7 mg, 0.029 mmol) was isolated as a white crystalline solid, m.p. 119-122 °C.

IR ν_{max} (solid): 2954, 2875, 2852, 1460 cm^{-1}; ^{1}H NMR (500 MHz, $CDCl_3$) δ : 4.64 (apparent d, *J* = 46.9 Hz, 3H, ring-CHF), 1.75 (apparent q, *J* = 7.4 Hz, 3H, ring-CHC), 1.44—1.39 (m, 6H, long chain-CH_2), 1.31—1.26 (m, 36H, long chain-CH_2), 0.88 (t, *J* = 6.8 Hz, 9H, CH_3); $^{19}F\{^{1}H\}$ NMR (470 MHz, $CDCl_3$) δ : -205.3 (br s, 3F); ^{13}C NMR (126 MHz, $CDCl_3$) δ : 94.8 -- 92.3 (m, CHF), 42.8 ($CHCH_2$), 32.1 ($CH_2CH_2CH_3$), 29.9 ($CH_2CH_2CH_2CH_3$), 29.7 ($CH_2CH_2CH_2CH_2CH_2CH_3$), 29.4 ($CH_2CH_2CH_2CH_2CH_3$), 27.8 ($CHCH_2$), 27.1 ($CHCH_2CH_2$), 22.8 (CH_2CH_3), 14.3 (CH_3); HRMS (ESI^+) $C_{30}H_{57}F_3$ [M+Na] found 497.431, requires 497.430.

All *cis*-trifluoro-2,4,6-tris(4-methylpentyl)cyclohexane 2.10

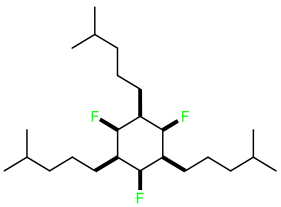

Following General Procedure **3**, **2.46** (292 mg, 0.760 mmol), Rh-CAAC-COD-Cl (6.50 mg, 0.011 mmol), 4Å molecular sieves (1.50 g), silica gel (700 mg), and hexane (15.0 mL) for

7 d, 50 °C, and at 50 bar H_2 gave, after purification by flash silica chromatography (25—42% diethyl ether in hexane) **2.10** (68%, 201 mg, 0.515 mmol) was isolated as a white crystalline solid, m.p. 123—130 °C.

IR ν_{max} (solid): 2899, 1462 cm^{-1}; ^1H NMR (500 MHz, $CDCl_3$) δ : 4.65 (dt, *J* = 48.0, 2.4 Hz, 3H, ring-C<u>H</u>F), 1.74 (q, *J* = 7.6 Hz, 3H, ring-C<u>H</u>), 1.62 – 1.49 (m, 12H, ring-CHC<u>H</u>$_2$C<u>H</u>$_2$CH$_2$CH$_2$CH *iso*CH$_3$), 1.48 – 1.36 (m, 3H, C<u>H</u> *iso*CH$_3$), 0.89 (d, *J* = 6.6 Hz, 18H, *iso*C<u>H</u>$_3$), 0.87 – 0.78 (m, 4H, C<u>H</u>$_2$CH isoCH$_3$); $^{19}F\{^1H\}$ NMR (470 MHz, $CDCl_3$) δ : -205.2 (s, 3F); ^{13}C NMR (126 MHz, $CDCl_3$) δ : 99.9 – 96.7 (m, <u>C</u>HF), 39.5 (<u>C</u>HCH$_2$), 39.1 (<u>C</u>H$_2$CH), 28.0 (<u>C</u>H$_2$CH$_2$CH$_2$CH), 27.9 (<u>C</u>H), 24.6 (<u>C</u>H$_2$CH$_2$CH), 22.8 (<u>C</u>H$_3$); HRMS (ESI^+) $C_{24}H_{45}F_3$ [M+K] found 429.310, requires 429.310.

(All *cis*-2,4,6-trifluorocyclohexane-1,3,5-triyl)tris(ethane-2,1-diyl))tricyclohexane 2.11

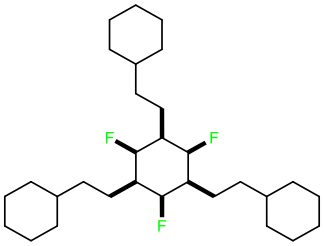

Following General Procedure **3**, **2.47** (361 mg, 0.780 mmol), Rh-CAAC-COD-Cl (6.40 mg, 0.013 mmol), 4Å molecular sieves (1.50 g), silica gel (700 mg), and hexane (15.0 mL) for 7 d, 50 °C, and at 50 bar H_2 gave, after purification by flash silica chromatography (0—5% Et_2O in hexane) **2.11** (31%, 113 mg, 0.240 mmol) was isolated as a white crystalline solid, m.p. 225—227 °C.

IR ν_{max} (solid): 3116, 1456 cm^{-1}; ^1H NMR (500 MHz, $CDCl_3$) δ: 4.64 (apparent dt, *J* = 48.0, 2.2 Hz, 3H, C<u>H</u>F), 1.42—1.38 (m, 3H, C<u>H</u>CH$_2$), 1.32—1.11 (m, 33H, sidering-<u>H</u>), 0.94—0.79 (m, 12H, C<u>H</u>$_2$C<u>H</u>$_2$); $^{19}F\{^1H\}$ NMR (470 MHz, $CDCl_3$) δ: -205.3 (s, 3F); ^{13}C NMR (126 MHz, $CDCl_3$) δ: 90.4 (br d, $^1J_{CF}$ = 204.1 Hz, 3C, ring-<u>C</u>F), 38.0 (br s, 3C, ring-<u>C</u>H), 34.7 (s, 3C, cyclohexane-<u>C</u>HCH$_2$), 33.5 (s, 6C, cyclohexane-*ortho*-<u>C</u>H$_2$), 26.8 (s, 6C, ring-CH<u>C</u>H$_2$<u>C</u>H$_2$), 26.5 (s, 6C, cyclohexane-*meta*-<u>C</u>H$_2$), 25.0 (s, 3C, cyclohexane-*para*-<u>C</u>H$_2$); HRMS (ESI^+) $C_{30}H_{51}F_3$ [M+Na] found 491.383, requires 491.384.

(All *cis*-2,4,6-trifluorocyclohexane-1,3,5-triyl)tris(propane-3,1-diyl))tris(oxy))tricyclohexane 2.12

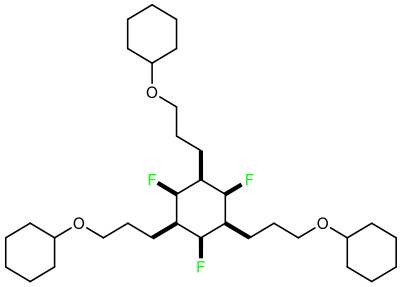

Following General Procedure **3**, **2.48** (410 mg, 0.740 mmol), Rh-CAAC-COD-Cl (12.7 mg, 0.022 mmol), 4Å molecular sieves (3.20 g), silica gel (1.60 g), and hexane (40.0 mL) for 8 d, 50 °C, and at 50 bar H_2 gave, after purification by flash silica chromatography (5—10% acetone in DCM) **2.12** (30%, 113 mg, 0.220 mmol) was isolated as a white crystalline solid, m.p. 91-92 °C.

IR ν_{max} (solid): 2926, 2852, 1446, 1076 cm^{-1}; ^1H NMR (500 MHz, $CDCl_3$) δ: 4.69 (apparent d, *J* = 47.7 Hz, 3H, CFH), 3.49 (t, *J* = 6.4 Hz, 6H, CH_2O), 3.21 (m, 3H, OCH), 1.89 (apparent q, *J* = 7.0, 5.1 Hz, 6H, *ortho*-C$\underline{H}_2$ top or bottom), 1.82 (apparent dd, *J* = 10.1, 5.6 Hz, 6H, *para*-C$\underline{H}_2$), 1.70 (apparent dt, *J* = 10.5, 6.7 Hz, 12H, C$\underline{H}_2$CH$_2$O & *meta*-C$\underline{H}_2$ top or bottom), 1.55—1.52 (m, 6H, CHC$\underline{H}_2$), 1.24 (apparent h, *J* = 10.0, 8.9 Hz, 15H, remaining H); $^{19}F\{^1H\}$ NMR (470 MHz, $CDCl_3$) δ: -205.6 (C$\underline{F}$H); ^{13}C NMR (126 MHz, $CDCl_3$) δ: 90.4 (br d, $^1J_{CF}$ = 181.6 Hz, 3C, $\underline{C}$FH), 77.7 (3C, $\underline{C}$HO), 68.0 ($\underline{C}H_2O$), 43.7 ($\underline{C}HCH_2$), 33.5 (6C, *ortho*-$\underline{C}H_2$), 27.4 (3C, $\underline{C}H_2CH_2O$), 26.0 (3C, CH$\underline{C}H_2$), 24.7 (3C, *para*-$\underline{C}H_2$), 24.3 (6C, *meta*-$\underline{C}H_2$); HRMS (ESI^+) $C_{33}H_{57}F_3O_3$ [M+Na] found 581.414, requires 581.416.

(All *cis*-1,3-bis(3,3-dimethylbutyl)-5-(4,4-dimethylpentyl)-2,4,6-trifluorocyclohexane 2.13

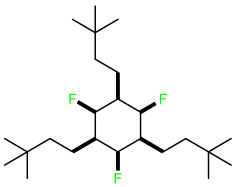

Following General Procedure **3**, **2.49** (286 mg, 0.744 mmol), Rh-CAAC-COD-Cl (7.80 mg, 0.014 mmol, 1.80 mol%), 4Å molecular sieves (2.40 g), silica (1.20 g), and hexane (40.0 mL) at 50 °C, for 6 d and at 50 bar H_2 gave, after purification by recrystallization in

acetone (washed with ice cold methanol) **2.13** (41%, 120 mg, 0.307 mmol) was obtained as a white crystal. m.p. 171—173 °C.

IR ν_{max} (solid): 2950, 1480 cm^{-1}; ^{1}H NMR (500 MHz, $CDCl_3$) δ : 4.69 (apparent dd, *J* = 45.5, 2.9 Hz, 3H ring-HF), 1.80 – 1.71 (m, 6H, ring-HCH_2), 1.35 – 1.28 (m, 6H, ring-HCH_2CH_2), 0.93 (s, 27H, CH_3), 0.89 (s, 3H, ring-HCH_2); $^{19}F\{^{1}H\}$ NMR (470 MHz, $CDCl_3$) δ : -205.4 (s, 3F); ^{13}C NMR (126 MHz, $CDCl_3$) δ : 90.5 (br d, $^{1}J_{CF}$ = 187.0 Hz, ring-CF), 45.1 (ring-CCH_2), 41.4 (ring-CCH_2CH_2), 30.5 (C), 29.5 (CH_3), 22.8 (ring-CCH_2); HRMS (ESI^+) $C_{24}H_{45}F_3$ [M+Na] found 413.336, requires 413.337.

All *cis*-1,3,5-triethyl-2,4,6-trifluorocyclohexane 2.14

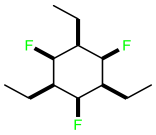

Following General Procedure **3**, **2.50** (27.5 mg, 0.130 mmol), Rh-CAAC-COD-Cl (2.00 mg, 0.002 mmol, 1.60 mol%), 4Å molecular sieves (700 mg), silica (400 mg), and hexane (4.00 mL) at 50 °C, for 6 d and at 50 bar H_2 gave, after purification by recrystallization in acetone (washed with ice cold methanol) **2.14** (35%, 9.80 mg, 0.044 mmol) was obtained as a white solid.

IR ν_{max} (solid): 2950, 1480 cm^{-1}; ^{1}H NMR (500 MHz, $CDCl_3$) δ : 4.71 (dt, *J* = 48.0, 2.6 Hz, 3H, HF), 1.82 (p, *J* = 7.5 Hz, 6H, CH_2), 1.39—1.36 (m, 3H, $CHCH_2$), 1.06 (t, *J* = 7.5 Hz, 9H, CH_3); $^{19}F\{^{1}H\}$ NMR (470 MHz, $CDCl_3$) δ : -205.8 (s, 3F); ^{13}C NMR (126 MHz, $CDCl_3$) δ : 92.3 (br d, $^{1}J_{CF}$ = 90.6 Hz, 3C, CF), 40.5 (3C, $CHCH_2$), 20.6 (3C, CH_2), 11.4 (3C, CH_3).

Acid stability test

Janus sample **2.1** (0.0025 mmol, 0.7 mg), **2.6** (0.0025 mmol, 1.0 mg), or **2.9** (0.0025 mmol, 1.2 mg) was added to separate NMR tubes with $CDCl_3$ (0.6 mL) then ^{19}F NMR spectra were taken. TFA (6.53 mmol, 0.5 mL, 2612 eq) was then added and after 1 h a second round of ^{19}F NMR spectra were taken. The resulting NMR spectra of *mono*-, *bis*- and *tris*-alkylated Janus molecules resulted in no degradation of *tris* and only partial degradation of *mono*-alkylated Janus compound (85% starting material **2.1** remains) and *bis*-alkylated Janus compound (92% starting material **2.6** remains).

Base stability test

Janus sample **2.1** (0.0025 mmol, 0.7 mg), **2.6** (0.0025 mmol, 1.0 mg), or **2.9** (0.0025 mmol, 1.2 mg) was added to separate NMR tubes with $CDCl_3$ (0.6 mL) then ^{19}F NMR spectra were taken. LiHMDS (1 M, 0.5 mL, 200 eq) was then added and after 1 h a second round of ^{19}F NMR spectra were taken. The resulting NMR spectra of *mono*-, *bis*- and *tris*-alkylated Janus molecules resulted in no degradation of tris and *bis*-alkylated Janus molecules and only partial degradation of *mono*-alkylated Janus compound (87% starting material **2.1** remains.

7.22 Experimental for Chapter 3

Methyl 2-(perfluorophenyl)acetate 3.6

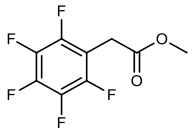

Pentafluoroacetic acid (5.00 g, 22.1 mmol) was dissolved in MeOH (40.0 mL) and HCl (2M, 1.00 mL) and heated to reflux overnight (24 h). The solution was allowed to cool to r.t. before being concentrated in vacuo. The mixture was then basified to pH 8 with $NaHCO_3$ and extracted with EtOAc (3x). The combined organic layers were washed with brine and dried over $MgSO_4$ before solvent was removed to afford the product (99%, 5.30 g, 22.1 mmol) as a clear oil. With spectroscopic data in accordance with the literature.[102]

IR νmax (solid): 1746 cm^{-1}; ^{1}H NMR (400 MHz, $CDCl_3$) δ : 3.74 (s, 3H, C$\underline{H}_3$), 3.73 (s, 2H, C$\underline{H}_2$); $^{19}F\{^{1}H\}$ NMR (377 MHz, $CDCl_3$) δ : -127.1 – -148.5 (m, *ortho*-F), -155.5 (t, *J* = 20.7 Hz, *para*-$\underline{F}$), -159.2 – -168.4 (m, *meta*-F); ^{13}C NMR (101 MHz, $CDCl_3$) δ : 168.9 ($\underline{C}$=O), 147.4 – 143.9 (m, 2C, *ortho*-$\underline{C}$F), 142.7 – 139.3 (m, *para*-$\underline{C}$F), 139.2 – 136.0 (m, 2C, *meta*-$\underline{C}$F), 108.2 (br tt, $^{2}J_{CF}$ = 18.5 Hz, $^{3}J_{CF}$ = 4.0 Hz, Ar-$\underline{C}CH_2$), 52.8 ($\underline{C}H_3$), 27.6 ($\underline{C}H_2$); HRMS (ESI^+) $C_9H_5F_5O_2$ [M+Na] found 263.010, requires 263.010.

Methyl 2-all *cis*-2,3,4,5,6-pentafluorocyclohexyl)acetate 3.7

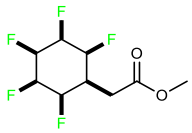

Following General Procedure **3**, methyl 2-(perfluorophenyl)acetate (950 mg, 3.95 mmol), Rh-CAAC-COD-Cl (5.00 mg, 0.008 mmol, 2 mol%), 4Å molecular sieves (8.00 g), and hexane (40.0 mL) at r.t, for 1d and at 50 bar H_2 gave, after purification by flash column chromatography (60% DCM in hexane) to yield the title compound (64%, 623 mg, 2.53 mmol) was obtained as a white crystal. m.p. 150—151 °C. With spectroscopic data in accordance with the literature.[102]

IR ν_{max} (solid): 1728 cm^{-1}; ^{1}H NMR (500 MHz, $CDCl_3$) δ : 5.34 (apparent br d, *J* = 54.0 Hz, 1H, *para*-C<u>H</u>), 5.00 (apparent br d, *J* = 49.0 Hz, 2H, *ortho*-C<u>H</u>), 4.69 – 4.32 (m, 2H, *meta*-C<u>H</u>), 3.75 (s, 3H, C<u>H</u>$_3$), 2.91 (d, *J* = 6.9 Hz, 2H, C<u>H</u>$_2$), 2.36 – 2.12 (m, 1H, C<u>H</u>); $^{19}F\{^{1}H\}$ NMR (470 MHz, $CDCl_3$) δ : -203.7 (br s, 2F, *meta*-F), -211.5 (br s, 2F, *ortho*-F), -216.8 (br s, *para*-<u>F</u>); ^{13}C NMR (126 MHz, $CDCl_3$) δ : 176.5 (C=O), 88.8 (br t, $^{2}J_{CF}$ = 15.9 Hz, *ortho*-<u>C</u>F), 87.5 – 86.0 (m, 2C, *para*-<u>C</u>F), 85.7 – 84.6 (m, 2C, *meta*-<u>C</u>F), 52.4 (O<u>C</u>H$_3$), 35.4 (<u>C</u>H), 30.5 (<u>C</u>H$_2$); HRMS (ESI$^+$) $C_9H_{11}F_5O_2$ [M+Na] found 269.057, requires 269.058.

2-(All *cis*-2,3,4,5,6-pentafluorocyclohexyl)ethan-1-ol 3.8

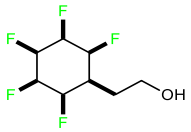

DIBAlH (1M in hexane, 13.4 mL, 13.4 mmol, 2.2 eq) was added dropwise to a solution of **3.7** (1.50 g, 6.09 mmol, 1 eq) in THF (30.0 mL) at 0 °C. The solution was slowly warmed to r.t. and stirred for 16 h. The reaction was then diluted with Et_2O (50.0 mL) cooled to 0 °C and quenched by the slow subsequent addition of water (0.400 mL), aqueous sodium hydroxide (15% w/w, 0.4 mL) and water (1.00 mL). The mixture was warmed to r.t. and stirred for 15 mins before $MgSO_4$ was added and the resulting suspension stirred for 15 mins. The suspension was then filtered to remove aluminium salts and the filtrate concentrated *in vacuo*. The crude product was purified by flash column chromatography (SiO_2, 60% EtOAc in hexane to 100% EtOAc) to give **3.8** as a white crystalline solid (99%, 1.33 g, 6.09 mmol) as a crystalline white solid, m.p. = 126 – 127 °C. With spectroscopic data in accordance with the literature.[102]

IR ν_{max} (solid): 3400, 2970, 1045 cm^{-1}; ^{1}H NMR (400 MHz, $CDCl_3$) δ : 5.35 (apparent d, *J* = 50.3 Hz, 1H, *para*-CF<u>H</u>), 5.00 (apparent d, *J* = 46.6 Hz, 2H, *ortho*-CF<u>H</u>), 4.61 – 4.27 (m, 2H, *meta*-CF<u>H</u>), 3.89 (apparent q, *J* = 5.2 Hz, 2H, C<u>H</u>$_2$OH), 3.71 (apparent t, *J* = 5.9 Hz, 1H, ring-C<u>H</u>), 2.13 (apparent q, *J* = 6.2 Hz, 2H, C<u>H</u>$_2$CH$_2$OH); $^{19}F\{^{1}H\}$ NMR (377 MHz, $CDCl_3$) δ : -203.18 (br dt, *J* = 11.9, 8.5 Hz, 2F, *meta*-F), -211.68 (br ddd, *J* = 26.3, 6.8, 6.6 Hz, 2F, *ortho*-F), -216.72 (br tt, *J* = 26.9, 14.1 Hz, *para*-C<u>F</u>H); ^{13}C NMR (CD_3OD, 126 MHz) δ : 89.9

(br s, *para*-CFH), 88.4 (br s, 2C, *ortho*-CFH), 87.1 (br s, 2C, *meta*-CFH), 59.3 ($\underline{C}H_2OH$), 36.0 ($\underline{C}FCH_2$), 29.8 ($\underline{C}H_2CH_2OH$); HRMS (EI) $C_8H_{11}F_5O$ [M] found 218.073, requires 218.072.

(All *cis*)-1-(2-Bromoethyl)-2,3,4,5,6-pentafluorocyclohexane 3.9

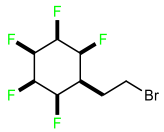

Ph_3P (3.16 g, 12.0 mmol, 2.1 eq) and CBr_4 (3.99 g, 12.0 mmol, 2.1 eq) were added to a solution of **3.8** (1.25 g, 5.73 mmol, 1 eq) in CH_3CN (40.0 mL) at r.t. for 16 h. The reaction mixture was concentrated *in vacuo* and purified directly by flash column chromatography (SiO_2, 40—60% EtOAc in hexane) to give the title compound as a white crystalline solid (88%, 1.41 g, 5.03 mmol), m.p. = 154-155 °C. With spectroscopic data in accordance with the literature.[102]

IR νmax (solid): 2900 cm^{-1}; ^1H NMR (500 MHz, $CDCl_3$) δ : 5.36 (apparent d, *J* = 52.7 Hz, 1H, *para*-CF$\underline{H}$), 4.95 (apparent d, *J* = 49.6 Hz, 2H, *ortho*-CF$\underline{H}$), 4.49 (apparent dt, *J* = 40.7, 26.3 Hz, 2H, *meta*-CF$\underline{H}$), 3.76 – 3.52 (m, 2H, $C\underline{H}_2Br$), 2.41 (q, *J* = 6.5 Hz, 2H, $C\underline{H}_2CH_2Br$); $^{19}F\{^1H\}$ NMR (470 MHz, $CDCl_3$) δ : -203.4 (br dt, *J* = 12.4, 8.5 Hz, 2F, *meta*-C$\underline{F}$H), -211.3 (br ddd, *J* = 27.2, 6.8, 6.1 Hz, 2F, *ortho*-C$\underline{F}$H), -216.8 (br tt, *J* = 26.1, 11.4 Hz, *para*-C$\underline{F}$H); ^{13}C NMR (126 MHz, $CDCl_3$) δ : 88.3 – 86.9 (m, 3C, *ortho*-$\underline{C}$FH & *para*-$\underline{C}$FH), 85.9 – 84.2 (m, 2C, *meta*-$\underline{C}$FH), 31.3 (ring-$\underline{C}HCH_2$), 30.7 ($\underline{C}H_2CH_2Br$), 28.4 ($\underline{C}H_2Br$); HRMS (EI) $C_8H_{10}F_5{}^{79}Br$ [M] found 279.988, requires 279.988.

1-(2-(All *cis*)-2,3,4,5,6-pentafluorocyclohexyl)ethyl)-4-(trifluoromethyl)benzene 3.10

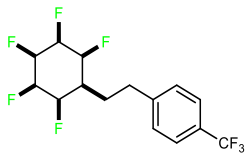

To a vial equipped with a stir bar was added photocatalyst $Ir[dF(CF_3)ppy]_2(dtbbpy)PF_6$ (1.40 mg, 0.001 mmol, 0.01 eq), 4-Bromobenzotrifluoride (0.020 mL, 0.130 mmol, 1 eq), **3.9** (52.8 mg, 0.190 mmol, 1.5 eq), tris(trimethylsilyl)silane (0.040 mL, 0.130 mmol, 1.0 eq), and anhydrous sodium carbonate (27.0 mg, 0.250 mmol, 2 eq). The vial was sealed and placed under nitrogen before 4.00 mL of DME was added. To a separate vial was

added $NiCl_2$•glyme (1.00 mg, 5.00 µmol, 0.01 eq) and 4,4'-di-tert-butyl-2,2'-bipyridine (1.30 mg, 5.00 µmol, 0.01 eq). The catalyst vial was sealed, purged with nitrogen then to it was added 2.00 mL of DME. The precatalyst solution was sonicated for 5 min to get a clear solution. After which, 0.250 mL (0.5 mol% catalyst, 1.25 µmol, 0.005 eq) was syringed into the reaction vessel. The solution was degassed by sparging with nitrogen while stirring for 10 min before sealing with Parafilm. The reaction was stirred and irradiated with a 34 W blue LED lamp (6-10 cm away, with cooling fan to keep the reaction temperature at 25 °C) for 17 h. The reaction was quenched by exposure to air and concentrated in vacuo. Purification by column chromatography (silica gel, 0—50% EtOAc in hexane) gave title compound (80%, 35.0 mg, 0.100 mmol, 82% conversion) as a pale white solid, m.p =140—141 °C.

IR ν_{max} (solid): 2927, 1620, 1330 cm^{-1}; ^1H NMR (500 MHz, $CDCl_3$) δ : 7.45 (dd, J = 125.5, 8.0 Hz, 4H, Ar-C<u>H</u>), 5.33 (apparent d, J = 52.5 Hz, 1H, *para*-CF<u>H</u>), 4.96 (apparent dd, J = 49.3, 5.0 Hz, 2H, *ortho*-CF<u>H</u>), 4.39 (apparent dd, J = 66.5, 27.9 Hz, 2H, *meta*-CF<u>H</u>), 2.88 (apparent t, J = 7.9 Hz, 2H, Ar-CHC<u>H</u>$_2$), 2.26 (apparent q, J = 7.7 Hz, 2H, Ar-CHCH$_2$C<u>H</u>$_2$), 1.10 (apparent t, J = 7.5 Hz, 1H, ring-C<u>H</u>); $^{19}F\{^1H\}$ NMR (470 MHz, $CDCl_3$) δ : -62.5 (br s, 3F, CF_3), -203.1 – -203.4 (m, 2F, CF, *meta*-F), -211.9 (br d, *J* = 27.0 Hz, 2F, CF, *ortho*-F), -216.7 (br tt, *J* = 26.1, 11.6 Hz, 1F, CF, *para*-CF); ^{13}C NMR (126 MHz, $CDCl_3$) δ : 146.6 (Ar-<u>C</u>CH$_2$), 137.9 (Ar-<u>C</u>CF$_3$), 128.6 (Ar-<u>C</u>H), 125.7 (Ar-<u>C</u>H), 119.6 — 115.8 (m, CF_3), 86.6 — 85.4 (5C, <u>C</u>FH), 32.1 (Ar-CHC<u>H</u>$_2$), 27.0 (Ar-CHCH$_2$C<u>H</u>$_2$), 12.2 (ring-C<u>H</u>); HRMS (ESI^+) $C_{15}H_{14}F_8$ [M+Na] found 369.086, requires 369.087.

1-(2-(All *cis*)-2,3,4,5,6-pentafluorocyclohexyl)ethyl)-3-(trifluoromethyl)benzene 3.11

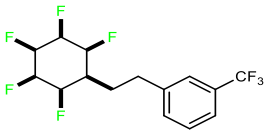

To a vial equipped with a stir bar was added photocatalyst $Ir[dF(CF_3)ppy]_2(dtbbpy)PF_6$ (1.40 mg, 0.001 mmol, 0.01 eq), 3-bromobenzotrifluoride (0.020 mL, 28.1 mg, 0.130 mmol, 1 eq), **3.9** (52.8 mg, 0.190 mmol, 1.5 eq), tris(trimethylsilyl)silane (0.040 mL, 0.130 mmol, 1.0 eq), and anhydrous sodium carbonate (27.0 mg, 0.250 mmol, 2 eq). The vial was sealed and placed under nitrogen before 4.00 mL of DME was added. To a

separate vial was added $NiCl_2$•glyme (1.00 mg, 5.00 µmol, 0.01 eq) and 4,4'-di-tert-butyl-2,2'-bipyridine (1.30 mg, 5.00 µmol, 0.01 eq). The catalyst vial was sealed, purged with nitrogen then to it was added 2 mL of DME. The precatalyst solution was sonicated for 5 min to get a clear solution. After which, 0.250 mL (0.5 mol% catalyst, 1.25 µmol, 0.005 eq) was syringed into the reaction vessel. The solution was degassed by sparging with nitrogen while stirring for 10 min before sealing with Parafilm. The reaction was stirred and irradiated with a 34 W blue LED lamp (6-10 cm away, with cooling fan to keep the reaction temperature at 25 °C) for 17 h. The reaction was quenched by exposure to air and concentrated in vacuo. Purification by column chromatography (silica gel, 0—50% Et_2O in hexane) gave Title Compound (76%, 32.7 mg, 0.094 mmol, 81% conversion) as a pale white solid, m.p. = 134—136 °C.

IR ν_{max} (solid): 2924, 1660, 1456, 1336 cm^{-1}; ^1H NMR (500 MHz, $CDCl_3$) δ : 7.53 – 7.37 (m, 4H, Ar-C<u>H</u>), 5.33 (apparent d, *J* = 53.0 Hz, 1H, *para*-CF<u>H</u>), 4.97 (apparent d, *J* = 50.1 Hz, 2H, *ortho*-CF<u>H</u>), 4.41 (apparent dt, *J* = 48.6, 27.3 Hz, 2H, *meta*-CF<u>H</u>), 2.94 – 2.79 (apparent t, *J* = 7.9 Hz, 2H, Ar-CHC<u>H</u>$_2$), 2.25 (apparent q, *J* = 7.7 Hz, 2H, Ar-CHCH$_2$C<u>H</u>$_2$), 1.10 (apparent t, *J* = 7.5 Hz, 1H, ring-C<u>H</u>); $^{19}F\{^1H\}$ NMR (470 MHz, $CDCl_3$) δ : -62.61 (br s, 3F, C<u>F</u>$_3$), -203.3 (br s, 2F, CF, *meta*-F), -211.73 – -211.94 (m, 2F, CF, *ortho*-F), -216.70 apparent (br tt, *J* = 26.9, 13.6 Hz, *para*-CF); ^{13}C NMR (126 MHz, $CDCl_3$) δ : 136.6 (Ar-<u>C</u>CH$_2$), 132.6 (C3), 131.8 (C6), 129.4 (C5), 125.1 (C2), 123.6 – 119.8 (2C, C4 & <u>C</u>F$_3$), 87.9 (br d, $^2J_{CF}$ = 17.2 Hz, 2C, <u>C</u>FH), 86.3 (br d, $^2J_{CF}$ = 17.2 Hz, 2C, <u>C</u>FH), 85.5— 84.3 (*para*-<u>C</u>FH), 32.3 (Ar-CH<u>C</u>H$_2$), 27.4 (Ar-CHCH$_2$<u>C</u>H$_2$), 11.3 (ring-<u>C</u>H); HRMS (ESI^+) $C_{15}H_{14}F_8$ [M+Na] found 369.086, requires 369.087.

1-(2-(All *cis*)-2,3,4,5,6-pentafluorocyclohexyl)ethyl)-2-(trifluoromethyl)benzene 3.12

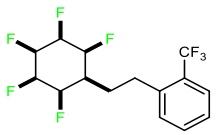

To a vial equipped with a stir bar was added photocatalyst Ir[dF(CF_3)ppy]$_2$(dtbbpy)PF_6 (1.40 mg, 0.001 mmol, 0.01 equiv.), 2-Bromobenzotrifluoride (0.020 mL, 28.1 mg, 0.130 mmol, 1 equiv.), **3.9** (52.8 mg, 0.190 mmol, 1.5 equiv.), tris(trimethylsilyl)silane (0.040 mL, 0.130 mmol, 1.0 equiv.), and anhydrous sodium carbonate (27.0 mg, 0.250 mmol,

2 equiv.). The vial was sealed and placed under nitrogen before 4.00 mL of DME was added. To a separate vial was added $NiCl_2$•glyme (1.00 mg, 5.00 µmol, 0.01 equiv.) and 4,4'-di-tert-butyl-2,2'-bipyridine (1.30 mg, 5.00 µmol, 0.01 equiv.). The catalyst vial was sealed, purged with nitrogen then to it was added 2.00 mL of DME. The precatalyst solution was sonicated for 5 min to get a clear solution. After which, 0.250 mL (0.5 mol% catalyst, 1.25 µmol, 0.005 equiv.) was syringed into the reaction vessel. The solution was degassed by sparging with nitrogen while stirring for 10 min before sealing with Parafilm. The reaction was stirred and irradiated with a 34 W blue LED lamp (6-10 cm away, with cooling fan to keep the reaction temperature at 25 °C) for 17 h. The reaction was quenched by exposure to air and concentrated in vacuo. Purification by column chromatography (silica gel, 0—50% Et_2O in hexane) gave Title Compound (39%, 16.8 mg, 0.049 mmol, 46% conversion) as a pale white solid, m.p. = 115—117 °C.

IR ν_{max} (solid): 3062, 1683, 1313 cm^{-1}; ^1H NMR (500 MHz, $CDCl_3$) δ : 7.51 (app. dd, *J* = 129.1, 7.8 Hz, 2H, Ar-C<u>H</u>), 7.42 (app. dt, *J* = 88.4, 7.6 Hz, 2H, Ar-C<u>H</u>), 5.34 (app. d, *J* = 52.7 Hz, 1H, *para*-CF<u>H</u>), 4.99 (app. d, *J* = 48.6 Hz, 2H, *ortho*-CF<u>H</u>), 4.45 (app. dt, *J* = 42.4, 26.7 Hz, 2H, *meta*-CF<u>H</u>), 3.00 – 2.88 (m, 2H, Ar-CHC<u>H</u>$_2$), 2.36 – 2.12 (m, 2H, Ar-CHCH$_2$C<u>H</u>$_2$), 1.10 (app. t, *J* = 7.5 Hz, 1H, ring-C<u>H</u>); $^{19}F\{^1H\}$ NMR (470 MHz, $CDCl_3$) δ : -59.5 (br s, 3F, <u>C</u>F_3), -202.1 – -203.4 (m, 2F, CF, *meta*-F), -212.0 (br ddd, *J* = 27.0, 8.0, 6.5 Hz, 2F, CF, *ortho*-F), -216.7 (tt, *J* = 26.2, 11.3 Hz, 1F, *para*-CF); ^{13}C NMR (126 MHz, $CDCl_3$) δ : 139.5 (Ar-<u>C</u>CH$_2$), 132.3 (2C, C4 & C5), 131.0 (C6), 126.7 (C2), 126.3 (C3), 123.7 (br s, CF_3), 88.0 br (d, $^2J_{CF}$ = 19.7 Hz, *para*-<u>C</u>FH), 86.5 (br d, $^2J_{CF}$ = 17.2 Hz, *ortho*-<u>C</u>FH), 85.6 (br d, $^2J_{CF}$ = 15.9 Hz, *meta*-<u>C</u>FH), 29.6 (Ar-CH<u>C</u>H$_2$), 28.0 (Ar-CHCH$_2$<u>C</u>H$_2$), 11.3 (ring-<u>C</u>H); HRMS (ESI^+) $C_{15}H_{14}F_8$ [M+Na] found 369.086, requires 369.087.

Methyl 4-(2-(All *cis*)-2,3,4,5,6-pentafluorocyclohexyl)ethoxy)benzoate 3.16

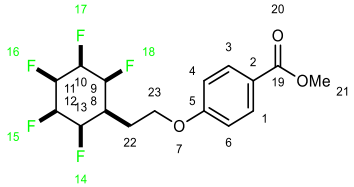

Methyl 4-hydroxybenzoate (54.2 mg, 0.360 mmol, 1 eq) was added to a solution of **3.9** (100 mg, 0.360 mmol, 1 eq) and Cs_2CO_3 (186 mg, 0.570 mmol, 1.6 eq) in DMF (10.0 mL)

and heated to 70 °C with stirring overnight. The solvent was then removed under reduced pressure and purified by flash column chromatography (0—80% EtOAc in hexane) to yield the title compound (87%, 109 mg, 0.309 mmol) as a white solid, m.p. = 179 —180 °C.

IR νmax (solid): 2956, 1718, 1255, 1043 cm^{-1}; ^{1}H NMR (500 MHz, $CDCl_3$) δ : 8.01 (d, *J* = 8.9 Hz, 2H, H3,H1-C<u>H</u>), 6.91 (d, *J* = 8.9 Hz, 2H, H4&H6-C<u>H</u>), 5.36 (app. d, *J* = 52.7 Hz, 1H, H11-CF<u>H</u>, C), 5.00 (app. d, *J* = 49.2 Hz, 2H, H9,H13-CF<u>H</u>), 4.48 (app. dd, *J* = 45.5, 21.5 Hz, 2H, H10,H12-CF<u>H</u>), 4.23 (app. t, *J* = 5.6 Hz, 2H, H23-OC<u>H_2</u>), 3.90 (s, 3H, H21-C<u>H_3</u>), 2.39 (q, *J* = 6.2 Hz, 2H, H22-OCH_2C<u>H_2</u>), 1.26 (app. s, 1H, H8); $^{19}F\{^{1}H\}$ NMR (470 MHz, $CDCl_3$) δ : -203.3 (br s, 2F, F15,F17-*meta*-C<u>F</u>), -211.6 (br d, *J* = 26.9 Hz, 2F, F14,H18-*ortho*-C<u>F</u>), -216.7 (br app. q, *J* = 15.3 Hz, F, F16-*para*-C<u>F</u>); ^{13}C NMR (126 MHz, $CDCl_3$) δ : 150.3 (C19), 147.3 (C5), 131.9 (C3 & C1), 127.6 (C2), 114.1 (C4 & C6), 89.0 (br d, $^{2}J_{CF}$ = 16.3 Hz, C11-*para*-<u>C</u>F), 88.3 (br s, 2C, C9,C13-*ortho*-<u>C</u>F), 87.9 (br d, $^{2}J_{CF}$ = 19.8 Hz, 2C, C10,C12-*meta*-<u>C</u>F), 68.1 (C23), 52.1 (C21), 29.9 (C8), 25.8 (C22); HRMS (ESI^{+}) $C_{16}H_{17}F_5O_3$ [M+Na] found 375.099, requires 375.100.

4-(2-(All *cis*)-2,3,4,5,6-pentafluorocyclohexyl)ethoxy)benzoic acid 3.17

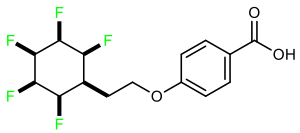

3.16 (318 mg, 0.903 mmol) was suspended in HCl (6M, 30.0 mL) and heated to reflux overnight, 16 h. The solvent was then removed under reduced pressure and purified by recrystallization with MeOH to yield the title compound (90%, 275 mg, 0.810 mmol) as a white solid, m.p. = 309—311 °C.

IR νmax (solid): 2960, 1672, 1257, 1041 cm^{-1}; ^{1}H NMR (400 MHz, DMSO-d_6) δ : 12.63 (s, 1H, O<u>H</u>), 7.89 (d, *J* = 8.9 Hz, 2H, Ar-C<u>H</u> COOH), 7.03 (d, *J* = 8.9 Hz, 2H, Ar-C<u>H</u> OCH_2), 5.66 – 4.60 (m, 5H, ring-F<u>H</u>), 4.22 (t, *J* = 6.0 Hz, 2H, OC<u>H_2</u>), 2.27 (t, *J* = 9.8 Hz, 1H, ring-C<u>H</u>CH_2), 2.14 (app. q, *J* = 6.0 Hz, 2H, OCH_2C<u>H_2</u>); $^{19}F\{^{1}H\}$ NMR (377 MHz, DMSO-d_6) δ : -202.5 – -204.1 (m, 2F, *meta*-C<u>F</u>), -211.5 (br d, *J* = 21.8 Hz, 2F, *ortho*-C<u>F</u>), -216.3 (tt, *J* = 23.8, 11.4 Hz, 1F, *para*-C<u>F</u>); ^{13}C NMR (101 MHz, DMSO-d_6) δ : 167.0 (<u>C</u>OOH), 162.0 (O-Ar-<u>C</u>), 146.7

(COOH-ring-C), 131.3 (COOH-ring-CH_2), 114.4 (2C, OC-ring-CH_2), 90.8 – 85.7 (m, 5C, CFH), 64.9 (OCH_2), 34.4 (br d, $^2J_{CF}$ = 19.0 Hz, ring-$CHCH_2$), 25.3 (ring-$CHCH_2$); HRMS (EI) $C_{15}H_{15}F_5O_3$ [M] found 338.093, requires 338.094.

Methyl 2-(2,4,6-trifluorophenyl)acetate 3.20

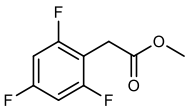

Pentafluoroacetic acid (3.00 g, 22.1 mmol) was dissolved in MeOH (40.0 mL) and HCl (2M, 1.00 mL) and heated to reflux overnight (24 h). The solution was allowed to cool to r.t. before being concentrated in vacuo. The Mixture was then basified to pH 8 with $NaHCO_3$ and extracted with EtOAc (3x). The combined organic layers were washed with brine and dried over $MgSO_4$ before solvent was removed to afford the product (99%, 5.30 g, 22.1 mmol) as a clear oil.

IR ν_{max} (solid): 2956, 1743, 1438 cm^{-1}; ^1H NMR (500 MHz, $CDCl_3$) δ : 6.72 – 6.62 (m, 2H, Ar-CH), 3.72 (s, 3H, CH_3), 3.66 (s, 2H, CH_2); $^{19}F\{^1H\}$ NMR (470 MHz, $CDCl_3$) δ : -109.0 (t, *J* = 5.3 Hz, 1F), -111.6 (d, *J* = 5.2 Hz, 2F); ^{13}C NMR (126 MHz, $CDCl_3$) δ : 170.0 (C=O), 162.2 (br dt, $^1J_{CF}$ = 249.0 Hz, $^2J_{CF}$ = 15.7 Hz, 2C, *ortho*-CF), 161.7 (br ddd, $^1J_{CF}$ = 249.2 Hz, $^2J_{CF}$ = 14.9 Hz, $^2J_{CF}$ = 10.9 Hz, *para*-CF), 106.9 (br td, $^2J_{CF}$ = 20.5 Hz, $^4J_{CF}$ = 4.7 Hz, Ar-CCH_2), 100.5 – 99.9 (m, 2C, *meta*-CH), 52.5 (CH_3), 27.5 (CH_2); HRMS (EI) $C_9H_7F_3O_2$ [M] found 204.039, requires 204.039.

Methyl 2-(All *cis*-2,4,6-trifluorocyclohexyl)acetate 3.21

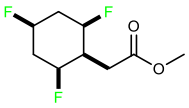

Following General Procedure **3** [10 batches], single batch was performed with **3.20** (0.285 mg, 1.40 mmol), Rh-CAAC-COD-Cl (3.00 mg, 0.005 mmol), 4Å molecular sieves (2.40 g), silica (0.60 g), and hexane (12.0 mL) at r.t., for 3d and at 50 bar H_2. The crude mixtures were pooled and after purification by flash column chromatography (60% DCM in hexane) to yield the title compound (45%, 1.33 g, 6.32 mmol) was obtained as a white crystal. m.p. 89—90 °C.

IR νmax (solid): 2953, 1730 cm^{-1}; ^{1}H NMR (400 MHz, $CDCl_3$) δ : 5.02 – 4.74 (m, 3H, HF), 3.72 (s, 3H,CH_3), 2.78 (d, *J* = 6.9 Hz, 2H, ring-$CHCH_2$), 2.71 – 2.54 (m, 2H, *meta*-CH), 2.30 (app. ddtd, *J* = 32.7, 29.9, 7.3, 6.9, 3.4 Hz, 1H, ring-CH), 1.87 (app. tdt, *J* = 40.2, 15.6, 3.3 Hz, 2H, meta-CH); $^{19}F\{^{1}H\}$ NMR (376 MHz, $CDCl_3$) δ : -177.9 (t, *J* = 13.8 Hz, 1F), -191.5 (d, *J* = 13.8 Hz, 2F); ^{13}C NMR (101 MHz, $CDCl_3$) δ : 166.8 (O=C), 87.5 (br d, $^{1}J_{CF}$ = 178.5 Hz, 2C, *ortho*-CF), 84.7 (br d, $^{1}J_{CF}$ = 175.2 Hz, *para*-CF), 52.1 (CH_3), 39.0 (ring-CH), 34.2 (O=CCH_2), 31.8 (br s, *meta*-CH_2); HRMS (EI) $C_9H_{13}F_3O_2$ [M] found 210.086, requires 210.086.

2-(All *cis*-2,4,6-trifluorocyclohexyl)ethan-1-ol 3.22

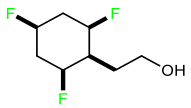

DIBAlH (1M in hexane, 13.6 mL, 13.6 mmol, 2.2 eq) was added dropwise to a solution of **3.21** (1.30 g, 6.18 mmol, 1 eq) in THF (30.0 mL) at 0 °C. The solution was slowly warmed to r.t. and stirred for 16 h. The reaction was then diluted with Et_2O (50.0 mL) cooled to 0 °C and quenched by the slow subsequent addition of water (0.400 mL), aqueous sodium hydroxide (15% w/w, 0.40 mL) and water (1.00 mL). The mixture was warmed to r.t. and stirred for 15 min before $MgSO_4$ was added and the resulting suspension stirred for 15 min. The suspension was then filtered to remove aluminium salts and the filtrate concentrated *in vacuo*. The crude product was purified by flash column chromatography (SiO_2, 60% EtOAc in hexane to 100% EtOAc) to give the title compound as a white crystalline (68%, 763 mg, 4.19 mmol), m.p. 86—87 °C.

IR ν_{max} (solid): 3614, 1010 cm^{-1}; ^{1}H NMR (500 MHz, $CDCl_3$) δ : 4.95 (app. p, *J* = 3.6 Hz, 1H, *para*-FH), 4.91 – 4.74 (m, 2H, *ortho*-FH), 3.92 – 3.79 (m, 2H, CH_2OH), 2.69 – 2.52 (m, 2H, CH_2CH_2OH), 2.13 – 1.74 (m, 5H, remaining H); $^{19}F\{^{1}H\}$ NMR (377 MHz, $CDCl_3$) δ : -178.0 (t, *J* = 13.0 Hz, 1F, *para*-F), -191.3 (d, *J* = 13.0 Hz, 2F, *ortho*-F); ^{13}C NMR (126 MHz, $CDCl_3$) δ : 87.6 (br d, $^{1}J_{CF}$ = 178.4 Hz, 2x ring-CF), 85.1 (br d, $^{1}J_{CF}$ = 174.6 Hz, ring-CF), 59.9 (CH_2OH), 38.6 (br t, $^{2}J_{CF}$ = 19.6 Hz, ring-$CHCH_2$), 35.0 – 33.9 (m, CH_2CH_2OH), 29.7 (2x ring-$CHCH_2$); HRMS (EI) $C_8H_{13}F_3O$ [M] found 182.092, requires 182.091.

(All *cis*)-2-(2-bromoethyl)-1,3,5-trifluorocyclohexane 3.23

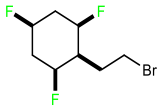

Ph_3P (2.28 g, 8.70 mmol, 2.1 eq) and CBr_4 (2.89 g, 8.70 mmol, 2.1 eq) were added to a solution of **3.22** (755 mg, 4.14 mmol, 1 eq) in CH_3CN (40.0 mL) at r.t. for 24 h. The reaction mixture was concentrated *in vacuo* and purified directly by flash column chromatography (SiO_2, 10—60% EtOAc in hexane) to give **3.23** as a white crystalline solid (82%, 830 mg, 3.39 mmol), m.p. 101—103 °C.

IR ν_{max} (solid): 2939, 650 cm^{-1}; ^1H NMR (500 MHz, $CDCl_3$) δ : 5.01 – 4.71 (m, 3H, CFH), 3.63 (t, *J* = 6.3 Hz, 2H, $BrCH_2$), 2.65 (dt, *J* = 15.5, 11.6 Hz, 2H, *meta* ring-CHH), 2.29 (q, *J* = 6.6 Hz, 2H, $BrCH_2CH_2$), 2.15 – 1.74 (m, 3H, *meta* ring-CHH & ring-CHCH$_2$); $^{19}F\{^1H\}$ NMR (377 MHz, $CDCl_3$) δ : -178.0 (t, *J* = 13.0 Hz, 1F, *para*-F), -191.3 (d, *J* = 13.0 Hz, 2F, *ortho*-F); ^{13}C NMR (126 MHz, $CDCl_3$) δ : 87.0 (br dd, $^1J_{CF}$ = 182.6 Hz, $^2J_{CF}$ = 3.1 Hz, 2C, *ortho*-CF), 84.9 (br d, $^1J_{CF}$ = 174.7 Hz, *para*-CF), 40.1 (br t, $^3J_{CF}$ = 19.4 Hz, ring-CHCH$_2$), 34.3 (br t, $^2J_{CF}$ = 20.7 Hz, ring-CH), 31.7 ($BrCH_2$), 29.7 (br s, 2C, *meta*-CH_2); HRMS (ESI^+) $C_8H_{12}F_3{}^{79}Br$ [M+Na] found 266.996, requires 266.997.

Methyl 4-(2-(All *cis*-2,4,6-trifluorocyclohexyl)ethoxy)benzoate 3.24

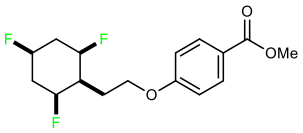

Methyl 4-hydroxybenzoate (425 mg, 2.79 mmol, 1.2 eq) was added to a solution of **3.23** (570 mg, 2.33 mmol, 1 eq) and Cs_2CO_3 (1.14 g, 3.72 mmol, 1.5 eq) in DMF (10.0 mL) and heated to 70 °C with stirring overnight. The solvent was then removed under reduced pressure and purified by flash column chromatography (0—80% EtOAc in hexane) to yield the title compound (72%, 755 mg, 2.39 mmol) as a white solid, m.p. 161—162 °C.

IR ν_{max} (solid): 2960, 1710, 1249 cm^{-1}; ^1H NMR (500 MHz, $CDCl_3$) δ : 7.99 (app. d, *J* = 8.9 Hz, 2H, COOMe-Ar-CH), 6.91 (app. d, *J* = 8.9 Hz, 2H, RO-Ar-CH), 4.89 (app. ddq, *J* = 48.1,

37.8, 3.5 Hz, 3H, CFH), 4.20 (t, *J* = 5.9 Hz, 2H, OCH$_2$), 3.89 (s, 3H, CH$_3$), 2.70 – 2.57 (m, 2H, ring-CH *meta*-CH), 2.26 (app. q, *J* = 6.3 Hz, 2H, OCH$_2$CH$_2$), 2.19 – 1.75 (m, 3H, *meta*-CHHCH); ^{19}F{^{1}H} NMR (377 MHz, $CDCl_3$) δ : -178.0 (br t, *J* = 13.4 Hz, *para*-CF), -191.3 (br d, *J* = 13.5 Hz, 2F, *ortho*-CF); ^{13}C NMR (126 MHz, $CDCl_3$) δ : 166.9 (C=O), 162.6 (O-Ar-C), 131.8 (2C, COOMe-Ar-CH), 123.0 (COOMe-Ar-C), 114.1 (2C, RO-Ar-CH), 88.2 – 86.4 (2C, *ortho*-CFH), 85.0 (br d, $^1J_{CF}$ = 174.8 Hz, *para*-CFH), 64.8 (OCH$_2$), 52.1 (OCH$_3$), 38.6 (br t, $^2J_{CF}$ = 19.6 Hz, CH), 34.6 – 34.1 (m, OCH$_2$CH$_2$), 26.7 (br t, $^2J_{CF}$ = 3.8 Hz, 2C, *meta*-CH$_2$); HRMS (ESI$^+$) $C_{16}H_{19}F_3O_3$ [M+H] found 317.136, requires 317.136.

4-(2-(All *cis*-2,4,6-trifluorocyclohexyl)ethoxy)benzoic acid 3.25

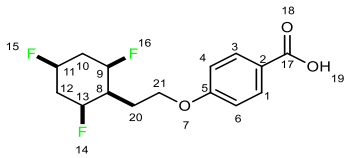

To a solution of the corresponding ester **3.24** (427 mg, 1.35 mmol, 1 eq) and sodium iodide (606 mg, 4.05 mmol, 3 eq) in acetonitrile (14.0 mL), chlorotrimethylsilane (0.510 mL, 4.05 mmol, 3 eq) was added with continuous good stirring. The reaction mixture was then heated under reflux (75 °C) for 35 h. Soon after the observed completion of reaction, the reaction mixture was cooled to r.t., and the product silyl esters were hydrolyzed to the corresponding carboxylic acids by adding water (50.0 mL). Subsequently, the reaction mixture was taken up in ether (50.0 mL x 2) and washed successively with water and sodium thiosulfate solution (10%, 25.0 mL) to remove inorganic salts and iodine, respectively. Water-insoluble carboxylic acids were then extracted by sodium bicarbonate solution (15%, 25.0 mL x 2) while the ether layer contained the unreacted starting ester. Pure carboxylic acids were obtained by acidification (2M HCl) of the bicarbonate extract and drying by freeze dryer overnight to obtain the title compound (55%, 226 mg, 0.750 mmol) as a white solid, m.p. 243—244°C decomposes.

IR νmax (solid): 2958, 1734, 1249 cm^{-1}; ^{1}H NMR (500 MHz, DMSO-d_6) δ : 12.58 (s, 1H, H19-COOH), 7.88 (d, *J* = 8.9 Hz, 2H, H1&H3-Ar-CH), 7.03 (d, *J* = 8.8 Hz, 2H, H4&H6-Ar-CH), 4.93 – 4.77 (m, 3H, H14,H15,H16-CFH), 4.19 (t, *J* = 6.1 Hz, 2H, H21-OCH$_2$), 2.37 (dt,

J = 14.3, 12.8 Hz, 2H, H20-$OCH_2C\underline{H}_2$), 2.16 – 1.85 (m, 5H, H8,H10,H12); $^{19}F\{^1H\}$ NMR (470 MHz, DMSO-d_6) δ : -175.4 (t, *J* = 12.8 Hz, 1F), -190.09 (d, *J* = 12.5 Hz, 2F); ^{13}C NMR (126 MHz, DMSO-d_6) δ : 167.1 (C17), 162.2 (C5), 131.4 (2C, C1&C3), 123.0 (C2), 114.4 (2C, C4&C6), 87.7 (br d, $^1J_{CF}$ = 177.7 Hz, 2C, C9&13), 85.2 (br d, $^1J_{CF}$ = 171.8 Hz, C11), 65.3 (C21), 37.8 (br t, $^2J_{CF}$ = 19.1 Hz, C8), 33.6 (C20), 26.5 (2C, C10&12); HRMS (EI) $C_{15}H_{18}F_3O_3$ [M] found 303.120, requires 303.120.

7.23 Experimental for Chapter 4

Diethyl (10-bromodecyl)phosphonate 4.4

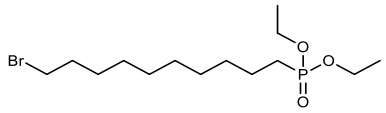

1,10-dibromodecane (24.0 g, 80.0 mmol, 1 eq) and triethyl phosphite (11.2 mL, 70.0 mmol, 0.880 eq) were added together and refluxed at 140 °C overnight. The reaction mixture was cooled to r.t. and purified by passing through a short column packed with silica gel and stored in freezer until its usage (80%, 23.0 g, 64.0 mmol). With spectroscopic data in accordance with the literature.[215]

IR νmax (solid): 2926, 1244 cm^{-1}; ^{1}H NMR (500 MHz, $CDCl_3$) δ : 4.06 (q, *J* = 7.5 Hz, 4H, $OC\underline{H}_2$), 3.38 (t, *J* = 6.8 Hz, 2H, $BrC\underline{H}_2$), 1.83 (app. p, *J* = 7.1 Hz, 2H, $PC\underline{H}_2$), 1.76 – 1.49 (m, 4H, $BrCH_2C\underline{H}_2$ & $PCH_2C\underline{H}_2$), 1.44 – 1.23 (m, 18H, $C\underline{H}_3$ & middle $C\underline{H}_2$); ^{31}P NMR (202 MHz, $CDCl_3$) δ : 32.6 (s, 1P); ^{19}C NMR (126 MHz, $CDCl_3$) δ : 61.5 (app. d, *J* = 6.4 Hz, 2x $O\underline{C}H_2$), 34.2 ($Br\underline{C}H_2$), 32.9 ($BrCH_2\underline{C}H_2$), 30.7 ($PCH_2CH_2\underline{C}H_2$), 29.6 – 28.8 (m, $BrCH_2CH_2CH_2\underline{C}H_2\underline{C}H_2\underline{C}H_2\underline{C}H_2\underline{C}H_2$), 28.3 ($BrCH_2CH_2\underline{C}H_2$), 25.8 (d, *J* = 140.3 Hz, $P\underline{C}H_2$), 22.5 (d, *J* = 5.2 Hz, $PCH_2\underline{C}H_2$), 16.6 (app. d, *J* = 6.0 Hz, 2x $\underline{C}H_3$); HRMS (ESI^+) $C_{14}H_{30}{}^{79}BrO_3P$ [M+H] found 357.119, requires 357.119.

Diethyl (10-(perfluorophenoxy)decyl)phosphonate 4.6

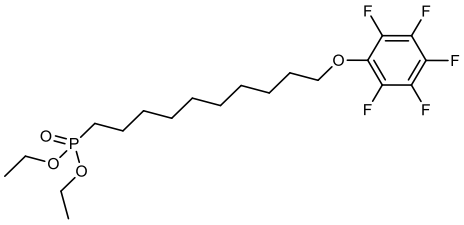

Potassium carbonate (2.24 g, 16.3 mmol, 3 eq) was added to pentafluorophenol (1.00 g, 5.43 mmol, 1 eq) in acetonitrile (30.0 mL) and stirred at 85 °C for 1 h. Diethyl (10-bromodecyl)phosphonate (2.33 g, 6.52 mmol, 1.2 eq) was then added to the mixture over a 15 min period and the reaction was heated to 90 °C for 18 h. After completion, the mixture was cooled to r.t., diluted with H_2O (100 mL), and extracted with hexane (2x 50.0 mL), and then with H_2O (1 x 100 mL), dried over anhydrous magnesium sulphate, filtered, evaporated under vacuum, and purified by flash column

chromatography (1—50% EtOAc in hexane) to yield the title compound (47%, 1.17 g, 2.54 mmol) as a clear oil.

IR ν_{max} (solid): 2927, 1480, 1241 cm^{-1}; ^{1}H NMR (500 MHz, $CDCl_3$) δ : 4.27 – 3.98 (m, 6H, POC$\underline{H}_2$ & Ar-OC$\underline{H}_2$), 1.83 – 1.65 (m, 4H, Ar-OCH$_2$C$\underline{H}_2$ & PC$\underline{H}_2$), 1.66 – 1.51 (m, 2H, PCH$_2$C$\underline{H}_2$), 1.44 (app. p, *J* = 7.2 Hz, 2H, Ar-OCH$_2$CH$_2$C$\underline{H}_2$), 1.39 – 1.25 (m, 16H, remaining $\underline{H}$); $^{19}F\{^{1}H\}$ NMR (470 MHz, $CDCl_3$) δ : -156.8 – -157.2 (m, 2F, *ortho*-C$\underline{F}$), -163.6 (t, *J* = 21.7 Hz, 2F, *meta*-C$\underline{F}$), -163.9 (t, *J* = 21.7 Hz, 1F, *para*-C$\underline{F}$); ^{31}P NMR (202 MHz, $CDCl_3$) δ : 32.6; ^{13}C NMR (126 MHz, $CDCl_3$) δ : 142.0 – 139.7 (m, 3F, *meta*/*para*-$\underline{C}$F), 138.5 – 138.0 (m, 2F, *ortho*-$\underline{C}$F), 136.35 (Ar-$\underline{C}$OR), 76.0 (Ar-O$\underline{C}H_2$), 61.50 (br d, $^{2}J_{CP}$ = 6.5 Hz, 2C, PO$\underline{C}H_2$), 30.7 (PCH$_2$CH$_2\underline{C}H_2$), 29.9 (Ar-OCH$_2\underline{C}H_2$), 29.7 – 29.0 (m, 4C, OCH$_2$CH$_2$CH$_2\underline{C}H_2\underline{C}H_2\underline{C}H_2\underline{C}H_2$), 25.8 (br d, $^{1}J_{CP}$ = 140.4 Hz, P$\underline{C}H_2$), 25.8 (Ar-OCH$_2$CH$_2\underline{C}H_2$), 22.5 (br d, $^{2}J_{CP}$ = 5.2 Hz, PCH$_2\underline{C}H_2$), 16.6 (app. d, *J* = 6.0 Hz, 2x $\underline{C}H_3$); HRMS (EI) $C_{20}H_{31}F_5O_4P$ [M] found 461.187, requires 461.187.

2,3,5,6-Tetrafluoro-4-iodophenol 4.9

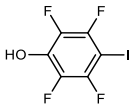

A mixture of potassium hydroxide (2.80 g, 50.0 mmol) in *tert*-butanol (40.0 mL) was heated to 65 °C. Iodopentafluorobenzene (2.67 mL, 20.0 mmol) was added in lots over 30 min to this mixture with constant stirring. After the addition, the temperature of the reaction was heated to reflux ~90 °C overnight. After completion the reaction was quenched by addition of water. The *tert*-butanol was removed under vacuum. The aqueous layer was extracted with methylene chloride (3 x 25.0 mL) to remove any unreacted iodopentafluorobenzene. The aqueous layer was acidified with concentrated hydrochloric acid (5.00 mL) and extracted with methylene chloride (3 x 25.0 mL). The organic phase was dried over magnesium sulphate and the solvent was removed under reduced pressure to obtain the title compound as a white crystal (67%, 3.90 g, 13.4 mmol), m.p. 163—165 °C. With spectroscopic date in accordance with the literature.[177]

IR ν_{max} (solid): 3313, 1641 cm^{-1}; $^{19}F\{^{1}H\}$ NMR (376 MHz, $CDCl_3$) δ : -122.14 – -122.31 (m, 2F), -159.78 – -159.97 (m, 2F); ^{13}C NMR (126 MHz, $CDCl_3$) δ : 209.1 (COH), 147.2 (d, $^{1}J_{CF}$ = 242.1 Hz, 2C, 3,5-CF), 137.6 (br d, $^{1}J_{CF}$ = 263.5 Hz, 2C, 2,6-CF), 60.9 (CI); HRMS (EI) C_6F_4IOH [M] found 291.900, requires 291.900.

Diethyl (10-(2,3,5,6-tetrafluoro-4-iodophenoxy)decyl)phosphonate 4.10

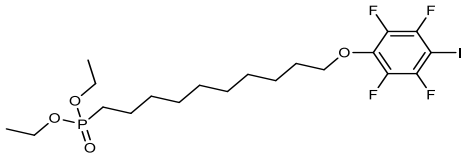

To a stirred solution of sodium iodide (513 mg, 3.43 mmol, 1 eq) in acetone (10.0 mL) was added Diethyl (10-bromodecyl)phosphonate (1.47 g, 4.11 mmol, 1.2 eq) and stirred at r.t. until no further precipitation was observed (20 min). The solution was filtered, and filtrate concentrated to give the corresponding crude iodide. A solution of 4-iodo-2,3,5,6-tetrafluorophenol (0.990 g, 3.43 mmol, 1 eq) and potassium carbonate (1.24 g, 10.3 mmol, 3 eq) was made in toluene (20.0 mL), the crude iodide was added into this and stirred at 88 °C temperature overnight. Water (50.0 mL) was added, and the layers separated. The aqueous layer was washed with DCM (3 x 50.0 mL) and combined organic layers were washed once with brine (50.0 mL) and dried over $MgSO_4$. The solvent was removed to afford the crude product. and purified by flash column chromatography (5—60% EtOAc in hexane) to yield the title compound (25%, 392 mg, 0.690 mmol) as a yellow oil.

IR ν_{max} (solid): 2929, 1510, 1450, 1024 cm^{-1}; ^{1}H NMR (500 MHz, $CDCl_3$) δ : 4.21 (t, *J* = 6.5 Hz, 2H), 4.14 – 4.01 (m, 4H), 1.89 – 1.66 (m, 4H), 1.64 – 1.52 (m, 2H), 1.47 – 1.22 (m, 18H); $^{19}F\{^{1}H\}$ NMR (470 MHz, $CDCl_3$) δ : -121.6 – -121.7 (m, 2F), -154.4 – -154.5 (m, 2F); ^{31}P NMR (202 MHz, $CDCl_3$) δ : 32.6; ^{13}C NMR (126 MHz, $CDCl_3$) δ : 147.5 (br d, *J* = 247.4 Hz, CF), 140.9 (br d, *J* = 267.8 Hz, 2C, CF), 138.5 (ArC-OCH_2), 75.5 (Ar-OCH_2), 71.1 (CI), 61.5 (2x POCH_2), 32.9 ($PCH_2CH_2CH_2$), 30.8 (Ar-$OCH_2CH_2CH_2CH_2$), 30.7 ($PCH_2CH_2CH_2CH_2$), 29.4 (Ar-$OCH_2CH_2CH_2CH_2CH_2$), 29.2 (Ar-$OCH_2CH_2CH_2CH_2CH_2CH_2$), 28.3 (Ar-$OCH_2CH_2$), 26.4 (Ar-$OCH_2CH_2CH_2$), 25.4 (br d, $^{1}J_{CP}$ = 141.6 Hz, PCH_2), 22.5 (d, $^{2}J_{CP}$ = 5.3 Hz, PCH_2CH_2),

16.6 (app. d, *J* = 6.0 Hz,2x CH_3); HRMS (ESI$^+$) $C_{20}H_{30}IF_4O_4P$ [M+H] found 569.094, requires 569.094.

Diethyl (10-((2,3,5,6-tetrafluoro-[1,1'-biphenyl]-4-yl)oxy)decyl)phosphonate 4.12

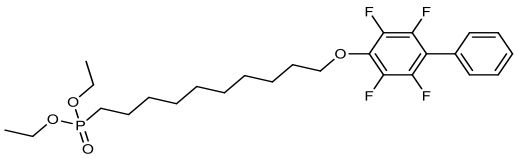

A solution of **4.10** (400 mg, 0.700 mmol, 1 eq) and phenylboronic acid (111 mg, 0.910 mmol, 1.3 eq) and potassium carbonate (195 mg, 1.41 mmol, 2 eq), tetrakis(triphenylphosphine)palladium(0) (65.0 mg, 0.056 mmol, 8 mol%) in 3:1 THF/H_2O (16.0 mL, 10.0 mL per mmol of aryl bromide) was stirred at 75 °C for 17 h. Subsequently, the reaction was cooled to r.t. and diluted with water (40.0 mL). The aqueous layer was extracted with DCM (3x 20.0 mL). The combined organic layers were washed with brine, dried over $MgSO_4$, filtered, and concentrated under vacuum. to afford the title compound (79%, 289 mg, 0.560 mmol) as a clear oil.

IR ν_{max} (solid): 2927, 1242 cm^{-1}; ^{1}H NMR (500 MHz, $CDCl_3$) δ : 7.50 – 7.40 (m, 5H, Ar-CH), 4.29 – 3.99 (m, 6H), 1.87 – 1.66 (m, 4H, Ar-OCH_2 & PCH_2), 1.64 – 1.49 (m, 2H, PCH$_2$CH_2), 1.32 – 1.29 (m, 18H, CH_3 & middle CH_2); ^{31}P NMR (202 MHz, $CDCl_3$) δ : 32.6 (s, 1P); ^{13}C NMR (101 MHz, $CDCl_3$) δ : 134.7 (br d, $^2J_{CF}$ = 6.3 Hz, 2C, ArCF Ar), 132.5 – 132.3 (m, 2C, ArCF OC), 132.1 (ArC- ArCF), 130.3 (ArCO), 129.0 (2C, *meta*-CH), 128.7 (ArC-Ar), 128.0 (br s, *ortho*-CH, *para*-CH), 75.8 – 75.1 (m, Ar-OCH$_2$), 61.5 (br s, 2C, POCH$_2$), 32.9 (PCH$_2$CH$_2$CH$_2$), 30.8 (Ar-OCH$_2$CH$_2$CH$_2$CH$_2$), 30.6 (PCH$_2$CH$_2$CH$_2$CH$_2$), 29.4 (Ar-OCH$_2$CH$_2$CH$_2$CH$_2$CH$_2$), 29.2 (Ar-OCH$_2$CH$_2$CH$_2$CH$_2$CH$_2$CH$_2$), 28.6 (Ar-OCH$_2$CH$_2$), 26.5 (Ar-OCH$_2$CH$_2$CH$_2$), 25.1 (br s, PCH$_2$), 22.5 (d, $^2J_{CF}$ = 5.1 Hz, PCH$_2$CH$_2$), 16.6 (app. d, *J* = 6.0 Hz, 2C, CH$_3$); HRMS (ESI$^+$) $C_{26}H_{35}F_4O_4P$ [M+Na] found 541.210, requires 541.211.

1-(*Tert*-butoxy)-2,3,4,5,6-pentafluorobenzene 4.19

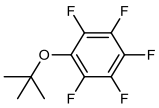

tert-BuOK (2.42 g, 21.6 mmol) was added to a stirred solution of hexafluorobenzene (4.99 g, 43.2 mmol) in THF (150 mL) at –8 °C. TLC of the resulting orange solution showed a single spot (1 h stirring). Further *tert*-BuOK (2.42 g, 21.6 mmol) was added and the mixture was stirred at –8 °C to 0 °C for 2 h. The product was isolated via removal of THF followed by a workup using H_2O (100 mL) and DCM (3x100 mL). The compound was then purified by column chromatography (hexane) resulting to yield the title compound (46%, 4.77 g, 19.9 mmol) as a clear oil. With spectroscopic data in accordance with the literature.[216]

IR ν_{max} (solid): 2985, 1506, 1004 cm^{-1}; ^1H NMR (500 MHz, $CDCl_3$) δ : 1.39 (apparent t, *J* = 1.4 Hz, 9H, C<u>H</u>$_3$); $^{19}F\{^1H\}$ NMR (470 MHz, $CDCl_3$) δ : -151.4 (dt, *J* = 23.8, 4.1 Hz, 2F, *ortho*-C<u>F</u>), -162.1 (tt, *J* = 21.9, 6.7 Hz, 1F, *para*-C<u>F</u>), -164.0 (ddt, *J* = 25.3, 21.5, 4.3 Hz, 2F, *meta*-C<u>F</u>); ^{13}C NMR (126 MHz, $CDCl_3$) δ : 145.9 – 141.8 (m, 3C, *meta*/*para*-<u>C</u>F), 138.0 (2C, br d, $^1J_{CF}$ = 249.1 Hz, *ortho*-<u>C</u>F), 130.2 (Ar-<u>C</u>OC), 85.2 (<u>C</u>), 28.4 (3C, <u>C</u>H$_3$); HRMS (EI) $C_{10}H_9F_5O$ [M] found 240.058, requires 240.057.

1-(*Tert*-butoxy)-2,3,5,6-tetrafluoro-4-(octyloxy)benzene 4.21

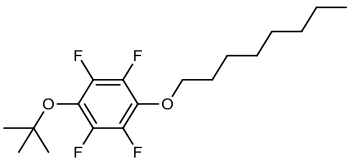

A mixture of potassium hydroxide (1.17 mg, 20.8 mmol) in 1-octanol (1.73 mL, 10.9 mmol) was heated to 65 °C and left stirring for 20 min. **4.19** (1.40 mL, 2.00 g, 8.32 mmol) was added in lots over 20 min to this mixture with constant stirring. After the addition, the temperature of the reaction was heated to reflux ~90 °C for 22 h. After completion the reaction was quenched by addition of water (50.0 mL). The hexanol was removed under vacuum. The aqueous layer was extracted with DCM (4 x 25.0 mL). The organic phase was dried over magnesium sulphate and the solvent was removed under reduced

pressure to obtain the title compound as a clear oil (54%, 1.56 g, 4.45 mmol) (including 10% *meta* product).

IR νmax (solid): 2929, 1494, 1174 cm^{-1}; ^{1}H NMR (500 MHz, $CDCl_3$) δ : 4.15 (t, *J* = 6.6 Hz, 2H, $OC\underline{H}_2$), 1.76 (dt, *J* = 14.6, 6.6 Hz, 2H, $OCH_2C\underline{H}_2$), 1.50 – 1.23 (m, 19H, remaining H), 0.89 (t, *J* = 7.0 Hz, 3H, $C\underline{H}_3$); $^{19}F\{^{1}H\}$ NMR (470 MHz, $CDCl_3$) δ : -153.0 (dd, *J* = 22.1, 5.9 Hz, C<u>F</u>Ot-butyl), -158.8 (dd, *J* = 22.1, 5.8 Hz, C<u>F</u>OCH_2); ^{13}C NMR (126 MHz, $CDCl_3$) δ : 145.5 – 139.7 (m, 4C, Ar<u>C</u>F), 131.4 (2C, Ar-<u>C</u>O), 84.4 (O<u>C</u>), 75.7 ($O\underline{C}H_2$), 31.9 ($\underline{C}H_2CH_2CH_3$), 30.0 (2C, $\underline{C}H_2\underline{C}H_2CH_2CH_2CH_3$), 29.3 ($OCH_2\underline{C}H_2$), 28.4 (3C, ^{t}butyl group), 25.7 ($OCH_2CH_2\underline{C}H_2$), 22.8 ($\underline{C}H_2CH_3$), 14.2 ($\underline{C}H_3$).

2,3,5,6-Tetrafluoro-4-(octyloxy)phenol 4.22

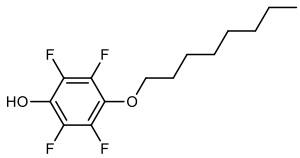

TFA (4.50 mL, 1 mL per mmol) was added to a solution of **4.21** (1.56 g, 4.50 mmol, 1 eq) in DCM (50.0 mL). After addition the reaction was stirred for 23 h. TFA and solvent were then removed via vacuo and gave, after purification by flash silica chromatography (0-10% EtOAc in hexane) the title compound (87%, 1.14 g, 3.88 mmol) as a yellow oil (including 9% *meta* product).

IR νmax (solid): 3320, 2929, 1494, 1174 cm^{-1}; ^{1}H NMR (500 MHz, $CDCl_3$) δ : 4.09 (t, *J* = 6.6 Hz, 2H, $OC\underline{H}_2$), 1.74 (tt, *J* = 8.0, 6.7 Hz, 2H, $OCH_2C\underline{H}_2$), 1.45 (app. p, *J* = 7.0 Hz, 2H,), 1.39 – 1.21 (m, 8H, remaining H), 0.88 (t, *J* = 7.1 Hz, 3H, $C\underline{H}_3$); $^{19}F\{^{1}H\}$ NMR (470 MHz, $CDCl_3$) δ : -158.2 (app. dd, *J* = 21.7, 5.0 Hz, C<u>F</u> COR), -164.8 (app. dd, *J* = 22.0, 5.5 Hz, C<u>F</u> COH); ^{13}C NMR (101 MHz, $CDCl_3$) δ : 142.2 (br d, $^{1}J_{CF}$ = 258.2 Hz, Ar-<u>C</u>F OH), 137.9 (br d, $^{1}J_{CF}$ = 222.5 Hz, Ar-<u>C</u>F OR), 130.3 (Ar-<u>C</u>OR), 125.3 (Ar-<u>C</u>OH), 76.0 ($O\underline{C}H_2$), 31.9 ($\underline{C}H_2CH_2CH_3$), 30.0 ($OCH_2\underline{C}H_2$), 29.4 ($\underline{C}H_2\underline{C}H_2CH_2CH_2CH_3$), 25.7 ($OCH_2CH_2\underline{C}H_2$), 22.8 ($CH_2CH_3$), 14.2 ($\underline{C}H_3$); HRMS ($ESI^-$) $C_{14}H_{18}F_4O_2$ [M-H] found 293.116, requires 293.117.

Diethyl (10-(2,3,5,6-tetrafluoro-4-(octyloxy)phenoxy)decyl)phosphonate 4.23

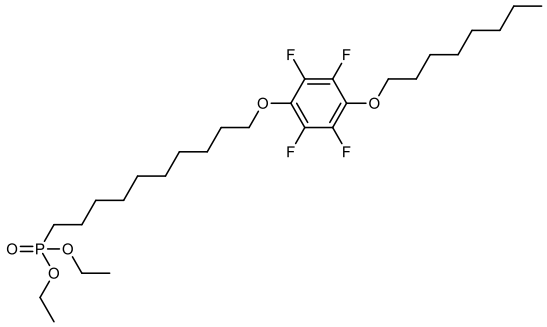

Potassium carbonate (1.41 g, 10.2 mmol, 3 eq) was added to **4.22** (1.00 g, 3.40 mmol, 1 eq) in acetonitrile (50.0 mL) and stirred at 85 °C for 1 h. Diethyl (10-bromodecyl)phosphonate (1.46 g, 4.10 mmol, 1.2 eq) was then added to the mixture over a 15 min period and the reaction was heated to 90 °C for 23 h. After completion, the mixture was cooled to r.t., diluted with H_2O (100 mL), and extracted with hexane (2x 50.0 mL), and then with H_2O (1 x 100 mL), dried over anhydrous magnesium sulphate, filtered, evaporated under vacuum, and purified by flash column chromatography (1—50% EtOAc in hexane) to yield the title compound (44%, 854 mg, 1.50 mmol) as a clear oil.

IR ν_{max} (solid): 2927, 1500, 1244 cm^{-1}; ^{1}H NMR (500 MHz, $CDCl_3$) δ : 4.15 – 3.98 (m, 8H, 2x $POCH_2$ & 2x Ar-$COCH_2$), 1.80 – 1.65 (m, 6H, PCH_2CH_2 & 2x Ar-$COCH_2CH_2$), 1.59 (app. ddt, *J* = 15.8, 11.2, 7.2 Hz, 2H, PCH_2), 1.44 (app. p, *J* = 7.4 Hz, 4H, 2x Ar-$COCH_2CH_2CH_2$), 1.30 (app. dt, *J* = 12.5, 6.2 Hz, 24H, remaining H), 0.88 (t, *J* = 6.8 Hz, 3H, CH_3); $^{19}F\{^{1}H\}$ NMR (470 MHz, $CDCl_3$) δ : -158.4 (br s, 4F); ^{31}P NMR (202 MHz, $CDCl_3$) δ : 32.6; ^{13}C NMR (126 MHz, $CDCl_3$) δ : 143.3 (br d, $^{2}J_{CF}$ = 14.1 Hz, 4C, Ar-CF), 140.9 (2C, Ar-COR), 75.72 (2C, Ar-$COCH_2$), 61.5 (br d, $^{2}J_{CP}$ = 6.5 Hz, 2C, $POCH_2$), 31.9 ($CH_2CH_2CH_3$), 30.7 ($CH_2CH_2CH_2P$), 30.1 – 29.4 (m, 6C, Ar-$COCH_2CH_2CH_2CH_2CH_2CH_2CH_2$ & Ar-$COCH_2CH_2CH_2CH_2CH_2$), 29.4 (CH_2CH_2O), 29.2 (CH_2CH_2O), 25.8 (br d, $^{1}J_{CP}$ = 140.3 Hz, CH_2P), 25.7 (2C, $CH_2CH_2CH_2O$), 22.8 (CH_2CH_3), 22.6 (br d, $^{2}J_{CP}$ = 5.1 Hz, CH_2CH_2P), 16.6 (2C, $POCH_2(CH_3)_2$), 14.2 (CH_3); HRMS (ESI^+) $C_{28}H_{47}F_4O_5P$ [M+H] found 571.317, requires 571.317.

Diethyl (10-((All *cis*-2,3,5,6-tetrafluoro-4-(octyloxy)cyclohexyl)oxy)decyl)phosphonate 4.24

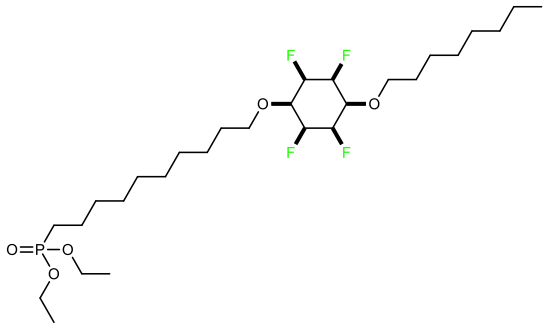

Following General Procedure **3**, **4.23** (700 mg, 1.23 mmol), Rh-CAAC-COD-Cl (14.0 mg, 0.025 mmol, 2 mol%), 4Å molecular sieves (8.00 g), silica (4.00 g), and hexane (40.0 mL) at 50 °C, for 2d and at 50 bar H_2 gave, title compound. However, it was not isolatable, and the crude was used for the final reaction.

HRMS (ESI^+) $C_{28}H_{53}F_4O_5P$ [M+H] found 577.364, requires 576.365.

(10-((All *cis*-2,3,5,6-tetrafluoro-4-(octyloxy)cyclohexyl)oxy)decyl)phosphonic acid 4.25

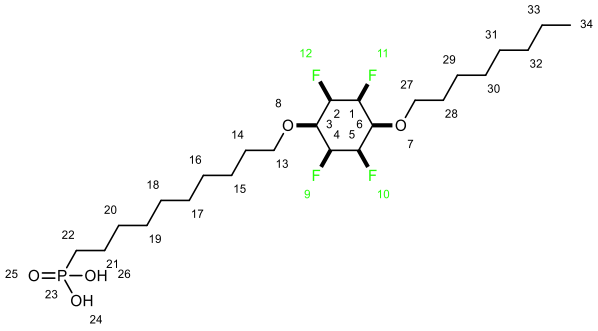

TMSBr (0.410 mL, 3.12 mmol, 3 eq) was added to a solution of **4.24** (600 mg, 1.04 mmol) in DCM (100 mL) and left to stir under argon for 24 h. The reaction was then concentrated via vacuo. The compound was then suspended in Na_2CO_3 and extracted (1x) with diethyl ether. The aqueous layer was then acidified to pH 3 with HCl (1M solution). The resulting mixture was then extracted with ethyl acetate (3x 50.0 mL). The organic layer was then washed with brine (2x 50.0 mL) dried over magnesium sulphate, filtered, and concentrated under reduced pressure to afford crude product. The crude was purified by reverse phase flash column chromatography (0—100% acetonitrile in

water) to yield the title compound (8%, 44.6 mg, 0.090 mmol) as a white powder. m.p. 149—150 °C.

IR ν_{max} (solid): 2922, 2851, 1456, 1107, 995 cm^{-1}; ^{1}H NMR (400 MHz, DMSO-d_6) δ : 5.26 – 4.47 (m, 4H, C1,2,4,5-C<u>H</u>F), 4.11 – 3.98 (m, 2H, C3&C6-C<u>H</u>O), 3.59 – 3.49 (m, 4H, C13&C27-C<u>H_2</u>), 1.80 – 1.57 (m, 2H, C22-PC<u>H_2</u>), 1.56 – 1.38 (m, 6H, C14&C21&C28), 1.28 – 1.22 (m, 22H, remaining-<u>H</u>), 0.85 (t, *J* = 6.7 Hz, 3H, C34-C<u>H_3</u>); $^{19}F\{^{1}H\}$ NMR (376 MHz, DMSO-d_6) δ : -206.71 (d, *J* = 15.5 Hz, $2F_{eq}$), -213.2 – -215.6 (m, $2F_{ax}$); ^{31}P NMR (202 MHz, DMSO-d_6) δ : 25.9; ^{13}C NMR (101 MHz, $CDCl_3$) attained from HSQC with multiplicity editing δ : 89.1—87.0 (C1,C2,C4,C,5), 73.6 (C3,C6), 69.9 (C13,27), 31.8 (C32), 30.4 (C20), 29.9 (C16,C17,C18,C19,C30,C31), 26.0 (C22), 22.8 (C15,C29), 22.6 (C33), 22.1 (C21), 14.3 (C34); Mass Spec HRMS (ESI^-) $C_{24}H_{45}F_4O_5P$ [M-H] found 519.287, requires 519.286.

1-(*Tert*-butoxy)-4-(cyclohexylmethoxy)-2,3,5,6-tetrafluorobenzene 4.27

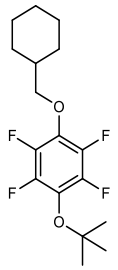

A mixture of potassium hydroxide (3.50 g, 63.4 mmol) in cyclohexanemethanol (4.00 mL, 31.7 mmol) was heated to 65 °C and left stirring for 20 min. 1-(*tert*-butoxy)-2,3,4,5,6- pentafluorobenzene (6.00 g, 25.0 mmol) was added in lots over 20 min to this mixture with constant stirring. After the addition, the temperature of the reaction was heated to reflux ~90 °C overnight. After completion the reaction was quenched by addition of water (50—100 mL). The hexanol was removed under vacuum. The aqueous layer was extracted with DCM (4 x 25.0 mL) and HCl (37%, 10.0 mL). The organic phase was dried over magnesium sulphate and the solvent was removed under reduced pressure to obtain the title compound as a clear oil (77%, 6.39 g, 19.1 mmol) (including 10% *meta* product).

IR ν_{max} (solid): 2927, 1494, 1041 cm^{-1}; ^{1}H NMR (500 MHz, $CDCl_3$) δ : 3.95 (d, *J* = 6.4 Hz, 2H, OC$\underline{H}_2$), 1.93 – 1.64 (m, 7H, C$\underline{H}$, *ortho*-C$\underline{H}_2$, top-*meta*-C$\underline{H}_2$), 1.38 (s, 9H, C$\underline{H}_3$), 1.34 – 1.12 (m, 4H, bottom-*meta*-C$\underline{H}_2$, *para*-C$\underline{H}_2$); $^{19}F\{^{1}H\}$ NMR (470 MHz, $CDCl_3$) δ : -153.0 (dd, *J* = 22.3, 5.7 Hz, 2F, C$\underline{F}$ CO^{t}butyl), -158.8 (dd, *J* = 21.7, 5.5 Hz, 2F, C$\underline{F}$ COCH$_2$); ^{13}C NMR (126 MHz, $CDCl_3$) δ : 143.9 (app. dd, $^{1}J_{CF}$ = 246.2 Hz, $^{2}J_{CF}$ = 12.8 Hz, Ar-$\underline{C}$F), 140.7 (br d, $^{2}J_{CF}$ = 5.5 Hz, Ar-$\underline{C}$OR), 84.4 (O$\underline{C}^{t}$butyl), 81.0 (O$\underline{C}$CH$_2$), 38.5 ($\underline{C}$H), 29.5 (2C, *ortho*-$\underline{C}$H$_2$), 28.4 (3C, $\underline{C}$H$_3$), 26.6 (2C, *meta*-$\underline{C}$H$_2$), 25.8 (*para*-$\underline{C}$H$_2$); HRMS (EI) $C_{17}H_{22}F_4O_2$ [M] found 334.155, requires 334.155.

4-(Cyclohexylmethoxy)-2,3,5,6-tetrafluorophenol 4.28

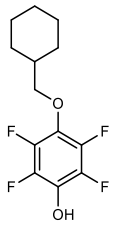

TFA (3.70 mL, 1 mL per mmol) was added to a solution of **4.27** (1.24 g, 3.71 mmol, 1 eq) in DCM (50.0 mL). After addition the reaction was stirred for 23 h. TFA and solvent were then removed via vacuo and gave, after purification by flash silica chromatography (0-10% EtOAc in hexane) the title compound (95%, 983 mg, 3.53 mmol) as a clear oil (including 10% *meta* product).

IR ν_{max} (solid): 3310, 2926, 1502, 1026 cm^{-1}; ^{1}H NMR (400 MHz, $CDCl_3$) δ : 5.38 (s, 1H, O$\underline{H}$), 3.88 (d, *J* = 6.4 Hz, 2H, OC$\underline{H}_2$), 1.94 – 1.64 (m, 7H, C$\underline{H}$, *ortho*-C$\underline{H}_2$, top-*meta*-C$\underline{H}_2$), 1.37 – 1.12 (m, 4H, bottom-*meta*-C$\underline{H}_2$, para-C$\underline{H}_2$); $^{19}F\{^{1}H\}$ NMR (377 MHz, $CDCl_3$) δ : -158.3 (dd, *J* = 21.8, 5.6 Hz, C$\underline{F}$ COR), -164.7 (dd, *J* = 21.8, 5.7 Hz, C$\underline{F}$ COH); ^{13}C NMR (101 MHz, $CDCl_3$) δ : 142.1 (br d, $^{1}J_{CF}$ = 246.3 Hz, Ar-$\underline{C}$F COH), 138.0 (br d, $^{1}J_{CF}$ = 255.6 Hz, Ar-$\underline{C}$F COR), 130.2 (br s, Ar-$\underline{C}$OR), 129.2 (Ar-$\underline{C}$OH), 81.4 (O$\underline{C}$CH$_2$), 38.5 ($\underline{C}$H), 29.6 (2C, *ortho*-$\underline{C}$H$_2$), 26.6 (2C, *meta*-$\underline{C}$H$_2$), 25.8 (*para*-$\underline{C}$H$_2$); HRMS (EI) $C_{17}H_{22}F_4O_2$ [M] found 334.155, requires 334.155.

Diethyl (10-(4-(cyclohexylmethoxy)-2,3,5,6-tetrafluorophenoxy)decyl)phosphonate 4.29

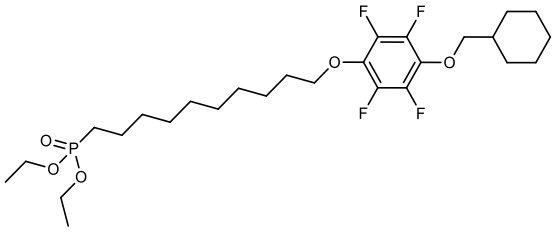

Potassium carbonate (1.49 g, 10.8 mmol, 3 eq) was added to **4.28** (1.00 g, 3.59 mmol, 1 eq) in acetonitrile (50.0 mL) and stirred at 85 °C for 1 h. Diethyl (10-bromodecyl)phosphonate (1.54 g, 4.31 mmol, 1.2 eq) was then added to the mixture over a 15 min period and the reaction was heated to 90 °C for 23 h. After completion, the mixture was cooled to r.t., diluted with H_2O (100 mL), and extracted with hexane (2x 50.0 mL), and then with H_2O (1 x 100 mL), dried over anhydrous magnesium sulphate, filtered, evaporated under vacuum, and purified by flash column chromatography (1—20% EtOAc in hexane) to yield the title compound (50%, 1.00 g, 1.81 mmol) as a clear oil.

IR ν_{max} (solid): 2927, 1500, 1467, 1033 cm^{-1}; ^1H NMR (400 MHz, $CDCl_3$) δ : 4.18 – 4.00 (m, 6H, POC$\underline{H}_2$ & Ar-OC$\underline{H}_2$-chain), 3.91 (d, *J* = 6.4 Hz, 2H, Ar-OC$\underline{H}_2$-ring), 1.79 – 1.64 (m, 9H, ring-*ortho*-C$\underline{H}_2$ & C$\underline{H}_2$CH$_2$P & Ar-OCH$_2$C$\underline{H}_2$ & ring-C$\underline{H}$), 1.64 – 1.51 (m, 2H, C$\underline{H}_2$P), 1.43 (app. td, *J* = 12.0, 10.1 Hz, 4H, ring-*meta*-C$\underline{H}_2$), 1.36 – 1.24 (m, 20H, remaining $\underline{H}$); $^{19}F\{^1H\}$ NMR (376 MHz, $CDCl_3$) δ : -158.5 (br s, 4F); ^{31}P NMR (202 MHz, $CDCl_3$) δ : 32.6; ^{13}C NMR (101 MHz, $CDCl_3$) δ : 143.2 (br d, $^2J_{CF}$ = 14.0 Hz, 4C, Ar-$\underline{C}$F), 140.8 (2C, Ar-$\underline{C}$OR), 81.1 (Ar-O$\underline{C}$H$_2$CH), 75.7 (Ar-O$\underline{C}$H$_2$CH$_2$), 61.5 (d, *J* = 6.5 Hz, 2C, PO$\underline{C}$H$_2$), 38.5 ($\underline{C}$H), 30.7 ($\underline{C}$H$_2$CH$_2$CH$_2$P), 30.0 (ring-*ortho*-$\underline{C}$H$_2$), 29.6 – 29.3 (4C, Ar-COCH$_2$CH$_2$CH$_2\underline{C}$H$_2\underline{C}$H$_2\underline{C}$H$_2\underline{C}$H$_2$), 29.2 (Ar-OCH$_2\underline{C}$H$_2$), 25.8 (br d, $^1J_{CP}$ = 142.3 Hz, 2C, $\underline{C}$H$_2$P & ring-*para*-$\underline{C}$H$_2$), 25.8 (2C, ring-*meta*-$\underline{C}$H$_2$), 25.7 (OCH$_2$CH$_2\underline{C}$H$_2$), 22.5 (br d, $^2J_{CP}$ = 5.2 Hz, $\underline{C}$H$_2$CH$_2$P), 16.6 (app. d, *J* = 6.0 Hz, 2C, POCH$_2$($\underline{C}$H$_3$)$_2$); HRMS (ESI$^+$) $C_{27}H_{43}F_4O_5P$ [M+Na] found 577.267, requires 577.268.

Diethyl (10-((All *cis*-4-(cyclohexylmethoxy)-2,3,5,6-tetrafluorocyclohexyl)oxy)decyl)phosphonate 4.30

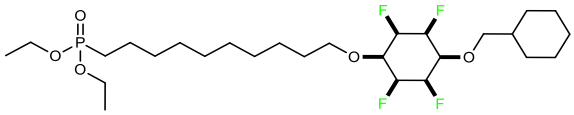

Following General Procedure **3**, **4.29** (900 mg, 1.62 mmol), Rh-CAAC-COD-Cl (19.0 mg, 0.032 mmol, 2 mol%), 4Å molecular sieves (8.00 g), silica (4.00 g), and hexane (40.0 mL) at 50 °C, for 2d and at 50 bar H_2 gave, a non-isolated title compound as a white powder.

HRMS (ESI$^+$) $C_{27}H_{49}F_4O_5P$ [M+H] found 561.333, requires 561.333.

(10-((All *cis*-4-(cyclohexylmethoxy)-2,3,5,6-tetrafluorocyclohexyl)oxy)decyl)phosphonic acid 4.31

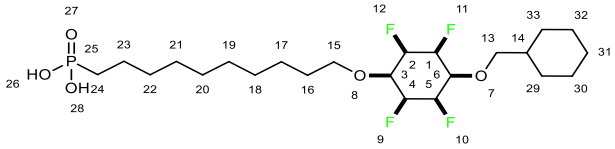

TMSBr (0.420 mL, 3.21 mmol, 3 eq) was added to a solution of **4.30** (600 mg, 1.07 mmol) in DCM (100 mL) and left to stir under nitrogen for 24 h. The reaction was then concentrated via vacuo. The compound was then suspended in Na_2CO_3 and extracted (1x) with diethyl ether. The aqueous layer was then acidified to pH 3 with HCl (1M solution). The resulting mixture was then extracted with ethyl acetate (3x 50.0 mL). The organic layer was then washed with brine (2x 50.0 mL) dried over magnesium sulphate, filtered, and concentrated under reduced pressure to afford crude product. The crude was purified by reverse phase flash column chromatography (0—100% acetonitrile in water) to yield the title compound (24%, 130 mg, 0.260 mmol) as a white powder. m.p. 162—163 °C.

IR ν_{max} (solid): 2920, 2851, 1466, 1119, 1083 cm^{-1}; ^{1}H NMR (500 MHz, DMSO-d_6) δ : 5.26 – 4.45 (m, 4H, C1,2,4,5-C<u>H</u>F), 3.96 – 3.66 (m, 2H, C3&C6-C<u>H</u>O), 3.53 (t, *J* = 6.6 Hz, 2H, C15-C<u>H</u>$_2$), 3.35 (d, *J* = 6.6 Hz, 2H, C13-C<u>H</u>$_2$), 1.81 – 1.75 (m, 2H, C24-PC<u>H</u>$_2$), 1.45 (app. d, *J* = 9.4 Hz, 5H, C16,C23,C28), 1.36 – 0.74 (m, 22H, remaining-<u>H</u>); ^{19}F{^{1}H} NMR (377 MHz, DMSO-d_6) δ : -205.3 – -207.3 (m, 2F$_{eq}$), -214.1 – -215.6 (m, 2F$_{ax}$); ^{31}P NMR (162

MHz, DMSO-d_6) δ : 26.0; ^{13}C NMR (101 MHz, $CDCl_3$) attained from HSQC with multiplicity editing δ : 89.2—87.0 (C1,C2,C4,C5), 77.0 (C3,C6), 74.6 (C13), 69.7 (C15), 38.4 (C14), 29.9 (C22), 29.6 (C29,C33), 29.5 (C18,C19,C20,C21), 29.3 (C16), 27.9 (C24), 26.0 (C17,C30,C32), 25.8 (C31), 23.3 (C23); HRMS (ESI^+) $C_{23}H_{42}F_4O_5P$ [M+H] found 505.270, requires 505.270.

7.24 Experimental for Chapter 5

General procedure 4 Synthesis methods and product characterization

General procedure **4.1** with pentafluoro anisole procedure

Stock solutions

MeOH	0.101 mL in 10 mL dry THF using 1 mL for reaction
*iso*propanol	0.1912 mL in 10 mL dry THF using 1 mL for reaction
^{t}-BuOH	185 mg in 10 mL dry THF using 1 mL for reaction
Pentafluoroanisole	0.99 g in 20 mL of dry THF using 2 mL for reaction

Stock solutions of alcohol and aromatic substrate were made using THF. To a stirred solution of MeOH/*iso*propanol/*tert*-BuOH (0.25 mmol, 0.5 eq) in dry THF (1 mL) in a flame-dried 25 mL round bottom flask, was added NaH (60% in paraffin oil, 15 mg, 0.375 mmol, 0.75 eq) portion wise under N_2. The resulting mixture was stirred for 20 min at r.t.. Then pentafluoroanisole (99 mg, 0.5 mmol, 1 eq) in dry THF (2 mL) was added all at once and the reaction was heated to 50 °C and monitored by NMR every 30 min.

General procedure **4.2** with pentafluoro-*iso*propoxybenzene

Stock solutions

MeOH	0.101 mL in 10 mL dry THF using 0.5 mL for reaction
*iso*propanol	0.1912 mL in 10 mL dry THF using 0.5 mL for reaction
^{t}-BuOH	185 mg in 10 mL dry THF using 0.5 mL for reaction
Pentafluoro-*iso*propoxybenzene	565.4 mg in 20 mL of dry THF using 2 mL for reaction

Stock solutions of alcohol and aromatic substrate were made using THF. To a stirred solution of MeOH/*iso*propanol/ *tert*-BuOH (0.125 mmol, 0.5 eq) in dry THF (0.5 mL) in a flame-dried 25 mL round bottom flask, was added NaH (60% in paraffin oil, 7.5 mg, 0.1875 mmol, 0.75 eq) portion wise under N_2. The resulting mixture was stirred for 20 min at r.t.. Then 1,2,3,4,5-pentafluoro-6-isopropoxybenzene (56.5 mg, 0.25 mmol, 1 eq) in dry THF (2 mL) was added all at once and the reaction was heated to 50 °C and monitored by NMR ever 30 min.

General procedure **4.3** with (*tert*-butoxy)-pentafluorobenzene

Stock solutions

MeOH	0.10 mL in 10 mL dry THF using 1 mL for reaction
*iso*propanol	0.1912 mL in 10 mL dry THF using 1 mL for reaction
^{t}-BuOH	185 mg in 10 mL dry THF using 1 mL for reaction
(*Tert*-butoxy)-pentafluorobenzene	1.20 g in 20 mL of dry THF using 2 mL for reaction

Stock solutions of alcohol and aromatic substrate were made using THF. To a stirred solution of MeOH / *iso*propanol / *tert*-BuOH (0.25 mmol, 0.5 eq) in dry THF (1 mL) in a flame-dried 25 mL round bottom flask, was added NaH (60% in paraffin oil, 15 mg, 0.375 mmol, 0.75 eq) portion wise under N_2. The resulting mixture was stirred for 20 min at r.t.. Then 1-(*tert*-butoxy)-2,3,4,5,6-pentafluorobenzene (120 mg, 0.5 mmol, 1 eq) in dry THF (2 mL) was added all at once and the reaction was heated to 50 °C and monitored by NMR every 30 min.

General procedure 5 S_NAr Scope experiments

A mixture of potassium hydroxide (2.5 eq) in appropriate alcohol (1.3 eq) was heated to 65°C and left stirring for 20 min. 1-(*tert*-butoxy)-2,3,4,5,6-pentafluorobenzene (1 eq) was added in lots over 20 min to this mixture with constant stirring. After the addition, the temperature of the reaction was heated to reflux 75-90 °C for 20-24 h. After completion the reaction was quenched by addition of water (50 mL). The hexanol was removed under vacuum. The aqueous layer was extracted with DCM (4 x 25 mL) and HCl (37%, 10 mL). The organic phase was dried over magnesium sulphate and the solvent was removed under reduced pressure then purified via flash column chromatography to obtain the title compound as a clear oil.

Table 5.1: Substrate (1.0 eq), nucleophile (0.5 eq), NaH (0.75 eq), THF (3 mL), 2.5 h, 50 °C

Substrate	Nucleophile	*para*/*meta* ratio at 2.5 hours	standard deviation	average	rounded average
C_6H_5-OMe	MeOH	1.752411576	0.01733632	1.755436621	1.8/1[a]
		1.774086379			
		1.73981191			
C_6H_5-OMe	IPA	1.98181818	0.17643587	1.83772623	1.8/1[a]
		1.89041096			
		1.64094955			
C_6H_5-OMe	^{tert}BuOH	2.11111	0.0711598	2.088461177	2.1/1[a]
		2.00873362			
		2.14553991			
C_6H_5-O*i*Pr	MeOH	1.77292576	0.033878406	1.756870053	1.8/1
		1.71794872			
		1.77973568			
C_6H_5-O*i*Pr	IPA	1.70940171	0.021548548	1.73428383	1.7/1
		1.74672489			
		1.74672489			
C_6H_5-O*i*Pr	^{tert}BuOH	2.25280899	0.398014503	2.408739857	2.4/1
		2.86111111			
		2.11229947			
C_6H_5-O*t*Bu	MeOH	3.67592593	0.12124999	3.677816017	3.7/1
		3.55752212			
		3.8			
C_6H_5-O*t*Bu	IPA	4.25	0.09989666	4.302388583	4.3/1
		4.41758242			
		4.23958333			
C_6H_5-O*t*Bu	^{tert}BuOH	7.40740741	0.29494267	7.066836947	7.1/1
		6.89655171			
		6.89655172			

[a] (*ortho* + *para*) : *meta* ratio. Maximum conversion of 50%.

1,2,3,4,5-Pentafluoro-6-isopropoxybenzene 5.22

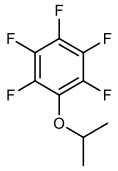

Sodium isopropoxide (1.00 g, 12.2 mmol) was added to a stirred solution of hexafluorobenzene (2.89 mL, 25.0 mmol) in THF (50.0 mL) at 0 °C. TLC of the resulting orange solution showed a single spot (1 h stirring). Further sodium isopropoxide (1.00 g, 12.2 mmol) was added and the mixture was stirred at 0 °C for 2 h. The product was isolated via removal of THF followed by a workup using H_2O (100 mL) and DCM (3x 100 mL). The compound was then purified by column chromatography (hexane) resulting to yield the title compound (11%, 601 mg, 2.66 mmol) as a clear yellow oil. With spectroscopic data in accordance with the literature.[217]

IR ν_{max} (solid): 2924, 1517, 1377, 1101, 1082 cm^{-1}; ^1H NMR (500 MHz, $CDCl_3$) δ : 4.49 – 4.39 (m, 1H, C<u>H</u>), 1.36 (d, *J* = 6.2 Hz, 6H, C<u>H</u>$_3$); $^{19}F\{^1H\}$ NMR (470 MHz, $CDCl_3$) δ : -155.8 – -156.0 (m, 2F, *ortho*-C<u>F</u>), -163.5 – -163.7 (m, *para*-C<u>F</u>), -163.7 – -163.9 (m, 2F, *meta*-C<u>F</u>); ^{13}C NMR (126 MHz, $CDCl_3$) δ : 142.6 (br dt, $^1J_{CF}$ = 250.0 Hz, $^2J_{CF}$ = 13.3 Hz, 2C, *meta*-<u>C</u>F), 138.5 (br s, *para*-<u>C</u>F), 139.5 – 137.0 (m, 2C, *ortho*-<u>C</u>F), 136.5 (Ar-<u>C</u>O), 78.8 (<u>C</u>H), 22.8 (2C, <u>C</u>H_3); HRMS (EI) $C_9H_7F_5O$ [M] found 226.041, requires 226.041.

1-(*Tert*-butoxy)-2,3,5,6-tetrafluoro-4-isopropoxybenzene 5.23_p

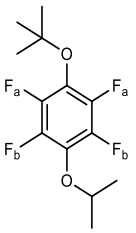

Stock solutions of alcohol and aromatic substrate were made using THF following general procedure **4.3**. To a stirred solution of isopropanol (15.0 mg, 0.019 mL, 0.250 mmol, 0.5 eq) in dry THF (1.00 mL) in a flame-dried 25 mL round bottom flask, was added NaH (60% in paraffin oil, 15.0 mg, 0.380 mmol, 0.75 eq) portion wise under N_2. The resulting mixture was stirred for 20 min at r.t.. Then 1-(*tert*-butoxy)-2,3,4,5,6-pentafluorobenzene (120 mg, 0.500 mmol, 1 eq) in dry THF (2.00 mL) was added all at

once and the reaction was heated to 50 °C and monitored by NMR. The *meta* and *para* ratios were taken every 30 min and the reaction was done two times, these ten ^{19}F NMR spectra were then averaged to obtain the averaged ratio of *para* and *meta* product. (*para* : *meta* = 4.3 ± 0.10 : 1).

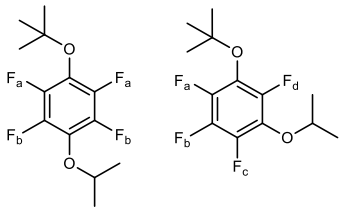

$^{19}F\{^{1}H\}$ NMR (377 MHz, $CDCl_3$) δ ***PARA* product**: -153.1 (dt, *J* = 22.0, 5.4 Hz, 2F, F_b), -157.8 (dt, *J* = 22.7, 5.2 Hz, 2F, F_a); $^{19}F\{^{1}H\}$ NMR (377 MHz, $CDCl_3$) δ ***META* product**: -144.2 (d, *J* = 5.6 Hz, F_d), -152.3 (dd, *J* = 22.4, 8.5 Hz, F_a), -155.6 (dd, *J* = 22.5, 8.2 Hz, F_c), -165.5 (tt, *J* = 22.8, 6.9 Hz, F_b).

1,2,4,5-Tetrafluoro-3,6-dimethoxybenzene 5.24_p

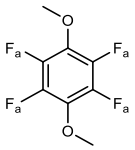

Stock solutions of alcohol and aromatic substrate were made using THF following general procedure **4.1**. To a stirred solution of MeOH (8.00 mg, 0.010 mL, 0.250 mmol, 0.5 eq) in dry THF (1.00 mL) in a flame-dried 25 mL round bottom flask, was added NaH (60% in paraffin oil, 15.0 mg, 0.380 mmol, 0.75 eq) portion wise under N_2. The resulting mixture was stirred for 20 min at r.t.. Then pentafluoroanisole (99.0 mg, 0.500 mmol, 1 eq) in dry THF (2.00 mL) was added all at once and the reaction was heated to 50 °C and monitored by NMR. The *ortho, meta,* and *para* ratios were taken every 30 min and the reaction was done two times, these ten ^{19}F NMR spectra were then averaged to obtain the averaged ratio of *para*, *meta* and *ortho* product. (*ortho* : *para* : *meta* = 0.55 : 1.27 : 1).

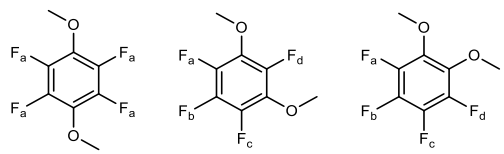

$^{19}F\{^{1}H\}$ NMR (470 MHz, $CDCl_3$) δ ***PARA* product**: -159.1 (app. d, *J* = 3.0 Hz, 4F, F_a); $^{19}F\{^{1}H\}$ NMR (470 MHz, $CDCl_3$) δ ***META* product**: -152.5 (d, J = 5.6 Hz, F_d, *iso* C<u>F</u>), -159.0 – -159.1

(m, 2F, C<u>F</u> OMe), -165.0 (app. q, *J* = 21.5 Hz, C<u>F</u>); $^{19}F\{^{1}H\}$ NMR (470 MHz, $CDCl_3$) δ ***<u>ORTHO</u>*** **<u>product</u>**: -158.8 – -158.8 (m, 2F, C<u>F</u> OMe), -164.7 (app d, *J* = 15.7, 9.0 Hz, 2F, C<u>F</u>).

1,2,4,5-Tetrafluoro-3-isopropoxy-6-methoxybenzene 5.25_p

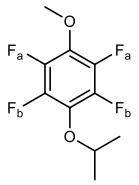

Stock solutions of alcohol and aromatic substrate were made using THF following general procedure **4.2**. To a stirred solution of isopropanol (7.52 mg, 0.130 mmol, 0.5 eq) in dry THF (0.500 mL) in a flame-dried 25 mL round bottom flask, was added NaH (60% in paraffin oil, 7.50 mg, 0.190 mmol, 0.75 eq) portion wise under N_2. The resulting mixture was stirred for 20 min at r.t.. Then pentafluoroanisole (99.0 mg, 0.500 mmol, 1 eq) in dry THF (2.00 mL) was added all at once and the reaction was heated to 50 °C and monitored by NMR. The *ortho, meta,* and *para* ratios were taken every 30 min and the reaction was done two times, these ten ^{19}F NMR spectra were then averaged to obtain the averaged ratio of *para*, *meta* and *ortho* product. (*ortho* : *para* : *meta* = 0.49 : 1.34 : 1).

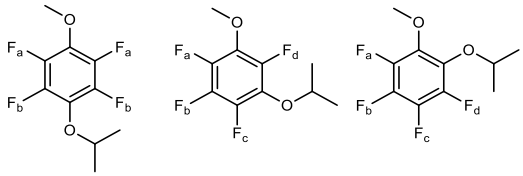

$^{19}F\{^{1}H\}$ NMR (470 MHz, $CDCl_3$) δ ***<u>PARA</u>*** **<u>product</u>**: -157.3 (dd, *J* = 21.8, 5.7 Hz, 2F, F_b, C<u>F</u> O^{i}-Pr), -159.3 (dd, *J* = 21.7, 5.8 Hz, 2F, F_a, C<u>F</u> OMe); $^{19}F\{^{1}H\}$ NMR (470 MHz, $CDCl_3$) δ ***<u>META</u>*** **<u>product</u>**: -150.7 (d, J = 5.8 Hz, F_d), -157.2 (dd, *J* = 22.1, 2.1 Hz, F_c, C<u>F</u> O^{i}-Pr), -158.7 (dd, *J* = 21.8, 1.9 Hz, F_a, C<u>F</u> OMe), -165.1 (td, *J* = 21.9, 5.8 Hz, F_b). $^{19}F\{^{1}H\}$ NMR (470 MHz, $CDCl_3$) δ ***<u>ORTHO</u>*** **<u>product</u>**: -156.0 (d, *J* = 21.4 Hz, F_d), - 159.0 (app. d, *J* = 13.5 Hz, F_a), -164.6 (td, *J* = 21.4, 2.4 Hz, F_c), -164.9 (td, *J* = 21.9, 2.8 Hz, F_b).

1-(*Tert*-butoxy)-2,3,5,6-tetrafluoro-4-methoxybenzene 5.26_p

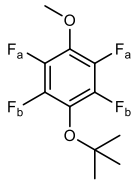

Stock solutions of alcohol and aromatic substrate were made using THF following general procedure **4.1**. To a stirred solution of *tert*-BuOH (9.25 mg, 0.130 mmol, 0.5 eq) in dry THF (1.00 mL) in a flame-dried 25 mL round bottom flask, was added NaH (60% in paraffin oil, 15.0 mg, 0.380 mmol, 0.75 eq) portion wise under N_2. The resulting mixture was stirred for 20 min at r.t.. Then pentafluoroanisole (99.0 mg, 0.500 mmol, 1 eq) in dry THF (2.00 mL) was added all at once and the reaction was heated to 50 °C and monitored by NMR. The *ortho, meta,* and *para* ratios were taken every 30 min and the reaction was done two times, these ten ^{19}F NMR spectra were then averaged to obtain the averaged ratio of *para*, *meta* and *ortho* product. (*ortho* : *para* : *meta* = 0.28 : 1.81 : 1).

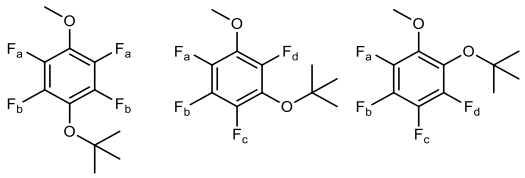

$^{19}F\{^1H\}$ NMR (470 MHz, $CDCl_3$) δ ***PARA* product**: -152.8 (dd, *J* = 21.9, 5.7 Hz, 2F, C<u>F</u> O^t-Bu), -159.5 (dd, *J* = 22.2, 6.2 Hz, 2F, C<u>F</u> OMe); $^{19}F\{^1H\}$ NMR (470 MHz, $CDCl_3$) δ ***META* product**: -146.1 (d, *J* = 5.8 Hz, *iso* C<u>F</u>), -152.6 (app. d, *J* = 22.5 Hz, C<u>F</u> O^t-Bu), -157.4 (app. d, *J* = 21.8 Hz, C<u>F</u> OMe), -165.2 (td, *J* = 22.3, 6.0 Hz, C<u>F</u>); $^{19}F\{^1H\}$ NMR (470 MHz, $CDCl_3$) δ ***ORTHO* product**: -152.2 (dt, *J* = 23.3, 5.4, 2.2 Hz, C<u>F</u> O^t-Bu), -158.9 (ddd, *J* = 21.8, 5.6, 3.0 Hz, C<u>F</u> OMe), -163.4 (app. d, *J* = 22.6 Hz, C<u>F</u> O^t-Bu), -165.0 (td, *J* = 22.3, 3.1 Hz, C<u>F</u> OMe); HRMS (EI) $C_{11}H_{12}F_4O_2$ [M] found 252.076, requires 252.077.

1,2,4,5-Tetrafluoro-3-isopropoxy-6-methoxybenzene 5.27_p

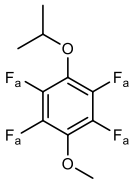

Stock solutions of alcohol and aromatic substrate were made using THF following general procedure **4.2**. To a stirred solution of MeOH (4.00 mg, 0.130 mmol, 0.5 eq) in dry THF (0.500 mL) in a flame-dried 25 mL round bottom flask, was added NaH (60% in paraffin oil, 7.50 mg, 0.190 mmol, 0.75 eq) portion wise under N_2. The resulting mixture was stirred for 20 min at r.t.. Then 1,2,3,4,5-pentafluoro-6-isopropoxybenzene (56.5 mg, 0.250 mmol, 1 eq) in dry THF (2.00 mL) was added all at once and the reaction was heated to 50 °C and monitored by NMR. The *meta* and *para* ratios were taken every 30 min and the reaction was done two times, these ten ^{19}F NMR spectra were then averaged to obtain the averaged ratio of *para* and *meta* product. (*para* : *meta* = 1.8 ± 0.034 : 1).

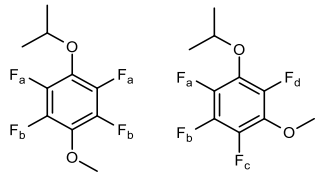

$^{19}F\{^1H\}$ NMR (470 MHz, $CDCl_3$) δ ***PARA* product**: -157.3 (dd, *J* = 21.8, 5.7 Hz, 2F, F_a, C<u>F</u> O^i-Pr), -159.3 (dd, *J* = 21.7, 5.8 Hz, 2F, F_b, C<u>F</u> OMe); $^{19}F\{^1H\}$ NMR (470 MHz, $CDCl_3$) δ ***META* product**: -150.7 (d, J = 5.8 Hz, F_d, *iso* C<u>F</u>), -157.2 (dd, *J* = 22.1, 2.1 Hz, F_c, C<u>F</u> O^i-Pr), -158.7 (dd, *J* = 21.8, 1.9 Hz, F_a, C<u>F</u> OMe), -165.1 (td, *J* = 21.9, 5.8 Hz, F_b, C<u>F</u>).

1,2,4,5-Tetrafluoro-3,6-diisopropoxybenzene 5.28_p

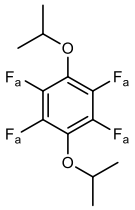

Stock solutions of alcohol and aromatic substrate were made using THF following general procedure **4.2**. To a stirred solution of isopropanol (7.52 mg, 0.125 mmol, 0.5 eq) in dry THF (0.500 mL) in a flame-dried 25 mL round bottom flask, was added NaH (60% in paraffin oil, 7.50 mg, 0.188 mmol, 0.75 eq) portion wise under N_2. The resulting

mixture was stirred for 20 min at r.t.. Then 1,2,3,4,5-pentafluoro-6-isopropoxybenzene (56.5 mg, 0.250 mmol, 1 eq) in dry THF (2.00 mL) was added all at once and the reaction was heated to 50 °C and monitored by NMR. The *meta* and *para* ratios were taken every 30 min and the reaction was done two times, these ten ^{19}F NMR spectra were then averaged to obtain the averaged ratio of *para* and *meta* product. (*para* : *meta* = 1.7 ± 0.022 : 1).

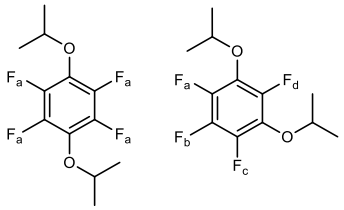

$^{19}F\{^{1}H\}$ NMR (470 MHz, $CDCl_3$) δ ***PARA* product**: -157.7 (d, *J* = 15.4 Hz, 4F, F_a); $^{19}F\{^{1}H\}$ NMR (470 MHz, $CDCl_3$) δ ***META* product**: -148.9 (d, *J* = 10.1 Hz, F_d), -157.2 (app. d, *J* = 24.3 Hz, 2F, F_{ac}), -165.6 (apparent s, F_b).

1-(*Tert*-butoxy)-2,3,5,6-tetrafluoro-4-isopropoxybenzene 5.29_p

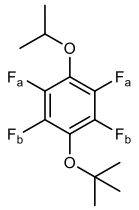

Stock solutions of alcohol and aromatic substrate were made using THF following general procedure **4.2**. To a stirred solution of *tert*-BuOH (9.25 mg, 0.125 mmol, 0.5 eq) in dry THF (0.500 mL) in a flame-dried 25 mL round bottom flask, was added NaH (60% in paraffin oil, 7.50 mg, 0.188 mmol, 0.75 eq) portion wise under N_2. The resulting mixture was stirred for 20 min at r.t.. Then 1,2,3,4,5-pentafluoro-6-isopropoxybenzene (56.5 mg, 0.250 mmol, 1 eq) in dry THF (2.00 mL) was added all at once and the reaction was heated to 50 °C and monitored by NMR. The *meta* and *para* ratios were taken every 30 min and the reaction was done two times, these ten ^{19}F NMR spectra were then averaged to obtain the averaged ratio of *para* and *meta* product. (*para* : *meta* = 2.4 ± 0.40 : 1).

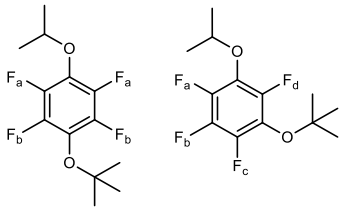

$^{19}F\{^{1}H\}$ NMR (377 MHz, $CDCl_3$) δ ***PARA* product**: -153.1 (dt, *J* = 22.0, 5.4 Hz, 2F, F_b), -157.8 (dt, *J* = 22.7, 5.2 Hz, 2F, F_a); $^{19}F\{^{1}H\}$ NMR (377 MHz, $CDCl_3$) δ ***META* product**: -144.2 (d, *J* = 5.6 Hz, F_d), -152.3 (dd, *J* = 22.4, 8.5 Hz, F_c), -155.6 (dd, *J* = 22.5, 8.2 Hz, F_a), -165.5 (tt, *J* = 22.8, 6.9 Hz, F_b).

1-(*Tert*-butoxy)-2,3,5,6-tetrafluoro-4-methoxybenzene 5.30_p

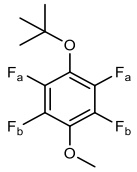

Stock solutions of alcohol and aromatic substrate were made using THF following general procedure **4.3**. To a stirred solution of MeOH (8.01 mg, 0.010 mL, 0.250 mmol, 0.5 eq) in dry THF (1.00 mL) in a flame-dried 25 mL round bottom flask, was added NaH (60% in paraffin oil, 15.0 mg, 0.375 mmol, 0.75 eq) portion wise under N_2. The resulting mixture was stirred for 20 min at r.t.. Then 1-(*tert*-butoxy)-2,3,4,5,6-pentafluorobenzene (120 mg, 0.500 mmol, 1 eq) in dry THF (2.00 mL) was added all at once and the reaction was heated to 50 °C and monitored by NMR. The *meta* and *para* ratios were taken every 30 min and the reaction was done two times, these ten ^{19}F NMR spectra were then averaged to obtain the averaged ratio of *para* and *meta* product. (*para* : *meta* = 3.7 ± 0.12 : 1).

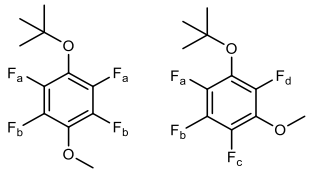

$^{19}F\{^{1}H\}$ NMR (470 MHz, $CDCl_3$) δ ***PARA* product**: -152.8 (dd, *J* = 21.9, 5.7 Hz, 2F, F_a), -159.5 (dd, *J* = 22.2, 6.2 Hz, 2F, F_b); $^{19}F\{^{1}H\}$ NMR (470 MHz, $CDCl_3$) δ ***META* product**: -146.1 (d, *J* = 5.8 Hz, F_d), -152.6 (app. d, *J* = 22.5 Hz, F_a), -157.4 (app. d, *J* = 21.8 Hz, F_c), -165.2 (td, *J* = 22.3, 6.0 Hz, F_b).

1,4-Di-*tert*-butoxy-2,3,5,6-tetrafluorobenzene 5.31_p

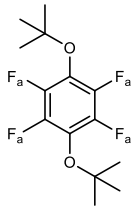

Stock solutions of alcohol and aromatic substrate were made using THF following general procedure **4.3**. To a stirred solution of *tert*-BuOH (18.5 mg, 0.250 mmol, 0.5 eq) in dry THF (1.00 mL) in a flame-dried 25 mL round bottom flask, was added NaH (60% in paraffin oil, 15.0 mg, 0.375 mmol, 0.75 eq) portion wise under N_2. The resulting mixture was stirred for 20 min at r.t.. Then 1-(*tert*-butoxy)-2,3,4,5,6-pentafluorobenzene (120 mg, 0.500 mmol, 1 eq) in dry THF (2.00 mL) was added all at once and the reaction was heated to 50 °C and monitored by NMR. The *meta* and *para* ratios were taken every 30 min and the reaction was done two times, these ten ^{19}F NMR spectra were then averaged to obtain the averaged ratio of *para* and *meta* product. (*para* : *meta* = 7.1 ± 0.29 : 1).

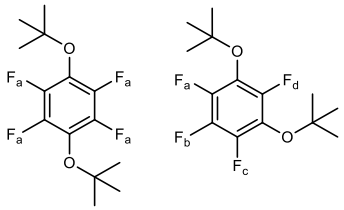

$^{19}F\{^1H\}$ NMR (470 MHz, $CDCl_3$) δ ***PARA* product**: -153.4 (F_a); $^{19}F\{^1H\}$ NMR (470 MHz, $CDCl_3$) δ ***META* product**: -139.8 (d, *J* = 5.8 Hz, F_d), -151.2 (d, *J* = 22.8 Hz, F_{ac}), -165.7 (td, *J* = 22.7, 5.8 Hz, F_b).

1-(*Tert*-butoxy)-2,3,5,6-tetrafluoro-4-methoxybenzene 5.41

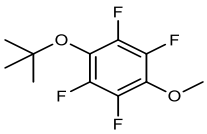

Following General Procedure **5** potassium hydroxide (584 mg, 10.4 mmol), methanol (0.900 mL, 5.46 mmol), and 1-(*tert*-butoxy)-2,3,4,5,6-pentafluorobenzene (0.700 mL, 1.00 g, 4.16 mmol) for 22 h, 90 °C gave, after purification by flash silica chromatography (hexane) title compound (36%, 374 mg, 1.48 mmol) was isolated as clear oil (including 9% *meta* product). Crude *(ortho* + *para*) : *meta* ratio = (0.55 + 1.33) : 1.

IR νmax (solid): 2981, 1496, 1047 cm^{-1}; ^{1}H NMR (500 MHz, $CDCl_3$) δ : 4.03 (d, *J* = 1.1 Hz, 3H, CH_3), 1.38 (t, *J* = 1.2 Hz, 9H, *t*-butyl); $^{19}F\{^{1}H\}$ NMR (470 MHz, $CDCl_3$) δ : -147.2 – -156.5 (m, 2F, Ar-F-O^{t}butyl), -155.0 – -163.9 (m, 2F, Ar-F-OCH_3); ^{13}C NMR (126 MHz, $CDCl_3$) δ : 145.3 – 142.8 (m, 2C, Ar-CF-OCH_3), 142.8 – 140.2 (m, 2C, Ar-CF-O^{t}butyl), 129.1 (app t, $^{2}J_{CF}$ = 13.7 Hz, 2C, Ar-COR), 84.5 (C), 62.5 (OCH_3), 28.4 (3C, CH_3); MS (EI) $C_{11}H_{12}F_4O_2$ [M] found 252.07, requires 252.07.

1-(*Tert*-butoxy)-2,3,5,6-tetrafluoro-4-isopropoxybenzene 5.42

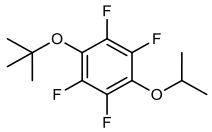

Following General Procedure **5** potassium hydroxide (584 mg, 10.4 mmol), isopropyl alcohol (0.420 mL, 5.46 mmol), and 1-(*tert*-butoxy)-2,3,4,5,6-pentafluorobenzene (0.700 mL, 1.00 g, 4.16 mmol) for 24 h, 90 °C gave, after purification by flash silica chromatography (hexane) title compound (23%, 271 mg, 0.970 mmol) was isolated as clear oil (including 19% *meta* product). Crude *para* : *meta* ratio = 3.50 : 1.

IR νmax (solid): 2981, 1490, 1039, 1012 cm^{-1}; ^{1}H NMR (500 MHz, $CDCl_3$) δ : 4.45 (hept, *J* = 6.2 Hz, 1H, OCH$(CH_3)_2$), 1.38 (s, 9H, ^{t}Bu), 1.35 (d, *J* = 6.1 Hz, 6H, ^{i}Pr); $^{19}F\{^{1}H\}$ NMR (470 MHz, $CDCl_3$) δ : -153.09 (br dt, *J* = 22.4, 5.7 Hz, 2F, Ar-F O^{t}Bu), -157.76 (br dt, *J* = 22.1, 5.6 Hz, Ar-F O^{i}Pr); ^{13}C NMR (126 MHz, $CDCl_3$) δ : 143.8 (br ddt, $^{1}J_{CF}$ = 246.0 Hz, $^{2}J_{CF}$ = 12.2 Hz, $^{3}J_{CF}$ = 4.7 Hz, 2C, Ar-CF O^{t}Bu), 142.5 (br ddt, $^{1}J_{CF}$ = 246.0 Hz, $^{2}J_{CF}$ = 13.6, $^{3}J_{CF}$ = 5.0 Hz, Ar-CF O^{i}Pr), 132.4 (Br t, $^{2}J_{CF}$ = 13.2 Hz, Ar-CO^{t}Bu), 129.2 (br t, $^{2}J_{CF}$ = 14.0 Hz, Ar-CO^{i}Pr), 84.5 (OC$(CH_3)_3$), 78.4 (OCH$(CH_3)_2$), 28.4 (3C, CH_3), 22.5 (2C, CH_3); HRMS (ESI^{+}) $C_{13}H_{16}F_4O_2$ [M+Na] found 303.098, requires 303.098.

4-((4-(*Tert*-butoxy)-2,3,5,6-tetrafluorophenoxy)methyl)-4'-propyl-1,1'-bi(cyclohexane) 5.43

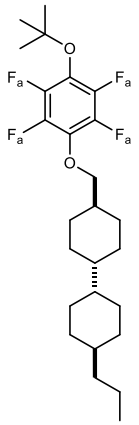

Following General Procedure **5** potassium hydroxide (584 mg, 10.4 mmol), alcohol (1.29 g, 5.41 mmol), THF (10.0 mL), and 1-(*tert*-butoxy)-2,3,4,5,6-pentafluorobenzene (0.700 mL, 1.00 g, 4.16 mmol) for 24 h, 75 °C gave, after purification by flash silica chromatography (0-5% EtOAc in hexane) title compound (52%, 988 mg, 2.15 mmol) was isolated as clear oil (including 14% *meta* product). Crude *para* : *meta* ratio = 4.38 : 1.

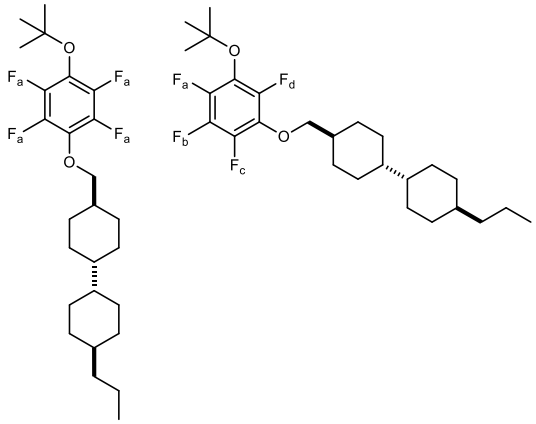

IR ν_{max} (solid): 2906, 1506, 1035 cm^{-1}; ^{1}H NMR (500 MHz, CDCl3) δ : 3.94 (d, *J* = 6.4 Hz, 2H, OCH_2), 1.96 – 1.89 (m, 2H, rings-C$\underline{H}_2$), 1.80 – 1.66 (m, 7H, rings-C$\underline{H}_2$, rings-C$\underline{H}_2$, rings-C$\underline{H}_2$, rings-HC-C$\underline{H}$), 1.38 (app. t, *J* = 1.2 Hz, 9H, ^{t}Bu), 1.29 (app. p, *J* = 7.2 Hz, 2H, C$\underline{H}_2CH_3$), 1.14 – 1.12 (m, 3H, rings-$\underline{H}$C-CH & C$\underline{H}_2CH_2CH_3$), 1.08 – 0.91 (m, 10H, rings-C$\underline{H}CH_2$, rings-C$\underline{H}CH_2$, rings-C$\underline{H}_2$, rings-C$\underline{H}_2$, rings-C$\underline{H}_2$, rings-C$\underline{H}_2$), 0.87 (t, *J* = 7.3 Hz, 3H, C$\underline{H}_3$); $^{19}F\{^{1}H\}$ NMR (470 MHz, $CDCl_3$) δ ***PARA* product**: -153.00 (dd, *J* = 22.3, 6.0 Hz, Ar-C$\underline{F}$ OC^{t}Bu), -158.84 (dd, *J* = 22.3, 6.0 Hz, Ar-C$\underline{F}$ OCH_2CH); $^{19}F\{^{1}H\}$ NMR (470 MHz, $CDCl_3$) δ ***META* product**: -145.40 (d, *J* = 5.8 Hz, F_d), -152.87 (dd, *J* = 22.9, 1.2 Hz, F_a), -156.61 (d, *J* = 21.5 Hz, F_c), -165.32 (td, *J* = 22.2, 5.8 Hz, F_b); ^{13}C NMR (126 MHz, $CDCl_3$) δ : 143.2 – 142.3 (m,

4C, Ar-CF), 136.8 – 136.2 (m, 2C, Ar-CO), 81.1 (OCH_2), 67.9 (OC^tBu), 43.5 (ring-$CHCH_2$), 43.4 (ring-$CHCH_2$), 40.0 ($CH_2CH_2CH_3$), 38.8 (rings-HC-CH), 37.8 (rings-HC-CH), 33.7 (2C, rings-CH_2), 30.4 – 29.1 (m, 6C, rings-CH_2), 28.4 (^tBu), 20.2 (CH_2CH_3), 14.5 (CH_3); HRMS (ESI^+) $C_{26}H_{38}F_4O_2$ [M+Na] found 481.271, requires 481.270.

1-(*Tert*-butoxy)-2,3,5,6-tetrafluoro-4-(hexyloxy)benzene 5.44

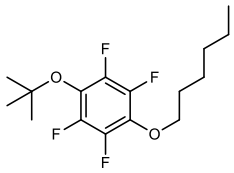

Following General Procedure **2** potassium hydroxide (1.40 g, 25.0 mmol), 1-hexanol (1.63 mL, 13.0 mmol), and 1-(*tert*-butoxy)-2,3,4,5,6-pentafluorobenzene (2.40 g, 10.0 mmol) for 22 h, 90 °C gave, after purification by flash silica chromatography (0-5% EtOAc in hexane) title compound (61%, 1.98 g, 6.14 mmol) was isolated as clear oil (including 12% *meta* product). Crude *para* : *meta* ratio = 4.52 : 1.

IR νmax (solid): 2933, 1494, 1174 cm^{-1}; ^1H NMR (500 MHz, $CDCl_3$) δ : 4.15 (t, *J* = 6.6 Hz, 2H, OCH_2), 1.76 (dq, *J* = 11.5, 5.8, 4.9 Hz, 2H, OCH_2CH_2), 1.40 – 1.30 (m, 15H, remaining H), 0.90 (t, *J* = 7.0 Hz, 3H, hexyl-CH_3); $^{19}F\{^1H\}$ NMR (470 MHz, $CDCl_3$) δ : -153.0 (dd, *J* = 22.1, 5.7 Hz, FO^tbu), -158.8 (dd, *J* = 22.6, 5.7 Hz $FOCH_2$); ^{13}C NMR (126 MHz, $CDCl_3$) δ : ^{13}C NMR (126 MHz, $CDCl_3$) δ : 145.4 – 140.2 (4C, m, Ar-CF), 133.8 (br s, 2C, Ar-CO), 84.5 (OC), 75.7 (OCH_2), 31.6 ($CH_2CH_2CH_3$), 30.0 ($CH_2CH_2CH_2CH_2CH_3$), 28.4 (3C, *t*-butyl group), 25.4 ($CH_2CH_2CH_2CH_3$), 22.7 (CH_2CH_3), 14.2 (CH_3); HRMS (ESI^+) $C_{16}H_{22}F_4O_2$ [M+Na] found 345.144, requires 345.145.

1-(*Tert*-butoxy)-4-(cyclohexyloxy)-2,3,5,6-tetrafluorobenzene 5.45

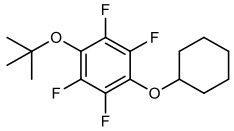

Following General Procedure **5** potassium hydroxide (584 mg, 10.4 mmol, 2.5 eq), cyclohexanol (0.570 mL, 5.46 mmol, 1.3 eq), and 1-(*tert*-butoxy)-2,3,4,5,6-pentafluorobenzene (0.700 mL, 1.00 g, 4.16 mmol, 1 eq) for 24 h, 90 °C gave, after

purification by flash silica chromatography (0-5% EtOAc in hexane) title compound (49%, 654 mg, 2.04 mmol) was isolated as clear oil (including 13% *meta* product). Crude *para* : *meta* ratio = 5.37 : 1.

IR vmax (solid): 2937, 1492, 1039 cm^{-1}; ^{1}H NMR (500 MHz, $CDCl_3$) δ : 4.14 (tt, *J* = 9.0, 4.0 Hz, 1H, ring-C<u>H</u>), 2.01 – 1.74 (m, 6H, *ortho*-C<u>H</u>$_2$ & *meta*-C<u>H</u>H), 1.66 – 1.48 (m, 4H, *meta*-CH<u>H</u> & *para*-C<u>H</u>$_2$), 1.38 (s, 9H, ^{t}Bu); $^{19}F\{^{1}H\}$ NMR (470 MHz, $CDCl_3$) δ : -153.15 (dd, *J* = 22.8, 5.7 Hz, 2F, Ar-<u>F</u> O^{t}Bu), -157.57 (dd, *J* = 22.6, 5.6 Hz, 2F, Ar-<u>F</u> OPh); ^{13}C NMR (126 MHz, $CDCl_3$) δ : 143.9 (ddt, $^{1}J_{CF}$ = 245.6 Hz, $^{2}J_{CF}$ = 12.2 Hz, $^{3}J_{CF}$ = 4.7 Hz, 2C, Ar-<u>C</u>F O^{t}Bu), 142.4 (br ddt, $^{1}J_{CF}$ = 246.0 Hz, $^{2}J_{CF}$ = 13.5 Hz, $^{3}J_{CF}$ = 5.0 Hz, 2C, Ar-<u>C</u>F Oring), 130.7 — 126.2 (m, 2C, Ar-<u>C</u>OR), 84.4 (O<u>C</u>(CH$_3$)$_3$), 83.3 (O<u>C</u>-ring), 32.3 (2C, ring-*ortho*-<u>C</u>H$_2$), 28.4 (3C, <u>C</u>H$_3$), 25.5 (ring-*para*-<u>C</u>H$_2$), 23.8 (2C, ring-*meta*-<u>C</u>H$_2$); HRMS (ESI^{+}) $C_{16}H_{20}F_4O_2$ [M+Na] found 343.130, requires 343.129.

1,4-Di-*tert*-butoxy-2,3,5,6-tetrafluorobenzene 5.46

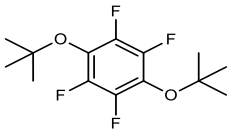

Following General Procedure **2** potassium hydroxide (832 mg, 14.8 mmol), *tert*-butanol (0.730 mL, 7.70 mmol), and 1-(*tert*-butoxy)-2,3,4,5,6-pentafluorobenzene (1.42 g, 5.93 mmol) for 22 h, 90 °C gave, after purification by flash silica chromatography (0-5% EtOAc in hexane) title compound (17%, 291 mg, 1.00 mmol) was isolated as clear oil (including 3% *meta* product). Crude *para* : *meta* ratio = 5.61 : 1. With spectroscopic data in accordance with the literature.[218]

IR ν_{max} (solid): 2940, 1496, 1032 cm^{-1}; ^{1}H NMR (400 MHz, $CDCl_3$) δ : 1.39 (s, 18H, C<u>H</u>$_3$); $^{19}F\{^{1}H\}$ NMR (376 MHz, $CDCl_3$) δ : -153.3 (4F); ^{13}C NMR (101 MHz, $CDCl_3$) δ : 142.6 (br s, 4C, <u>C</u>F), 99.6 (br s, 2C, <u>C</u>O), 72.6 (2C, O<u>C</u>(CH$_3$)$_3$), 28.5 (6C, <u>C</u>H$_3$); HRMS (EI) $C_{14}H_{18}F_4O_2$ [M] found 294.125, requires 294.124.

1-(*Tert*-butoxy)-2,3,5,6-tetrafluoro-4-phenoxybenzene 5.47

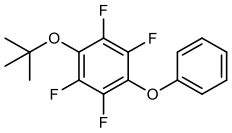

Following General Procedure **2** potassium hydroxide (292 mg, 5.20 mmol), phenol (0.240 mL, 2.71 mmol), and 1-(*tert*-butoxy)-2,3,4,5,6-pentafluorobenzene (0.350 mL, 500 mg, 2.08 mmol) for 24 h, 90 °C gave, after purification by flash silica chromatography (0-5% EtOAc in hexane) title compound (8%, 107 mg, 0.339 mmol) was isolated as clear oil (including 14% *meta* product). Crude *para* : *meta* ratio = 5.90 : 1.

IR vmax (solid): 2924, 1506, 1143 cm^{-1}; ^{1}H NMR (500 MHz, $CDCl_3$) δ : 7.33 (dd, *J* = 8.7, 7.3 Hz, 2H, *meta*-CH), 7.11 (td, *J* = 7.4, 1.1 Hz, 1H, *para*-CH), 6.97 (d, *J* = 8.2 Hz, 2H, *ortho*-CH), 1.43 (app. t, *J* = 1.2 Hz, 9H, ^{t}Bu); $^{19}F\{^{1}H\}$ NMR (470 MHz, $CDCl_3$) δ : -151.6 – -151.7 (m, 2F, CF O^{t}Bu), -156.1 – -156.2 (m, 2F, CF OPh); ^{13}C NMR (126 MHz, $CDCl_3$) δ : 157.5 (OCPh), 145.3 – 144.9 (2C, m, Ar-CF), 143.7 – 142.6 (m, 2C, Ar-CF), 141.5 – 140.9 (2C m, Ar-CO), 129.9 (2C, *meta*-CH), 123.7 (*para*-CH), 115.5 (2C, *ortho*-CH), 85.1 (C ^{t}Bu), 28.4 (3C, ^{t}Bu); HRMS (EI) $C_{16}H_{14}F_4O_2$ [M] found 314.093, requires 314.092.

4-(4-(*Tert*-butoxy)-2,3,5,6-tetrafluorophenoxy)-4'-propyl-1,1'-bi(cyclohexane) 5.48

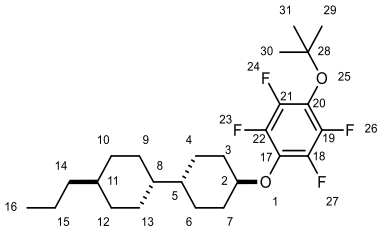

A mixture of potassium hydroxide (584 mg, 10.4 mmol), (1*r*,1'*s*,4*R*,4'*R*)-4'-propyl-[1,1'-bi(cyclohexan)]-4-ol (1.22 g, 5.41 mmol) in THF (10.0 mL) was heated to 65 °C and left stirring for 20 min. 1-(*tert*-butoxy)-2,3,4,5,6-pentafluorobenzene (0.700 mL, 1.00 g, 4.16 mmol) was added in lots over 20 min to this mixture with constant stirring. After the addition, the temperature of the reaction was heated to reflux ~90 °C for 24 h. After completion the reaction was quenched by addition of water (50.0 mL). The THF was removed under vacuum. The aqueous layer was extracted with DCM (4 x 25.0 mL) and HCl (37%, 10.0 mL). The organic phase was dried over magnesium sulphate and the solvent was removed under reduced pressure. The compound was then purified by

column chromatography (0-5% EtOAc in hexane) resulting to yield the title compounds as a white solid (64%, 735 mg, 1.65 mmol) (including 13% *meta* product), m.p. = 60—61 °C. Crude *para* : *meta* ratio = 6.10 : 1.

IR ν_{max} (solid): 2922, 1492, 1369, 1039, 979 cm^{-1}; ^{1}H NMR (500 MHz, $CDCl_3$) δ : 4.01 (tt, *J* = 10.6, 4.5 Hz, 1H, H2), 2.12 (dd, *J* = 13.2, 3.8 Hz, 2H, 1H3&H7), 1.88 – 1.63 (m, 8H, H10&H12, 1H4&H6&H9&H13), 1.55 – 1.43 (m, 2H, 1H3&H7), 1.38 (s, 9H, ^{t}Bu), 1.33 – 1.24 (m, 2H, H15), 1.13 (t, *J* = 6.0 Hz, 4H, H5&H8&H14), 1.09 – 0.91 (m, 5H, H11, 1H4&H6&H9&H13), 0.87 (t, *J* = 8.2 Hz, 3H, H16); $^{19}F\{^{1}H\}$ NMR (470 MHz, $CDCl_3$) δ : -153.1 (dd, *J* = 22.7, 5.9 Hz, Ar-CF OC^{t}Bu), -157.5 (dd, *J* = 22.7, 5.8 Hz, Ar-CF OCH); ^{13}C NMR (126 MHz, $CDCl_3$) δ : 145.3 – 143.3 (m, 4C, C18,C19,C21,C22), 143.3 – 141.0 (m, 2C, C17&C20), 84.5 (C2), 84.4 (C28), 42.6 (C11), 39.9 (2C, C5&C8), 37.7 (C14), 33.6 (2C, C10C&12), 32.7 (2C, C3&C7), 30.3 (2C, C9&C13), 28.4 (3C, ^{t}Bu), 28.0 (2C, C4&C6), 20.2 (C15), 14.6 (C16); HRMS (ESI^{+}) $C_{25}H_{36}F_4O_2$ [M+Na] found 467.254, requires 467.254.

1-(*Tert*-butoxy)-2,3,5,6-tetrafluoro-4-(((1*R*,2*S*,5*R*)-2-isopropyl-5-methylcyclohexyl)oxy)benzene 5.49

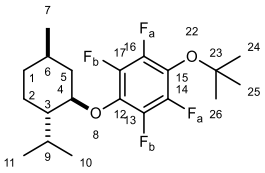

Following General Procedure **5** potassium hydroxide (584 mg, 10.4 mmol), L-menthol (1.63 g, 10.4 mmol, 2.5 eq), THF (10.0 mL), and 1-(*tert*-butoxy)-2,3,4,5,6-pentafluorobenzene (1.00 g, 4.16 mmol) for 24 h, 75 °C gave, after purification by flash silica chromatography (0-5% EtOAc in hexane) title compound (38%, 589 mg, 1.56 mmol) was isolated as clear oil (including 8% *meta* product). Crude *para* : *meta* ratio = 7.32 : 1.

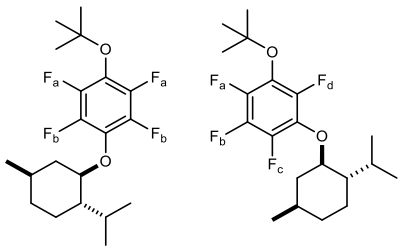

IR νmax (solid): 2895, 1467, 1342, 1093 cm^{-1}; ^{1}H NMR (400 MHz, CDCl3) δ : 4.04 (td, *J* = 10.6, 4.4 Hz, 1H, H4), 2.40 (pd, *J* = 7.0, 2.6 Hz, 1H, H9), 1.88 (app. d, *J* = 11.9 Hz, 1H, H5), 1.77 – 1.63 (m, 2H, H2), 1.54 (ddt, *J* = 13.0, 10.2, 3.2 Hz, 1H, H6), 1.44 – 1.24 (m, 11H, H1,H24,H25,H26), 1.19 – 0.99 (m, 2H, H5), 0.97 (d, *J* = 7.0 Hz, 3H, H10 or H11), 0.90 (d, *J* = 6.5 Hz, 3H, H11 or H10), 0.87 (d, *J* = 6.9 Hz, 3H, H7); $^{19}F\{^{1}H\}$ NMR (377 MHz, $CDCl_3$) δ **Major *Para* Product**: -153.1 (dd, *J* = 22.6, 6.2 Hz, 2F, F_a), -157.2 (dd, *J* = 22.2, 6.3 Hz, 2F, F_b); $^{19}F\{^{1}H\}$ NMR (377 MHz, $CDCl_3$) δ ***Meta* product** (8%): -143.71 (d, *J* = 6.0 Hz, F_d), -152.49 (d, *J* = 22.8 Hz, F_a), -154.84 (d, *J* = 22.0 Hz, F_c), -165.42 (td, *J* = 22.5, 6.1 Hz, F_b); ^{13}C NMR (101 MHz, $CDCl_3$) δ : 143.9 (br ddt, $^{1}J_{CF}$ = 245.8 Hz, $^{2}J_{CF}$ = 12.6 Hz, $^{3}J_{CF}$ = 4.5 Hz, 2C, C14,C16), 142.4 (br ddt, $^{1}J_{CF}$ = 245.9 Hz, $^{2}J_{CF}$ = 13.9 Hz, $^{3}J_{CF}$ = 5.4 Hz, 2C, C13,C17), 140.1 (br s, 2C, C12,C15), 84.4 (C23), 84.2 (C4), 48.6 (C3), 40.6 (C5), 34.3 (C1), 31.6 (C6), 28.4 (3C, ^{t}Bu, C24,C25,C26), 25.8 (C9), 23.3 (C2), 22.2 (*iso* $\underline{C}H_3$,C10 or C11), 21.1 (*iso* $\underline{C}H_3$, C10 or C11), 16.1 ($\underline{C}H_3$, C7); HRMS (ESI^+) $C_{20}H_{28}F_4O_2$ [M+Na] found 399.192, requires 399.192.

1,4-Diethoxy-2,3,5,6-tetrafluorobenzene 5.50

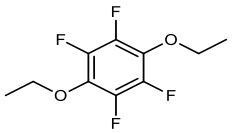

EtONa (1.77 g, 26.0 mmol) was added to a stirred solution of hexafluorobenzene (1.00 mL, 8.67 mmol) in THF (25.0 mL) at r.t and stirred for 24 h. The product was isolated via removal of THF followed by a workup using H_2O (50.0 mL) and DCM (3x 50.0 mL). The compound was then purified by flash column chromatography (0-20% EtOAc in hexane) resulting to yield the title compound (37%, 764 mg, 3.21 mmol) as a clear oil (including 20% *meta* product). With spectroscopic data in accordance with the literature.[219]

IR νmax (solid): 2989, 1500, 987 cm^{-1}; ^{1}H NMR (500 MHz, $CDCl_3$) δ : 4.20 (q, *J* = 7.0 Hz, 4H, $C\underline{H}_2$), 1.40 (t, *J* = 7.0 Hz, 6H, $C\underline{H}_3$); $^{19}F\{^{1}H\}$ NMR (470 MHz, $CDCl_3$) δ : -158.4 (4F); ^{13}C NMR (126 MHz, $CDCl_3$) δ : 143.1 (app. br dd, $^{2}J_{CF}$ = 15.3, $^{3}J_{CF}$ = 4.9 Hz, 4C, Ar-$\underline{C}$F), 141.7 – 140.8 (m, 2C, Ar-$\underline{C}$O), 71.3 (2C, $\underline{C}H_2$), 15.5 (3C, $\underline{C}H_3$); HRMS (EI) $C_{10}H_{10}F_4O_2$ [M] found 238.062, requires 238.061.

All *cis*-1,4-diethoxy-2,3,5,6-tetrafluorocyclohexane 5.51

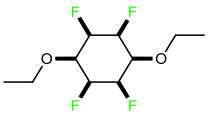

Following General Procedure **3**, 1,4-diethoxy-2,3,5,6-tetrafluorobenzene (100 mg, 0.420 mmol), Rh-CAAC-COD-Cl (4.00 mg, 0.067 mmol, 1.6 mol%), silica (1.00 g), and hexane (40.0 mL) at r.t., for 1 d and at 50 bar H_2 gave, after purification by flash column chromatography (60% DCM in hexane) to yield the title compound (43%, 44.3 mg, 0.180 mmol) was obtained as a white crystal (including 3% *meta* product). m.p. = 138—141 °C.

IR ν_{max} (solid): 2951, 1381, 1103 cm^{-1}; ^1H NMR (500 MHz, $CDCl_3$) δ : 5.13 (apparent d, *J* = 51.9 Hz, 2H, CFH), 4.39 (apparent d, *J* = 47.5 Hz, 2H, CFH), 3.98 – 3.58 (m, 4H, OCH_2), 3.41 – 3.07 (m, 2H, ring-CHO), 1.25 (s, 6H, CH_3); $^{19}F\{^1H\}$ NMR (470 MHz, $CDCl_3$) δ : -206.5 ($2F_{eq}$), -214.8 ($2F_{ax}$); $^{19}F\{^1H\}$ NMR (470 MHz, $CDCl_3$) δ ***Meta* product** (3%) : -193.7 (app. d, *J* = 12.5 Hz), -197.0 (d, *J* = 19.0 Hz), -215.0 – -215.1 (m), -215.8 – -216.3 (m); ^{13}C NMR (126 MHz, $CDCl_3$) δ : 88.1 – 85.0 (m, 4C, CFH), 73.0 (2C, CH), 29.9 (2C, CH_2), 15.4 (2C, CH_3); HRMS (EI) $C_{10}H_{16}F_4O_2$ [M] found 244.108, requires 244.108.

4',4'''-(((Perfluoro-1,4-phenylene)bis(oxy))bis(methylene))bis(4-propyl-1,1'-bi(cyclohexane)) 5.54

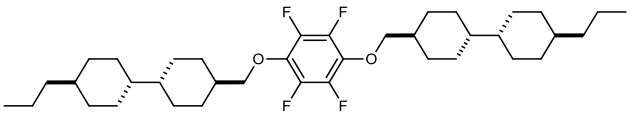

A mixture of potassium hydroxide (608 mg, 10.8 mmol), alcohol (3.10 g, 13.0 mmol) in THF (1.00 mL) was heated to 65 °C and left stirring for 20 min. Hexafluorobenzene (0.500 mL, 4.33 mmol) was added in lots over 20 min to this mixture with constant stirring. After the addition, the temperature of the reaction was heated to reflux ~90 °C for 24 hours. After completion the reaction was quenched by addition of water (50.0 mL). The THF was removed under vacuum. The aqueous layer was extracted with DCM (4 x 25.0 mL) and HCl (37%, 10.0 mL). The organic phase was dried over magnesium sulphate and the solvent was removed under reduced pressure. The compound was then purified by column chromatography (0-5% EtOAc in hexane) resulting to yield the

title compounds (*meta*+*para*) as a white solid (12%, 314 mg, 0.520 mmol) (including 32% *meta* product), m.p. = 126—129 °C.

IR ν_{max} (solid): 2904, 1496, 1035 cm^{-1}; ^{1}H NMR (500 MHz, $CDCl_3$) δ : 3.90 (d, *J* = 6.4 Hz, 4H, $OC\underline{H}_2$), 1.93 – 1.85 (m, 4H, rings-$C\underline{H}_2$), 1.82 – 1.64 (m, 14H, rings-$C\underline{H}_2$, rings-$C\underline{H}_2$, rings-$C\underline{H}_2$, rings-HC-C<u>H</u>), 1.36 – 1.24 (m, 4H, $C\underline{H}_2CH_3$), 1.14 (app. t, *J* = 6.0 Hz, 6H, rings-<u>H</u>C-CH & $C\underline{H}_2CH_2CH_3$), 1.08 – 0.92 (m, 20H, rings-C<u>H</u>CH_2, rings-C<u>H</u>CH_2, rings-$C\underline{H}_2$, rings-$C\underline{H}_2$, rings-$C\underline{H}_2$, rings-$C\underline{H}_2$), 0.87 (t, *J* = 7.3 Hz, 6H, $C\underline{H}_3$); $^{19}F\{^{1}H\}$ NMR (470 MHz, $CDCl_3$) δ : -158.5 (s, 4F); ^{13}C NMR (126 MHz, $CDCl_3$) δ : 144.3 – 142.0 (m, 4C, Ar-<u>C</u>F), 136.6 – 135.4 (m, 2C, Ar-<u>C</u>O), 81.2 (2C, $O\underline{C}H_2$), 43.5 (2C, ring-<u>C</u>HCH_2), 43.4 (2C, ring-<u>C</u>HCH_2), 40.0 (2C, $\underline{C}H_2CH_2CH_3$), 38.8 (2C, rings-HC-<u>C</u>H), 37.8 (2C, rings-H<u>C</u>-CH), 33.7 (4C, rings-$\underline{C}H_2$), 30.4 – 29.2 (m, 12C, rings-$\underline{C}H_2$), 20.2 (2C, $\underline{C}H_2CH_3$), 14.6 (2C, $\underline{C}H_3$); HRMS (EI) $C_{38}H_{62}F_4O_2$ [M] found 625.462, requires 625.460.

All *cis*-2,3,5,6-tetrafluorocyclohexane-1,4-diyl)bis(oxy))bis(methylene))bis(4-propyl-1,1'-bi(cyclohexane)) 5.55

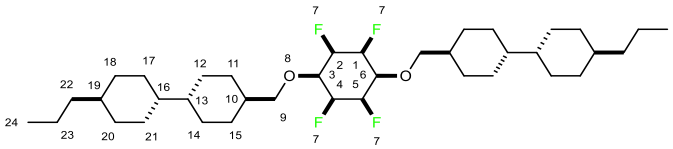

Following General Procedure **3**, **5.54** (300 mg, 0.480 mmol), Rh-CAAC-COD-Cl (5.50 mg, 0.010 mmol, 2 mol%), 4Å molecular sieves (1.0 g), silica (500 mg), and hexane (20.0 mL) at r.t., for 5d and at 50 bar H_2 gave, after purification by flash column chromatography (20-40% EtOAc in hexane) to yield the title compound (4%, 13.0 mg, 0.021 mmol) as a white rubbery white solid, decomposes above 240 °C.

IR ν_{max} (solid): 2918, 1500, 1066, 916 cm^{-1}; ^{1}H NMR (400 MHz, $CDCl_3$) δ : 5.10 (app. d, *J* = 49.4 Hz, 2H, H2 & H4 eq), 4.35 (app. d, *J* = 64.0 Hz, 2H, H1 & H5 ax), 3.74 (app. d, *J* = 27.1 Hz, 2H, H3 & H6), 3.57 – 3.33 (m, 4H, H13), 1.85 (app. d, *J* = 10.7 Hz, 4H, H14 & H23), 1.73 (app. d, *J* = 13.4 Hz, 16H, H15 & H19 & 1H16 & 1H18 & 1H22 & 1H24), 1.33 – 1.27 (m, 6H, H21 & 1H16), 1.16 – 1.09 (m, 6H, H25 & 1H18), 1.03 – 0.90 (m, 16H, H27 & H17 & H20 & 1H22 & 1H24 & H26), 0.86 (t, *J* = 7.3 Hz, 6H, H28); $^{19}F\{^{1}H\}$ NMR (376 MHz,

$CDCl_3$) δ : -206.5 (app. s, 2F, $F_{equatorial}$), -214.8 (app. s, 2F, F_{axial}); ^{13}C NMR (101 MHz, $CDCl_3$) δ : 92.7 – 89.7 (m, 4C, C1,C2,C4,C5), 86.9 (2C, C3,C6), 71.2 (2C, C13), 43.5 (4C, C14,C23), 40.0 (2C, C26), 37.8 (4C, C17 & C20), 33.8 – 33.0 (m, 4C, C22,C24), 30.7 – 29.2 (m, 12C, C15,C16,C18,C19,C21,C25), 20.2 (2C, C27), 14.6 (2C, C28); HRMS (ESI^+) $C_{38}H_{64}F_4O_2$ [M+Na] found 651.473, requires 651.473.

All *cis*-1-(*tert*-butoxy)-2,3,5,6-tetrafluoro-4-methoxycyclohexane 5.56

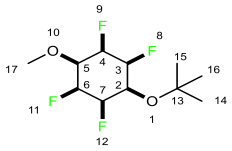

Following General Procedure **3**, 1-(*tert*-butoxy)-2,3,5,6-tetrafluoro-4-methoxybenzene (360 mg, 1.43 mmol), Rh-CAAC-COD-Cl (13.0 mg, 0.023 mmol, 1.6 mol%), 4Å molecular sieves (8.00 g), silica (4.00 g), and hexane (40.0 mL) at r.t., for 2d and at r.t. H_2 gave, after purification by flash column chromatography (2% EtOAc in DCM) to yield the title compound (29%, 106 mg, 0.410 mmol) was obtained as a white crystal. m.p. 180—181 °C.

IR ν_{max} (solid): 2960, 1091 cm^{-1}; ^1H NMR (500 MHz, $CDCl_3$) δ : 5.35 – 4.12 (m, 4H, HF), 3.60 (app. d, *J* = 25.7 Hz, 3H, CH_3), 3.52 – 2.21 (m, 2H, CHO), 1.35 – 1.16 (m, 9H, ^{t}Bu); $^{19}F\{^1H\}$ NMR (470 MHz, $CDCl_3$) δ : -206.2 (2F), -215.7 (2F); ^{13}C NMR (126 MHz, $CDCl_3$) δ : 109.7 (br d, $^1J_{CF}$ = 108.0 Hz, 4C, ring-CF, C2,C3,C5,C6), 77.4 (2C, ring-CO, C4,C7), 73.3 (C13), 56.4 (C17), 28.1 (3C, C14,C15,C16); HRMS (ESI^+) $C_{11}H_{18}F_4O_2$ [M+H] found 259.131, requires 259.132.

1-Butoxy-4-(cyclohexylmethoxy)-2,3,5,6-tetrafluorobenzene 5.58

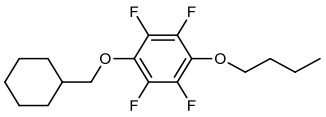

Potassium carbonate (1.49 g, 10.8 mmol, 3 eq) was added to 4-(cyclohexylmethoxy)-2,3,5,6-tetrafluorophenol (1.00 g, 3.59 mmol, 1 eq) in acetonitrile (50.0 mL) and stirred at 85 °C for 1 h. 1-bromobutane (591 mg, 4.31 mmol, 1.2 eq) was then added to the mixture over a 15 min period and the reaction was heated to 90 °C for 23 h. After completion, the mixture was cooled to r.t., diluted with H_2O (100 mL), and extracted with hexane (2x 50.0 mL), and then with H_2O (1 x 100 mL), dried over anhydrous magnesium sulphate, filtered, evaporated under vacuum, and purified by flash column chromatography (1—20% EtOAc in hexane) to yield the title compound (74%, 887 mg, 2.65 mmol) as a clear oil (including 10% *meta* product).

IR ν_{max} (solid): 2927, 1498, 1300 cm^{-1}; ^1H NMR (500 MHz, $CDCl_3$) δ : 4.12 (t, *J* = 6.5 Hz, 2H, $OC\underline{H}_2CH_2$), 3.92 (d, *J* = 6.4 Hz, 2H, $OC\underline{H}_2CH$), 1.86 (app. d, *J* = 13.3 Hz, 2H, ring *ortho*-$C\underline{H}_2$), 1.82 – 1.65 (m, 6H, CH & ring *meta*-C<u>H</u>H & ring *para*-C<u>H</u>H), 1.49 (h, *J* = 7.4 Hz, 2H, $C\underline{H}_2CH_3$), 1.35 – 1.13 (m, 3H, ring *meta*-CH<u>H</u> & ring *para*-CH<u>H</u>), 1.05 (qd, *J* = 12.2, 3.4 Hz, 2H, ring *ortho*-$C\underline{H}_2$), 0.97 (t, *J* = 7.4 Hz, 3H, $C\underline{H}_3$); $^{19}F\{H^1\}$ NMR (470 MHz, $CDCl_3$) δ : -158.5 (4F); ^{13}C NMR (126 MHz, $CDCl_3$) δ : 143.5 – 142.6 (m, 4C, Ar-<u>C</u>F), 141.9 – 140.8 (m, 2C, Ar-<u>C</u>O), 81.1 ($O\underline{C}H_2CH$), 75.5 ($O\underline{C}H_2CH_2$), 38.5 (<u>C</u>H), 32.0 ($OCH_2\underline{C}H_2$), 29.5 (2C, ring *ortho*-$\underline{C}H_2$), 26.6 (ring *para*-$\underline{C}H_2$), 25.8 (2C, ring *meta*-$\underline{C}H_2$), 19.0 ($\underline{C}H_2CH_3$), 13.8 ($\underline{C}H_3$); HRMS (EI) $C_{17}H_{22}F_4O_2$ [M] found 334.154, requires 334.155.

All *cis*-1-butoxy-4-(cyclohexylmethoxy)-2,3,5,6-tetrafluorocyclohexane 5.59

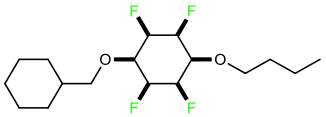

Following General Procedure **3**, 1-butoxy-4-(cyclohexylmethoxy)-2,3,5,6-tetrafluorobenzene (620 mg, 1.85 mmol), Rh-CAAC-COD-Cl (20.0 mg, 0.037 mmol, 2 mol%), 4Å molecular sieves (8.00 g), silica (2.00 g), and hexane (40.0 mL) at r.t., for 4 d and at 50 bar H_2 gave, after purification by flash column chromatography (60% DCM in

hexane) to yield the title compound, (53%, 335 mg, 0.984 mmol) as a white crystal. m.p. 138—140 °C.

IR ν_{max} (solid): 2924, 1377, 1085 cm^{-1}; ^{1}H NMR (500 MHz, $CDCl_3$) δ : 5.12 (app. d, *J* = 50.9 Hz, 2H, ring-CF<u>H</u>), 4.51 – 4.22 (m, 3H, ring-CF<u>H</u> & ring-CO<u>H</u>CH_2), 3.57 (app. dd, *J* = 107.4, 39.4 Hz, 4H, OC<u>H</u>$_2$$CH_2$ & OC<u>H</u>$_2$CH), 3.20 (app. q, *J* = 25.3, 23.7 Hz, 1H, ring-CO<u>H</u>CH), 1.80 (app. d, *J* = 12.8 Hz, 2H, *ortho*-C<u>H</u>$_2$), 1.66 (app. s, 9H, *ortho*-C<u>H</u>$_2$ & C<u>H</u> & OCH_2C<u>H</u>$_2$ & *para*-C<u>H</u>$_2$), 1.41 (app. d, *J* = 8.1 Hz, 2H, OCH_2CH_2C<u>H</u>$_2$), 1.24 (app. q, *J* = 25.9, 20.2 Hz, 4H, *meta*-C<u>H</u>$_2$), 1.02 – 0.84 (m, 3H, C<u>H</u>$_3$); $^{19}F\{^{1}H\}$ NMR (470 MHz, $CDCl_3$) δ **Major conformer**: -206.4 (s, 2F, F_{eq}), -214.8 (s, 2F, F_{ax}); $^{19}F\{^{1}H\}$ NMR (470 MHz, $CDCl_3$) δ **Minor conformer**: -206.5 (s, 2F, F_{ax}), -214.9 (s, 2F, F_{ax}); ^{13}C NMR (126 MHz, $CDCl_3$) δ : 86.76 (dd, $^{1}J_{CF}$ = 191.5 Hz, $^{2}J_{CF}$ = 48.3 Hz, 4C, <u>C</u>FH), 76.4 (br s, ring-<u>C</u>HO), 75.7 (O<u>C</u>$H_2$$CH_2$), 73.9 (O<u>C</u>$H_2$CH), 73.0 (<u>C</u>HO), 38.3 (<u>C</u>H), 31.7 (OCH_2<u>C</u>H_2), 29.8 (2C, *ortho*-<u>C</u>H_2), 26.7 (*para*-<u>C</u>H_2), 26. (2C, *meta*-<u>C</u>H_2), 19.3 (OCH_2CH_2<u>C</u>H_2), 14.0 (<u>C</u>H_3); HRMS (EI) $C_{17}H_{29}F_4O_2$ [M] found 341.209, requires 341.210.

2,3,5,6-Tetrafluoro-4-(((1*R*,2*S*,5*R*)-2-isopropyl-5-methylcyclohexyl)oxy)phenol 5.60

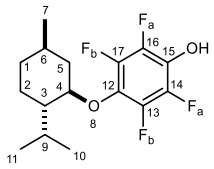

TFA (2.60 mL, 1 mL per mmol) was added to a solution of **5.49** (952 mg, 2.53 mmol, 1 eq) in DCM (50.0 mL). After addition the reaction was stirred for 48 h. TFA and solvent were then removed via vacuo and gave, after purification by flash silica chromatography (0-20% EtOAc in hexane) the title compound (quantitative, 851 mg, 2.50 mmol) as a clear oil (including 8% *meta* product).

IR ν_{max} (solid): 3660, 2900, 1320, 1097 cm^{-1}; ^{1}H NMR (400 MHz, $CDCl_3$) δ : 5.60 – 5.02 (m, 1H, OH, H22), 3.94 (td, *J* = 10.6, 4.4 Hz, 1H, H4), 2.42 (app. pd, *J* = 7.0, 2.6 Hz, 1H, H9), 1.86 (app. d, *J* = 12.4 Hz, 1H, H1), 1.70 (app. ddq, *J* = 16.2, 12.7, 3.3 Hz, 2H, H5), 1.52 (app. ddd, *J* = 16.3, 9.5, 3.1 Hz, 1H, H3), 1.26 (app. t, *J* = 7.2 Hz, 2H, H6 & H2), 1.16 – 1.01 (m, 2H, H1 & H2), 0.97 (d, *J* = 7.1 Hz, 3H, H10 or H11), 0.90 (d, *J* = 6.5 Hz, 3H, H10

or H11), 0.87 (d, *J* = 6.9 Hz, 3H, H7); $^{19}F\{^{1}H\}$ NMR (376 MHz, $CDCl_3$) δ : -156.7 (br dq, *J* = 19.7, 5.9 Hz, 2F, F_b), -164.7 – -164.9 (m, 2F, F_a); ^{13}C NMR (101 MHz, $CDCl_3$) δ : 140.5 (br s, 2C, C14 & C16), 134.7 (br s, 2C, C13 & C17), 113.9 (C12), 101.5 (C15), 84.3 (C4), 48.6 (C3), 40.4 (C1), 34.3 (C5), 31.6 (C6), 25.7 (C9), 23.2 (C2), 22.3 (C10 or C11), 21.1 (C10 or C11), 16.1 (C7); HRMS (ESI^+) $C_{16}H_{20}F_4O_2$ [M+Na] found 319.133, requires 319.132.

1-Butoxy-2,3,5,6-tetrafluoro-4-(((1*R*,2*S*,5*R*)-2-isopropyl-5-methylcyclohexyl)oxy)benzene 5.61

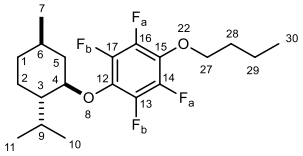

Potassium carbonate (2.57 g, 18.6 mmol, 3 eq) was added to **5.60** (1.99 g, 6.21 mmol, 1 eq) in acetonitrile (20.0 mL) and THF (10.0 mL) and stirred at 85 °C for 30 min. bromobutane (0.880 mL, 8.07 mmol, 1.3 eq) was then added to the mixture over a 15 min period and the reaction was heated to 75 °C for 24 h. After completion, the mixture was cooled to r.t., diluted with H_2O (50.0 mL), and extracted with hexane (2x 100 mL), dried over anhydrous magnesium sulphate, filtered, evaporated under vacuum to yield the title compound (65%, 1.51 g, 4.01 mmol) as a clear liquid (including 8% *meta* product).

IR νmax (solid): 2873, 1496, 1340, 1095 cm^{-1}; ^1H NMR (400 MHz, $CDCl_3$) δ : 4.17 – 4.11 (m, 2H, H27), 4.00 (td, *J* = 10.6, 4.4 Hz, 1H, H4), 2.40 (septd, *J* = 6.9, 2.6 Hz, 1H, H9), 1.87 (app. d, *J* = 12.2 Hz, 1H, H1), 1.80 – 1.63 (m, 4H, H5,H28), 1.60 – 1.46 (m, 3H, H3,H29), 1.39 – 1.31 (m, 2H, H6,H2), 1.18 – 1.02 (m, 2H, H1,H2), 1.00 – 0.94 (m, 6H, H10,H11), 0.92 – 0.85 (m, 6H, H7,H30); $^{19}F\{H^1\}$ NMR (377 MHz, $CDCl_3$) δ : -156.8 (dd, *J* = 21.8, 5.9 Hz, 2F, F_b), -158.7 (dd, *J* = 21.9, 5.7 Hz, 2F, F_a); ^{13}C NMR (101 MHz, $CDCl_3$) δ : 144.0 – 143.1 (m, 2C, C14,C16), 141.6 – 140.5 (m, 2C, C13,C17), 131.7 – 130.3 (m 2C, C12,C15), 84.2 (C4), 75.4 (C27), 48.6 (C3), 40.5 (C1), 34.3 (C5), 32.0 (C28), 31.6 (C6), 25.7 (C9), 23.3 (C2), 22.2 (C10 or C11), 21.1 (C10 or C11), 19.0 (C29), 16.1 (C7), 13.9 (C30); HRMS (ESI^+) $C_{20}H_{28}F_4O_2$ [M+Na] found 399.192, requires 399.192.

All *cis*-1-butoxy-2,3,5,6-tetrafluoro-4-(((1*R*,2*S*,5*R*)-2-isopropyl-5-methylcyclohexyl)oxy)cyclohexane 5.62

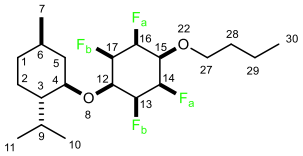

Following General Procedure **3**, **5.61** (400 mg, 1.06 mmol), Rh-CAAC-COD-Cl (11.0 mg, 0.019 mmol, 1.8 mol%), 4Å molecular sieves (8.00 g), silica (4.00 g), and hexane (40.0 mL) at r.t., for 4 d and at 50 bar H_2 gave, after purification by flash column chromatography (50-70% DCM in hexane) to yield the title compound (64%, 261 mg, 0.682 mmol) as a white powder (including 3% *meta* product). m.p. 99—100 °C, $[a]^{25}_D$ = -59.4° (DCM).

IR νmax (solid): 2908, 1465, 1105, 1095 cm^{-1}; ^1H NMR (400 MHz, $CDCl_3$) δ : 5.26 – 4.75 (m, 2H, H13 & H17), 4.63 – 4.16 (m, 2H, H14 & H16), 3.80 – 3.54 (m, 2H, H27), 3.43 – 3.16 (m, 2H, H12 & H15), 2.62 – 2.23 (m, 1H, H4), 2.18 – 1.89 (m, 2H, H5), 1.74 – 1.47 (m, 5H, H1 & H2 & H6), 1.47 – 1.16 (m, 6H, H3 & H9 & H28 & H29), 0.90 (d, *J* = 6.5 Hz, 9H, H7 & H10 & H11), 0.75 (d, *J* = 6.9 Hz, 3H, H30); $^{19}F\{^1H\}$ NMR (470 MHz, $CDCl_3$) δ **Major conformer**: -206.4 (app. dd, J = 47.8, 11.2 Hz, $2F_{eq}$, 2F, F_b), -214.5 (app. d, *J* = 13.3 Hz, $2F_{ax}$, 2F, F_a); $^{19}F\{^1H\}$ NMR (470 MHz, $CDCl_3$) δ **Minor conformer**: -205.7 (d, *J* = 10.2 Hz, $2F_{ax}$, F_b), -214.1 (d, *J* = 16.9, $2F_{eq}$, F_a); $^{19}F\{^1H\}$ NMR (470 MHz, $CDCl_3$) δ ***meta* product** (3%): -206.6 (t, *J* = 11.3 Hz), -214.2 (app. td, *J* = 24.4, 17.1 Hz), -214.9 – -215.5 (m, 2F); ^{13}C NMR (101 MHz, $CDCl_3$) δ : 88.2 – 85.2 (m, 4C, C13,C14,C16,C17), 79.0 (2C, C12,C15), 76.2 (C4), 74.1 (C27), 48.2 (C3), 40.8 (C5), 34.4 (C1), 32.2 (C28), 31.7 (C9), 31.1 (C6), 23.1 (C2), 22.4 (2C, C10 & C11), 19.1 (C29), 16.0 (C30), 14.0 (C7); HRMS (ESI^+) $C_{20}H_{34}F_4O_2$ [M+Na] found 405.239, requires 405.239.

2,3,5,6-Tetrafluoro-4-((-4'-propyl-[1,1'-bi(cyclohexan)]-4-yl)methoxy)phenol 5.63

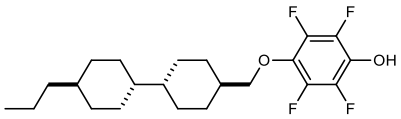

TFA (1.45 mL, 1 mL per mmol) was added to a solution of **5.43** (664 mg, 1.45 mmol, 1 eq) in DCM (50.0 mL). After addition the reaction was stirred for 23 h. TFA and solvent were then removed via vacuo and gave, after purification by flash silica chromatography (0-20% EtOAc in hexane) the title compound (82%, 480 mg, 1.19 mmol) as a white solid (including 14% *meta* product), m.p. 119-120 °C.

IR vmax (solid): 3600, 2908, 1483, 1375, 1020, 1015 cm^{-1}; ^{1}H NMR (500 MHz, $CDCl_3$) δ : 5.10 (s, 1H, O<u>H</u>), 3.88 (d, *J* = 6.4 Hz, 2H, $OC\underline{H}_2$), 1.97 – 1.87 (m, 2H, rings-$C\underline{H}_2$), 1.82 – 1.66 (m, 7H, rings-$C\underline{H}_2$, rings-$C\underline{H}_2$, rings-$C\underline{H}_2$, rings-HC-C<u>H</u>), 1.29 (app. td, *J* = 13.7, 12.6, 6.3 Hz, 2H, $C\underline{H}_2CH_3$), 1.17 – 1.10 (m, 3H, rings-<u>H</u>C-CH & $C\underline{H}_2CH_2CH_3$), 1.08 – 0.91 (m, 10H, rings-C<u>H</u>CH_2, rings-C<u>H</u>CH_2, rings-$C\underline{H}_2$, rings-$C\underline{H}_2$, rings-$C\underline{H}_2$, rings-$C\underline{H}_2$), 0.87 (t, *J* = 7.3 Hz, 3H, $C\underline{H}_3$); $^{19}F\{^{1}H\}$ NMR (470 MHz, $CDCl_3$) δ : -158.2 (dd, *J* = 21.8, 5.6 Hz, Ar-C<u>F</u> OCH_2CH), -164.8 (dd, *J* = 21.9, 5.7 Hz, Ar-C<u>F</u> OH); ^{13}C NMR (126 MHz, $CDCl_3$) δ : 143.1 – 142.4 (m, 4C, Ar-<u>C</u>F), 136.6 – 135.5 (m, 2C, Ar-<u>C</u>O), 81.4 ($O\underline{C}H_2$), 43.5 (ring-<u>C</u>HCH_2), 43.4 (ring-<u>C</u>HCH_2), 40.0 ($C\underline{H}_2CH_2CH_3$), 38.8 (rings-HC-<u>C</u>H), 37.8 (rings-H<u>C</u>-CH), 33.7 (2C, rings-$\underline{C}H_2$), 30.3 – 29.3 (m, 6C, rings-$\underline{C}H_2$), 20.2 ($\underline{C}H_2CH_3$), 14.6 ($\underline{C}H_3$); HRMS (ESI^+) $C_{22}H_{30}F_4O_2$ [M+Na] found 425.209, requires 425.207.

4-((4-Butoxy-2,3,5,6-tetrafluorophenoxy)methyl)-4'-propyl-1,1'-bi(cyclohexane) 5.64

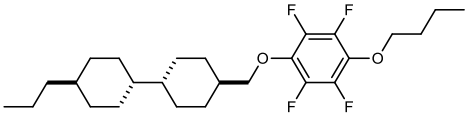

Potassium carbonate (328 mg, 2.37 mmol, 3 eq) was added to **5.63** (318 mg, 0.790 mmol, 1 eq) in acetonitrile (20.0 mL) and THF (10.0 mL) and stirred at 85 °C for 1 h. bromobutane (0.110 mL, 0.950 mmol, 1.2 eq) was then added to the mixture over a 15 min period and the reaction was heated to 85 °C for 23 h. After completion, the mixture was cooled to r.t., diluted with H_2O (50.0 mL), and extracted with hexane (2x 100 mL), dried over anhydrous magnesium sulphate, filtered, evaporated under vacuum, and purified by flash column chromatography (1—20% EtOAc in hexane) to yield the title

compound (67%, 242 mg, 0.528 mmol) as an off white solid (including 13% *meta* product). m.p. 76—78 °C

IR ν_{max} (solid): 2850, 1498, 1107, 1043 cm^{-1}; ^{1}H NMR (500 MHz, $CDCl_3$) δ : 4.12 (t, *J* = 6.5 Hz, 2H, $OC\underline{H}_2CH_2$), 3.91 (d, *J* = 6.4 Hz, 2H, $OC\underline{H}_2$ ring), 1.94 – 1.88 (m, 2H, rings-$C\underline{H}_2$), 1.81 – 1.66 (m, 10H, rings-$C\underline{H}_2$, rings-$C\underline{H}_2$, rings-$C\underline{H}_2$, rings-$C\underline{H}_2$, rings-$C\underline{H}_2$), 1.55 – 1.43 (m, 2H, $OCH_2CH_2C\underline{H}_2CH_3$), 1.30 (app. dq, *J* = 14.8, 7.5 Hz, 3H, ring-$CH_2C\underline{H}_2CH_3$, rings-HC-C$\underline{H}$), 1.16 – 1.12 (m, 3H, $C\underline{H}_2CH_2CH_3$, rings-$\underline{H}$C-CH), 1.08 – 0.99 (m, 8H, rings-C$\underline{H}CH_2$, rings-C$\underline{H}CH_2$, rings-$C\underline{H}_2$, rings-$C\underline{H}_2$, rings-$C\underline{H}_2$), 0.97 (t, *J* = 7.4 Hz, 3H, $CH_2C\underline{H}_3$), 0.87 (t, *J* = 7.3 Hz, 3H, ring-$C\underline{H}_3$); $^{19}F\{H^1\}$ NMR (470 MHz, $CDCl_3$) δ : -158.5 (br s, 4F); ^{13}C NMR (126 MHz, $CDCl_3$) δ : 143.3 – 142.3 (m, 4C, Ar-$\underline{C}$F), 136.9 – 135.4 (m, 2C, Ar-$\underline{C}$O), 81.2 ($O\underline{C}H_2$ ring), 75.5 ($O\underline{C}H_2CH_2$), 43.5 (ring-$\underline{C}HCH_2$), 43.4 (ring-$\underline{C}HCH_2$), 40.0 ($\underline{C}H_2CH_2CH_3$), 38.8 (rings-HC-$\underline{C}$H), 37.8 (rings-H$\underline{C}$-CH), 33.7 (2C, rings-$\underline{C}H_2$), 32.0 ($OCH_2\underline{C}H_2CH_2CH_3$), 30.3 – 29.3 (m, 6C, rings-$\underline{C}H_2$), 20.2 ($\underline{C}H_2CH_3$), 19.0 ($OCH_2CH_2\underline{C}H_2CH_3$), 14.6 ($\underline{C}H_3$), 13.9 ($OCH_2CH_2CH_2\underline{C}H_3$); HRMS (EI) $C_{26}H_{38}F_4O_2$ [M] found 458.282, requires 458.281.

4-(((All *cis*-4-butoxy-2,3,5,6-tetrafluorocyclohexyl)oxy)methyl)-4'-propyl-1,1'-bi(cyclohexane) 5.65

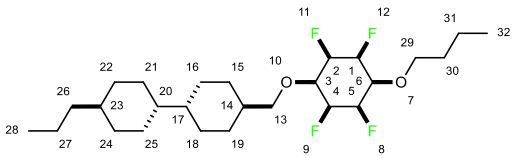

Following General Procedure **3**, **5.64** (550 mg, 1.20 mmol), Rh-CAAC-COD-Cl (12.3 mg, 0.220 mmol, 2 mol%), 4Å molecular sieves (8.00 g), silica (4.00 g), and hexane (40.0 mL) at r.t., for 5 d and at 50 bar H_2 gave, after purification by flash column chromatography (30 -60% DCM in hexane) to yield the title compound (54%, 302 mg, 0.651 mmol) as a white rubbery white solid (including 12% *meta* product), m.p. 174—175 °C.

IR ν_{max} (solid): 2910, 1107, 1043 cm^{-1}; ^{1}H NMR (500 MHz, $CDCl_3$) δ : 5.32 – 5.03 (m, 2H, H2 & H4), 4.53 – 4.22 (m, 2H, H1 & H5), 3.68 (app. t, *J* = 6.6 Hz, 2H, 2H, H3 & H6), 3.49 (dd, *J* = 31.1, 6.0 Hz, 2H, H13), 3.37 – 3.10 (m, 2H, H29), 1.88 (app. d, *J* = 10.5 Hz, 3H,

H14 & H30), 1.80 – 1.57 (m, 10H, H15 & H19 & 1H16 & 1H18 & 1H22 & 1H24 & 1H21 & 1H25), 1.44 (app. p, *J* = 7.4 Hz, 3H, H17 & H31), 1.36 – 1.26 (m, 9H, 1H16 & 1H18 & 1H22 & 1H24 & 1H21 & 1H25 & H23 & H27), 1.20 – 1.11 (m, 3H, H26 & H20), 0.98 – 0.86 (m, 6H, H28 & H32); $^{19}F\{^{1}H\}$ NMR (470 MHz, $CDCl_3$) δ **Major conformer**: -206.4 ($2F_{eq}$, F9&F11), -214.7 (s, $2F_{ax}$, F8&F12); $^{19}F\{^{1}H\}$ NMR (470 MHz, $CDCl_3$) δ **Minor conformer**: -206.5 ($2F_{ax}$, F9&F11), -214.9 (s, $2F_{eq}$, F8&F12); $^{19}F\{^{1}H\}$ NMR (470 MHz, $CDCl_3$) δ ***meta* product** (12%): -206.8 (t, *J* = 11.5 Hz), -214.2 (t, *J* = 24.5 Hz), -215.3 – -215.4 (m, 2F); ^{13}C NMR (101 MHz, $CDCl_3$) δ : 112.6 – 105.7 (m, 4C, C1,C2,C4,C5), 80.0 (2C, C3,C6), 68.1 (2C, C13,C29), 43.6 (2C, C14,C23), 40.0 (C26), 37.8 (2C, C17,C20), 33.8 (2C, C22,C24), 31.8 (C30), 30.6 – 29.1 (m, 6C, C15,C16,C18,C19,C21,C25), 20.2 (C27), 19.2 (C31), 14.6 (C28), 14.0 (C32); HRMS (ESI^+) $C_{26}H_{44}F_4O_2$ [M+Na] found 487.317, requires 487.318.

4-Propyl-4'-((2,3,5,6-tetrafluoro-4-methoxyphenoxy)methyl)-1,1'-bi(cyclohexane) 5.67

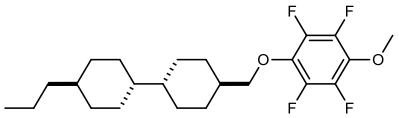

Potassium carbonate (484 mg, 3.50 mmol, 3 eq) was added to 4-(cyclohexylmethoxy)-2,3,5,6-tetrafluorophenol (470 mg, 1.17 mmol, 1 eq) in acetonitrile (50.0 mL) and stirred at 85 °C for 1 h. Methyl iodide (0.100 mL, 1.99 mg, 1.40 mmol, 1.2 eq) was then added to the mixture over a 15 min period and the reaction was heated to 90 °C for 23 h. After completion, the mixture was cooled to r.t., diluted with H_2O (100 mL), and extracted with hexane (2x 50.0 mL), and then with H_2O (1 x 100 mL), dried over anhydrous magnesium sulphate, filtered, evaporated under vacuum, and purified by flash column chromatography (1—20% EtOAc in hexane) to yield the title compound (57%, 278 mg, 0.670 mmol) as an clear oil (including 15% *meta* product).

IR ν_{max} (solid): 2922, 1498, 1394, 1045 cm^{-1}; ^{1}H NMR (500 MHz, $CDCl_3$) δ : 3.99 (s, 3H, OCH_3), 3.91 (d, *J* = 6.4 Hz, 2H, OCH_2), 1.95 – 1.87 (m, 2H, rings-CH_2), 1.81 – 1.65 (m, 7H, rings-CH_2, rings-CH_2, rings-CH_2, rings-HC-CH), 1.29 (app. dt, *J* = 14.4, 7.4 Hz, 2H, CH_2CH_3), 1.14 (app. t, *J* = 6.0 Hz, 3H, rings-HC-CH & $CH_2CH_2CH_3$), 1.06 – 0.92 (m, 10H, rings-$CHCH_2$, rings-$CHCH_2$, rings-CH_2, rings-CH_2, rings-CH_2, rings-CH_2), 0.87 (t, *J* = 7.3 Hz, 3H, CH_3);

$^{19}F\{^{1}H\}$ NMR (470 MHz, $CDCl_3$) δ : -158.3 (dd, *J* = 21.4, 5.5 Hz, Ar-C<u>F</u> OCH_2CH), -159.1 (dd, *J* = 21.5, 5.7 Hz, Ar-C<u>F</u> OMe); ^{13}C NMR (101 MHz, $CDCl_3$) δ : 141.9 (br d, $^{1}J_{CF}$ = 244.4 Hz, 4C, Ar-<u>C</u>F), 139.5 – 138.2 (m, 2C, Ar-<u>C</u>O), 81.2 (O<u>C</u>H_2), 43.5 (ring-<u>C</u>HCH_2), 43.4 (ring-<u>C</u>HCH_2), 40.0 (<u>C</u>$H_2CH_2CH_3$), 38.8 (rings-HC-<u>C</u>H), 37.8 (rings-H<u>C</u>-CH), 33.7 (2C, rings-<u>C</u>H_2), 30.5 (O<u>Me</u>), 30.7 – 28.8 (m, 6C, rings-<u>C</u>H_2), 20.2 (<u>C</u>H_2CH_3), 14.6 (<u>C</u>H_3); HRMS (EI) $C_{23}H_{32}F_4O_2$ [M] found 416.233, requires 416.233.

4-Propyl-4'-(((All *cis*-2,3,5,6-tetrafluoro-4-methoxycyclohexyl)oxy)methyl)-1,1'-bi(cyclohexane) 5.68

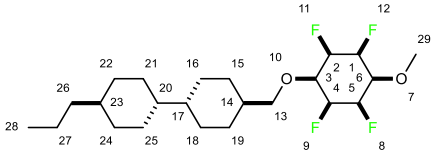

Following General Procedure **3**, **5.67** (110 mg, 0.260 mmol), Rh-CAAC-COD-Cl (3.00 mg, 0.005 mmol, 1-2 mol%), 4Å molecular sieves (1.00 g), silica (250 mg), and hexane (20.0 mL) at r.t, for 5 d and at 50 bar H_2 gave, after purification by flash column chromatography (50-70% DCM in hexane) to yield the title compound (45%, 50.0 mg, 0.118 mmol) as a white powder (including 15% *meta* product). m.p. 210—211 °C.

IR ν_{max} (solid): 2906, 1444, 1392, 1107, 1047 cm^{-1}; ^{1}H NMR (400 MHz, $CDCl_3$) δ : 5.14 (d, *J* = 50.0 Hz, 2H, H2 & H4), 4.56 – 4.20 (m, 2H, H1 & H5), 3.79 – 3.68 (m, 2H, H3 & H6), 3.58 (s, 3H, H29), 3.44 (d, *J* = 6.5 Hz, 2H, H13), 1.85 (app. dt, *J* = 6.6, 3.0 Hz, 2H, H14 & H23), 1.79 – 1.50 (m, 8H, H15 & H19 & 1H16 & 1H18 & 1H22 & 1H24), 1.35 – 1.22 (m, 3H, H21 & 1H16), 1.18 – 1.08 (m, 3H, H25 & 1H18), 0.95 (app. dd, *J* = 20.0, 9.7 Hz, 8H, H27 & H17 & H20 & 1H22 & 1H24 & H26), 0.86 (t, *J* = 7.3 Hz, 3H, H28); $^{19}F\{^{1}H\}$ NMR (470 MHz, $CDCl_3$) δ **Major conformer**: -206.6 ($2F_{eq}$, F9&F11), -215.1 (s, $2F_{ax}$, F8&F12); $^{19}F\{^{1}H\}$ NMR (470 MHz, $CDCl_3$) δ **Minor conformer**: -206.5 ($2F_{ax}$, F9&F11), -215.0 (s, $2F_{eq}$, F8&F12); $^{19}F\{^{1}H\}$ NMR (470 MHz, $CDCl_3$) δ ***meta*** **product** (15%): -206.9 (t, *J* = 11.2 Hz), -214.4 (t, *J* = 24.5 Hz), -215.5 (app. ddd, *J* = 30.5, 24.5, 11.1 Hz, 2F); ^{13}C NMR (101 MHz, $CDCl_3$) δ : 93.0 – 90.5 (m, 4C, C1 & C2 & C4 & C5), 87.9 – 85.2 (m, 2C, C3 & C6), 72.8 (C13), 66.2 (C29), 43.5 (2C, C14 & C23), 40.0 (C26), 37.8 (2C, C17 & C20), 33.8 (2C, 22 &

C24), 30.6 – 29.2 (m, 6C, C15 & C16 & C18 & C19 & C21 & C25), 20.2 (C27), 14.6 (C28); HRMS (ESI^+) $C_{23}H_{38}F_4O_2$ [M+Na] found 445.270, requires 445.271.

2,3,5,6-Tetrafluoro-4-((-4'-propyl-[1,1'-bi(cyclohexan)]-4-yl)oxy)phenol) 5.69

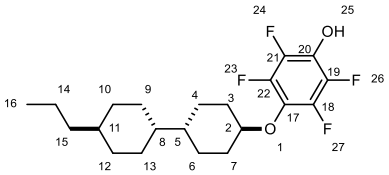

TFA (1.57 mL, 1 mL per mmol) was added to a solution of **5.48** (700 mg, 1.57 mmol, 1 eq) in DCM (50.0 mL). After addition the reaction was stirred for 23 h. TFA and solvent were then removed via vacuo and gave, after purification by flash silica chromatography (0-20% EtOAc in hexane) the title compound (94%, 571 mg, 1.47 mmol) as a white solid (including 11% *meta* product), m.p. = 120—121 °C.

IR νmax (solid): 3360, 2908, 1494, 1037, 974 cm^{-1}; ^1H NMR (400 MHz, $CDCl_3$) δ : 5.08 (s, 1H, OH), 3.92 (td, *J* = 11.0, 5.4 Hz, 1H, H2), 2.16 – 2.06 (m, 2H, 1H3&H7), 1.86 – 1.65 (m, 8H, H10&H12, 1H4&H6&H9&H13), 1.47 (q, *J* = 12.4, 11.9 Hz, 2H, 1H3&H7), 1.36 – 1.24 (m, 2H, H15), 1.13 (t, *J* = 5.9 Hz, 4H, H5&H8&H14), 1.08 – 0.92 (m, 5H, H11, 1H4&H6&H9&H13), 0.86 (t, *J* = 7.3 Hz, 3H, H16); $^{19}F\{^1H\}$ NMR (470 MHz, $CDCl_3$) δ : -156.8 (dd, *J* = 22.1, 5.9 Hz, Ar-CF OCH), -164.9 (dd, *J* = 22.2, 5.7 Hz, Ar-CF OH); ^{13}C NMR (101 MHz, $CDCl_3$) δ : 146.0 – 142.8 (m, 4C, C18,C19,C21,C22), 137.5 – 135.5 (m, 2C, C17&C20), 84.6 (C2), 42.6 (d, *J* = 48.3 Hz, C11), 39.9 (2C, C5&C8), 37.7 (C14), 33.6 (2C, C10C&12), 32.6 (2C, C3&C7), 30.3 (2C, C9&C13), 28.0 (2C, C4&C6), 20.2 (C15), 14.6 (C16); HRMS (ESI^-) $C_{21}H_{27}F_4O_2$ [M-H] found 387.196, requires 387.195.

4-(4-Butoxy-2,3,5,6-tetrafluorophenoxy)-4'-propyl-1,1'-bi(cyclohexane) 5.70

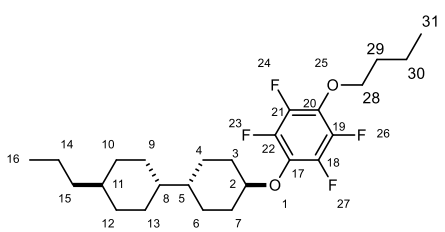

words Potassium carbonate (589 mg, 4.26 mmol, 3 eq) was added to **5.69** (550 mg, 1.42 mmol, 1 eq) in acetonitrile (50.0 mL) and THF (10.0 mL) and stirred at 85 °C for 1 h.

bromobutane (0.230 mL, 2.13 mmol, 1.2 eq) was then added to the mixture over a 15 min period and the reaction was heated to 90 °C for 23 h. After completion, the mixture was cooled to r.t., diluted with H_2O (100 mL), and extracted with hexane (2 x 50.0 mL), and then with H_2O (1 x 100 mL), dried over anhydrous magnesium sulphate, filtered, evaporated under vacuum, and purified by flash column chromatography (1—20% EtOAc in hexane) to yield the title compound (66%, 414 mg, 0.93 mmol) as an gummy solid (including 10% *meta* product), m.p. = 38—40 °C.

IR vmax (solid): 2922, 1494, 1039, 981 cm^{-1}; ^1H NMR (500 MHz, $CDCl_3$) δ : 4.13 (t, *J* = 6.5 Hz, 2H, H28), 3.97 (td, *J* = 10.8, 5.3 Hz, 1H, H2), 2.14 – 2.07 (m, 2H, 1H3&H7), 1.74 (app. tq, *J* = 20.7, 10.7 Hz, 8H, 1H3&H7,1H4&H6, 1H9&H13, 1H10&H12), 1.49 (app. dt, *J* = 14.6, 7.3 Hz, 4H, H29&H30), 1.30 (dq, *J* = 15.4, 8.0 Hz, 2H, H15), 1.13 (app. t, *J* = 5.9 Hz, 4H, H14,H5&H8), 1.10 – 0.99 (m, 7H, H11, 1H4&H6, 1H9&H13, 1H10&H12) 0.97 (t, *J* = 7.4 Hz, 3H, H31), 0.87 (t, *J* = 7.3 Hz, 3H, H16); $^{19}F\{^1H\}$ NMR (470 MHz, $CDCl_3$) δ : -157.1 (dd, *J* = 21.9, 5.7 Hz, 2F, F23&F27), -158.63 (dd, *J* = 21.9, 5.8 Hz, 2F, F24&F26); ^{13}C NMR (126 MHz, $CDCl_3$) δ : 144.2 – 141.1 (m, 4C, C18,C19,C21,C22), 137.7 – 135.6 (m, 2C, C17&C20), 84.6 (C2), 75.4 (C28), 42.6 (C11), 39.9 (2C, C5&C8), 37.7 (C14), 33.6 (2C, C10C&12), 32.7 (2C, C3&C7), 32.0 (C29), 30.3 (2C, C9&C13), 28.0 (2C, C4&C6), 20.2 (C15), 19.0 (C30), 14.6 (C16), 13.9 (C31); HRMS (ESI^+) $C_{25}H_{36}F_4O_2$ [M+Na] found 467.254, requires 467.255.

4-((All *cis*-4-butoxy-2,3,5,6-tetrafluorohexyl)oxy)-4'-propyl-1,1'-bi(cyclohexane) 5.71

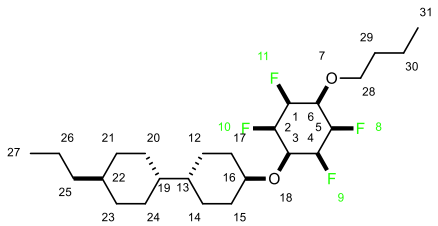

Following General Procedure **3**, **5.70** (390 mg, 0.880 mmol), Rh-CAAC-COD-Cl (10.0 mg, 0.018 mmol, 2 mol%), 4Å molecular sieves (1.00 g), silica (500 mg), and hexane (20.0 mL) at r.t., for 3 d, and at 50 bar H_2 gave, after purification by flash column chromatography (30-60% DCM in hexane) to yield the title compound (72%, 283 mg,

0.630 mmol) as a white gummy solid (including 6% *meta* product). m.p. = 236—238 °C dec.

IR vmax (solid): 2922, 1450, 1043, 871 cm^{-1}; ^{1}H NMR (400 MHz, $CDCl_3$) δ : 5.22 – 4.90 (m, 4H, H1,H2,H4,H5), 4.55 – 4.15 (m, 2H, H3&H6), 3.80 – 3.57 (m, 2H, H28), 3.54 – 3.32 (m, 1H, H16), 2.12 – 1.96 (m, 2H, 1H15&H17), 1.80 – 1.56 (m, 8H, 1H15&H17, 1H12&H14, 1H20&H24, 1H21&H23), 1.41 (app. td, *J* = 14.4, 6.8 Hz, 4H, H29&H30), 1.29 (app. dd, *J* = 16.2, 9.8 Hz, 2H, H15), 1.17 – 1.09 (m, 4H, H25, H13&H19), 1.03 – 0.87 (m, 1H, H22, 1H12&H14, 1H20&H24, 1H21&H23, H31), 0.86 (t, *J* = 7.4 Hz, 3H, H27); $^{19}F\{^{1}H\}$ NMR (376 MHz, $CDCl_3$) δ **Major conformer**: -206.3 ($2F_{eq}$, F9&F10), -214.7 (s, $2F_{ax}$, F8&F11); $^{19}F\{^{1}H\}$ NMR (376 MHz, $CDCl_3$) δ **Minor conformer**: -206.8 ($2F_{ax}$, F9&F10), -214.5 (s, $2F_{eq}$, F8&F11); $^{19}F\{^{1}H\}$ NMR (376 MHz, $CDCl_3$) δ ***meta*** **product** (6%): -206.6 (t, *J* = 11.5 Hz), -214.1 (t, *J* = 24.5 Hz), -215.3 (app. dd, *J* = 24.1, 11.5 Hz); ^{13}C NMR (101 MHz, $CDCl_3$) δ : 148.7 – 145.3 (m, 4C, C1,C2,C4,C5), 140.1 – 137.0 (m, 2C, C3,C6), 85.5 (C16), 75.1 (C28), 42.7 (C22), 39.9 (2C, C13&C19), 37.7 (C25), 33.7 (2C, C21&C23), 32.7 (2C, C15&C17), 32.1 (C29), 30.3 (2C, C20&C24), 28.2 (2C, C12&C14), 20.2 (C26), 19.1 (C30), 14.6 (C27), 14.0 (C31); HRMS (ESI^+) $C_{25}H_{42}F_4O_2$ [M+Na] found 473.301, requires 473.302.

4-((Perfluorophenoxy)methyl)-4'-propyl-1-1'-bi(cyclohexane) 5.74

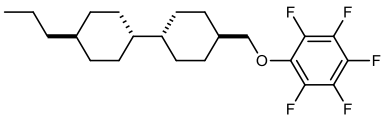

A mixture of potassium hydroxide (729 mg, 13.0 mmol, 1.5 eq), alcohol (3.10 mg, 13.0 mmol, 1.5 eq) in THF (15.0 mL) was heated to 65 °C and left stirring for 20 min. Hexafluorobenzene (1.00 mL, 8.66 mmol, 1 eq) was added in lots over 20 min to this mixture with constant stirring. After the addition, the temperature of the reaction was heated to reflux ~75 °C for 23 h. After completion the reaction was quenched by addition of water (50.0 mL). The THF was removed under vacuum. The aqueous layer was extracted with DCM (4 x 25.0 mL) and HCl (37%, 10.0 mL). The organic phase was dried over magnesium sulphate and the solvent was removed under reduced pressure. The compound was then purified by column chromatography (0-5% EtOAc in hexane)

resulting to yield the title compounds as a white crystalline solid (61%, 2.12 g, 5.24 mmol), m.p. = 50—51 °C.

IR ν_{max} (solid): 2904, 1508, 1028, 985 cm^{-1}; ^{1}H NMR (500 MHz, $CDCl_3$) δ : 3.94 (d, *J* = 6.4 Hz, 2H, O$\underline{C}H_2$), 1.91 (app. d, *J* = 7.0 Hz, 2H, rings-$\underline{C}H_2$), 1.81 – 1.67 (m, 7H, rings-$\underline{C}H_2$, rings-$\underline{C}H_2$, rings-$\underline{C}H_2$, rings-HC-$\underline{C}H$), 1.29 (app. td, *J* = 13.5, 12.1, 6.2 Hz, 2H, $\underline{C}H_2CH_3$), 1.14 (app. t, *J* = 6.0 Hz, 3H, rings-$\underline{H}C$-CH & $\underline{C}H_2CH_2CH_3$), 1.09 – 0.92 (m, 10H, rings-$\underline{C}HCH_2$, rings-$\underline{C}HCH_2$, rings-$\underline{C}H_2$, rings-$\underline{C}H_2$, rings-$\underline{C}H_2$, rings-$\underline{C}H_2$), 0.87 (t, *J* = 7.3 Hz, 3H, $\underline{C}H_3$); $^{19}F\{^{1}H\}$ NMR (470 MHz, $CDCl_3$) δ : -157.0 (dt, *J* = 20.0, 3.3 Hz), -163.5 – -163.9 (m), -164.3 (tt, *J* = 22.7, 3.3 Hz); ^{13}C NMR (126 MHz, $CDCl_3$) δ : 144.6 – 143.1 (m, 5C, Ar-$\underline{C}F$), 137.9 – 136.5 (m, Ar-$\underline{C}O$), 81.4 (O$\underline{C}H_2$), 43.5 (ring-$\underline{C}HCH_2$), 43.4 (ring-$\underline{C}HCH_2$), 40.0 ($\underline{C}H_2CH_2CH_3$), 38.8 (rings-HC-$\underline{C}H$), 37.8 (rings-H$\underline{C}$-CH), 33.7 (2C, rings-$\underline{C}H_2$), 30.4 – 29.2 (m, 6C, rings-$\underline{C}H_2$), 20.2 ($\underline{C}H_2CH_3$), 14.6 ($\underline{C}H_3$); HRMS (EI) $C_{22}H_{29}F_5O$ [M] found 404.214, requires 404.213.

4-(((All *cis*-2,3,4,5,6-pentafluorocyclohexyl)oxy)methyl)-4'-propyl-1,1'-bi(cyclohexane) 5.75

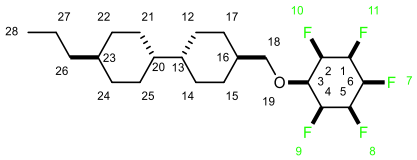

Following General Procedure **3**, **5.74** (490 mg, 1.21 mmol), Rh-CAAC-COD-Cl (14.0 mg, 0.024 mmol, 2 mol%), 4Å molecular sieves (8.00 g), silica (2.00 g), and hexane (40.0 mL) at r.t., for 4 d and at 50 bar H_2 gave, after purification by flash column chromatography (60% DCM in hexane) to yield the title compound (5%, 27.0 mg, 0.066 mmol) as a white crystal, decomposes above 120 °C.

IR ν_{max} (solid): 2906, 1452, 1055, 954 cm^{-1}; ^{1}H NMR (400 MHz, DMSO-d_6) δ : 5.79 – 4.43 (m, 5H, H1,H2,H4,H5,H6), 4.32 (t, *J* = 5.3 Hz, 1H, H3), 3.45 (d, *J* = 6.7 Hz, 2H, H18), 1.83 – 1.60 (m, 10H, H15&H17,1H12&H14,1H21&H25,1H22&H24), 1.34 – 1.17 (m, 4H, H16,H27,H23), 1.11 (app. t, *J* = 6.2 Hz, 4H, H26,H13&H20), 1.07 – 0.88 (m, 6H, 1H12&H14,1H21&H25,1H22&H24), 0.84 (t, *J* = 7.2 Hz, 3H, H28); $^{19}F\{^{1}H\}$ NMR (377 MHz,

DMSO-d_6) δ : -209.3 – -209.8 (m, 2F, *meta*-F, $F_{equatorial}$), -215.5 (app. d, *J* = 23.4 Hz, 2F, *ortho*-F, F_{axial}), -216.2 – -216.8 (m, 1F, *para*-F); ^{13}C NMR (101 MHz, DMSO-d_6) δ : 112.6 – 94.6 (m, 5C, C1,C2,C4,C5,C6), 74.3 (C3), 66.7 (C18), 37.1 (C16), 35.9 (C23), 34.5 (app. d, *J* = 2.9 Hz, 2C, C13&C20), 33.1 (C26), 29.7 (2C, C22&C24), 29.6 – 28.7 (m, 6C, C12,C14,C15,C17,C21,C25), 19.5 (C27), 14.3 (C28); HRMS (ESI^+) $C_{22}H_{35}F_5O$ [M+Na] found 433.250, requires 433.251.

8: References

1 A. Harsanyi and G. Sandford, *Green Chemistry*, 2015, **17**, 2081–2086.
2 G. Villalba, R. U. Ayres and H. Schroder, *J. Ind. Ecol.*, 2007, **11**, 85–101.
3 O. Glemser, U. Biermann and S. P. V Halasz, *Inorg. Nucl. Chem. Letters*, 1969, **5**, 501–508.
4 J. Behrman, *J. Chem. Edu.*, 2006, **83**, 1138–1139.
5 R. E. Banks and J. C. Tatlow, *J. Fluorine Chem.*, 1986, **33**, 71–108.
6 F. Swarts, *Bull. Acad. Roy. Belg*.
7 M. Inoue, Y. Sumii and N. Shibata, *ACS Omega*, 2020, **5**, 10633–10640.
8 Y. Ogawa, E. Tokunaga, O. Kobayashi, K. Hirai and N. Shibata, *iScience*, 2020, **23**, 101467.
9 S. Ebnesajjad, in *Applied Plastics Engineering Handbook: Processing and Materials*, Elsevier Inc., London, 2013, pp. 63–89.
10 Fortune Business Insights, Plastics Polymers and Resins, https://www.fortunebusinessinsights.com/plastics-polymers-and-resins-industry#, (accessed 22 December 2024).
11 E. Clementi, D. L. Raimondi and W. P. Reinhardt, *J. Chem. Phys.*, 1967, **47**, 1300–1307.
12 P. Y. Lien, R. M. You and W. P. Hu, *J. Phys. Chem.*, 2001, **105**, 2391–2400.
13 K. B. Wiberg, *Acc. Chem. Res.*, 1996, **29**, 229–234.
14 P. Kirsch, *Modern Fluoroorganic Chemistry*, Wiley, 2013.
15 A. Bondi, *J. Phys. Chem.*, 1964, **68**, 441–451.
16 R. S. Rowland and R. Taylor, *J. Phys. Chem.*, 1996, **100**, 7384–7391.
17 D. O'Hagan, *Chem. Soc. Rev.*, 2008, **37**, 308–319.
18 H. A. Bent, *Chem. Rev.*, 1961, **61**, 275–311.
19 A. D. McNaught and A. Wilkinson, in *The IUPAC Compendium of Chemical Terminology*, International Union of Pure and Applied Chemistry (IUPAC), Research Triangle Park, NC, 2014.
20 M. L. Trapp, J. K. Watts, N. Weinberg and B. M. Pinto, *Can. J. Chem.*, 2006, **84**, 692–701.
21 N. C. Craig, A. Chen, K. H. Suh, S. Klee, G. C. Mellau, B. P. Winnewisser and M. Winnewisser, *J. Am. Chem. Soc.*, 1997, **119**, 4789–4790.
22 D. O'Hagan, *Chem. Soc. Rev.*, 2008, **37**, 308–319.
23 L. Goodman, H. Gu and V. Pophristic, *J. Phys. Chem.*, 2005, **109**, 1223–1229.
24 I. Rayment, in *Encyclopedia of Physical Science and Technology*, Elsevier, 2003, pp. 191–218.
25 J. W. Banks, A. S. Batsanov, J. A. K. Howard, D. O'Hagan, H. S. Rzepa and S. Martin-Santamaria, *J. Chem. Soc., Perkin Trans. 2*, 1999, 2409–2411.
26 C. A. Lipinski, *Elsevier*, 2004, preprint, DOI: 10.1016/j.ddtec.2004.11.007.
27 C. A. Lipinski, F. Lombardo, B. W. Dominy and P. J. Feeney, *Adv. Drug Deliv. Rev.*, 2001, **46**, 3–26.
28 D. O'Hagan, *Chem. Eur. J.*, 2020, **26**, 7981–7997.
29 S. Purser, P. R. Moore, S. Swallow and V. Gouverneur, *Chem. Soc. Rev.*, 2008, **37**, 320–330.
30 V. P. Reddy, in *Organofluorine Compounds in Biology and Medicine*, Elsevier, 2015, pp. 179–199.
31 Ozone Secretariat, https://ozone.unep.org/kigali-amendment-nine-parties-montreal-protocol-have-ratified, (accessed 7 January 2021).
32 D. Gordon, *W.B. Saunders*, 2020, preprint, DOI: 10.1016/j.anclin.2020.06.006.

33 S. Shi, Y. Li, Z. Cui, Y. Yan, X. Zhang, J. Tang and S. Xiao, *Chem. Eng. J.*, 2023, **470**, 144166.
34 N. Gargiulo and A. Peluso, *J. Colloid Interface Sci.*, 2019, **554**, 463–464.
35 J. L. Clark, A. Taylor, A. Geddis, R. M. Neyyappadath, B. A. Piscelli, C. Yu, D. B. Cordes, A. M. Z. Slawin, R. A. Cormanich, S. Guldin and D. O'Hagan, *Chem. Sci.*, 2021, **12**, 9712–9719.
36 C. R. Patrick and G. S. Prosser, *Nature*, 1960, **187**, 102–103.
37 P. Panini and D. Chopra, in *Hydrogen Bonded Supramolecular Structures*, Springer, Berlin, Heidelberg, 2015, vol. 87, pp. 37–67.
38 Arunan E, Desiraju GR, Klein RA, Sadlej J, Scheiner S, Alkorta I, Alkorta I, Clary DC, Crabtree RH, Dannenberg JJ, Hobza P, Kjaeergaard HG, Legon AC, Mennucci B and Nesbitt DJ, *Defining the hydrogen bond: an account (IUPAC Technical Report)*, 2011.
39 D. Chopra and T. N. G. Row, *CrystEngComm*, 2011, **13**, 2175–2186.
40 C. Yu, A. Kütt, G. V. Röschenthaler, T. Lebl, D. B. Cordes, A. M. Z. Slawin, M. Bühl and D. O'Hagan, *Angew. Chem. Int. Ed.*, 2020, **59**, 19905–19909.
41 L. N. Kuleshova and P. M. Zorkii, *Acta Cryst.*, 1981, **37**, 1363–1366.
42 A. Abad, C. Agulló, A. C. Cuñat, C. Vilanova and M. C. Ramírez De Arellano, *Cryst Growth Des*, 2006, **6**, 46–57.
43 M. V. Ponomarenko, N. Kalinovich, Y. A. Serguchev, M. Bremer and G. V. Röschenthaler, *J. Fluor. Chem.*, 2012, **135**, 68–74.
44 M. Hird, *Chem. Soc. Rev.*, 2007, **36**, 2070–2095.
45 S. Ziherl, J. Pavlin, K. Susman, S. A. Glažar, M. Čepič and N. Vaupotic, 2010, preprint.
46 F. Reinitzer, *Monatshefte für Chemie - Chemical Monthly*, 1888, **9**, 421–441.
47 O. Lehmann, *Zeitschrift für Physikalische Chemie*, 1889, **4U**, 462–472.
48 P. J. Collings and J. W. Goodby, *Introduction to Liquid Crystals*, CRC Press, Boca Raton, Florida, 2nd edn., 2019.
49 https://www.vedantu.com/evs/types-of-crystals.
50 M. Qaddoura and K. Belfield, *Int. J. Mol.*, 2009, **10**, 4772–4788.
51 Y. Chen, F. Peng, T. Yamaguchi, X. Song and S.-T. Wu, *Crystals (Basel)*, 2013, **3**, 483–503.
52 A. Takeda, S. Kataoka, T. Sasaki, H. Chida, H. Tsuda, K. Ohmuro, T. Sasabayashi, Y. Koike and K. Okamoto, *Sid. Int. Symp. Dig. Tec.*, 1998, **29**, 1077–1080.
53 2006-2024 NXP Semiconductors, LCD Drivers.
54 Joshua Clark, the University of St Andrews, 2021.
55 L. Hunter, *Beilstein J. Org. Chem.*, 2010, **6**, 38.
56 L. Hunter, P. Kirsch, A. M. Z. Slawin and David O'Hagan, *Angew. Chem. Int. Ed.*, 2009, **48**, 5457–5460.
57 A. J Durie, A. M. Z. Slawin, T. Label, P. Kirsch and David O'Hagan, *Chem. Commun.*, 2011, **47**, 8265.
58 N. Santschi and R. Gilmour, *Nat. Chem.*, 2015, **7**, 467–468.
59 A. J. Durie, A. M. Z. Slawin, T. Lebl, P. Kirsch and D. O'Hagan, *Chem. Commun.*, 2012, **48**, 9643.
60 N. S. Keddie, A. M. Z. Slawin, T. Lebl, D. Philp and D. O'Hagan, *Nat. Chem.*, 2015, **7**, 483–488.
61 Y. Wei, B. Rao, X. Cong and X. Zeng, *J. Am. Chem. Soc.*, 2015, **137**, 9250–9253.

62 M. P. Wiesenfeldt, Z. Nairoukh, W. Li and F. Glorius, *Science (1979)*, 2017, **357**, 908–912.
63 Z. Nairoukh, M. Wollenburg, C. Schlepphorst, K. Bergander and F. Glorius, *Nat. Chem.*, 2019, **11**, 264–270.
64 B. L. Tran, J. L. Fulton, J. C. Linehan, J. A. Lercher and R. M. Bullock, *ACS Catal.*, 2018, **8**, 8441–8449.
65 B. L. Tran, J. L. Fulton, J. C. Linehan, M. Balasubramanian, J. A. Lercher and R. M. Bullock, *ACS Catal.*, 2019, **9**, 4106–4114.
66 D. Moock, M. P. Wiesenfeldt, M. Freitag, S. Muratsugu, S. Ikemoto, R. Knitsch, J. Schneidewind, W. Baumann, A. H. Schäfer, A. Timmer, M. Tada, M. R. Hansen and F. Glorius, *ACS Catal.*, 2020, **10**, 6309–6317.
67 X. Zhang, L. Ling, M. Luo and X. Zeng, *Angew. Chem. Int. Ed.*, 2019, **58**, 16785–16789.
68 S. V. Haridas and M. von Delius, *Chem. Commun.*, 2024, **60**, 606–609.
69 O. Shyshov, K. A. Siewerth and M. von Delius, *Chem. Commun.*, 2018, **54**, 4353–4355.
70 S. M. Pratik, A. Nijamudheen and A. Datta, *ChemPhysChem*, 2016, **17**, 2373–2381.
71 H. Tsuji, G. Cantagrel, Y. Ueda, T. Chen, L. J. Wan and E. Nakamura, *Chem.-Asian J.*, 2013, **8**, 2377–2382.
72 P. R. Varadwaj, A. Varadwaj and B.-Y. Jin, *PCCP*, 2015, **17**, 31624–31645.
73 S. Tsuzuki, T. Uchimaru and M. Mikami, *J. Phys. Chem.*, 2006, **110**, 2027–2033.
74 Cihang Yu, The University of St Andrews, 2022.
75 S. M. Pratik, A. Nijamudheen and A. Datta, *J. Phys. Chem. C*, 2017, **121**, 1752–1762.
76 T. J. Poskin, B. A. Piscelli, K. Yoshida, D. B. Cordes, A. M. Z. Slawin, R. A. Cormanich, S. Yamada and D. O'Hagan, *Chem. Commun.*, 2022, **58**, 7968–7971.
77 R. A. Cormanich, N. S. Keddie, R. Rittner, D. O'Hagan and M. Bühl, *PCCP*, 2015, **17**, 29475–29478.
78 O. Shyshov, S. V. Haridas, L. Pesce, H. Qi, A. Gardin, D. Bochicchio, U. Kaiser, G. M. Pavan and M. von Delius, *Nat. Commun.*, 2021, **12**, 3134.
79 F. Bellotti, A. De Gloria, A. Poggi, L. Andreone, S. Damiani and P. Knoll, *Cogn. Technol. Work.*, 2004, **6**, 247–265.
80 J. Fan, H. Roehrig, M. K. Sundareshan, E. Krupinski, W. J. Dallas and K. Gandhi, *Med Phys*, 2005, **32**, 578–587.
81 L. Pingping and Q. Danhao, *IOP Conf. Ser. Mater. Sci. Eng.*, 2019, **631**, 052004.
82 K. J. Kim and S. S. Sundar, in *INTERACT 2011, Part II*, IFIP International Federation for Information Processing, 2011, pp. 281–288.
83 Z. Wu, C. Chen and Z. Zhao, *SID Symposium Digest of Technical Papers*, 2019, **50**, 534–537.
84 J. Ma, Y.-C. Yang, Z. Zheng, J. Shi and W. Cao, *Displays*, 2009, **30**, 185–189.
85 C.-H. Liu, C.-Y. Hsiao, J.-C. Gu, K.-Y. Liu, C.-H. Chang, C.-E. Lee and S.-F. Yan, *Appl. Sci.*, 2021, **11**, 11153.
86 J. T. Abel, P. Ouillette, C. L. Williams, J. Blau, J. Cheng, K. Yao, W. Y. Lee, T. C. Cornish, U. G. J. Balis and D. S. McClintock, *J. Pathol. Inform.*, 2020, **11**, 23.
87 K. J. Kim and S. S. Sundar, in *INTERACT 2011, Part II*, IFIP International Federation for Information Processing, 2011, pp. 281–288.

88 J. Jung, H. Park, H. Y. Jung, S. E. Jung, S. G. Kim, T. H. Kim, Y. J. Lim, B.-C. Ku, M. Kim and S. H. Lee, *J. Inf. Disp.*, 2024, **25**, 121–142.

89 H. Chen, Y. Liu, M. Chen, T. Jiang, Z. Yang and H. Yang, *Mol.*, 2022, **27**, 7150.

90 T. Bykova, N. Al-Maharik, A. M. Z. Slawin and D. O'Hagan, *Beilstein J. Org. Chem.*, 2017, **13**, 728–733.

91 T. Bykova, N. Al-Maharik, A. M. Z. Slawin, M. Bühl, T. Lebl and D. O'Hagan, *Chem. - Eur. J.*, 2018, **24**, 13290–13296.

92 M. S. Ayoup, D. B. Cordes, A. M. Z. Slawin and D. O'Hagan, *Beilstein J. Org. Chem.*, 2015, **11**, 2671–2676.

93 B. E. Ziegler, M. Lecours, R. A. Marta, J. Featherstone, E. Fillion, W. S. Hopkins, V. Steinmetz, N. S. Keddie, D. O'Hagan and T. B. McMahon, *J. Am. Chem. Soc.*, 2016, **138**, 7460–7463.

94 M. J. Lecours, R. A. Marta, V. Steinmetz, N. Keddie, E. Fillion, D. O'Hagan, T. B. McMahon and W. S. Hopkins, *J. Phys. Chem. Lett.*, 2017, **8**, 109–113.

95 A. Theodoridis, G. Papamokos, M. P. Wiesenfeldt, M. Wollenburg, K. Müllen, F. Glorius and G. Floudas, *J. Phys. Chem. B*, 2021, **125**, 3700–3709.

96 R. Mondal, M. Agbaria and Z. Nairoukh, *Chem. – Eur. J.*, 2021, **27**, 7193–7213.

97 R. F. W. Bader and R. F. Bader, *Bader Atoms in Molecules: A Quantum Theory*, Clarendon Press, Oxford, 1990.

98 J. Contreras-García, E. R. Johnson, S. Keinan, R. Chaudret, J.-P. Piquemal, D. N. Beratan and W. Yang, *J. Chem. Theory Comput.*, 2011, **7**, 625–632.

99 A. Altun, F. Neese and G. Bistoni, *J. Chem. Theory Comput.*, 2019, **15**, 215–228.

100 D. Herschlag and M. M. Pinney, *Biochemistry*, 2018, **57**, 3338–3352.

101 H.-J. Schneider, *Chem. Sci.*, 2012, **3**, 1381.

102 J. L. Clark, R. M. Neyyappadath, C. Yu, A. M. Z. Slawin, D. B. Cordes and D. O'Hagan, *Chem. – Eur. J.*, 2021, **27**, 16000–16005.

103 G. Hennrich and A. M. Echavarren, *Tetrahedron Lett.*, 2004, **45**, 1147–1149.

104 T. Charvillat, P. Bernardelli, M. Daumas, X. Pannecoucke, V. Ferey and T. Besset, *Chem. Soc. Rev.*, 2021, **50**, 8178–8192.

105 E. C. Taylor and P. M. Harrington, *J. Org. Chem.*, 1990, **55**, 3222–3227.

106 B. M. Trost, J. Xie and J. D. Sieber, *J. Am. Chem. Soc.*, 2011, **133**, 20611–20622.

107 J. Sklyaruk, V. Zubar, J. C. Borghs and M. Rueping, *Org. Lett.*, 2020, **22**, 6067–6071.

108 Z. Wu, X. Liu, C. Ji, L. Li, S. Wang, Y. Peng, K. Tao, Z. Sun, M. Hong and J. Luo, *J. Am. Chem. Soc.*, 2019, **141**, 3812–3816.

109 A. Jain, Y. G. Wang and L. N. Shi, *J. Alloys Compd.*, 2022, **928**, 167066.

110 S. Yamada, Y. Wang, M. Morita, Q. Zhang, D. O'Hagan, M. Nagata, T. Agou, H. Fukumoto, T. Kubota, M. Hara and T. Konno, *Crystals (Basel)*, 2021, **11**, 450.

111 J. Zheng, Z. He, C. Li, Z. Miao, D. Wang, Y. Luan, Y. Li, Y. Zhao, H. Cao, W. He and Z. Yang, *Dyes Pigm.*, 2022, **205**, 110598.

112 P. A. Wright, *Microporous Framework Solids*, The Royal Society of Chemistry, 1st edn., 2008.

113 B. F. Abrahams, B. F. Hoskins, D. M. Michail and R. Robson, *Nature*, 1994, **369**, 727–729.

114 H. Li, M. Eddaoudi, M. O'Keeffe and O. M. Yaghi, *Nature*, 1999, **402**, 276–279.

115 O. M. Yaghi and H. Li, *J. Am. Chem. Soc.*, 1995, **117**, 10401–10402.

116 X. Zhang, Z. Chen, X. Liu, S. L. Hanna, X. Wang, R. Taheri-Ledari, A. Maleki, P. Li and O. K. Farha, *Chem. Soc. Rev.*, 2020, **49**, 7406–7427.
117 H. D. Lawson, S. P. Walton and C. Chan, *ACS Appl. Mater. Interfaces.*, 2021, **13**, 7004–7020.
118 V. Pascanu, G. González Miera, A. K. Inge and B. Martín-Matute, *J. Am. Chem. Soc.*, 2019, **141**, 7223–7234.
119 A. E. Baumann, D. A. Burns, B. Liu and V. S. Thoi, *Commun. Chem.*, 2019, **2**, 86.
120 Sujit K. Ghosh and S. Kitagaw, *Metal-Organic Frameworks (MOFs) for Environmental Applications*, Elsevier, Amsterdam, 1st edn., 2019.
121 D. Alezi, Y. Belmabkhout, M. Suyetin, P. M. Bhatt, Ł. J. Weseliński, V. Solovyeva, K. Adil, I. Spanopoulos, P. N. Trikalitis, A.-H. Emwas and M. Eddaoudi, *J. Am. Chem. Soc.*, 2015, **137**, 13308–13318.
122 D. Li, A. Yadav, H. Zhou, K. Roy, P. Thanasekaran and C. Lee, *Global Challenges*, DOI:10.1002/gch2.202300244.
123 K. Xuan, Y. Pu, F. Li, J. Luo, N. Zhao and F. Xiao, *Chinese Journal of Catalysis*, 2019, **40**, 553–566.
124 J.-R. Li, R. J. Kuppler and H.-C. Zhou, *Chem. Soc. Rev.*, 2009, **38**, 1477.
125 X. Zhao, P. Pachfule and A. Thomas, *Chem. Soc. Rev.*, 2021, **50**, 6871–6913.
126 O. Buyukcakir, S. H. Je, S. N. Talapaneni, D. Kim and A. Coskun, *ACS Appl. Mater. Interfaces.*, 2017, **9**, 7209–7216.
127 H. R. Abuzeid, A. F. M. EL-Mahdy and S.-W. Kuo, *Giant*, 2021, **6**, 100054.
128 P. Kuhn, M. Antonietti and A. Thomas, *Angew. Chem. Int. Ed.*, 2008, **47**, 3450–3453.
129 L. Chen, B. Zhang, L. Chen, H. Liu, Y. Hu and S. Qiao, *Mater Adv*, 2022, **3**, 3680–3708.
130 P. Soleimani Abhari, S. Gholizadeh, F. Rouhani, Y.-L. Li, A. Morsali and T.-F. Liu, *Inorg. Chem. Front.*, 2023, **10**, 6134–6159.
131 Z.-J. Lin, S. A. R. Mahammed, T.-F. Liu and R. Cao, *ACS Cent. Sci.*, 2022, **8**, 1589–1608.
132 Y. Liu and B. Yan, *Inorg. Chem. Front.*, 2024, **11**, 1099–1107.
133 J. Li and B. Chen, *Chem. Sci.*, 2024, **15**, 9874–9892.
134 B. Wang, R. He, L.-H. Xie, Z.-J. Lin, X. Zhang, J. Wang, H. Huang, Z. Zhang, K. S. Schanze, J. Zhang, S. Xiang and B. Chen, *J. Am. Chem. Soc.*, 2020, **142**, 12478–12485.
135 N. Huang, P. Wang and D. Jiang, *Nat. Rev. Mater.*, 2016, **1**, 16068.
136 L. Jiao, J. Y. R. Seow, W. S. Skinner, Z. U. Wang and H.-L. Jiang, *Mater. Today*, 2019, **27**, 43–68.
137 X. Qi, N. Shen, A. Al Othman, A. Mezentsev, A. Permyakova, Z. Yu, M. Lepoitevin, C. Serre and M. Durymanov, *Int. J. Pharm.*, 2023, **15**, 1521.
138 L. Chen, B. Zhang, L. Chen, H. Liu, Y. Hu and S. Qiao, *Mater. Adv.*, 2022, **3**, 3680–3708.
139 Z. Meng and K. A. Mirica, *Chem. Soc. Rev.*, 2021, **50**, 13498–13558.
140 F. Ambroz, T. J. Macdonald, V. Martis and I. P. Parkin, *Small Methods*, 2018, **2**, 1800173.
141 P. Zhang, C. C. Le and D. W. C. MacMillan, *J. Am. Chem. Soc.*, 2016, **138**, 8084–8087.
142 World Intellectual Property Organization, WO2017088738 A1, 2017.
143 J. C. Biffinger, H. W. Kim and S. G. DiMagno, *ChemBioChem*, 2004, **5**, 622–627.

144 C. Yu, B. A. Piscelli, N. Al Maharik, D. B. Cordes, A. M. Z. Slawin, R. A. Cormanich and D. O'Hagan, *Chem. Commun.*, 2022, **58**, 12855–12858.
145 R. K. Kunz, S. Rumfelt, N. Chen, D. Zhang, A. S. Tasker, R. Bürli, R. Hungate, V. Yu, Y. Nguyen, D. A. Whittington, K. L. Meagher, M. Plant, Y. Tudor, M. Schrag, Y. Xu, G. Y. Ng and E. Hu, *BMCL*, 2008, **18**, 5115–5117.
146 CN115340528 A, 2022.
147 L. Benco, D. Tunega, J. Hafner and H. Lischka, *J. Phys. Chem. B.*, 2001, **105**, 10812–10817.
148 S. Dai, C. Simms, I. Dovgaliuk, G. Patriarche, A. Tissot, T. N. Parac-Vogt and C. Serre, *Chem. Mater.*, 2021, **33**, 7057–7066.
149 V. Garcia and M. Bibes, *Nat. Commun.*, 2014, **5**, 4289.
150 Werner Känzig, *Solid State Physics*, Academic Press, 1957, vol. 4.
151 H. Liu, Y. Ye, X. Zhang, T. Yang, W. Wen and S. Jiang, *J. Mater. Chem. C*, 2022, **10**, 13676–13689.
152 A. S. Tayi, A. Kaeser, M. Matsumoto, T. Aida and S. I. Stupp, *Nat. Chem.*, 2015, **7**, 281–294.
153 S. Horiuchi, R. Kumai and Y. Tokura, *J. Am. Chem. Soc.*, 2005, **127**, 5010–5011.
154 S. Horiuchi, Y. Tokunaga, G. Giovannetti, S. Picozzi, H. Itoh, R. Shimano, R. Kumai and Y. Tokura, *Nature*, 2010, **463**, 789–792.
155 A. S. Tayi, A. K. Shveyd, A. C.-H. Sue, J. M. Szarko, B. S. Rolczynski, D. Cao, T. J. Kennedy, A. A. Sarjeant, C. L. Stern, W. F. Paxton, W. Wu, S. K. Dey, A. C. Fahrenbach, J. R. Guest, H. Mohseni, L. X. Chen, K. L. Wang, J. F. Stoddart and S. I. Stupp, *Nature*, 2012, **488**, 485–489.
156 J. Harada, T. Shimojo, H. Oyamaguchi, H. Hasegawa, Y. Takahashi, K. Satomi, Y. Suzuki, J. Kawamata and T. Inabe, *Nat. Chem.*, 2016, **8**, 946–952.
157 H.-Y. Ye, Y.-Y. Tang, P.-F. Li, W.-Q. Liao, J.-X. Gao, X.-N. Hua, H. Cai, P.-P. Shi, Y.-M. You and R.-G. Xiong, *Science (1979)*, 2018, **361**, 151–155.
158 C. Huang, Y. Li, Y. Xie, Y. Du, H. Peng, Y. Zeng, J. Liu and R. Xiong, *Angew. Chem. Int. Ed.*, 2021, **60**, 16668–16673.
159 Y. Ai, P.-F. Li, M.-J. Yang, Y.-Q. Xu, M.-Z. Li and R.-G. Xiong, *Chem. Sci.*, 2022, **13**, 748–753.
160 A. Safari, R. K. Panda and V. F. Janas, *Key Eng Mater*, 1996, **122–124**, 35–70.
161 R. Whatmore, in *Springer Handbook of Electronic and Photonic Materials*, Springer, Cham, 2017, pp. 1–1.
162 M. Owczarek, K. A. Hujsak, D. P. Ferris, A. Prokofjevs, I. Majerz, P. Szklarz, H. Zhang, A. A. Sarjeant, C. L. Stern, R. Jakubas, S. Hong, V. P. Dravid and J. F. Stoddart, *Nat. Commun.*, 2016, **7**, 13108.
163 J. M. Dlugosch, H. Seim, A. Bora, T. Kamiyama, I. Lieberman, F. May, F. Müller-Plathe, A. Nefedov, S. Prasad, S. Resch, K. Saller, C. Seim, M. Speckbacher, F. Voges, M. Tornow and P. Kirsch, *ACS Appl. Mater. Interfaces.*, 2022, **14**, 31044–31053.
164 I. K. Schuller, R. Stevens, R. Pino and M. Pechan, *Neuromorphic Computing – From Materials Research to Systems Architecture Roundtable*, 2015.
165 G. Indiveri, *Neuromorphic Computing and Engineering*, 2021, **1**, 010401.
166 R. Bez, E. Camerlenghi, A. Modelli and A. Visconti, *Proc. IEEE*, 2003, **91**, 489–502.
167 J. Elerath, *Commun. ACM*, 2009, **52**, 38–45.
168 B. Jacob, S. W. Ng and D. T. Wang, *Memory systems: cache, DRAM, disk*, Morgan Kaufmann Publishers, 2010.

169 R. Micheloni, A. Marelli and K. Eshghi, *Inside Solid State Drives (SSDs)*, Springer, 2012.
170 B. J. Cafferty, A. S. Ten, M. J. Fink, S. Morey, D. J. Preston, M. Mrksich and G. M. Whitesides, *ACS Cent. Sci.*, 2019, **5**, 911–916.
171 D. Villemin, F. Simeon, H. Decreus and P.-A. Jaffres, *Phosphorus, Sulfur, Silicon Relat. Elem.*, 1998, **133**, 209–213.
172 Y. P. Subedi, M. N. Alfindee, J. P. Shrestha, G. Becker, M. Grilley, J. Y. Takemoto and C.-W. T. Chang, *BMCL*, 2018, **28**, 3034–3037.
173 M. Ikenberry, L. Peña, D. Wei, H. Wang, S. H. Bossmann, T. Wilke, D. Wang, V. R. Komreddy, D. P. Rillema and K. L. Hohn, *Green Chem.*, 2014, **16**, 836–843.
174 S. Lu and H. Alper, *Chem. Eur. J.*, 2007, **13**, 5908–5916.
175 Y. Yang, L. Yuan, B. Shan, Z. Liu and Q. Miao, *Chem. Eur. J.*, 2016, **22**, 18620–18627.
176 J. Wen, H. Yu and Q. Chen, *J. Mater. Chem.*, 1994, **4**, 1715.
177 C. B. Aakeröy, S. Panikkattu, P. D. Chopade and J. Desper, *CrystEngComm*, 2013, **15**, 3125–3136.
178 S. Rohrbach, A. J. Smith, J. H. Pang, D. L. Poole, T. Tuttle, S. Chiba and J. A. Murphy, *Angew. Chem. Int. Ed.*, 2019, **58**, 16368–16388.
179 H. Finkelstein, *Berichte der deutschen chemischen Gesellschaft*, 1910, **43**, 1528–1532.
180 T. W. Baughman, J. C. Sworen and K. B. Wagener, *Tetrahedron*, 2004, **60**, 10943–10948.
181 K. Matos and J. A. Soderquist, *J. Org. Chem.*, 1998, **63**, 461–470.
182 G. B. Smith, G. C. Dezeny, D. L. Hughes, A. O. King and T. R. Verhoeven, *J. Org. Chem.*, 1994, **59**, 8151–8156.
183 C. Amatore, A. Jutand and G. Le Duc, *Chem. Eur. J.*, 2011, **17**, 2492–2503.
184 C. L. Cheong and B. J. Wakefield, *J. Chem. Soc. Perkin Trans.*, 1988, **1**, 3301–3305.
185 A. Ahmed, R. Sanedrin, T. Willers and P. R. Waghmare, *J. Colloid Interface Sci.*, 2022, **608**, 1086–1093.
186 Y. F. Miura, M. Takenaga, T. Koini, M. Graupe, N. Garg, , Robert L. Graham and T. R. Lee, *Langmuir*, 1998, **14**, 5821–5825.
187 C. Fischer, S. Das, Q. Zhang, Y. Liu, L. Weinhardt, D. O'Hagan, M. Zharnikov and A. Terfort, *Nano Res.*, 2023, **16**, 11030–11041.
188 A. Lapworth, *J. Chem. Soc., Trans.*, 1903, **83**, 995–1005.
189 J. F. Bunnett and R. E. Zahler, *Chem. Rev.*, 1951, **49**, 273–412.
190 K. Kikushima, H. Koyama, K. Kodama and T. Dohi, *Molecules*, 2021, **26**, 1365.
191 C. Bakewell, B. J. Ward, A. J. P. White and M. R. Crimmin, *Chem. Sci.*, 2018, **9**, 2348–2356.
192 E. E. Kwan, Y. Zeng, H. A. Besser and E. N. Jacobsen, *Nat. Chem.*, 2018, **10**, 917–923.
193 A. J. J. Lennox, *Angew. Chem. Int. Ed.*, 2018, **57**, 14686–14688.
194 N. El Guesmi, G. Berionni and B. H. Asghar, *Monatsh. Chem.*, 2013, **144**, 1537–1545.
195 H. C. Sample and M. O. Senge, *EurJOC*, 2021, **2021**, 7–42.
196 S. Scales, S. Johnson, Q. Hu, Q.-Q. Do, P. Richardson, F. Wang, J. Braganza, S. Ren, Y. Wan, B. Zheng, D. Faizi and I. McAlpine, *Org. Lett.*, 2013, **15**, 2156–2159.
197 G. M. Brooke, J. Burdon and J. C. Tatlow, *J. Chem. Soc.*, 1962, **0**, 3253–3254.

198 H. Sun and S. G. DiMagno, *Angew. Chem. Int. Ed.*, 2006, **45**, 2720–2725.
199 J. Kvíčala, M. Beneš, O. Paleta and V. Král, *J. Fluor. Chem.*, 2010, **131**, 1327–1337.
200 V. E. Terekhov, O. S. Morozov, E. S. Afanaseva, B. A. Bulgakov, A. V. Babkin, A. V. Kepman and V. V. Avdeev, *Mendeleev Communications*, 2020, **30**, 671–673.
201 M. R. Cargill, G. Sandford, A. J. Tadeusiak, G. D. Love, N. Hollfelder, F. Pleis, G. Nelles and P. Kilickiran, *Liq. Cryst.*, 2011, **38**, 1069–1078.
202 A. S. Henderson, S. Medina, J. F. Bower and M. C. Galan, *Org. Lett.*, 2015, **17**, 4846–4849.
203 J. Campos, M. Loubidi, M.-C. Scherrmann and S. Berteina-Raboin, *Molecules*, 2018, **23**, 684.
204 S. Rohrbach, J. A. Murphy and T. Tuttle, *JACS*, 2020, **142**, 14871–14876.
205 M. Hird, *Liq. Cryst. Today*, 2005, **14**, 9–21.
206 R. Karapinar, M. O'Neill and M. Hird, *J. Phys. D Appl. Phys.*, 2002, **35**, 900–905.
207 W. C. Yip, C. Welch, G. H. Mehl and T. D. Wilkinson, *J. Mol. Liq.*, 2020, **299**, 112141.
208 D. Camuffo, in *Microclimate for Cultural Heritage*, Elsevier, 2019, pp. 459–482.
209 L. Kumar, Md. S. Alam, C. L. Meena, R. Jain and A. K. Bansal, in *Profiles of Drug Substances, Excipients and Related Methodology*, National Institute of Pharmaceutical Education and Research, Punjab, 2009, vol. 34, pp. 153–192.
210 N. H. Daraghmeh, B. Z. Chowdhry, S. A. Leharne, M. M. Al Omari and A. A. Badwan, in *Profiles of Drug Substances, Excipients and Related Methodology*, The Jordanian Pharmaceutical Manufacturing Company, Naor, 2011, vol. 36, pp. 35–102.
211 Y. Li, H. Shi and G. Yin, *Nat. Rev. Chem.*, 2024, **8**, 535–550.
212 J. Luo, A. H. Jensen, N. R. Brooks, J. Sniekers, M. Knipper, D. Aili, Q. Li, B. Vanroy, M. Wübbenhorst, F. Yan, L. Van Meervelt, Z. Shao, J. Fang, Z.-H. Luo, D. E. De Vos, K. Binnemans and J. Fransaer, *Energy Environ. Sci.*, 2015, **8**, 1276–1291.
213 M. Suzuki, S. Ohara, M. Sakamoto, K. Noda, T. Sasaki, N. Kawatsuki and H. Ono, *Opt. Mater. Express*, 2024, **14**, 1857.
214 O. Sato, N. Iwata, J. Kawamura, T. Maeda, Y. Tsujii, J. Watanabe and M. Tokita, *J. Mater. Chem. C.*, 2017, **5**, 4384–4387.
215 D. Villemin, F. Simeon, H. Decreus and P.-A. Jaffres, *Phosphorus, Sulfur, Silicon Relat. Elem.*, 1998, **133**, 209–213.
216 W. Chang, H. Randel, T. Weyhermüller, A. A. Auer, C. Farès and C. Werlé, *Angew. Chem. Int. Ed.*, 2023, **62**, e2022191.
217 G. M. Brooke and A. C. Young, *J. Fluor. Chem.*, 1976, **8**, 223–241.
218 C. L. Cheong and B. J. Wakefield, *J. Chem. Soc., Perkin Trans. 1*, 1988, 3301.
219 J. H. James, M. E. Peach and C. R. Williams, *J. Fluor. Chem.*, 1985, **27**, 91–104.

9: Appendix

(Published papers)

ChemComm

ROYAL SOCIETY OF CHEMISTRY

COMMUNICATION

View Article Online
View Journal | View Issue

Check for updates

Cite this: *Chem. Commun.*, 2022, **58**, 7968

Received 27th May 2022,
Accepted 18th June 2022

DOI: 10.1039/d2cc03010a

rsc.li/chemcomm

Janus faced fluorocyclohexanes for supramolecular assembly: synthesis and solid state structures of equatorial mono-, di- and tri alkylated cyclohexanes and with tri-axial C–F bonds to impart polarity†

Thomas J. Poskin,[a] Bruno A. Piscelli,[b] Keigo Yoshida,[c] David B. Cordes,[a] Alexandra M. Z. Slawin,[a] Rodrigo A. Cormanich,[b] Shigeyuki Yamada[c] and David O'Hagan*[a]

Concise and general synthesis protocols are reported to generate all-*syn* mono-, di- and tri-alkylated cyclohexanes where a single fluorine is located on the remaining carbons of the ring. The alkyl groups are positioned to lie equatorially and to have triaxial C–F bonds imparting polarity to these ring systems. Intermolecular electrostatic interactions in the solid-state structure of the trialkylated systems are explored and the resultant supramolecular order opens up prospects for design in soft materials.

We have demonstrated that certain arrangements in selectively fluorinated cyclohexanes possess highly polar properties, particularly if the fluorines are strategically located on one face of the cyclohexane ring.[1] All-*syn*-1,2,3,4,5,6-hexafluorocyclohexane **1** is the flagship molecule in this regard, and its unusual polarity is evinced by a very high melting point (mp ~208 °C) as well as a high molecular dipole of μ = 5.89 D.[2] The origin of this polarity lies predominantly in the tri-axial alignment of three of the six C–F bonds, a situation that is always maintained in interconverting chair conformations. This imparts a polarity to the molecule and generates an electronegative (fluorine) and electropositive (hydrogen) face and the rings tends to associate electrostatically (hydrogen to fluorine faces) in the solid-state, with fluorine to hydrogen contacts, rather than fluorous clustering.[3,4] The term 'Janus faced' cyclohexane[5] has been applied to such cycloalkanes for this reason.

Given that the alignment of the axial C–F bonds is particularly significant in terms of inducing polarity in these systems, it can be anticipated that if the equatorial C–F bonds are replaced with alkyl groups, the polarity should be maintained. This was exemplified recently in the solid-state structures of a range of monoalkylated pentafluorocyclohexyl derivatives, where it emerged that the rings adopt the most polar conformation with triaxial C–F bonds and an equatorial alkyl substituent.[6] Theory offers partial support where the methyl substituent in, for example, cyclohexane **2** illustrated in Fig. 1, has a small energy preference (−0.51 kcal mol^{-1}) for the equatorial methyl conformation.[6a] In this paper we demonstrate an increasing

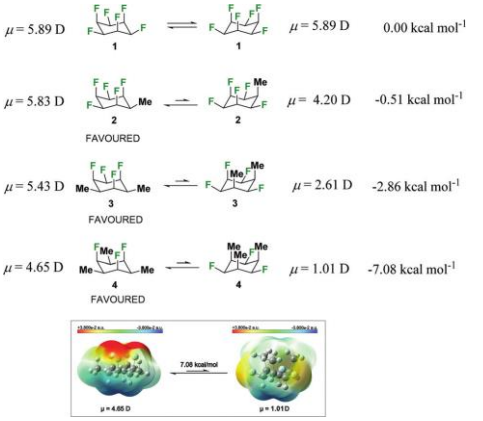

Fig. 1 Structures of **1–4** optimized at the B3LYPD3/def2-TZVP theory level, with calculated conformational Gibbs free energy differences and molecular dipole moments between the chair conformations of some selectively fluorinated all-*syn* fluorocyclohexanes.[7] The lower image shows a surface electrostatic potential map for the conformers of **4**.

[a] *University of St Andrews, School of Chemistry, North Haugh, St Andrews, Fife, KY16 9ST, UK. E-mail: do1@st-andrews.ac.uk; Fax: 01334 463800; Tel: 01334 467171*
[b] *University of Campinas, Chemistry Institute, Monteiro Lobato Street, Campinas, Sao Paulo, Brazil 13083-862. E-mail: cormanich@unicamp.br*
[c] *Faculty of Molecular Chemistry and Engineering, Kyoto Institute of Technology, Matsugasaki, Sakyo-ku, Kyoto, 606-8585, Japan*

† Electronic supplementary information (ESI) available. CCDC 2174305–2174309. For ESI and crystallographic data in CIF or other electronic format see DOI: https://doi.org/10.1039/d2cc03010a

This journal is © The Royal Society of Chemistry 2022

Open Access Article. Published on 20 June 2022. Downloaded on 7/11/2022 11:46:59 AM.
This article is licensed under a Creative Commons Attribution 3.0 Unported Licence.

preference for the triaxial C–F conformer with di- and tri-alkylated derivatives. This is predicted by the computational outcomes presented in Fig. 1 for cyclohexanes **3** and **4**. Progressive methylation at alternate positions around the ring is predicted to increase the triaxial C–F preference and increase the bias towards the more polar arrangements. The calculated[7] molecular dipole moments (μ) for the conformers of **4** indicate that it is the triaxial arrangement of the fluorines which contributes most significantly to molecular polarity (μ = 4.65 D), the ring inverted conformer with equatorial fluorines is much less polar (μ = 1.01 D). With this background it became an objective to prepare a range of all-*syn* 2,4,6-trialkylated-1,3,5-trifluorocyclohexanes **16**, to assess their structures and properties, particularly as they are predicted to be strongly trifluoro-triaxial with the more polar conformations dominating. A general route was devised to this class of compounds which also allowed mono- and di-alkylated cyclohexane rings of this class to be prepared as shown in Scheme 1.

The syntheses sequences start with Sonogashira protocols[8] coupling the appropriate commercially available fluoroiodobenzene **5**, **9** or **13** with terminal acetylenes. The resultant aryl-acetylenes **6**, **10a–c** or **14a–f** were then hydrogenated under standard conditions over Pd/C to generate alkyl-fluoroaryls **7**, **11a–c** or **15a–f** respectively with saturated side chains. These products were then subject to aryl ring hydrogenations under the conditions recently reported by Glorius[8] for the preparation of fluorocyclohexanes from aromatic precursors, using the [CAAC]-COD Rh catalyst **17**.[9] Although these aryl hydrogenation reactions proved to be slow (H_2, 50–70 bar, 1–10 d) conversions overall are moderate to good and it offered a direct approach to this class of compounds generating products **8**, **12a–b** and **16a–f** as illustrated in Fig. 2. Some of the products were amenable to X-ray structure analysis, such as the monosubstituted derivative **8**, the disubstituted derivative **12c** and trisubstituted trifluorocyclohexanes **16d**, **16e** and **16f**. The offset in the stacking arrangement of the fluorocyclohexyl rings, as observed for the monosubstituted derivatives[2,6] was not observed for the di- and tri-substituted systems.

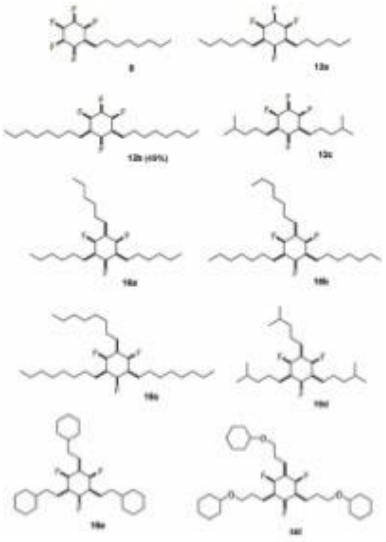

Fig. 2 Structures of the product mono-**8**, di-**12a–b** and tri-**16a–f** fluoroalkylated cyclohexanes prepared in this study.

On the other hand, in the cases of the di- and tri-substituted derivatives **12c**, **16d** and **16e**, the cyclohexane rings stack directly, one on top of another as illustrated in Fig. 3 for **16e** (see also Fig. SI6–SI8, ESI†). It is also interesting to note that the alkyl substituents in the di- and tri-substituted systems lie in the plane of the stacked rings very different to the monosubstituted all-*syn* pentafluorocyclohexyl systems such as **8** and as previously disclosed in other cases where there is an angular herringbone arrangement of the side chains to the rings in the solid-state.[6a] The more ordered stacking arrangement of the trialkyls **16** as a class was explored computationally in the dimeric and trimeric molecular assemblies for compound **4** as a model.

The surface electrostatic potential map for the triaxial arrangement of the fluorines in **4** as illustrated in Fig. 1,

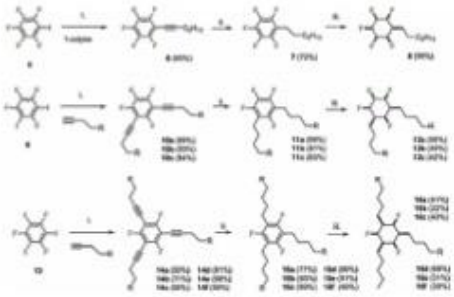

Scheme 1 Reaction conditions: (i) **5**, **9**, **13** (2.5 mmol); terminal alkyne (3–9 mmol), bis(PPh$_3$)PdCl$_2$ (0.375 mmol), Cu(I)I (0.357 mmol), DIPA (25 mL), 80 °C, 24 h; (ii) **6**, **10**, **14** (0.3–2 mmol), 10% Pd/C (10% wt eq), hexane or MeOH (10–100 mL), H_2 (3–15 bar), 20 °C, 16–72 h.; (iii) **7**, **11**, **15** (0.17–0.78 mmol), Rh(CAAC)-COD **17** (1.6 mol%), silica (0.2–1.6 g)/4 Å mol sieves (0.2–3.2 g), hexane (2–40 mL), H_2 (50–70 bar), 25–50 °C, 1–10 d.

Fig. 3 Structure of **16e** showing perpendicular ring stacks in three isolated molecules.

This journal is © The Royal Society of Chemistry 2022

Open Access Article. Published on 20 June 2022. Downloaded on 7/11/2022 11:46:59 AM.
This article is licensed under a Creative Commons Attribution 3.0 Unported Licence.

highlights the Janus face character of this cyclohexane, with a highly negative (red) electrostatic potential associated with the triaxial fluorine face and a highly positive (blue) electrostatic potential associated with the triaxial hydrogens. On the other hand, the polarization diminishes considerably upon ring inversion, and the Janus face characteristic is lost for the triaxial alkyl groups in compound **4**. It is notable that the stacking of the cyclohexane rings in the tri-substituted derivatives further increases the attractive intermolecular interaction between positive and negative ring faces, as evidenced by the surface electrostatic potential maps for the dimer and trimer as illustrated in Fig. 4a, and by the interactions obtained through QTAIM and NCI calculations between axial fluorines and axial hydrogens (Fig. 4b and c, respectively).[10] The strong attractive F–H interactions significantly stabilize these arrangements, with calculated complexation energies for the dimer and trimer of -8.04 kcal mol^{-1} and -17.40 kcal mol^{-1} respectively, the latter value essentially being the sum of two such intermolecular interactions. Therefore, it can be anticipated that it is the array of F···H contacts which are responsible for stabilizing the intermolecular cyclohexane interactions, leading to stabilization of the crystalline supramolecular assembly of the trialkyl-substituted cyclohexanes.

Only in the trisubstituted structures **16** are the ring stacks completely insulated from each other by the alkyl substituents. In the mono- and di-substituted systems *e.g.* **8** and **12c** there is lateral contact between fluorocyclohexane ring stacks (see ESI†)

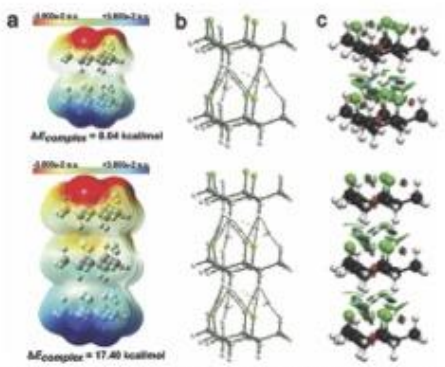

Fig. 4 (a) Surface electrostatic potential maps for dimeric and trimeric arrangements of the polar conformer of **4** obtained at the PBE0/def2-TZVP theory level. Both dimer and trimer are characterized by the electrostatic attraction between the hydrogen and fluorine faces. (b) QTAIM molecular graphics obtained from the PBE0/def2-TZVP electron density, with bond critical points (BCPs) represented by green spheres and ring critical points (RCPs) and cage critical points (CCPs) represented by small red and blue spheres, respectively. (c) NCI iso-surfaces obtained from PBE0/def2-TZVP electron density using reduced density gradient (RDG) = 0.5 and blue–green–red colour scale ranging from $-0.015 <$ sign(λ_2)$\rho(r) <$ 0.015 a.u. Complexation energies were calculated at B3LYP-D3/def2-TZVP optimised geometries using the HFLD method and with the aug-cc-pVTZ basis set.[10]

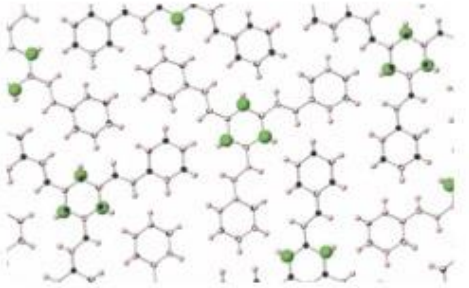

Fig. 5 The solid-state packing arrangements in the structure of **16e** showing that the all-*syn* fluorocyclohexane stacks are isolated and insulated laterally from each other by the hydrocarbon side chains. This is not the case for the mono- and di-substituted alkyl systems *e.g.* **8** and **12c** (see ESI†).

whereas there is a complete insulation of ring stacks in the solid-state structure of the trisubstituted compounds as illustrated for **16e** in Fig. 5. This suggests a characteristic of the trisubstituted systems in the solid-state.

Differential scanning calorimetry (DSC) and polarising optical microscopy (POM) analyses were carried out to assess if these materials were predisposed to polymorphism and/or liquid crystalline phases.[11] The analyses for compounds **16a–f** is presented in the ESI† and illustrated here for compound **16d** in Fig. 6. DSC analysis indicated that for some of the compounds only a single phase transition (melting point) was apparent, however for others, such as **16d**, there is clear polymorphic behaviour with a distinct transition at 97 °C prior to melting at 141 °C. The POM image of this polymorphic phase for **16d** has a clearly contrasted and highly orientated fibrous aspect typical of an ordered supramolecular structure, and this is found in several of the other systems too (see ESI† for **16a** & **16e**) although characteristics vary with different alkyl functionality.

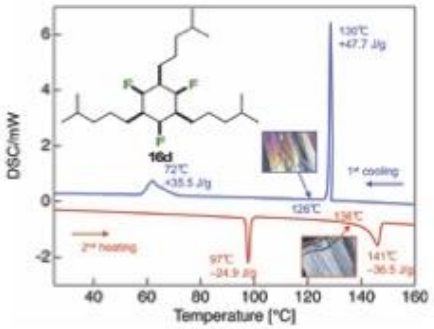

Fig. 6 DSC trace of **16d** illustrating polymorphic phases (mp = 141 °C) during the 1st cooling and 2nd heating cycle.

Open Access Article. Published on 20 June 2022. Downloaded on 7/11/2022 11:46:59 AM. This article is licensed under a Creative Commons Attribution 3.0 Unported Licence.

In conclusion we have presented a synthesis approach to selectively alkylated all-*syn* alkylated cyclohexanes that also contain triaxial C–F bonds, and we profile the alternating 2,4,6-trialkyl motifs in particular. The parallel orientation of the C–F bonds imparts a high polarity to these ring systems, and in selected cases the alkyl chains completely insulate the Janus ring stacks from each other, an arrangement which is not observed for the mono- and di-alkylated systems. The predisposition of the polar Janus rings to assemble in stacks due to electrostatic attraction between the alternating faces of the rings holds promise for ordering supramolecular assemblies with polar properties and offers an approach to designing next generation soft materials such as polar liquid crystals.

We thank the EPSRC for a studentship (TJP) through the CRITICAT Doctoral Training Centre. FAPESP is also gratefully acknowledged for a studentship (BAP, #2021/09716-5) and a Young Researcher Award (RAC, #2018/03910-1). CENAPAD-SP, CESUP and SDumont are also acknowledged for the computational resources used in theory calculations.

Conflicts of interest

There are no conflicts to declare.

References

1 (*a*) C. Yu, A. Kütt, G.-V. Röschenthaler, T. Lebl, D. B. Cordes, A. M. Z. Slawin, M. Bühl and D. O'Hagan, *Angew. Chem., Int. Ed.*, 2020, **59**, 19905–19909; (*b*) D. O'Hagan, *Chem. – Eur. J.*, 2020, **26**, 7981–7997; (*c*) T. Bykova, N. Al-Maharik, A. M. Z. Slawin, M. Bühl, T. Lebl and D. O'Hagan, *Chem. – Eur. J.*, 2018, **24**, 13290–13296; (*d*) T. Bykova, N. Al-Maharik, A. M. Z. Slawin and D. O'Hagan, *Beilstein J. Org. Chem.*, 2017, **13**, 728–733; (*e*) M. Salah Ayoup, D. B. Cordes, A. M. Z. Slawin and D. O'Hagan, *Beilstein J. Org. Chem.*, 2015, **11**, 2671–2676.

2 N. S. Keddie, A. M. Z. Slawin, T. Lebl, D. Philp and D. O'Hagan, *Nat. Chem.*, 2015, **7**, 483–488.

3 (*a*) R. A. Cormanich, N. Keddie, R. Rittner, D. O'Hagan and M. Bühl, *Phys. Chem. Chem. Phys.*, 2015, **44**, 29475–29478; (*b*) B. E. Ziegler, M. Lecours, R. A. Marta, J. Featherstone, E. Fillion, W. S. Hopkins, V. Steinmetz, N. S. Keddie, D. O'Hagan and T. B. McMahon, *J. Am. Chem. Soc.*, 2016, **138**, 7460–7463; (*c*) M. J. Lecours, R. A. Marta, V. Steinmetz, N. Keddie, E. Fillion, D. O'Hagan, T. B. McMahon and W. S. Hopkins, *J. Phys. Chem. Lett.*, 2017, **8**, 109–113.

4 (*a*) O. Shyshov, S. V. Haridas, L. Pesce, H. Y. Qi, A. Gardin, D. Bochicchio, U. Kaiser, G. M. Pavan and M. von Delius, *Nat. Commun.*, 2021, **12**, 3134; (*b*) A. Theodoridis, G. Papamokos, M. P. Wiesenfeldt, M. Wollenburg, K. Mullen, F. Glorius and G. Floudas, *J. Phys. Chem. B*, 2021, **125**, 3700–3709; (*c*) R. Mondal, M. Agbaria and Z. Nairoukh, *Chem. – Eur. J.*, 2021, **27**, 7193–7213.

5 N. Santschi and R. Gilmour, *Nat. Chem.*, 2015, **7**, 467–468.

6 (*a*) J. L. Clark, A. Taylor, A. Geddis, R. M. Neyyappadath, B. A. Piscelli, C. Yu, D. B. Cordes, A. M. Z. Slawin, R. A. Cormanich, S. Guldin and D. O'Hagan, *Chem. Sci.*, 2021, **12**, 9712–9719; (*b*) J. L. Clark, R. M. Neyyappadath, C. Yu, A. M. Z. Slawin, D. B. Cordes and D. O'Hagan, *Chem. – Eur. J.*, 2021, **27**, 16000–16005.

7 H. Tsuji, G. Cantagrel, Y. Ueda, T. Chen, L. J. Wan and E. Nakamura, *Chem. – Asian J.*, 2013, **8**, 2377–2382.

8 (*a*) T. Charvillat, P. Bernardelli, M. Daumas, X. Pannecoucke, V. Ferey and T. Besset, *Chem. Soc. Rev.*, 2021, **50**, 8178–8192; (*b*) Z. Nairoukh, M. Wollenburg, C. Schlepphorst, K. Bergander and F. Glorius, *Nat. Chem.*, 2019, **11**, 264–270; (*c*) M. P. Wiesenfeldt, Z. Nairoukh, W. Li and F. Glorius, *Science*, 2017, **357**, 908–912.

9 (*a*) X. Zhang, L. Ling, M. Luo and X. Zeng, *Angew. Chem., Int. Ed.*, 2019, **58**, 16785–16789; (*b*) Y. Wei, B. Rao, X. Cong and X. Zeng, *J. Am. Chem. Soc.*, 2015, **137**, 9250–9253.

10 (*a*) R. F. W. Bader, *Atoms in Molecules: A Quantum Theory*, Claredon, Oxford, 1990; (*b*) J. Contreras-García, E. R. Johnson, S. Keinan, R. Chaudret, J. Piquemal, D. N. Beratan and W. Yang, *J. Chem. Theory Comput.*, 2011, **7**(3), 625–632; (*c*) A. Altun, F. Neese and G. Bistoni, *J. Chem. Theory Comput.*, 2019, **15**(11), 5894–5907.

11 S. Yamada, M. Morita, Y. Wang, Q. Zhang, D. O'Hagan, T. Agou, H. Fukumoto, T. Kubota, M. Hara and T. Konno, *Crystals*, 2021, **11**, 450.

JOC The Journal of Organic Chemistry

Open Access
This article is licensed under CC-BY 4.0

pubs.acs.org/joc Article

Synthesis of Janus All-*Cis* Tetrafluorocyclohexanes Carrying 1,4-Diether Motifs

Thomas J. Poskin, Bruno A. Piscelli, Aidan P. McKay, David B. Cordes, Yuto Eguchi, Shigeyuki Yamada, Rodrigo A. Cormanich,* and David O'Hagan*

Cite This: J. Org. Chem. 2024, 89, 18445−18451 Read Online

ACCESS | Metrics & More | Article Recommendations | * Supporting Information

ABSTRACT: Nucleophilic aromatic substitutions (S_NAr) of alkoxides on pentafluoroaryl ethers are explored as a first step in a synthesis sequence to generate all-*cis* 2,3,5,6-tetrafluorocyclohexyl-1,4-dialkyl ethers 1. The S_NAr reaction was explored both experimentally and theoretically to rationalize *ortho*/*para*/*meta* selectivities. *tert*-Butyl deprotection of products followed by phenol alkylations introduces versatility to the synthesis. The final Rh(CAAC) 3 catalyzed aryl hydrogenation step of intermediate tetrafluoroaryl-1,4-diethers generated cyclohexane products 1. This chemistry introduces a new class of Janus fluorocyclohexane derivatives with ether substituents placed 1,4- to each other.

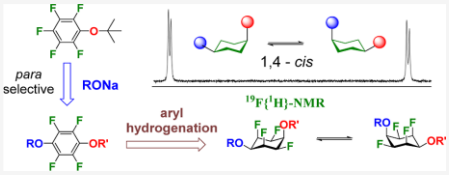

Downloaded via 136.37.78.197 on December 23, 2024 at 15:43:18 (UTC).
See https://pubs.acs.org/sharingguidelines for options on how to legitimately share published articles.

INTRODUCTION

There has been a recent discussion regarding the synthesis and properties of "thermodynamically disfavored" cyclohexanes,[1] where there is an *ax*/*eq* or *eq*/*ax* conformational ambiguity, such as is found in *cis*-1,2, *trans*-1,3, and *cis*-1,4 cyclohexanes, as illustrated in Figure 1. Chemistry to access such substitutions will generally tend toward thermodynamically preferred diequatorial isomers, and thus, specific methods have to be devised to achieve these thermodynamically disfavored *cis*-configurations. The relatively low representation of such compounds across the large organic molecule demographic runs counter to a wider consensus that molecules with an increased dimensionality offer new prospects for uncovering innovative properties from materials[2] to bioactives.[3]

In this paper, we explore the preparation of *cis*-1,4 cyclohexyl ethers 1, where the cyclohexane ring also has four fluorine atoms arranged around the ring and with an all-*cis* configuration. This is an extension of our current interest in facially polarized Janus cyclohexanes.[4] All-*cis*-1,2,3,4,5,6-hexafluorocyclohexane 2 has attracted some interest due to its high polarity, particularly as it is a cyclohexane, which as a class is generally found to be hydrophobic.[5] In the interconverting chair conformations of this cyclohexane, there are always triaxial C−F bonds pointing in the same direction, which impart a strong molecular dipole. It is the coalignment of the axial C−F bonds, which contribute most significantly to its the molecular polarity.[6]

These systems have been termed Janus cyclohexanes[7] as they have two faces (electropositive-H and electronegative-F face). The first preparation of 2 in our laboratory[5] from inositol was significantly improved by the Glorius laboratory,[8] who developed a direct aryl hydrogenation of hexafluorobenzene. The method involves high pressure hydrogenations (~50 bar H_2) using a Rh catalyst, which was applied to aryl hydrogenations by Zeng et al.[9] The catalyst 3 shown in Figure 2 contains the strongly electron-donating cyclic alkyl amino carbene ligand (CAAC) and reactions are carried out in low polarity solvents. This combination suppressed competing dehydrofluorination reactions, generating a series of Janus cyclohexanes with good efficiency. For the preparation of ethers, Glorius et al.[8c] exemplified the aryl hydrogenation of fluorophenyl silyl (TBS) ethers to the corresponding all-*cis* pentafluorocyclohexyl ethers, such as 4a. Subsequently, von Delius's laboratory[10] demonstrated aryl hydrogenation to methyl ether 4b from the pentafluoroanisole precursor. This methyl ether could be converted to alcohol 4c and derivatized to acetate 4c and more elaborate esters, such as 4e, which acted as monomers displaying interesting dynamic behavior due to self-assembly equilibria between the Janus rings. Most recently,[11] von Delius's laboratory has extended to examples of all-*cis* 1,3,5-triethers 7a and 7b (via triol 6), which have been prepared by aryl hydrogenations of trifluorotrimethoxybenzene 5 followed by demethylation. The three ether substituents in 7a and 7b adopt a thermodynamically favorable triequatorial conformation, and as a consequence, the three C−F bonds are triaxial. This arrangement is attractive as it offers trisubstituted

Received: September 19, 2024
Revised: October 29, 2024
Accepted: November 19, 2024
Published: November 27, 2024

ACS Publications
© 2024 The Authors. Published by American Chemical Society

https://doi.org/10.1021/acs.joc.4c02345
J. Org. Chem. 2024, 89, 18445−18451

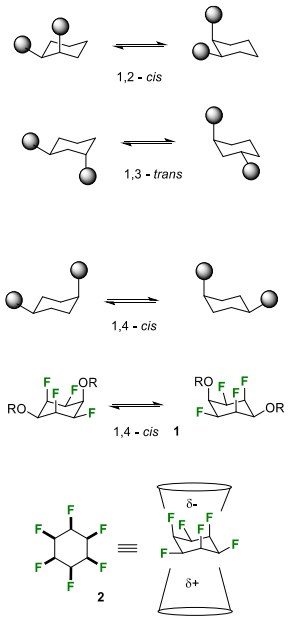

Figure 1. "Thermodynamically disfavored" cyclohexanes and all-*cis*-1,2,3,4,5,6-hexafluorocyclohexane **2**.

cyclohexanes with a large dipole due to the oriented C−F bonds.

We address here the synthesis of all-*cis* tetrafluoro disubstituted cyclohexanes **1**, where alkyl ether substituents are *cis*-1,4 to each other. They are a class of Janus cyclohexanes where oxygens replace the 1,4-fluorines; however, there will always be an axial and an equatorial C-OR bond in interconverting chair conformations rendering these "thermodynamically disfavored". The only example of a 1,4-ether that we are aware of is *bis* silyl ether **8**, which was reported in the original Glorius paper.[8] The new class of Janus 1,4-dialkyl ethers may offer some advantages in that they will have more complex 3D arrangements and will be more dynamic in supramolecular assemblies. The route to these 1,4-cyclohexyl diethers exploits a *para* selective S_NAr reaction on *t*ButO-pentafluorophenol ether **10** and then aryl hydrogenations offer access to molecules of class **1**.

RESULTS AND DISCUSSION

A general route to 1,4-disubstituted tetrafluorocyclohexyl ether **1** is outlined in Scheme 1. For S_NAr reactions on pentafluoroaryl rings, a regiochemical preference for *para* over *meta* attack by nucleophiles is generally observed; although the bias is dependent on the indigenous substituent.

For example, S_NAr reactions on C_6F_5X systems with electron-withdrawing groups (−NO_2, −CN) are very highly selective for *para* products[12] as is a −Ph substituent[13] or even an unsubstituted −H substituent.[14] For pentafluoroaryl ethers such as X = OMe, the *para* over the *meta* directing effect is much more modest relative to −H[14] and −Ph,[13] due to the mesomeric donor ability of the methoxyl group. In order to maximize the regiochemical preference in favor of *para* addition for an alkoxide nucleophile to a pentafluoroaryl ether, an exploration of progressively larger indigenous ether substituents (−OMe **9**, −O*i*Pr **10**, and −O*t*But **11**) was conducted and with progressively larger alkoxide nucleophiles to enhance both steric and stereoelectronic factors. Reactions were conducted in THF with **9**, **10**, and **11** reacting with sodium methoxide (OMe^-), *iso*-propoxide ($iPrO^-$) and *tert*-butoxide ($tBuO^-$) as nucleophiles. The *ortho*/*para*/*meta* product ratios are represented in Table 1. It emerged that the *meta*/*para* ratio is the lowest in the reactions conducted on the *t*ButO-aryl ether **11** and with $tBuO^-$ as a nucleophile.

It is not clear where the origin of this selectivity arises. In aryl ethers (anisoles), the MeO^- substituent tends to adopt a planar orientation with respect to the aromatic ring, maximizing oxygen lone pair conjugation into the ring whereas the $tBuO^-$ group adopts a perpendicular conformation, which will reduce the donor potential of the oxygen lone pairs.[15] However, the *ortho* fluorines in **9** also direct the −OMe to a

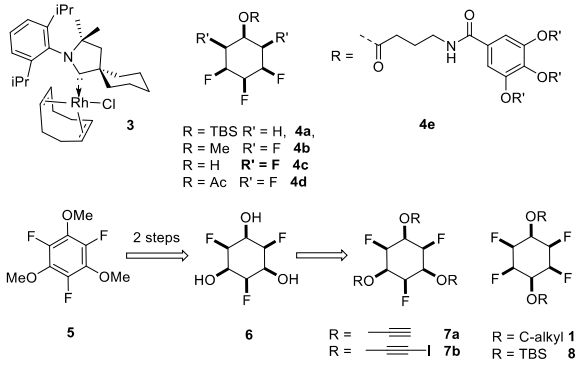

Figure 2. CAAC catalyst **3** and Janus ether substituted cyclohexanes.[8−10]

https://doi.org/10.1021/acs.joc.4c02345
J. Org. Chem. 2024, 89, 18445−18451

The Journal of Organic Chemistry pubs.acs.org/joc Article

Scheme 1. Synthesis Routes to All-*Cis* Tetrafluorocyclohexyl Diethers 1a−1e from *t*ButO Ether 11

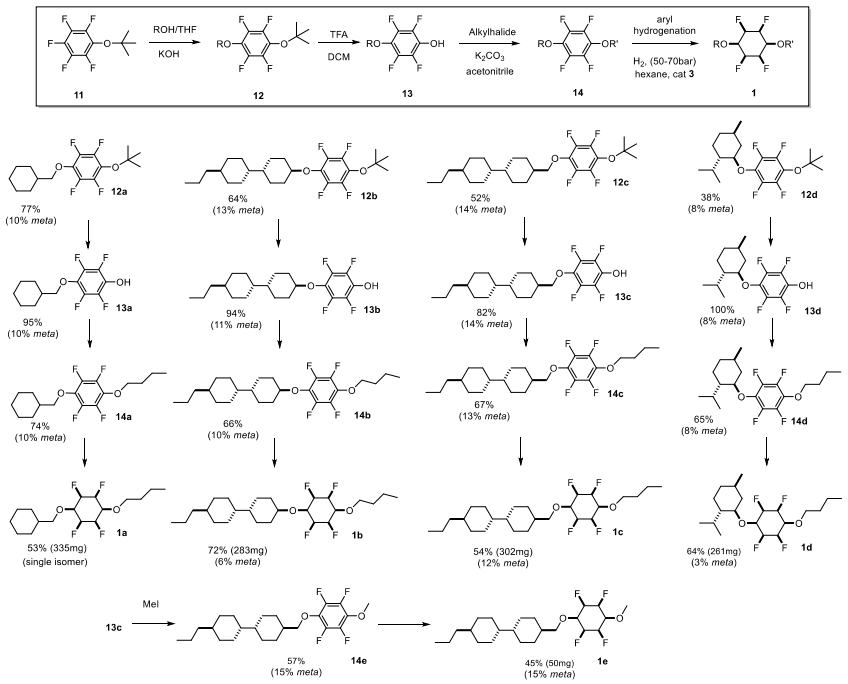

Table 1. *Ortho*/*Para*/*Meta* Ratios of Products from Reactions of 9−11 with Alkoxide Nucleophiles[a]

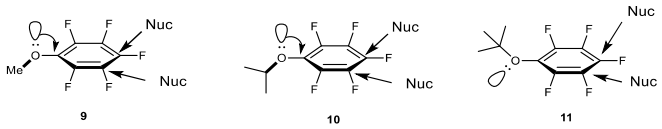

nucleophile	9 (MeO)			10 (*i*PrO)			11 (*t*ButO)		
	ortho	*para*	*meta*	*ortho*	*para*	*meta*	*ortho*	*para*	*meta*
MeONa	0.55	1.27	1.0	0.0	1.8	1.0	0.0	3.7	1.0
*i*PrONa	0.49	1.34	1.0	0.0	1.7	1.0	0.0	4.3	1.0
*t*ButONa	0.28	1.81	1.0	0.0	2.4	1.0	0.0	7.1	1.0

[a]Conditions: **9**, **10** or **11** (1.0 equiv), alcohol (0.5 equiv), NaH (0.75 equiv), THF (3 mL), 2.5 h, 50 °C. (Ratios are an averages of triplicates).

more favored perpendicular conformation,[16] so stereoelectronically the MeO- and *t*ButO-ethers are more equivalent in this perfluorinated series. In order to explore these effects further, reaction profiles with an alkoxide nucleophile were conducted computationally for MeO- ether **9** and *t*ButO-ether **11**. In each case, reaction profiles were modeled for *para* and *meta* trajectories and with MeO^- and $tButO^-$ as nucleophiles.

It proved challenging to locate transition states (TSs), but they could be found employing a developing version of Autobench[17] for energy reaction barriers. Considering the methoxyl ether **9** as the substrate and with MeO^- as the nucleophile, the energies of the TSs are very similar and only a little (1.3 and 1.6 kcal mol^{-1}) above the ground state energy of **9**, as illustrated in Figure 3a. In each case, the reaction is highly exergonic (ΔG^0 = −14.9 and −17.8 kcal mol^{-1}) with a high barrier to reversibility and thus the *meta*/*para* ratio appears to be determined kinetically with the *meta* TS a little higher ($\Delta\Delta G^{\ddagger}$ = 0.8 kcal mol^{-1}) than that of the *para* TS (Figure 4). When **11** is the substrate and with MeO^- again as the nucleophile, the reaction follows a trend similar to that of **9**, with a $\Delta\Delta G^{\ddagger}$ = 0.9 kcal mol^{-1}, but the reaction is very much more exergonic for the *meta*/*para* products (ΔG^0 = −29.6 and

https://doi.org/10.1021/acs.joc.4c02345
J. Org. Chem. 2024, 89, 18445−18451

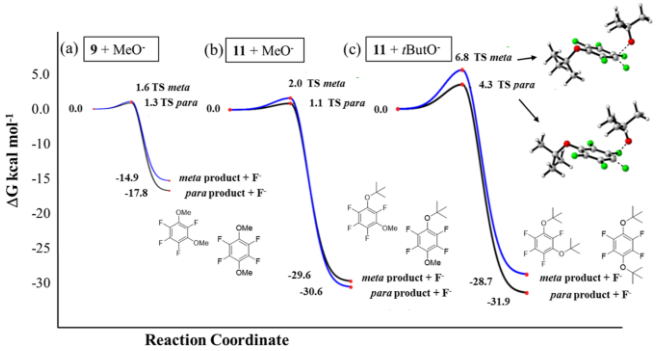

Figure 3. Reaction profiles for S_NAr reactions of (a) **9** with OMe^-; (b) **11** with OMe^-; and (c) **11** with $tBuO^-$; each attacking either at the *meta* or *para* positions calculated at the M06-2X/6-311++G** level. The *para* reaction course is kinetically favored in each case.

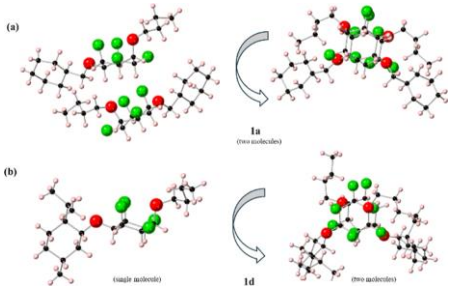

Figure 4. X-ray structures of 1,4-diethers (a) **1a** and (b) **1d** viewed from two trajectories.

−30.6 kcal mol^{-1}), as illustrated in Figure 3b. On the other hand, when $tBuO^-$ is the nucleophile combining with tBuO ether **11**, there is an increase in the reaction energy barriers to $\Delta\Delta G^{\ddagger}$ = 2.5 kcal mol^{-1} favoring the *para* TS, and the reaction is also high exergonic, as illustrated in Figure 3c. In all of these reactions, intermediate Meisenheimer complexes could not be located computationally, and these reactions appear to progress through a concerted S_NAr substitution process. Concerted processes have already been proposed for S_NAr of perfluoroaromatics,[18,19] and this general mechanism for S_NAr reactions was evaluated by Jacobsen[20] and has been discussed more widely.[21]

With the knowledge that the *para*/*meta* ratio is most influenced by an incipient *t*BuO ether, **11** emerged as an attractive starting material in order to most effectively influence the *para*/*meta* regiochemistry. S_NAr reactions generated the *t*BuO ether products **12**, predominantly as the *para* products, with lesser levels of *meta* isomers (≤15%), as illustrated in Scheme 1. The ethers were then conveniently cleaved to aryl ether phenols **13** by treatment with trifluoroacetic acid. Subsequent alkylation of phenols **13**, in this case with 1-bromobutane or methyl iodide-generated diaryl ethers **14**.

The resultant ethers **14** were then subject to aryl hydrogenations (H_2 50 bar, cat **3**)[8] to generate a range of all-*cis* tetrafluoro-substituted cyclohexyl diethers **1**. The approach could reasonably be applied quite widely although the reactions explored here were conducted with well-known liquid crystal motifs as the targets.[22]

In the case of **1b−e**, differential scanning calorimetry and polarized optical microscopy analysis showed significant levels of crystalline polymorphism in each case, although no LC phases were observed during both the heating and cooling processes (see Figures S1−S4). In all Janus *cis*-tetrafluorocyclohexane **1b−e**, the alkoxy moieties introduced at the 1,4-positions occupy axial and equatorial positions, forming a bent structure, which appears to prevent LC phase formation.

1,4-Diether products **1a−e** were solids and single crystals of **1a** and **1d** were obtained and submitted for X-ray structure analysis. The resultant structures are illustrated in Figure 4. In each case, the structures adopt the expected chair conformations in the solid state and, consequently, the 1,4-substitution dictates an axial and an equatorial ether bond in each cyclohexane. In both cases, it is the *n*-butyl ether that adopts the axial orientation. One feature of both structures is that the cyclohexane rings do not stack directly above each other; instead, they rotate such that the C−O bonds eclipse C−F bonds in the ring stacks. Essentially, there is less order in ring stacking relative to compounds where the substituents are all equatorial.[23]

In the solid state, only a single conformer is adopted; however, in solution, ^{19}F-[^1H}NMR analysis indicates that these compounds adopt ∼1:1 mixed ratios of presumably the chair conformers, when the ether substituents are non-equivalent and with these nonequivalent substituents switching between axial and equatorial orientations. This is obvious in the representative NMR spectra of **1a**, as illustrated in Figure 5.

The pathway and energy barrier to this interconversion was explored theoretically for the symmetric tetrafluoro dimethyl ether **1f** and barriers to interconversion were compared relative to all-*cis*-hexafluorofluorocyclohexane **2** and to cyclohexane **15** itself to act as points of reference. Calculations were carried out at the M06-2X/6-311++G** theory level.[24,25] The resultant interconversion pathways and energy barriers are illustrated in Figure 6.

The values computed here for the TSs and, also the twisted boat intermediates, are similar to those reported in previous

https://doi.org/10.1021/acs.joc.4c02345
J. Org. Chem. 2024, 89, 18445−18451

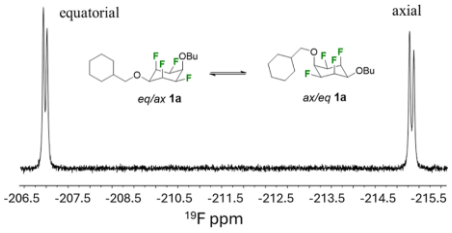

Figure 5. $^{19}F\{^{1}H\}$-NMR of **1a** showing an equilibrium mix of *eq*/*ax* **1a** and *ax*/*eq* **1a** in solution.

studies for both all-*cis*1,2,3,4,5,6-hexafluorocyclohexane **2**[26] and cyclohexane **15**[27] and, therefore, we assume that the calculated conformational energy profile for **1f** is relatively accurate. It is notable that the highest barrier to interconversion for **1f** at the "half-chair" structure is close to that for **2** at its "half-chair" intermediate, suggesting a similar level of negative electrostatic interaction between the C−O and C−F bonds in **1f**, and C−F and C−F bonds in **2** as the conformational profile progresses through these two intermediates. In fact, the "half-chair" TS in **1f** is 0.8 kcal mol^{-1} lower in energy compared to **2** (15.0 against 15.8 kcal mol^{-1}), which is attributed to the formation of OC−H···F stabilizing contacts formed between methoxy groups and fluorine atoms (Figure S8). These half−chair TSs are ∼4.0 kcal mol^{-1} above that for cyclohexane **15**, where only C−H/C−H bond contacts are present. There are two conformational profiles for **1f**, corresponding to two possible symmetrical boat intermediate structures where either two C−O or two C−F bonds occupy the apical positions of the TS structure (see Figure 6b). Ethoxylation at positions 1 and 4 on the fluorinated systems does not significantly affect the ring-flip energy barriers, which are around 15 kcal mol^{-1} and easily surmountable at room temperature. As a result, it is expected that asymmetric compounds **1a−e**, despite showing a single conformer in the solid state, are in a rapid equilibrium between both chair conformers in solution.

In conclusion, we present a synthesis to all-*cis* 2,3,5,6-tetrafluorocyclohexanes **1** carrying 1,4-diether moieties, as a new class of Janus cyclohexanes. These were prepared by S_NAr chemistry with various alkoxide nucleophiles on pentafluoroaryl ether **11**. Cleavage of the *t*ButO ethers **12** followed by alkylation of the resultant phenols **13**, allowed a range of 1,4 diethers **14** to be prepared, and these were subjected to aryl hydrogenations to generate cyclohexanes of class **1**. Low levels of the *meta* isomers were evident from the S_NAr reaction, a reaction that was investigated computationally. This analysis indicated a maximum energy difference (∼2.5 kcal mol^{-1}) between *para* and *meta* TSs, for *t*ButO ether **11** and *t*BuO^- as a nucleophile, which is consistent with the experimental outcomes. These "thermodynamically disfavored" compounds form less ordered arrangements in the solid state than previous prepared all-*cis*-fluorocyclohexanes.[23,28]

■ ASSOCIATED CONTENT

Data Availability Statement

The data underlying this study are available in the published article and its Supporting Information.

Supporting Information

The Supporting Information is available free of charge at https://pubs.acs.org/doi/10.1021/acs.joc.4c02345.

Experimental details and analyses of prepared compounds **1a−1e**, copies of ^{1}H, $^{13}C\{^{1}H\}$ and $^{19}F\{^{1}H\}$ NMR spectra, X-ray data **1a** and **1d**, details of computation reaction barriers for S_NAr reactions on **9** and **11**, and interconversion barriers for cyclohexanes **1f**, **2**, and **15** (PDF)

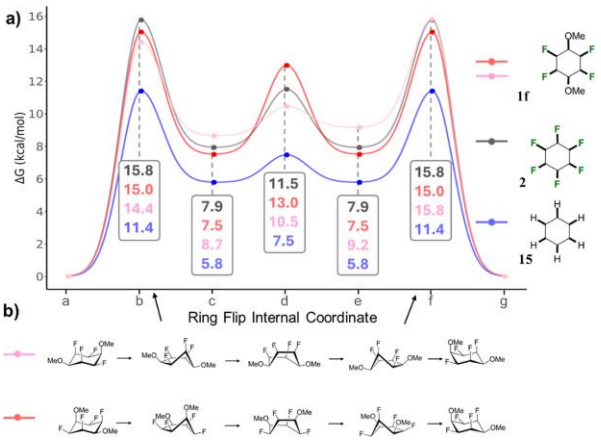

Figure 6. (a) Comparative cyclohexyl interconversion energy profiles for dimethoxy ether **1f**, all-*cis*1,2,3,4,5,6-exafluorocyclohexane **2** and cyclohexane **15** showing the relative energies of intermediates. Energy values in kcal mol^{-1}. (b) Schematic of the two interconversion pathways for cyclohexane **1f**.

https://doi.org/10.1021/acs.joc.4c02345
J. Org. Chem. 2024, 89, 18445−18451

Accession Codes

Deposition numbers 2384410−2384411 contain the supplementary crystallographic data for this paper. These data can be obtained free of charge via the joint Cambridge Crystallographic Data Centre (CCDC) and Fachinformationszentrum Karlsruhe Access Structures service.

AUTHOR INFORMATION

Corresponding Authors

Rodrigo A. Cormanich − *Instituto de Química, Departamento de Química Orgânica, Universidade Estadual de Campinas, Campinas, São Paulo 13083-970, Brazil*; orcid.org/0000-0001-7659-1749; Email: cormanich@unicamp.br

David O'Hagan − *School of Chemistry, University of St Andrews, St Andrews KY16 9ST, U.K.*; orcid.org/0000-0002-0510-5552; Email: do1@st-andrews.ac.uk

Authors

Thomas J. Poskin − *School of Chemistry, University of St Andrews, St Andrews KY16 9ST, U.K.*

Bruno A. Piscelli − *Instituto de Química, Departamento de Química Orgânica, Universidade Estadual de Campinas, Campinas, São Paulo 13083-970, Brazil*

Aidan P. McKay − *School of Chemistry, University of St Andrews, St Andrews KY16 9ST, U.K.*; orcid.org/0000-0002-8578-7054

David B. Cordes − *School of Chemistry, University of St Andrews, St Andrews KY16 9ST, U.K.*; orcid.org/0000-0002-5366-9168

Yuto Eguchi − *Faculty of Molecular Chemistry and Engineering, Kyoto Institute of Technology, Sakyo-ku, Kyoto 606-8585, Japan*

Shigeyuki Yamada − *Faculty of Molecular Chemistry and Engineering, Kyoto Institute of Technology, Sakyo-ku, Kyoto 606-8585, Japan*; orcid.org/0000-0002-6379-0447

Complete contact information is available at: https://pubs.acs.org/10.1021/acs.joc.4c02345

Notes

The authors declare no competing financial interest.

ACKNOWLEDGMENTS

We thank EPSRC (EP/S030506) UK, and FAPESP Brazil are thanked for a Young Researcher Award to R.A.C. (#2018/03910-1) and Scholarships to B.A.P. (#2023/14064-2 and #2022/10156-7). CNPq is acknowledged for a fellowship to R.A.C. (#306912/2023-6) and FAEPEX for research funding. CENAPAD-SP and CESUP computational resources are also gratefully acknowledged.

REFERENCES

(1) Li, Y.; Shi, H.; Yin, G. Synthetic techniques for thermodynamically disfavoured substituted six-membered rings. *Nat. Rev. Chem* **2024**, *8*, 535−550.

(2) (a) Chang, J.; Chen, F.; Li, H.; Suo, J.; Zheng, H.; Zhang, J.; Wang, Z.; Valtchev, V.; Qiu, S.; Fang, Q. Three-dimensional covalent organic frameworks with nia nets for efficient separation of benzene/cyclohexane mixtures. *Nat. Commun.* **2024**, *15*, 813. (b) Ma, X.; Scott, T. F. Approaches and challenges in the synthesis of three-dimensional covalent-organic frameworks. *Commun. Chem.* **2018**, *1*, 98.

(3) (a) Wang, Z.; Sharma, P. P.; Rathi, B.; Xie, M.; De Clercq, E.; Pannecouque, C.; Kang, D.; Zhan, P.; Liu, X. Escaping from Flatland: Multiparameter Optimization Leads to the Discovery of Novel Tetrahydropyrido[4,3-d]pyrimidine Derivatives as Human Immunodeficiency Virus-1 Non-nucleoside Reverse Transcriptase Inhibitors with Superior Antiviral Activities against Non-nucleoside Reverse Transcriptase Inhibitor-Resistant Variants and Favorable Drug-like Profiles. *J. Med. Chem.* **2023**, *66*, 8643−8665. (b) Lovering, F. Escape from Flatland 2: Complexity and Promiscuity. *MedChemComm* **2013**, *4*, 515−519.

(4) O'Hagan, D. The Emergence and Properties of Selectively Fluorinated 'Janus' Cyclohexanes. *Chem. Rec.* **2023**, *23*, No. e202300027.

(5) Keddie, N. S.; Slawin, A. M. Z.; Lebl, T.; Philp, D.; O'Hagan, D. All-cis 1,2,3,4,5,6-Hexafluorocyclohexane is a Facially Polarized Cyclohexane. *Nat. Chem.* **2015**, *7*, 483−488.

(6) (a) Lecours, M. J.; Marta, R. A.; Steinmetz, V.; Keddie, N. S.; Fillion, E.; O'Hagan, D.; McMahon, T. B.; Hopkins, W. S. Interaction of $B_{12}F_{12}^{2-}$ with All-cis 1,2,3,4,5,6 Hexafluorocyclohexane in the Gas Phase. *J. Phys. Chem. Lett.* **2017**, *8*, 109−113. (b) Ziegler, B. E.; Lecours, M.; Marta, R. A.; Featherstone, J.; Fillion, E.; Hopkins, W. S.; Steinmetz, V.; Keddie, N. S.; O'Hagan, D.; McMahon, T. B. Janus Face Aspect of All-cis 1,2,3,4,5,6-Hexafluorocyclohexane Dictates Remarkable Anion and Cation Interactions In the Gas Phase. *J. Am. Chem. Soc.* **2016**, *138*, 7460−7463.

(7) Santschi, N.; Gilmour, R. A Janus Cyclohexane Ring. *Nat. Chem.* **2015**, *7*, 467−468.

(8) (a) Nairoukh, Z.; Wollenburg, M.; Schlepphorst, C.; Bergander, K.; Glorius, F. The Formation of All-cis-(Multi)Fluorinated Piperidines by a Dearomatization-Hydrogenation Process. *Nat. Chem.* **2019**, *11*, 264−270. (b) Wiesenfeldt, M. P.; Knecht, T.; Schlepphorst, C.; Glorius, F. Silylarene Hydrogenation: A Strategic Approach that Enables Direct Access to Versatile Silylated Saturated Carbo- and Heterocycles. *Angew. Chem., Int. Ed.* **2018**, *57*, 8297−8300. (c) Wiesenfeldt, M. P.; Nairoukh, Z.; Li, W.; Glorius, F. Hydrogenation of Fluoroarenes. Direct Access to All-cis (Multi)-Fluorinated Cycloalkanes. *Science* **2017**, *357*, 908−912.

(9) (a) Zhang, X.; Ling, L.; Luo, M.; Zeng, X. Accessing Difluoromethylated and Trifluoromethylated cis-Cycloalkanes and Saturated Heterocycles: Preferential Hydrogen Addition to the Substitution Sites for Dearomatization. *Angew. Chem., Int. Ed.* **2019**, *58*, 16785−16789. (b) Wei, Y.; Rao, B.; Cong, X.; Zeng, X. Highly Selective Hydrogenation of Aromatic Ketones and Phenols Enabled by Cyclic (Amino)(alkyl)carbene Rhodium Complexes. *J. Am. Chem. Soc.* **2015**, *137*, 9250−9253.

(10) (a) Haridas, S. V.; Shyshov, O.; von Delius, M. Supramolecular Polymerization of All-cis Fluorinated Cyclohexanes: Influence of Side Chains. *Org. Mater.* **2023**, *5*, 166−174. (b) Shyshov, O.; Haridas, S. V.; Pesce, L.; Qi, H.; Gardin, A.; Bochicchio, D.; Kaiser, U.; Pavan, G. M.; von Delius, M. Living Supramolecular Polymerization of Fluorinated Cyclohexanes. *Nat. Commun.* **2021**, *12*, 3134. (c) Shyshov, O.; Siewerth, K. A.; von Delius, M. Evidence for Anion-Binding of All-cis Hexafluorocyclohexane in Solution and Solid State. *Chem. Commun.* **2018**, *54*, 4353−4355.

(11) Haridas, S. V.; von Delius, M. Synthesis and Supramolecular Properties of All-cis-2,4,6-Trifluorocyclohexane-1,3,5-triol. *Chem. Commun.* **2024**, *60*, 606−609.

(12) Burdon, J.; Hollyhead, W. B.; Patrick, C. R.; Wilson, K. V. 1184. Kinetics of nucleophilic substitution in polyfluoro-aromatic compounds. Part I. The reaction of sodium methoxide with some pentafluorophenyl-compounds. *J. Chem. Soc.* **1965**, 6375−6379.

(13) Kvíčala, J.; Beneš, M.; Paleta, O.; Král, V. Regiospecific Nucleophilic Substitution in 2,3,4,5,6-Pentafluorobiphenyl as Model Compound for Supramolecular Systems. Theoretical Study of Transition States and Energy Profiles, Evidence for Tetrahedral S_N2 Mechanism. *J. Fluorine Chem.* **2010**, *131*, 1327−1337.

(14) Brooke, G. M.; Burdon, J.; Tatlow, J. C. J. Aromatic Polyfluoro Compounds XII. Orientation Reactions of Pentafluorobenzene. *Chem. Soc.* **1962**, 3253−3254.

(15) Tsuzuki, S.; Houjou, H.; Nagawa, Y.; Hiratani, K. High-Level Ab-initio Calculations of Torsional Potential of Phenol, Anisole, and o-Hydroxyanisole: Effects of Intramolecular Hydrogen Bond. *J. Phys. Chem. A* **2000**, *104*, 1332−1336.

https://doi.org/10.1021/acs.joc.4c02345
J. Org. Chem. 2024, 89, 18445−18451

(16) Belyakov, A. V.; Kieninger, M.; Cachau, R. E.; Ventura, O. N.; Oberhammer, H. Molecular Structure and Internal Rotation in 2,3,5,6-Tetrafluoroanisole as Studied by Gas-Phase Electron Diffraction and Quantum Chemical Calculations. *J. Phys. Chem. A* **2005**, *109*, 394−399.
(17) Cormanich, R. A.; da Silva, G. D. Autobench V1.0: Benchmarking Automation for Electronic Structure Calculations. *J. Chem. Inf. Model.* **2024**, *64*, 3322−3331.
(18) Sadowsky, D.; McNeill, K.; Cramer, C. J. Dehalogenation of Aromatics by Nucleophilic Aromatic Substitution. *Environ. Sci. Technol.* **2014**, *48*, 10904−10911.
(19) Kikushima, K.; Grellier, M.; Ohashi, M.; Ogoshi, S. Transition-Metal-Free Catalytic Hydrodefluorination of Polyfluoroarenes by Concerted Nucleophilic Aromatic Substitution With a Hydrosilicate. *Angew. Chem., Int. Ed.* **2017**, *56*, 16191−16196.
(20) Kwan, E. E.; Zeng, Y.; Besser, H. A.; Jacobsen, E. N. Concerted Nucleophilic Aromatic Substitutions. *Nat. Chem.* **2018**, *10*, 917−923.
(21) Rohrbach, S.; Smith, A. J.; Pang, J. H.; Poole, D. L.; Tuttle, T.; Chiba, S.; Murphy, J. A. Concerted Nucleophilic Aromatic Substitution Reactions. *Angew. Chem., Int. Ed.* **2019**, *58*, 16368−16388.
(22) Kirsch, P.; Bremer, M. Nematic Liquid Crystals for Active Matrix Displays: Molecular Design and Synthesis. *Angew. Chem., Int. Ed.* **2000**, *39*, 4216−4235.
(23) Poskin, T. J.; Piscelli, B. A.; Yoshida, K.; Cordes, D. B.; Slawin, A. M. Z.; Cormanich, R. A.; Yamada, S.; O'Hagan, D. Janus Faced Fluorocyclohexanes for Supramolecular Assembly: Synthesis and Solid-State Structures of Equatorial Mono-Di- and Tri Alkylated Cyclohexanes and With Tri-Axial C-F Bonds to Impart Polarity. *Chem. Commun.* **2022**, *58*, 7968−7971.
(24) Bannwarth, C.; Ehlert, S.; Grimme, S. GFN2-xTB-An Accurate and Broadly Parametrized Self-Consistent Tight-Binding Quantum Chemical Method with Multipole Electrostatics and Density-Dependent Dispersion Contributions. *J. Chem. Theory Comput.* **2019**, *15*, 1652−1671.
(25) Zhao, Y.; Truhlar, D. G. The M06 suite of density functionals for main group thermochemistry, thermochemical kinetics, noncovalent interactions, excited states, and transition elements: two new functionals and systematic testing of four M06-class functionals and 12 other functionals. *Theor. Chem. Acc.* **2008**, *120*, 215−241.
(26) Pratik, S. M.; Nijamudheen, A.; Datta, A. Janus All-cis-1,2,3,4,5,6-Hexafluorocyclohexane: A Molecular Motif for Aggregation-Induced Enhanced Polarization. *ChemPhysChem* **2016**, *17*, 2373−2381.
(27) (a) Anet, F. A. L.; Bourn, A. J. R. Nuclear Magnetic Resonance Line-Shape and Double-Resonance Studies of Ring Inversion in Cyclohexane-d_{11}. *J. Am. Chem. Soc.* **1967**, *89*, 760−768. (b) Hendrickson, J. B. Molecular geometry. VII. Modes of interconversion in the medium rings. *J. Am. Chem. Soc.* **1967**, *89*, 7047−7061.
(28) Clark, J. L.; Taylor, A.; Geddis, A.; Neyyappadath, R. M.; Piscelli, B. A.; Yu, C.; Cordes, D. B.; Slawin, A. M. Z.; Cormanich, R. A.; Guldin, S.; O'Hagan, D. Supramolecular packing of alkyl substituted Janus face all-cis 2,3,4,5,6-pentafluorocyclohexyl motifs. *Chem. Sci.* **2021**, *12*, 9712−9719.

https://doi.org/10.1021/acs.joc.4c02345
J. Org. Chem. 2024, 89, 18445−18451